

**Seismic Reflection Experiments  
Imaging the Physical Nature of  
Crustal Structures in Southern California**

**Thesis by  
John Nikolai Louie**

**In Partial Fulfillment of the Requirements  
for the Degree of  
Doctor of Philosophy**

**California Institute of Technology  
Pasadena, California**

**1987**

**(submitted March 2, 1987)**

KNOWLEDG

To my parents,  
Mary Dugan and Nikolai Louie,  
who should be held responsible.

## ACKNOWLEDGEMENTS

My stay here at Caltech's Seismological Laboratory has been made most pleasant and inspirational by all of the people who I have been privileged to know. In the first place, I am very grateful for the generous support I have been provided with throughout my graduate career. A three-year fellowship granted by the AMOCO Foundation, in particular, enabled me to pursue projects based on my own interests instead of on funding availability. This rare freedom was a boon to my creativity, and I am thankful to Dr. Leon Thomsen of AMOCO, who was instrumental in arranging for the fellowship. Valuable support was also provided by an Institute Fellowship during my first year, and through research assistantships provided by Sun Oil Company, the U. S. Geological Survey, and the National Science Foundation.

I am especially grateful to my advisor for this thesis, Dr. Robert W. Clayton, for having enough confidence to allow me to work more or less independently for long periods. Yet he provided insightful ideas and inspirations at just the right times, keeping my work on track. Many of his ideas are represented in this thesis. Rob's weekly seminars, in which his students could informally discuss the progress of their research, formed a very large part of my geophysical education. I was also advised by Dr. Clarence R. Allen, to whom I am indebted for guiding me through the field of earthquake prediction research. He has also been an outstanding model of professional integrity and thoroughness.

One of the most remarkable privileges that I enjoyed at the Seismo Lab was the interaction I had with the late C. Hewitt Dix. He had many insights into every aspect of geophysics, from theory to field operations, which cut through the obfuscations so common in reflection seismology and got right to the heart of the scientific issues. If I have been able to absorb only a small percentage of what he tried to teach me, then I have still benefitted enormously.

The other faculty of the Seismo Lab deserve credit at least for their efforts to preserve the Lab's unique atmosphere. Their emphasis on research, their treatment of students as colleagues, and the relative lack of scrambling for stipend support make graduate study here an unparalleled opportunity for education and productive work. I feel as though I have been insulated from most of the negative aspects of graduate school.

Of course, most of my interaction at the Lab has been with other students. Those in my class, Ann Mori, Steve Salyards, David Scott, and Richard Stead, have been particularly valued colleagues and companions over the past five years. They have often gone out of their way to help me out. Ronan LeBras has also been an excellent collaborator and friend, whose impact on my work is shown most clearly in Chapter 1 of this thesis. I simply cannot list all of the other people at the Lab who have helped me, since I have been able to interact positively with everyone with whom I shared time here.

I must, however, thank those who have freely, and literally, given their sweat and blood to assist me during the field experiments described in Chapter 2. I do not understand why so many people were willing to work so hard so far out in such a torrid desert. But they all deserve medals for valor against

heatstroke, callouses, cholla, and warm beer. L. Astiz, J. Choy, H. Davies, S. Grand, B. Hager, J. Hasse, T. Hearn, H. Houston, R. LeBras, V. LeFevre, H. Magistrale, C. Polanskey, M. Richards, S. Salyards, C. Schmitt, D. Schmitt, R. Stead, C. Stork, J. Tyburczy, J. Vidale, and H.-W. Zhou are among those who contributed to this thesis through such hard work, and through valuable suggestions.

Data were obtained through methods easier than fieldwork. I am indebted to Sid Kauffman of COCORP at Cornell University for kindly providing the data from their lines through Parkfield and the western Mojave. A generous grant from ARCO Research Company covered the cost of reproducing the large Mojave dataset.

The formation of the Calcrust crustal reflection profiling consortium concurrently with my stay at Caltech was a tremendous boon to my career. Calcrust was conceived by Tom L. Henyey, Robert W. Clayton, John C. Crowell, Greg A. Davis, Perry Ehlig, Eric G. Frost, Peter C. Leary, Peter E. Malin, Tom V. McEvelly, and Leon T. Silver. It was through their untiring efforts and guidance that the project reported in Chapters 2 and 3 was brought to fruition. I must also thank David A. Okaya, whose footsteps I have in many ways been trying to follow. Many people from USC, UC Santa Barbara, and UC Berkeley contributed immensely to the project. John McRaney, John Morton, and Michelle Robertson have been among the most competent and cooperative. Thanks are also due to CGG crew 510, and AMOCO, for working most cooperatively with us in the eastern Mojave under trying conditions. A debt is due to S. Biehler and his students at UC Riverside for their generosity with equipment and expertise. None of the fieldwork could have been

carried out without the gracious cooperation of the Southern Pacific Railroad, the Metropolitan Water District, and the U. S. Bureau of Land Management, who taught us how to work with minimum impact.

Finally, I am grateful to Penn State for giving me a job so I could get off my duff and write this thesis in the wonderfully short period of three weeks. My mother and father have been constant sources of support and advice. My father is responsible for introducing me to folk dancing while I was at Caltech. The new friends I found there have made what might have been a humdrum life of science one full of variety and joy. *at multiple effects becomes tractable*

## ABSTRACT

Seismic reflection methods have been extensively used to probe the Earth's crust and suggest the nature of its formative processes. The analysis of multi-offset seismic reflection data extends the technique from a reconnaissance method to a powerful scientific tool that can be applied to test specific hypotheses. The treatment of reflections at multiple offsets becomes tractable if the assumptions of high-frequency rays are valid for the problem being considered. Their validity can be tested by applying the methods of analysis to full wave synthetics.

Three studies illustrate the application of these principles to investigations of the nature of the crust in southern California. A survey shot by the COCORP consortium in 1977 across the San Andreas fault near Parkfield revealed events in the record sections whose arrival time decreased with offset. The reflectors generating these events are imaged using a multi-offset three-dimensional Kirchhoff migration. Migrations of full wave acoustic synthetics having the same limitations in geometric coverage as the field survey demonstrate the utility of this back projection process for imaging. The migrated depth sections show the locations of the major physical boundaries of the San Andreas fault zone. The zone is bounded on the southwest by a near-vertical fault juxtaposing a Tertiary sedimentary section against uplifted crystalline rocks of the fault zone block. On the northeast, the fault zone is bounded by a fault dipping into the San Andreas, which includes slices of serpentized

ultramafics, intersecting it at 3 km depth. These interpretations can be made despite complications introduced by lateral heterogeneities.

In 1985 the Calcrust consortium designed a survey in the eastern Mojave desert to image structures in both the shallow and the deep crust. Preliminary field experiments showed that the major geophysical acquisition problem to be solved was the poor penetration of seismic energy through a low-velocity surface layer. Its effects could be mitigated through special acquisition and processing techniques. Data obtained from industry showed that quality data could be obtained from areas having a deeper, older sedimentary cover, causing a re-definition of the geologic objectives. Long offset stationary arrays were designed to provide reversed, wider angle coverage of the deep crust over parts of the survey. The preliminary field tests and constant monitoring of data quality and parameter adjustment allowed 108 km of excellent crustal data to be obtained.

This dataset, along with two others from the central and western Mojave, was used to constrain rock properties and the physical condition of the crust. The multi-offset analysis proceeded in two steps. First, an increase in reflection peak frequency with offset is indicative of a thinly layered reflector. The thickness and velocity contrast of the layering can be calculated from the spectral dispersion, to discriminate between structures resulting from broad scale or local effects. Second, the amplitude effects at different offsets of P-P scattering from weak elastic heterogeneities indicate whether the signs of the changes in density, rigidity, and Lamé's parameter at the reflector agree or are opposed. The effects of reflection generation and propagation in a heterogeneous, anisotropic crust were contained by the design of the experiment and the

simplicity of the observed amplitude and frequency trends. Multi-offset spectra and amplitude trend stacks of the three Mojave Desert datasets suggest that the most reflective structures in the middle crust are strong Poisson's ratio ( $\sigma$ ) contrasts. Porous zones or the juxtaposition of units of mutually distant origin are indicated. Heterogeneities in  $\sigma$  increase towards the top of a basal crustal zone at  $\sim 22$  km depth. The transition to the basal zone and to the mantle include increases in  $\sigma$ . The Moho itself includes  $\sim 400$  m layering having a velocity higher than that of the uppermost mantle. The Moho maintains the same configuration across the Mojave despite 5 km of crustal thinning near the Colorado River. This indicates that Miocene extension there either thinned just the basal zone, or that the basal zone developed regionally after the extensional event.

## Table of Contents

Acknowledgements .....	iii
Abstract .....	vii
Glossary .....	xii
<b>Introduction</b> .....	<b>1</b>
<b>Chapter 1: 3-d imaging of steeply dipping structure near the San Andreas fault, Parkfield, California</b> .....	<b>148</b>
Abstract .....	3
1. Introduction .....	4
2. Characteristics of the survey .....	8
3. Imaging method .....	17
Approximations to the wave equation .....	17
4. Migration results .....	33
5. Conclusions .....	40
<b>Chapter 2: Seismic acquisition case history of the Calcrust Mojave-Sonoran deep crustal survey</b> .....	<b>210</b>
Abstract .....	42
1. Introduction .....	43
2. Goals of the survey .....	45
3. Preliminary field tests .....	48
Determining the seismic character of the target structure .....	51
Large-scale reflection tests .....	57
Finite difference modeling .....	61
Attenuation of multiply reflected basement refractions .....	73
4. Acquisition Strategy .....	82
5. Vibrator system field tests .....	88
6. Acquisition parameters .....	91
7. Description of the data .....	94
8. Conclusions .....	106

**Chapter 3: Constraints on the physical nature of deep crustal structures in the Mojave Desert, California**

Abstract .....	109
1. Introduction .....	110
2. Datasets used .....	120
Description of Calcrust WM-1 data .....	122
Crustal velocities .....	130
3. Reflection spectral analysis .....	138
Thin layer reflection spectra at multi-offset .....	138
Analysis of reflection spectra .....	148
4. Reflection amplitude analysis .....	172
Effects on seismic amplitudes .....	176
Recording and processing effects .....	176
Surface consistent effects .....	179
Propagation effects .....	182
Reflector effects .....	189
Multi-offset reflection amplitudes from the Mojave Desert .....	196
Eastern Mojave .....	197
Central Mojave .....	207
Western Mojave .....	213
5. Conclusions .....	246
<b>Recommendations</b> .....	<b>254</b>
<b>References</b> .....	<b>258</b>
<b>Appendix: Acquisition parameters of the 1985 Calcrust survey</b> .....	<b>271</b>

## GLOSSARY

- Acoustic** Pertaining to pressure waves in a fluid medium.
- Air Wave** The acoustic wave propagating within the air.
- Array** A distribution of seismic sources or receivers over a small area of the ground surface, with the separate elements summed together into one record or channel.
- Automatic Gain Control (AGC)** A method of equalizing different parts of a data trace relative to one another for clearer display.
- Basement** The generally older and higher-velocity plutonic and metamorphic rocks below the younger sedimentary and extrusive rocks.
- Cable** The signal conductor linking all of the groups to the recorder. Typically spans the offset range of the receivers.
- Channel** The recorder input carrying the response of a single receiver group.
- Correlation** In vibrator work, the cross-correlation of the chirp nominally swept through by the vibrator, and of the ground motion recorded on a single channel over a complete shot record, to mimic an explosion record.
- Depth Section** A cross-section of some property in a 3-dimensional body relating horizontal location and depth.
- Elastic** Pertaining to elastic waves in a linear elastic medium.
- Equalization** Multiplication of all or parts of a data trace by a scalar, or a smooth set of scalars.
- Finite Difference** A discretization of differentials into subtractions over a discretized medium, used to solve wave equations for model calculations.
- First Break** The initial deflection of a trace corresponding to the initial arrival of shot energy at that offset in the gather.
- Gain** The amplification applied to a recorded channel to yield a data trace.

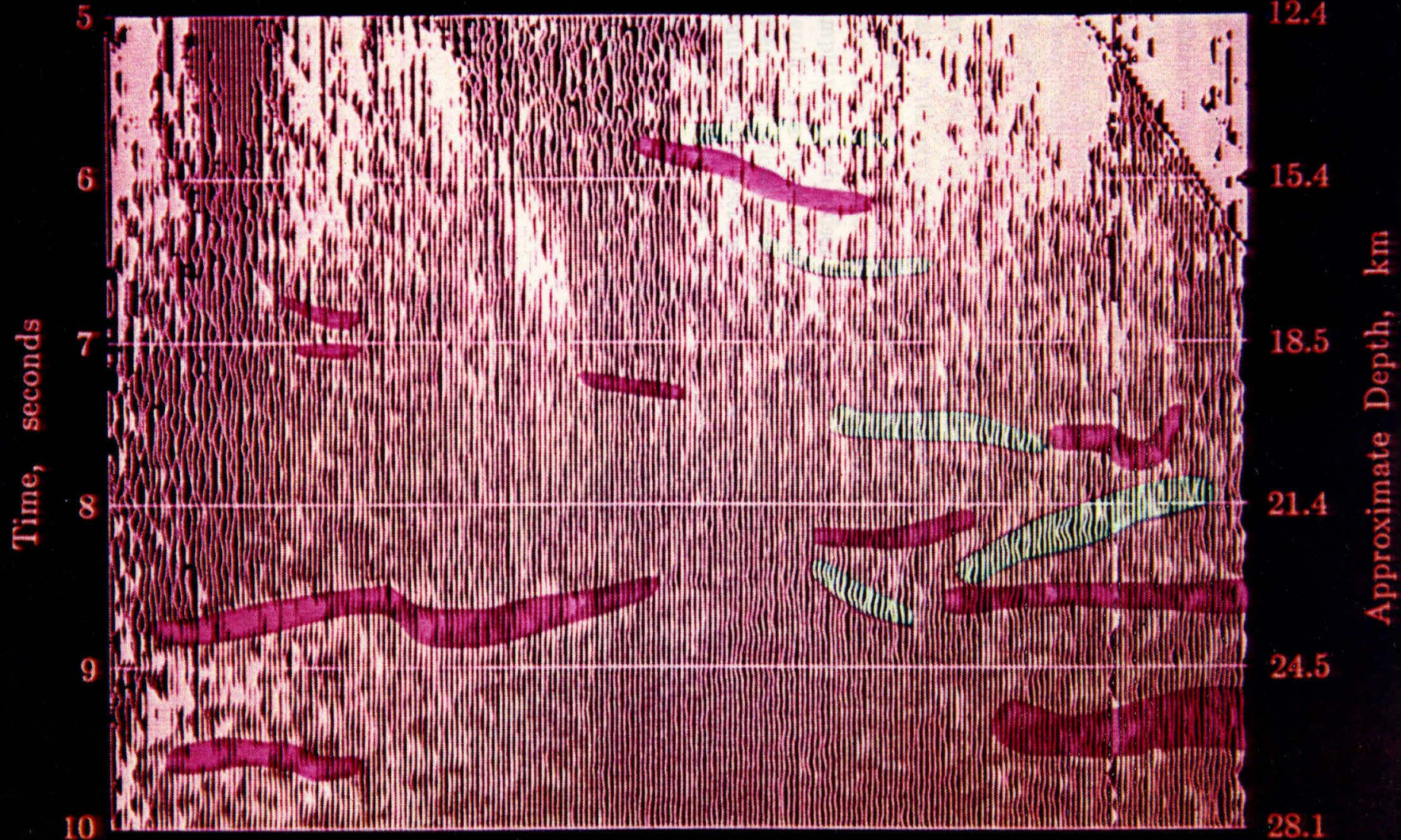
<b>Gather</b>	A record section of traces having some common attribute, such as their shots or midpoints, usually ordered according to their offsets.
<b>Geophone</b>	An individual seismometer, forming one element of a receiver group.
<b>Ground Roll</b>	The surface waves generated by a shot.
<b>Group</b>	Several geophones, connected to sum electrically and set into the surface to form a receiver array. Recorded by a single channel.
<b>Image</b>	An inversion, migration, backprojection, or focusing of wavefield data into some representation of subsurface structure.
<b>Jug</b>	A geophone.
<b>Line</b>	The path followed by a roll-along seismic reflection survey, often consisting of a number of overlapping spreads.
<b>Midpoint</b>	(MP) The point on the surface midway between the source and receiver.
<b>Migration</b>	The conversion of a reflection wavefield from a time section into a depth section.
<b>Moveout</b>	The apparent velocity of an arrival on a gather.
<b>Moveup</b>	Motion of the vibrators between separate sweeps of a single shot, forming the spacing of the source array.
<b>Mute</b>	To zero out unwanted parts of a gather.
<b>Normal Moveout</b>	(NMO) The hyperbolic increase in arrival time of a reflection as offset increases.
<b>Offset</b>	The distance between the source and receiver, which can be signed to indicate their orientation relative to the roll-along direction.
<b>Out-of-Plane</b>	Not directly beneath the line.
<b>Overburden</b>	The veneer of low-velocity material at the surface.
<b>Quantile</b>	Of a set of numbers, that value such that a certain percentage of the set is lesser.
<b>Raytracing</b>	Derivation of the propagation of a wavefield using high-frequency optical ray approximations.

<b>Record</b>	A gather of traces sorted to represent the results of a physical seismic experiment.
<b>Roll-Along</b>	The progression of the combination of sources and receivers relative to the fixed survey line.
<b>Semblance</b>	The similarity of an event in a gather to the shape sought by a linear operator applied to the gather.
<b>Shot</b>	The combination of separate vibrator sweeps for which the resulting records are summed together to mimic a single larger source.
<b>Sort</b>	The arrangement of traces into gathers having a particular attribute in common.
<b>Spread</b>	A set of receiver groups laid in some geometry along the line, or the physical receiver geometry relative to the source location.
<b>Stack</b>	The reduction of a gather containing traces recorded at multiple offsets to a single trace, mimicking a zero-offset trace.
<b>Static</b>	A deviation of arrival amplitude or phase, constant throughout the trace.
<b>Surface Consistent</b>	Of an arrival characteristic or a static, dependence on only the surface location of the source or receiver, and often independent of the incident angle.
<b>Sweep</b>	A single "chirp" by a vibrator, or the time series controlling it.
<b>Time Section</b>	The record of a wavefield recorded at the surface, represented as horizontal distance against time.
<b>Trace</b>	The seismogram recorded by a single receiver group on one channel, in response to a single shot.
<b>Vertical Seismic Profile</b>	(VSP) A time section recorded from seismometers located at different depths of a well or drill hole.
<b>Vibrator</b>	A machine used to impart an oscillatory force upon the ground surface having controlled amplitude and phase.
<b>Window</b>	The culling out of a part of a gather over some continuous interval of time and distance.
<b>Zero-Offset</b>	Having the source and receiver at the same location.

SOUTH

Linear Amplitude—Offset Trends

NORTH



Horizontal Exaggeration 2.4 : 1

- AX -

**Frontispiece:** Linear amplitude versus offset trend stack of Calcrust line WM-1 in Ward Valley, eastern Mojave Desert, California. The long-offset range gathers incorporated in this stack were produced by merging data from distant stationary arrays with the records of a high-resolution seismic reflection survey. The image presents a cross section of the deep crust 8.3 km wide, between about 12.4 and 28.1 km depth. The slope of the change in reflection amplitude with source-to-receiver offset, found by linear regression, is plotted for each point of a stacked time section. Light-colored areas indicate where reflection amplitudes increase as offset increases. Trace deflections to the left indicate where amplitudes decrease with offset.

Areas of this image having strong amplitude trends, associated with strong reflections that obey the assumptions of the stacking process, are indicated with contrasting colors. Dark red shows areas of strong increases, aqua shows areas of strong decreases. The north-dipping interface at 15.4 km produces the strongest mid-crustal reflection in the section. Its large increase in amplitude with offset indicates strong variations in Poisson's ratio at that depth. The basal crustal zone between 23.5 and 26.5 km depth is bounded by interfaces showing amplitude increases, including the Mohorovicic discontinuity on the bottom. Since both are transitions to materials having higher P velocities, they also form strong increases in Poisson's ratio. The decreasing trends just above the basal zone at 22 km indicate a high degree of Poisson's ratio heterogeneity radiating up from the top of the zone. Such heterogeneity is evidence of active crustal processes, such as the intrusion of fluids.

## INTRODUCTION

The projects presented in this thesis are linked by a common methodology for the analysis of seismic reflection data. Chapter 1 sets the tone of this method. Dissatisfaction with the results of conventional methods of analysis, such as stacking, prompts a search through the data in the domain of the physical seismic experiment for phenomena that may carry more information. These phenomena are usually associated with the properties of reflections as observed over a range of offsets between the seismic source and receiver. Synthetic seismograms are then used to gain an understanding of the phenomena in question. It is hoped that the analysis of the reflections can then be simplified through the application of high-frequency ray approximations to the wave equation that governs the whole process. The method of analysis, and its results, are kept simple to compensate for the many sources of interference that cannot be easily evaluated. The effects analyzed typically result from contrasts in the physical properties of the crust, which do not necessarily correspond with the boundaries important to geological interpretations.

Analyses can be motivated by considerations other than the observation of an unusual phenomenon in the data. As discussed in Chapter 2, experiments can be designed with the resolution of specific geological or geophysical problems in mind. Effects specific to the site of the experiment may frustrate the constraint of one problem, yet benefit the resolution of another.

The benefits of this kind of approach become clear in the conclusions reached in Chapters 1 and 3. Where standard methods have missed important structures, or have left too many unanswered questions as to their origin, this more focused approach provides much new information. In Chapter 3, the variation of reflection frequency and amplitude with source-to-receiver offset is investigated. Simple models and theory are used to establish the connection of these properties with the presence of thinly-layered structures and changes in Poisson's ratio. The lessons learned on seismic reflection experimental design in Chapter 2 are then applied to investigate such reflector properties in three datasets spanning the Mojave Desert. This investigation brings to light formative processes operating within the Earth's crust, which are at present poorly understood.

## Chapter 1

### 3-D Imaging of Steeply Dipping Structure Near the San Andreas Fault, Parkfield, California

#### ABSTRACT

Shot gathers from the Parkfield, California, deep crustal seismic reflection line, recorded in 1977 by COCORP, reveal coherent events having horizontal to inverse moveouts. These events are migrated using a multi-offset three dimensional Kirchhoff sum method. This method is a ray equation back projection inversion of the acoustic wavefield, which is valid under the Born, WKBJ, and far-field assumptions. Migrations of full wave acoustic synthetics, having the same limitations in geometric coverage as the COCORP survey, demonstrate the utility of the imaging process. The images resulting from back projection of the survey data suggest that the Gold Hill fault carries ultramafic rocks from the surface to 3 km depth at a dip greater than  $45^\circ$ , where it joins the San Andreas fault, which may cut through more homogeneous materials at shallow depths. To the southwest, a 2 km Tertiary sedimentary section appears to terminate against a near-vertical fault. The zone between this fault and the San Andreas may be floored at 3 km by flat-lying ultramafics. Lateral velocity inhomogeneities are not accounted for in the migration, but in this case do not seriously hinder the

reconstruction of reflectors.

## 1. INTRODUCTION

The conventional process of stacking seismic reflection data depends for its validity as an imaging process on a number of assumptions about the character of the subsurface. Principally, the velocity of the medium must vary only slowly in the lateral direction. Where this constraint does not apply, a stacked section may not be interpretable. Some other method must be used to examine the data in the multi-offset form of the physical seismic experiment.

This chapter presents an excellent example of a seismic reflection dataset, which cannot be fully interpreted using the stacking process and its underlying assumptions. It was recorded across a rather spectacular lateral heterogeneity—the San Andreas fault zone. It will be seen how the interpretations of this survey done previously could not image the strongest reflections in the dataset. Then a method will be described for imaging these events and the less restrictive assumptions that underlie it. Its effectiveness will be demonstrated through imaging of synthetic data. Finally, the imaging of the field dataset will provoke conclusions on the relationship of the geological and physical setting both of the area near the San Andreas and of seismic reflection targets in general.

In 1977 COCORP recorded 27 km of deep crustal reflection data on a route crossing the San Andreas fault in Monterey County, California, near the town of Parkfield. This section of the fault has long been of interest to seismologists because of the regular occurrence of moderate earthquakes on it.

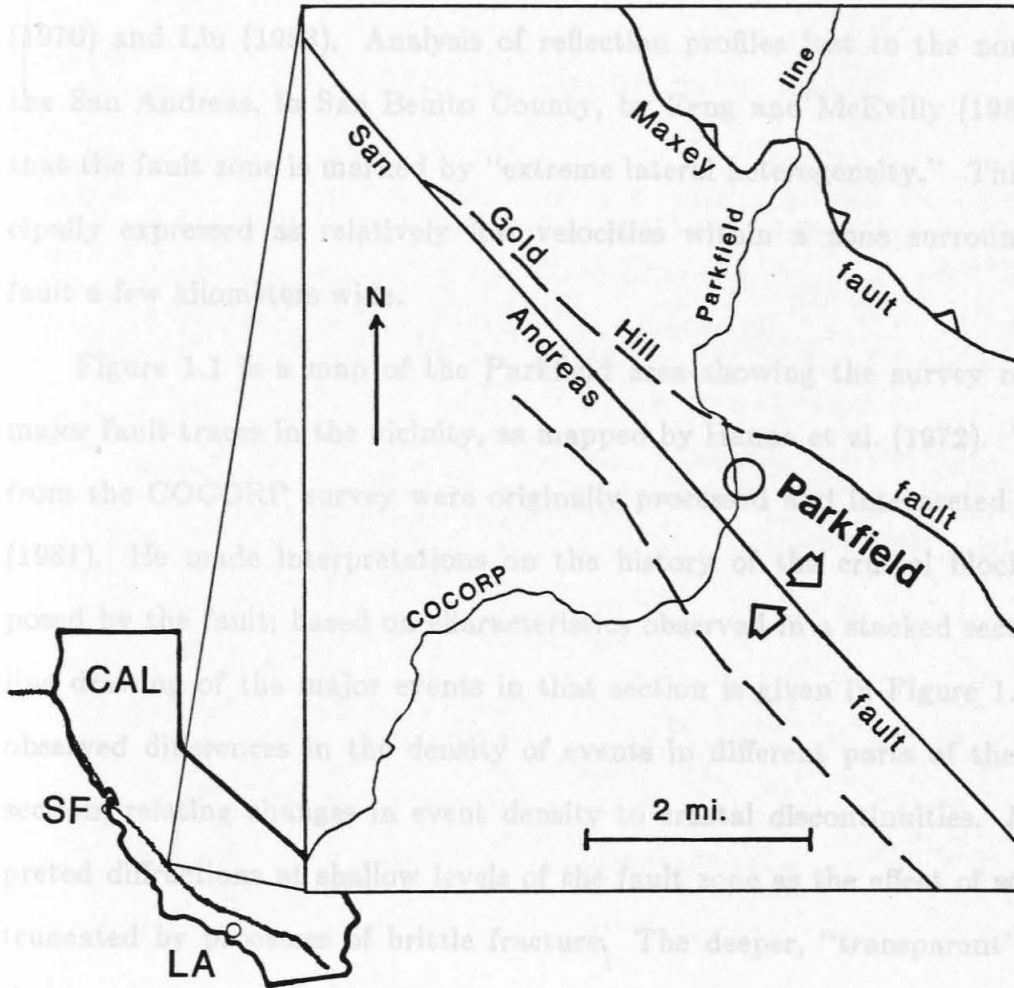


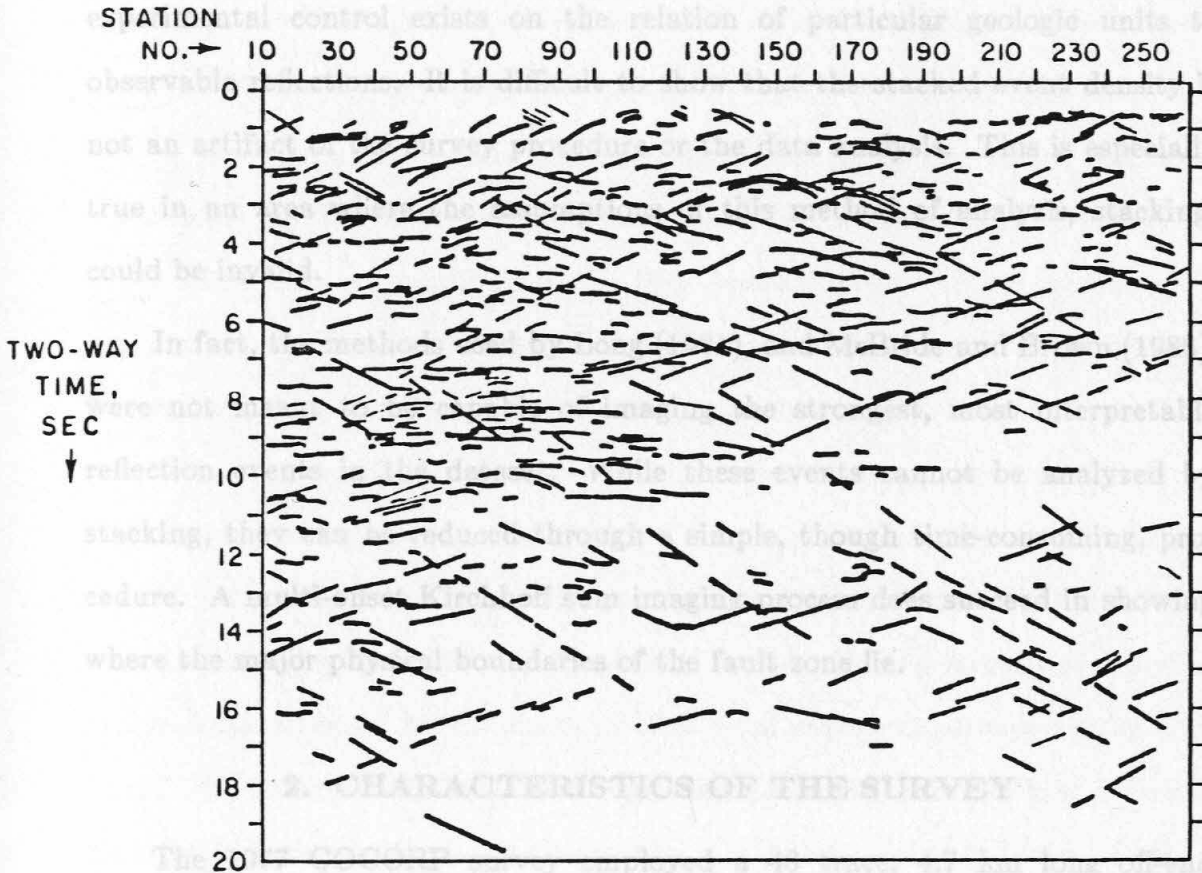
**Fig. 1.1:** Map of the vicinity of the town of Parkfield, showing the route of the COCORP survey, and fault traces taken from Hanna et al. (1972).

Evaluations of velocities and other seismic characteristics of the region have attended several studies of seismic activity, such as those by Eaton et al. (1970) and Liu (1983). Analysis of reflection profiles just to the north along the San Andreas, in San Benito County, by Feng and McEvelly (1983) shows that the fault zone is marked by "extreme lateral heterogeneity." This is principally expressed as relatively low velocities within a zone surrounding the fault a few kilometers wide.

Figure 1.1 is a map of the Parkfield area showing the survey route and major fault traces in the vicinity, as mapped by Hanna et al. (1972). The data from the COCORP survey were originally processed and interpreted by Long (1981). He made interpretations on the history of the crustal blocks juxtaposed by the fault, based on characteristics observed in a stacked section. His line drawing of the major events in that section is given in Figure 1.2. Long observed differences in the density of events in different parts of the stacked section, relating changes in event density to crustal discontinuities. He interpreted diffractions at shallow levels of the fault zone as the effect of structures truncated by processes of brittle fracture. The deeper, "transparent" part of the zone represents a region of ductile flow. Because of the poor quality of the stack, these conclusions could not be made firm.

A better approach was undertaken by McBride and Brown (1986). They present a complete reworking of the dataset facilitated by the, previously unavailable, detailed control of the data processing and reduction. Pre-correlation and pre-stack balancing, filtering, and editing contribute to an overall improvement in the stacked section. The density of stacked events was again used to make associations with regionally known crustal structures.

COCORP - PARKFIELD, CALIF.



From Long, 1981

**Fig. 1.2:** Line drawing by Long (1981) of a COCORP preliminary stack of the Parkfield survey. The station numbers increase from southwest to northeast, with the San Andreas fault near station 140.

This kind of interpretation is limited in that it is based on the validity of the stacking process, which, as Feng and McEvilly (1983) showed, is thoroughly violated in this region. Further, it attempts to assign geologic interpretations to a physical phenomenon, stacked event density, where little experimental control exists on the relation of particular geologic units to observable reflections. It is difficult to show that the stacked event density is not an artifact of the survey procedure or the data analysis. This is especially true in an area where the assumptions of this method of analysis, stacking, could be invalid.

In fact, the methods used by Long (1981), and McBride and Brown (1986), were not meant to be capable of imaging the strongest, most interpretable reflection events in the dataset. While these events cannot be analyzed by stacking, they can be reduced through a simple, though time-consuming, procedure. A multi-offset Kirchhoff sum imaging process does succeed in showing where the major physical boundaries of the fault zone lie.

## 2. CHARACTERISTICS OF THE SURVEY

The 1977 COCORP survey employed a 48 trace, 4.7 km long off-end receiver spread with a minimum offset of 0.45 km. The vibrators started at the southwest end of the line and pushed the spread to the northeast, shooting at 100 m intervals. The line is, however, sinuous over distances smaller than the length of the receiver spread, as shown by Figure 1.1. This sinuosity has the effect of spreading the midpoints of the recordings from different pairs of sources and receivers over a substantial area, as discussed by McBride and Brown (1986). In particular, the midpoints of receivers at shorter offsets are

close to the line, while the long offset midpoints are more distant, generally following a straighter path than the line. This kind of geometric discrepancy is damaging to the stacking process since short offset raypaths may pass through different near-surface heterogeneities than the long offset raypaths. It offers some advantages, however, for true three-dimensional analysis techniques, since the line sinuosity provides some three-dimensional coverage.

A large number of field records distributed along the entire line were examined. By far the strongest, most coherent events observable in the multi-offset data appeared near the San Andreas fault. These events show horizontal or reverse moveouts, in that their arrival times decrease with increasing offset, and have amplitudes comparable to the direct arrivals (Figure 1.3). They are found on all of the reasonably clean gathers near the fault. The timing and apparent velocity of the events change rapidly as the orientation of the survey line changes. These factors suggested that the events may have originated as sidewall reflections from steeply dipping structures. Similar events were observed by Robinson in 1945 from reflection surveys on the Gulf Coast. He interpreted them as horizontally propagating refractions reflected off lateral discontinuities in the refracting structures, probably faults. From a number of surveys in different orientations, he was able to locate the faults by relating the arrival time of the events to the propagation time along the refractor.

Some compensation for the sinuosity of the COCORP line can be made by sorting out common midpoint (CMP) gathers of the data. All traces whose midpoint fell within 230 m of a node of a two-dimensional grid of points with the same spacing were sorted into a gather for that node, regardless of the

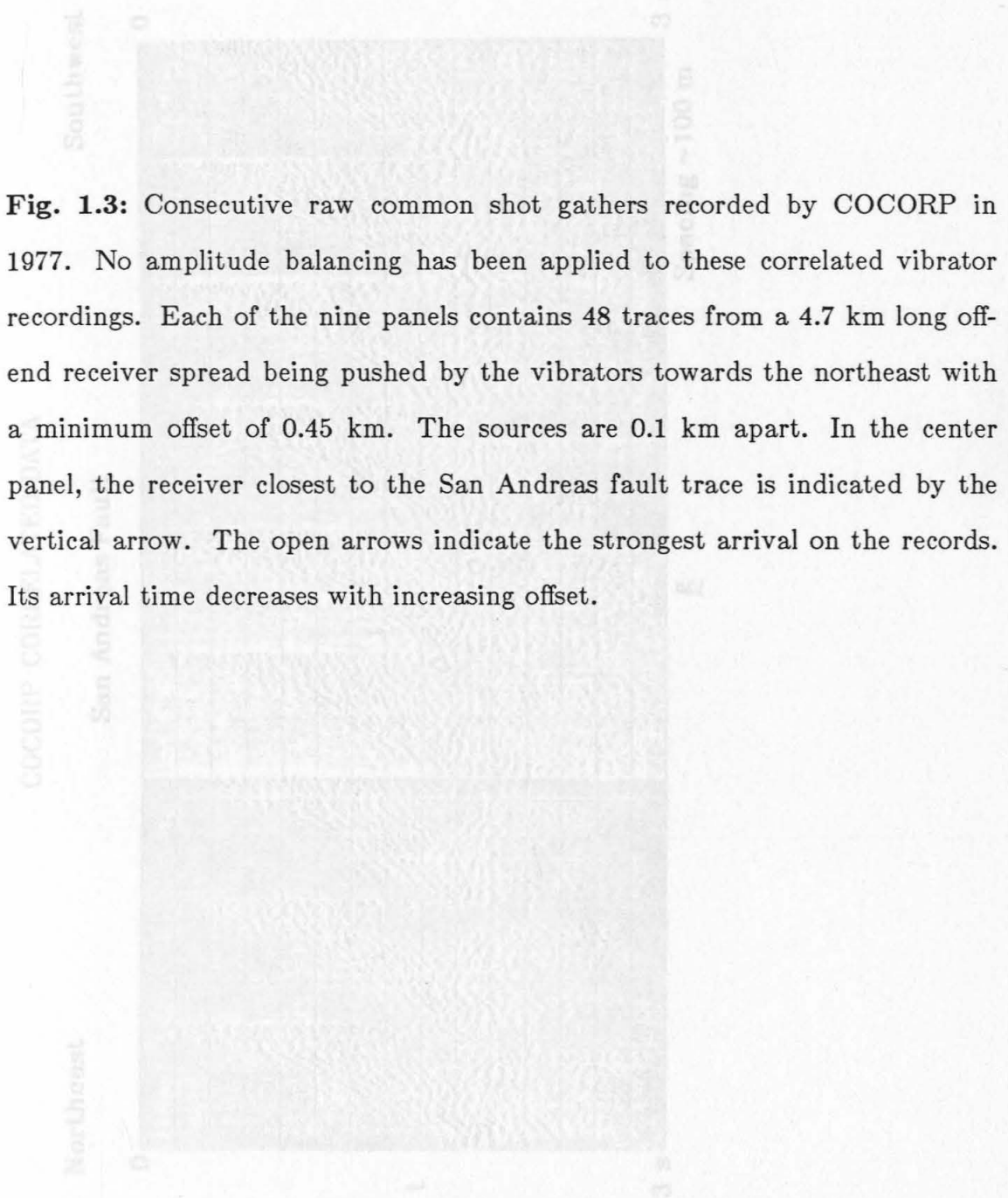


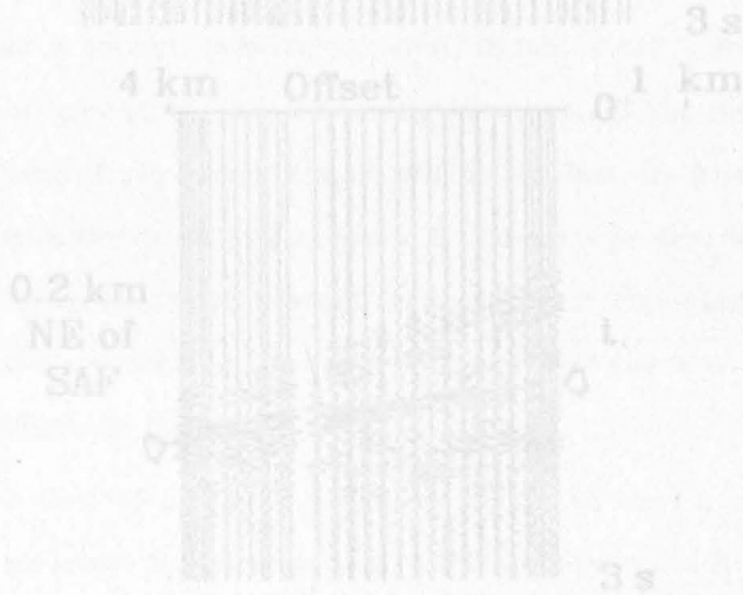
**Fig. 1.3:** Consecutive raw common shot gathers recorded by COCORP in 1977. No amplitude balancing has been applied to these correlated vibrator recordings. Each of the nine panels contains 48 traces from a 4.7 km long off-end receiver spread being pushed by the vibrators towards the northeast with a minimum offset of 0.45 km. The sources are 0.1 km apart. In the center panel, the receiver closest to the San Andreas fault trace is indicated by the vertical arrow. The open arrows indicate the strongest arrival on the records. Its arrival time decreases with increasing offset.



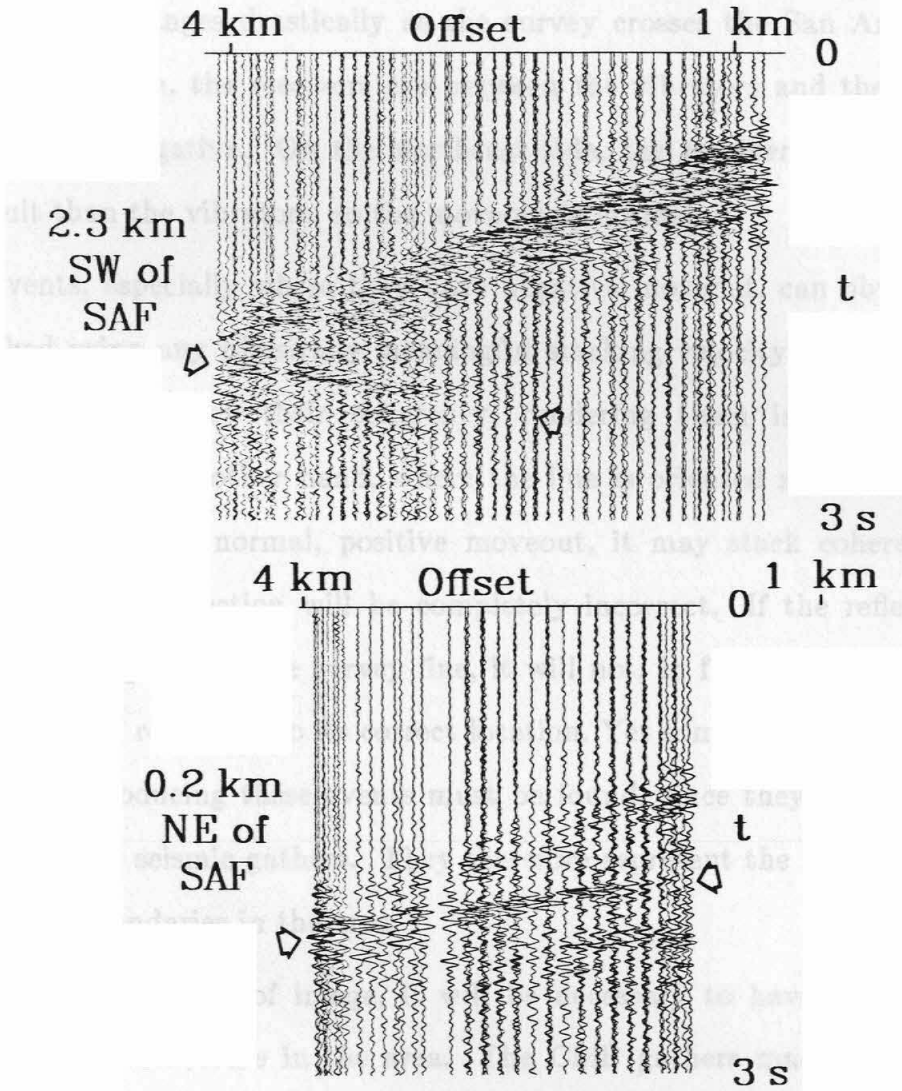
COCORP - 12 - CORRELATED DATA  
Common-Midpoint Gathers  
True Amplitude

4 km Offset 1 km

**Fig. 1.4:** Two common midpoint gathers of unequalized traces assembled within two-dimensional bins 460 m wide at different locations near the San Andreas. The open arrows indicate the positions of a strong reflection from the steeply dipping fault zone. The timing and apparent velocity of the sidewall reflection change as the geometric relationship of the shots and receivers relative to the fault changes.



COCORP CORRELATED DATA  
Common-Midpoint Gathers  
True Amplitude

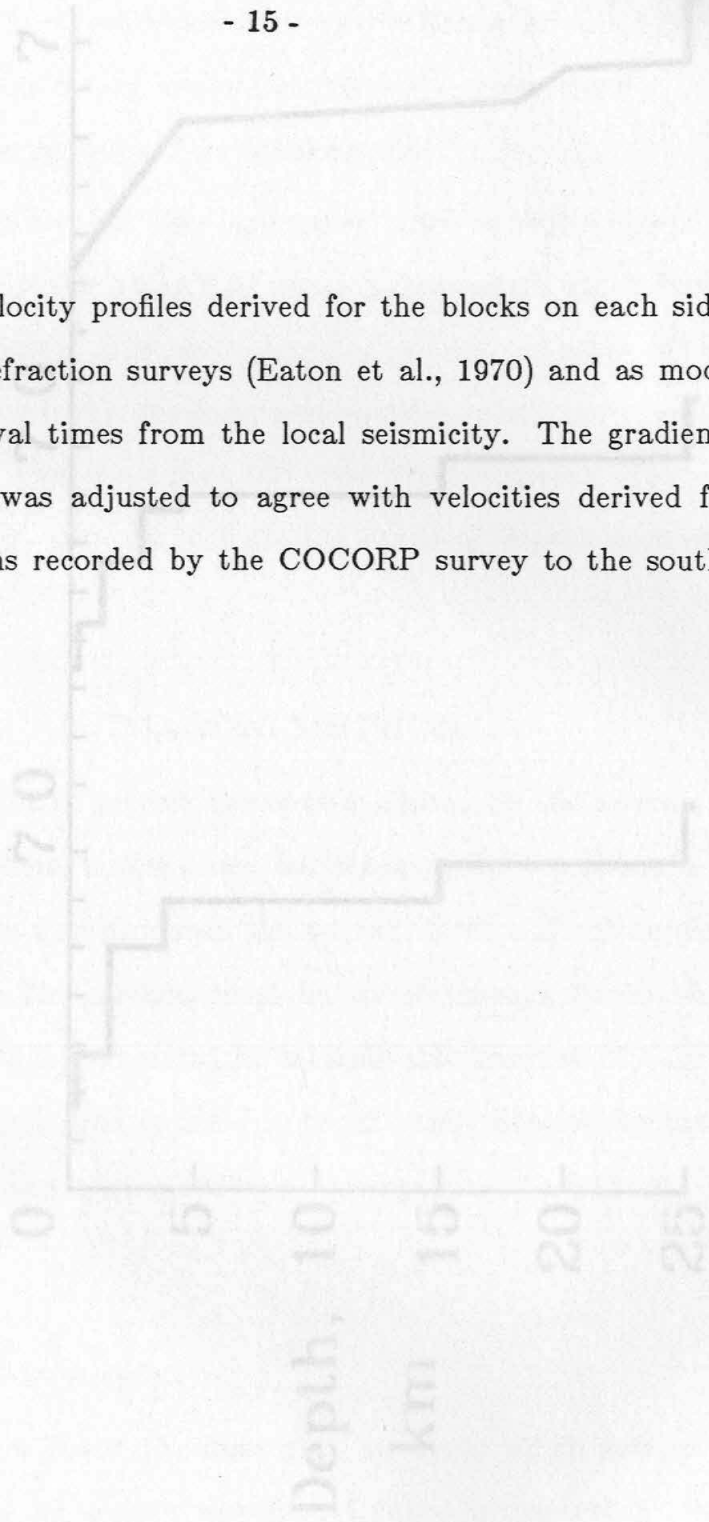


orientation of the shot-receiver pair. Two of these gathers are shown in Figure 1.4. The unusual arrivals at about 2 seconds at the farther offsets can be found on many gathers. As the figure shows, the apparent velocity of the sidewall reflection changes drastically as the survey crosses the San Andreas. On the southwest side, the receivers are between the vibrators and the fault, so the moveout is negative. On the northeast side, the receivers are farther from the fault than the vibrators, so the moveout is normal.

Such events, especially where they have negative moveout, can obviously not be stacked using any physically meaningful stacking velocity. The stacking process would destroy their coherency, rendering them invisible in a stacked section. On the other hand, where the line is oriented such that the sidewall reflection has a normal, positive moveout, it may stack coherently, but its location in the section will be completely incorrect. If the reflection point is not in the plane of the survey line, it will not, in fact, be possible to migrate the stacked reflection to its correct location. Yet some process of imaging the reflector producing these events must be found, since they carry most of the energy in the seismic gathers. They therefore represent the most fundamental physical boundaries in the area.

In obtaining this kind of image, it will be necessary to have a starting idea of the velocity structure in the area. The CMP gathers made from the southwest part of the line did show coherent reflections from near-horizontal structures in the upper 3 km of the crust. Interval velocities calculated from velocity semblances of these gathers indicated a strong velocity gradient in this area similar to that found by Liu (1983) from seismicity analysis. The gradient is shown in Figure 1.5, which also incorporates deeper velocity

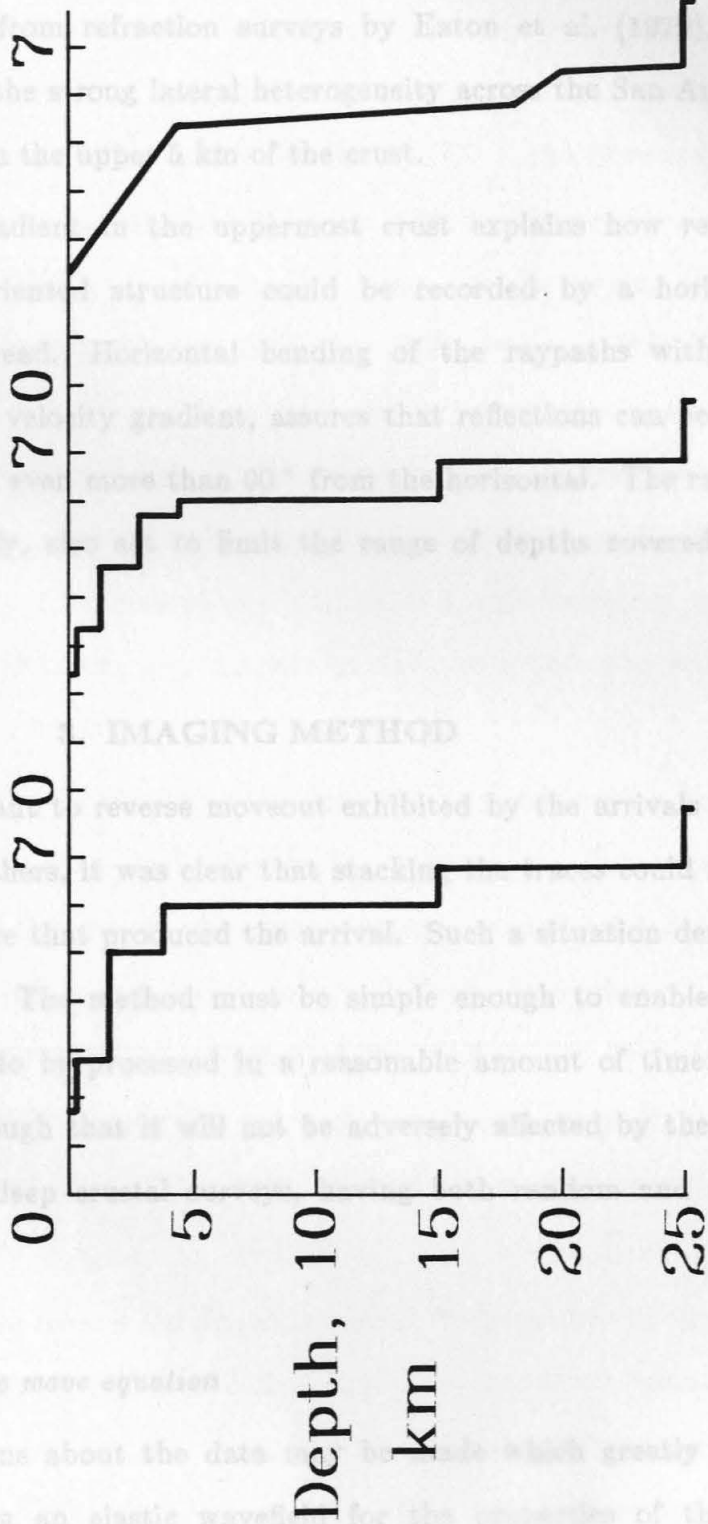
**Fig. 1.5:** Crustal velocity profiles derived for the blocks on each side of the San Andreas from refraction surveys (Eaton et al., 1970) and as modified by Liu (1983) with arrival times from the local seismicity. The gradient at the top of Liu's profile was adjusted to agree with velocities derived from the moveout of reflections recorded by the COCORP survey to the southwest of the San Andreas.



# VELOCITY PROFILES

P Velocity, km / s

SW of SAF NE of SAF This Study



from Eaton (1970) from Liu (1983)

## Approximations to the wave equation

Some assumptions about the data are made which greatly simplify the task of inverting an elastic wavelet for the properties of the Earth through which it has propagated. Le Bras (1983) develops representations of

information derived from refraction surveys by Eaton et al. (1970). These profiles suggest that the strong lateral heterogeneity across the San Andreas is limited to velocities in the upper 5 km of the crust.

The velocity gradient in the uppermost crust explains how reflections from a vertically oriented structure could be recorded by a horizontally oriented receiver spread. Horizontal bending of the raypaths with depth, within such a strong velocity gradient, assures that reflections can be located on structures dipping even more than  $90^\circ$  from the horizontal. The ray bending will, unfortunately, also act to limit the range of depths covered by the recorded reflections.

### 3. IMAGING METHOD

Given the constant to reverse moveout exhibited by the arrivals in question on the CMP gathers, it was clear that stacking the traces could not help to image the structure that produced the arrival. Such a situation demands a pre-stack migration. The method must be simple enough to enable tens of thousands of traces to be processed in a reasonable amount of time. Yet it should be robust enough that it will not be adversely affected by the copious noise seen on such deep crustal surveys, having both random and coherent character.

Since the purpose here is simply to establish the geometry of the scatterer, the amplitude corrections become due to

*Approximations to the wave equation*

Some assumptions about the data may be made which greatly simplify the task of inverting an elastic wavefield for the properties of the Earth through which it has propagated. Le Bras (1985) developed representations of

the acoustic and the elastic wave equations, based on several assumptions which reduced the inversion of reflection data to a process very similar to the Kirchhoff sum migration of Jain and Wren (1980). First, the Born approximation considers the scattered wavefield to result from small, rapid variations in material properties, which are superposed on larger, slowly varying properties, which affect only the propagation of the wave. This approximation allows the effect of scattering at varying incidence angle to be linearized as presented by Wu and Aki (1985). Second, the WKBJ approximation, which assumes that the medium parameters vary slowly along the propagation path, allows the propagation through the medium to be regarded as a high-frequency ray. This is also dependent on the third approximation, that the source and receiver are in the far field relative to the reflector.

With these three approximations the data can be considered to be a linear superposition of rays from individual point scatterers. The tomographic approximation of the inverse of this superposition, as discussed by Le Bras (1985), is simply the superposition of rays from individually recorded reflections. Thus, the scattering potential of the medium can be estimated as the sum of the reflections recorded by each source-receiver pair, positioned according to the travel time of the rays between the surface points and the subsurface reflector.

Since the purpose here is simply to establish the geometry of the scatterers within the medium, I will ignore the amplitude correction factors due to the angle of incidence on the scatterer, and to the length of the travel path. Further, the scatterer will be represented by the sum of reflection wavelets without cross correlation with the source wavelet, since a source wavelet is not

# GEOMETRY

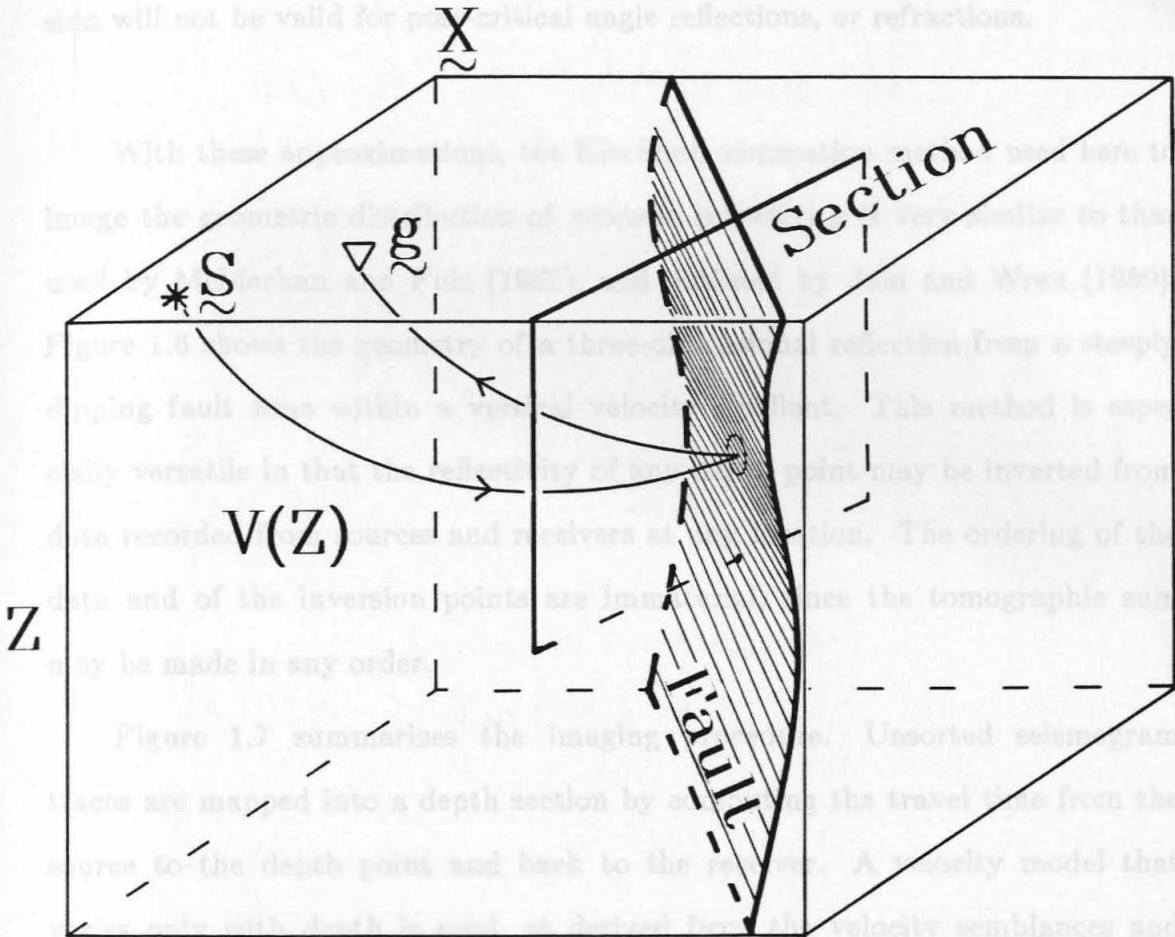


**Fig. 1.6:** Geometry of a sidewall reflection from a fault zone within a medium showing an increase in velocity with depth  $Z$ .  $S$  and  $g$  are the source and receiver positions, respectively.

available. Certain restrictions will apply. The data put into the inversion should contain only primary P-to-P wave reflections. In addition, the inversion will not be valid for post-critical angle reflections, or refractions.

With these approximations, the Kirchhoff summation method used here to image the geometric distribution of acoustic reflectivity is very similar to that used by McMechan and Fuis (1987), and outlined by Jain and Wren (1980). Figure 1.6 shows the geometry of a three-dimensional reflection from a steeply dipping fault zone within a vertical velocity gradient. This method is especially versatile in that the reflectivity of any depth point may be inverted from data recorded from sources and receivers at any location. The ordering of the data and of the inversion points are immaterial, since the tomographic sum may be made in any order.

Figure 1.7 summarizes the imaging procedure. Unsorted seismogram traces are mapped into a depth section by computing the travel time from the source to the depth point and back to the receiver. A velocity model that varies only with depth is used, as derived from the velocity semblances and the model of Liu (1983; Figure 1.5). The travel time calculation included turning rays, which allows the imaging of structures with greater than  $90^\circ$  dips. To allow for propagation through a laterally heterogeneous medium, the travel time calculation could take the form of raytracing through a variable velocity medium. If, however, the bulk of the travel path can be constrained to a part of the medium in which velocity varies principally with depth, then a simple raytracing through a vertically varying medium can be used for data with any orientation of the source-receiver offset. This allows the travel times to be

### KIRCHHOFF-SUM ALGORITHM

$$R(\underline{X}, Z) \leftarrow \sum_{\substack{\underline{S} \\ \underline{g} \\ \underline{X} \\ Z}} \text{Data}(t(\underline{S}, \underline{g}, \underline{X}, Z))$$

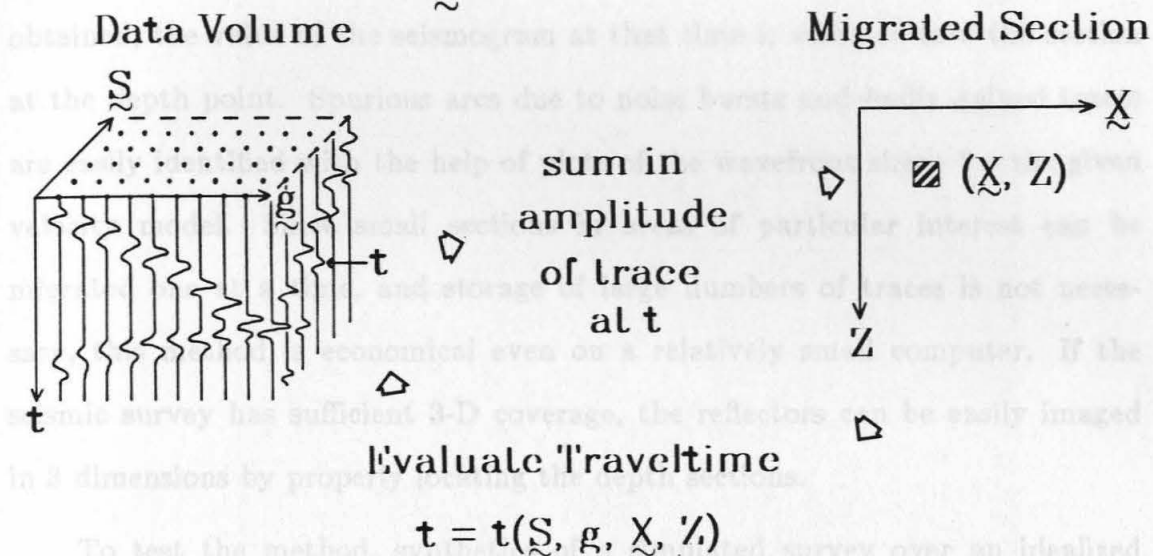


**Fig. 1.7:** Schematic representation of of a Kirchhoff sum algorithm used to form a migrated image of multi-offset reflection data. For each recorded source-receiver pair  $(\underline{S}, \underline{g})$ , over each point  $(\underline{X}, Z)$  in some depth section, a travel time is calculated. The amplitude of the recorded trace at that time is then summed into the point of the depth section.

Synthetics were calculated with shot and receiver spacings meant to simulate the Parkfield survey, but with poorer coverage. The synthetic gathers, given in Figure 1.9, show strong reflections from both sides of the near-vertical fault zone, which are quite similar to the arrivals in the Parkfield data. The travel times calculated

calculated only once, for the range of offset and depth of the experiment, greatly speeding the imaging process. For this reason the migrations performed here will employ mainly sources and receivers on just one side of a major lateral discontinuity such as the San Andreas.

Once the travel time down to and up from the depth point has been obtained, the value of the seismogram at that time is summed into the section at the depth point. Spurious arcs due to noise bursts and badly gained traces are easily identified with the help of plots of the wavefront shape for the given velocity model. Since small sections in areas of particular interest can be migrated one at a time, and storage of large numbers of traces is not necessary, this method is economical even on a relatively small computer. If the seismic survey has sufficient 3-D coverage, the reflectors can be easily imaged in 3 dimensions by properly locating the depth sections.

To test the method, synthetics of a simulated survey over an idealized model of a steeply dipping fault zone were calculated. A finite difference solution of the two-dimensional acoustic wave equation was used. This solution included all acoustic multiples, post-critical reflections, and refractions. The velocity model was identical to the one identified in Figure 1.5, except that a 2 km-wide fault zone having a 20% lower velocity at a given depth, and a sinusoidal profile in cross section, was introduced to test the ability of the method to resolve vertically complex fault geometries (Figure 1.8). Synthetics were calculated with shot and receiver spacings meant to simulate the Parkfield survey, but with poorer coverage. The synthetic gathers, given in Figure 1.9, show strong reflections from both sides of the near-vertical fault zone, which are quite similar to the arrivals in the Parkfield data. The travel times calculated

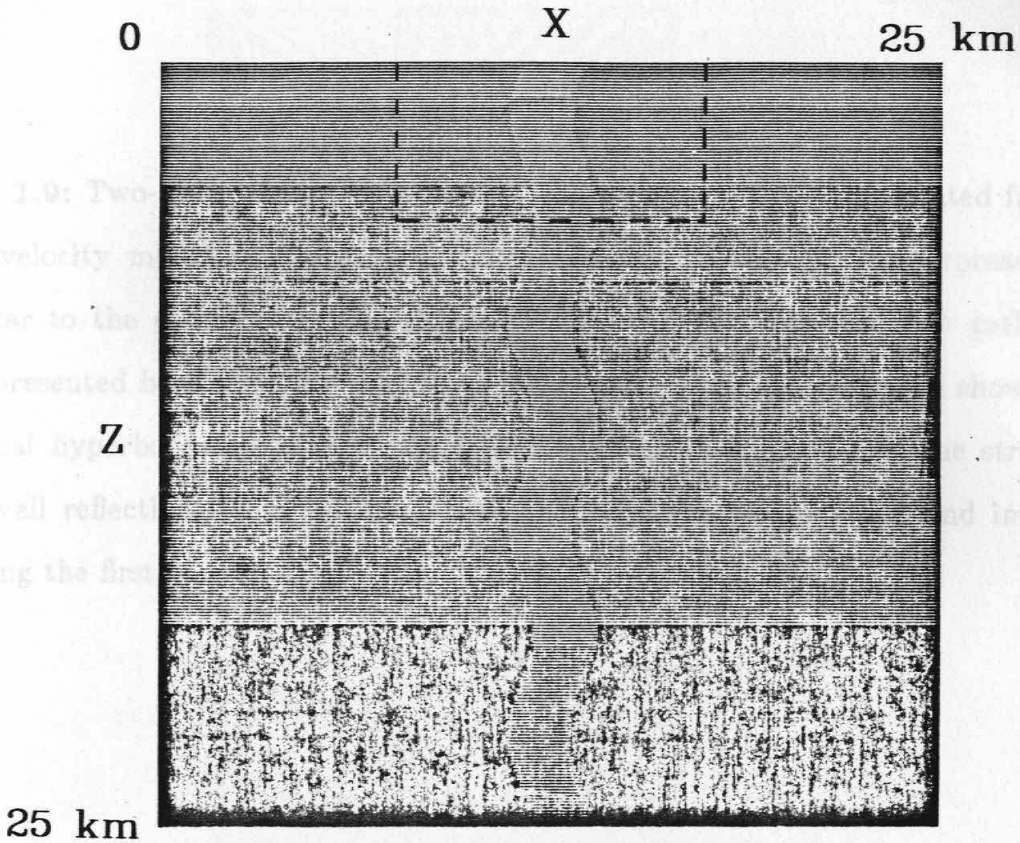
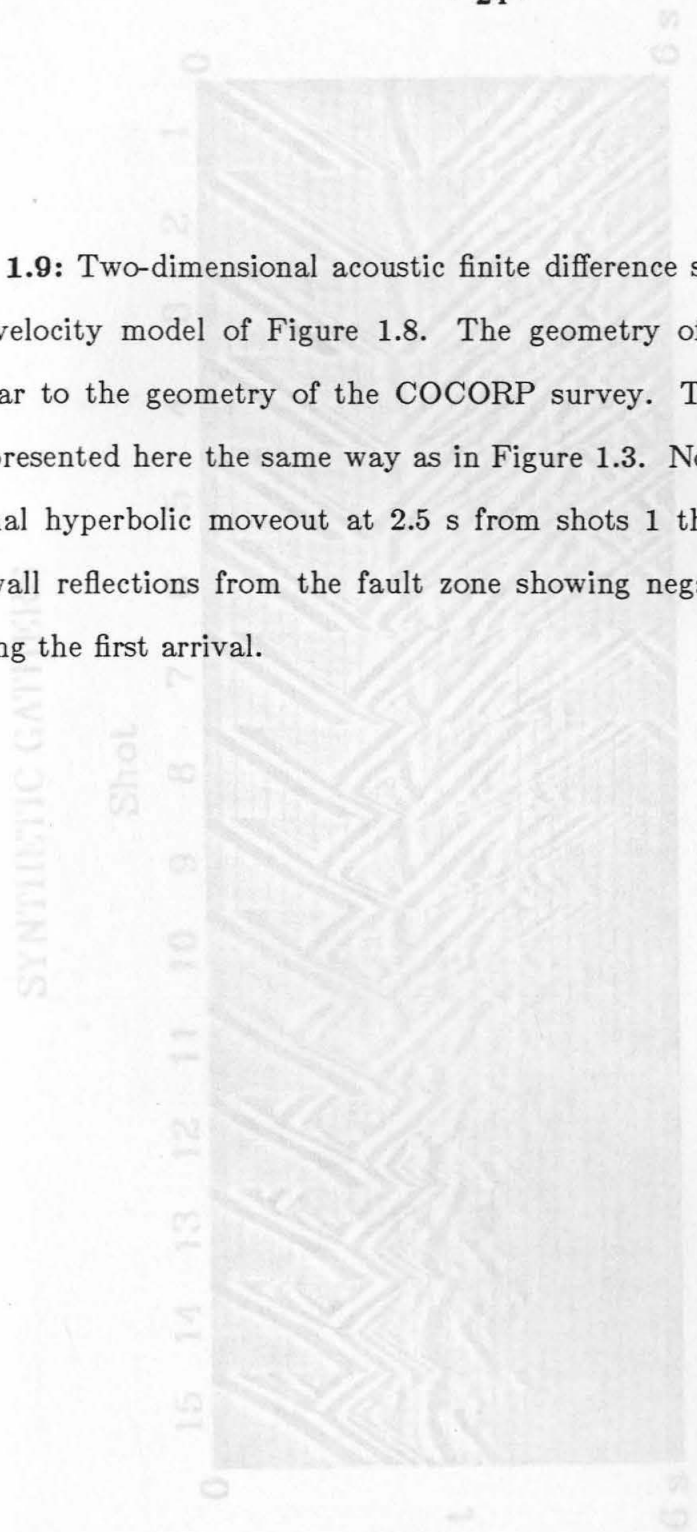
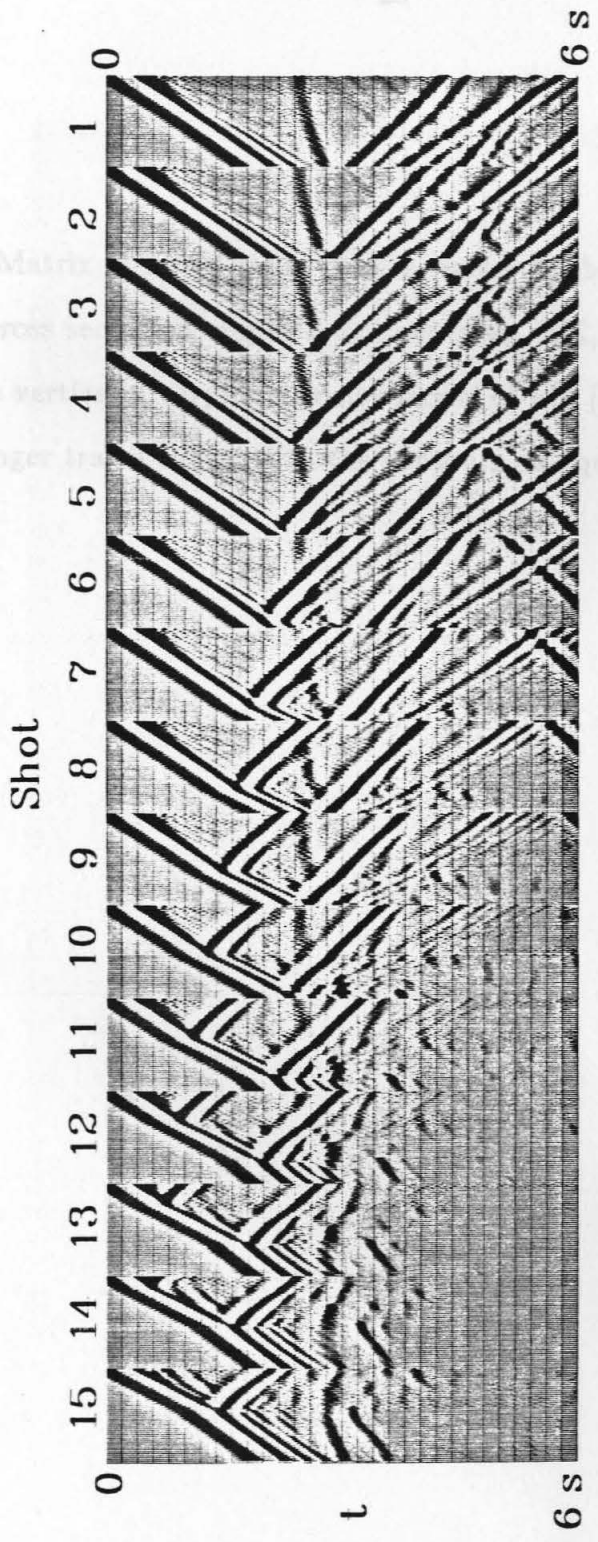


**Fig. 1.8:** Two-dimensional velocity model representing a cross section 25 km wide by 25 km deep across a fault zone having a sinuous profile. The zone, 2 km wide, has a velocity 20% lower than the adjacent regions. Outside the fault zone the model is that of Liu (1983; Figure 1.5), which varies only with depth. The dashed box is region imaged in Figures 1.11 and 1.12.

**Fig. 1.9:** Two-dimensional acoustic finite difference synthetics generated from the velocity model of Figure 1.8. The geometry of the synthetic spread is similar to the geometry of the COCORP survey. The common shot gathers are presented here the same way as in Figure 1.3. Note the reflection showing normal hyperbolic moveout at 2.5 s from shots 1 through 5, and the strong sidewall reflections from the fault zone showing negative moveout and intersecting the first arrival.

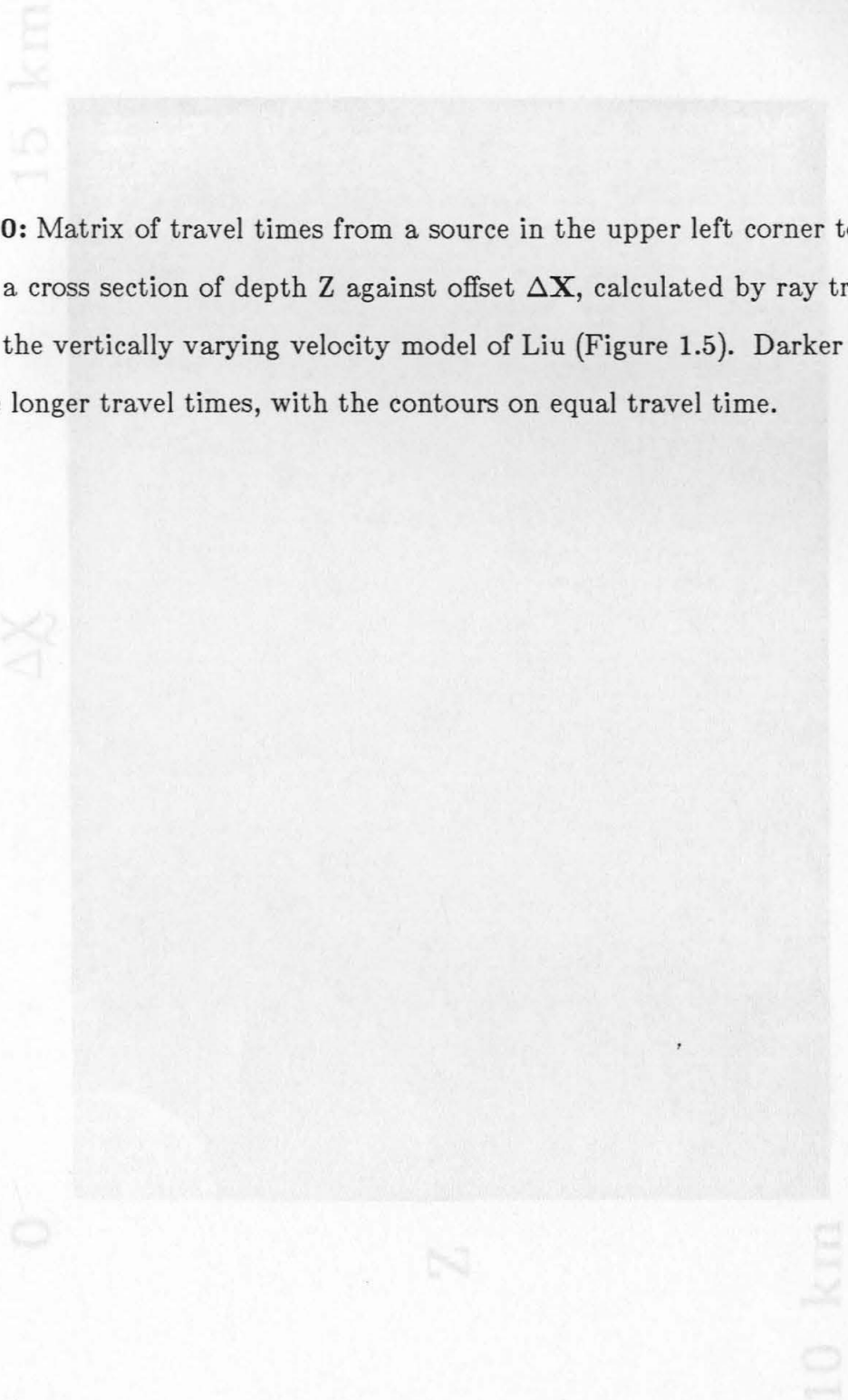


# SYNTHETIC GATHERS



23

**Fig. 1.10:** Matrix of travel times from a source in the upper left corner to any point in a cross section of depth  $Z$  against offset  $\Delta X$ , calculated by ray tracing through the vertically varying velocity model of Liu (Figure 1.5). Darker areas have the longer travel times, with the contours on equal travel time.

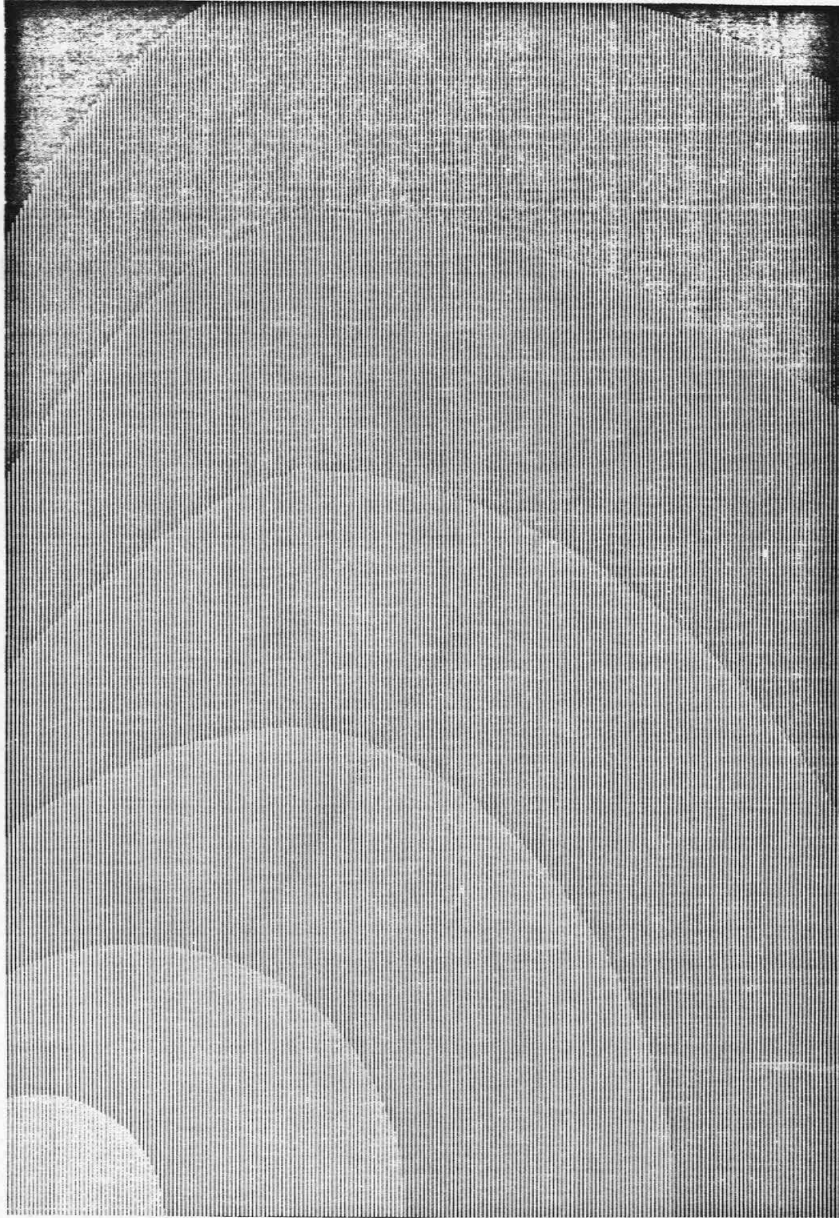


# TRAVELTIME MATRIX

15 km

$\Delta X_2$

0



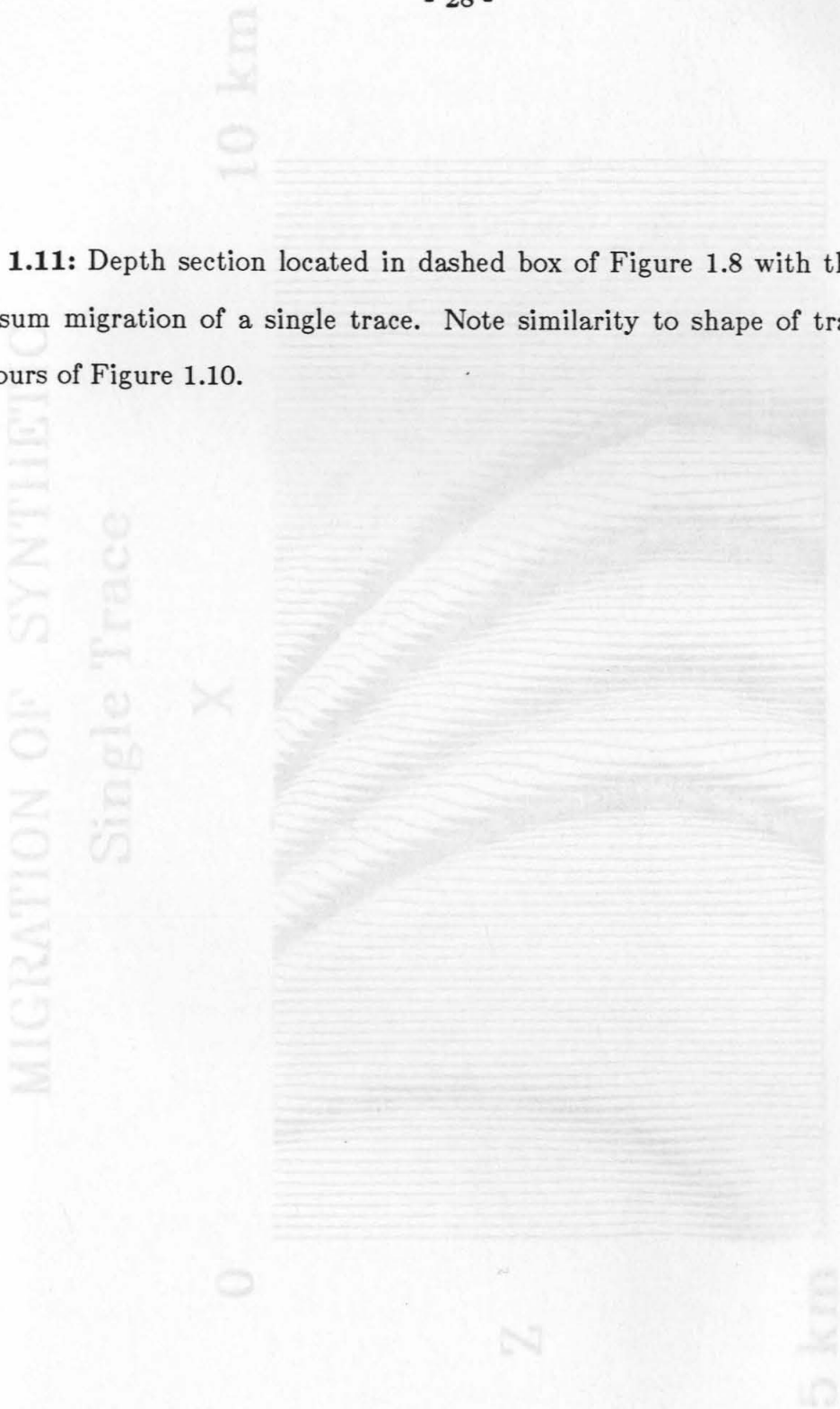
Z

10 km

Fig. 1.11: D  
hoff sum m  
contours of P

Kirch-  
of time

**Fig. 1.11:** Depth section located in dashed box of Figure 1.8 with the Kirchhoff sum migration of a single trace. Note similarity to shape of travel time contours of Figure 1.10.



# MIGRATION OF SYNTHETIC Single Trace

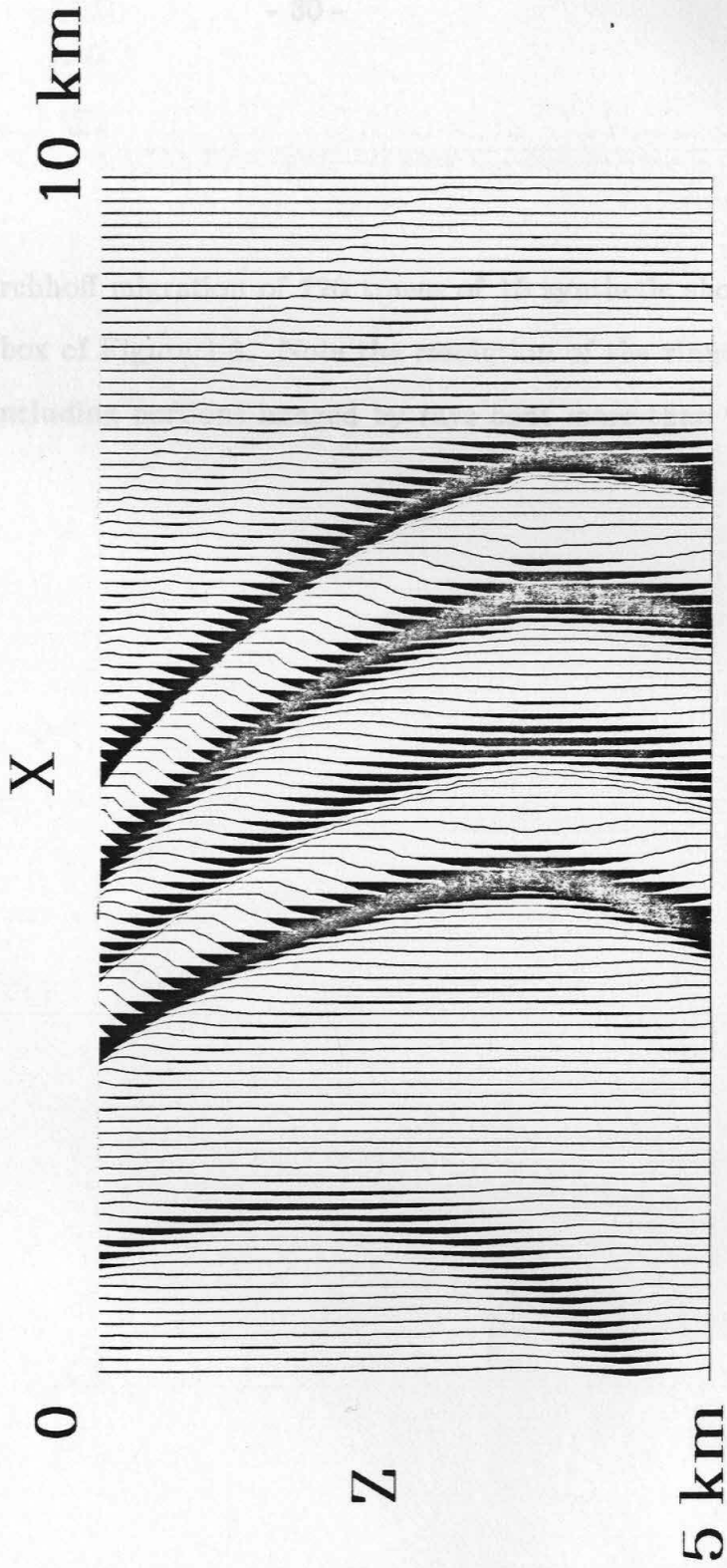
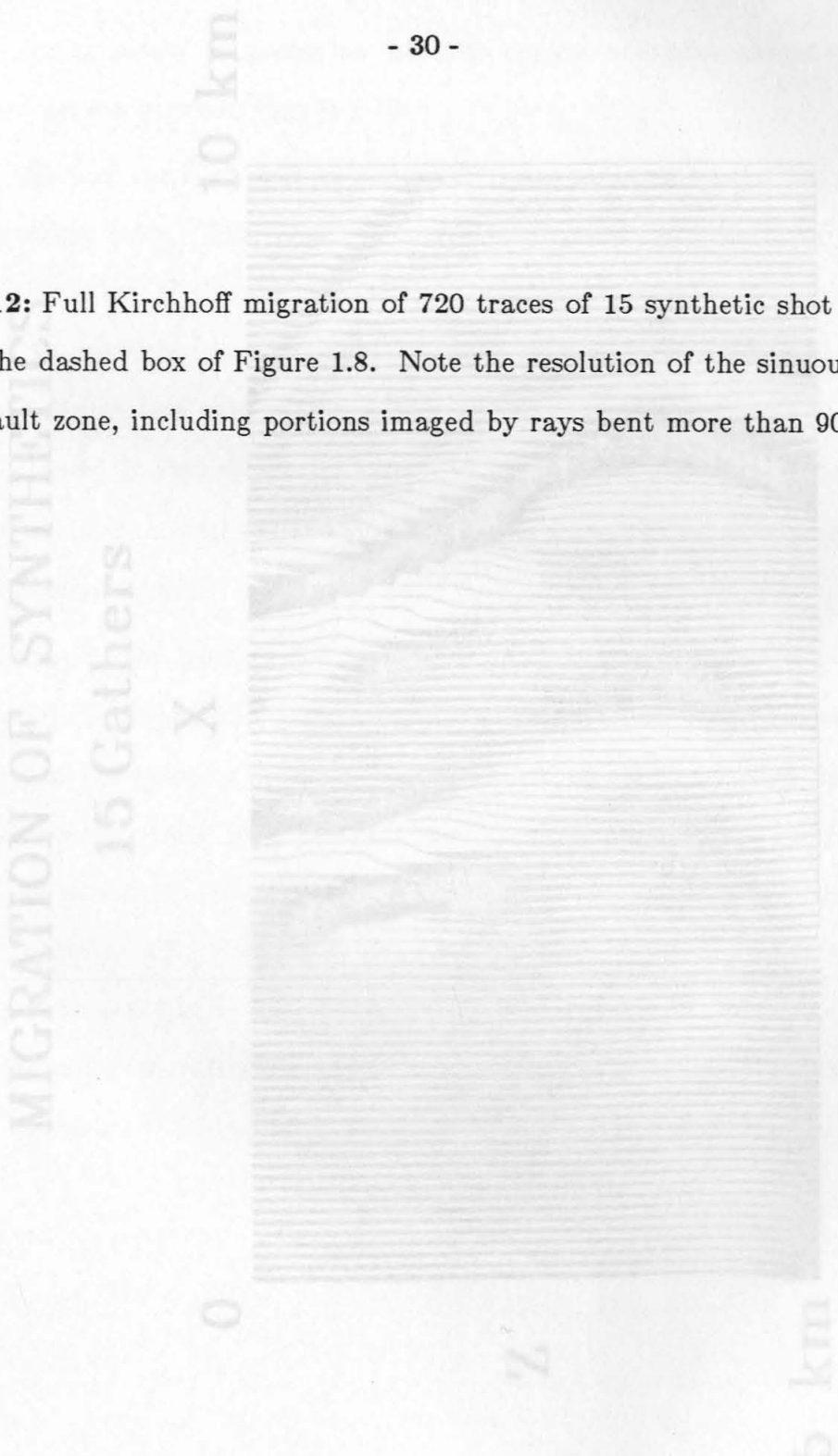
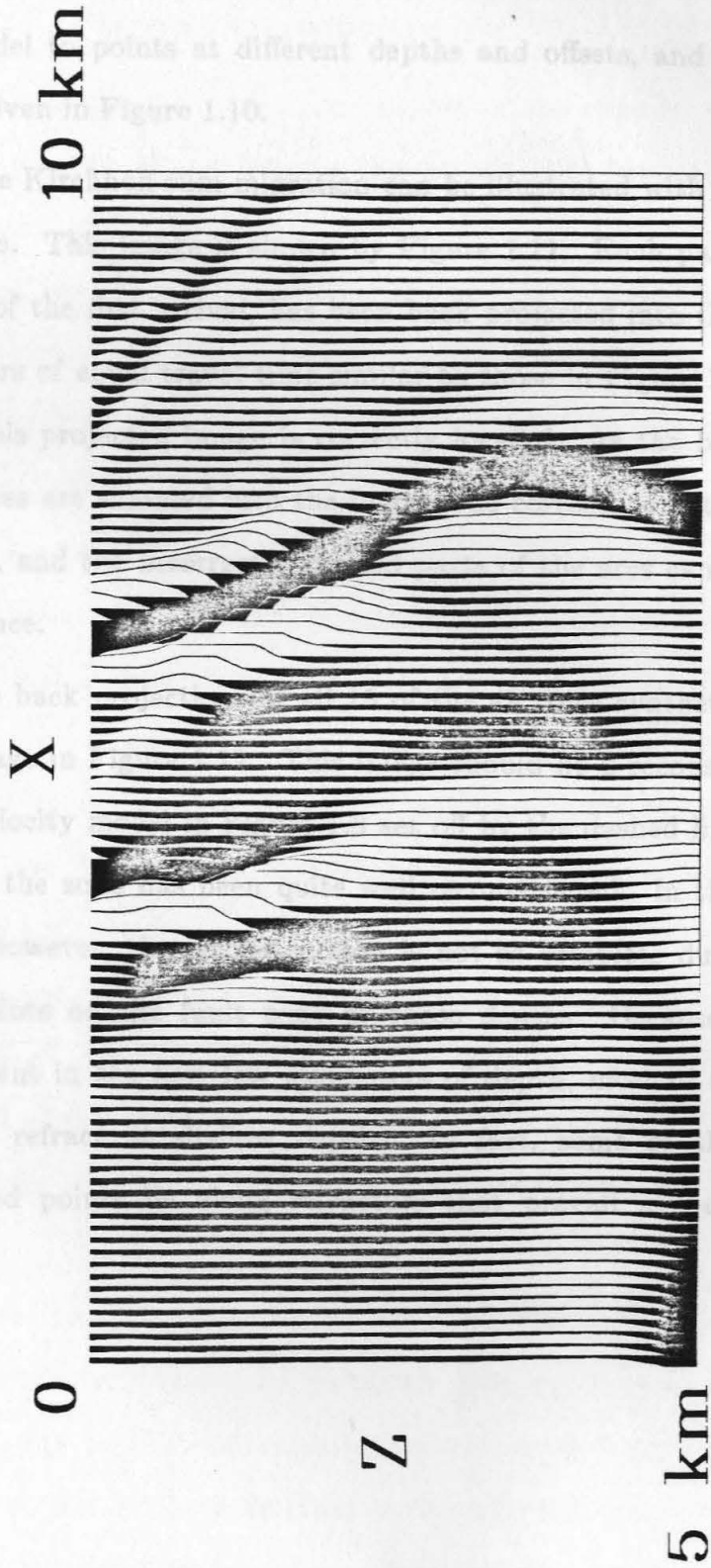


**Fig. 1.12:** Full Kirchhoff migration of 720 traces of 15 synthetic shot gathers within the dashed box of Figure 1.8. Note the resolution of the sinuous shape of the fault zone, including portions imaged by rays bent more than 90° from vertical.



# MIGRATION OF SYNTHETICS

15 Gathers



for the velocity model to points at different depths and offsets, and used for the inversions, are given in Figure 1.10.

The effect of the Kirchhoff sum migration can be illustrated with a migration of a single trace. This image is shown by Figure 1.11. Each part of the trace, after muting of the first arrival, has been back projected into the depth section along contours of equal travel time similar to those in Figure 1.10. At least one point of this projected image is correctly located. As the back projections of more traces are summed into the image, the correctly located point should be reinforced, and the incorrectly located parts of the arcs canceled by destructive interference.

Summing in the back projections of all 15 of the 48 trace synthetic gathers produced the image in Figure 1.12. This image should be a reconstruction of the part of the velocity model in Figure 1.8 set off by the dashed line. The sinuous geometry of the zone has been quite well reconstructed. In the lower third of the image, however, the reconstruction is not as complete due to the lack of reflection points on the fault zone at those depths. Because of the strong velocity gradient in the first few kilometers of depth, most of the rays turn horizontally or refract at shallow depths. In fact, some of the most strongly reconstructed points lie along refractors that prevail at particular depths.

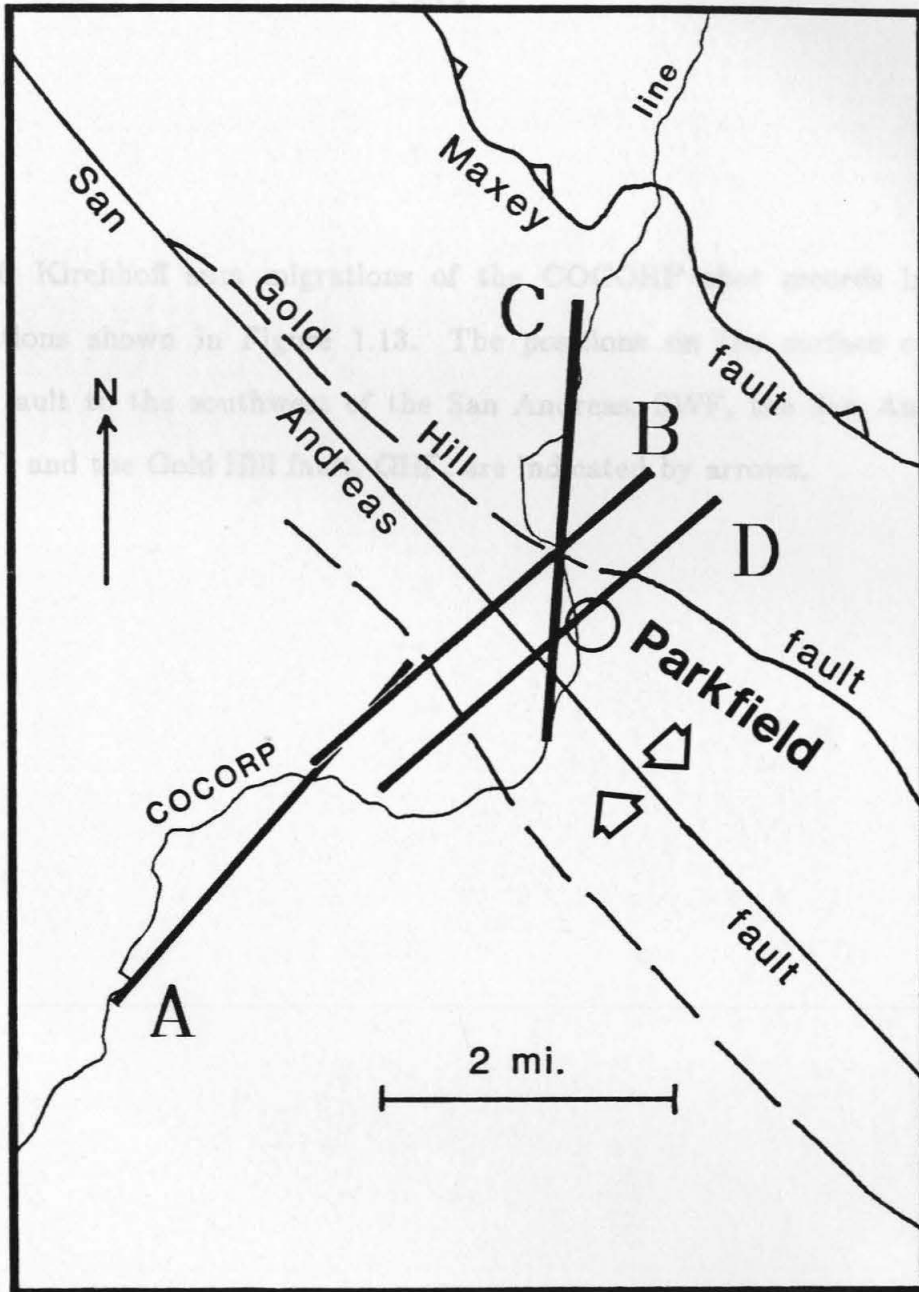
The back projected depth sections are shown in Figure 1.14. Many parts of these images are artifacts. Where the geometric coverage is poor, because of the layout of the line or the concentration of raypaths along refracting structures, the arching tails of the individual back-projected events may not be canceled. It is most useful to look for strong images that are at least

#### 4. MIGRATION RESULTS

Despite all the approximations, the poor quality of the records, and large uncertainties in the velocity model, images can be obtained from the actual COCORP survey data. The reflections to be back projected are clear, high-amplitude events that are most prominent on the records in Figures 1.3 and 1.4. Because of the high signal-to-noise ratio, there can be fair confidence in this case that the migrated images will not be dominated by the effects of spurious high-amplitude noise.

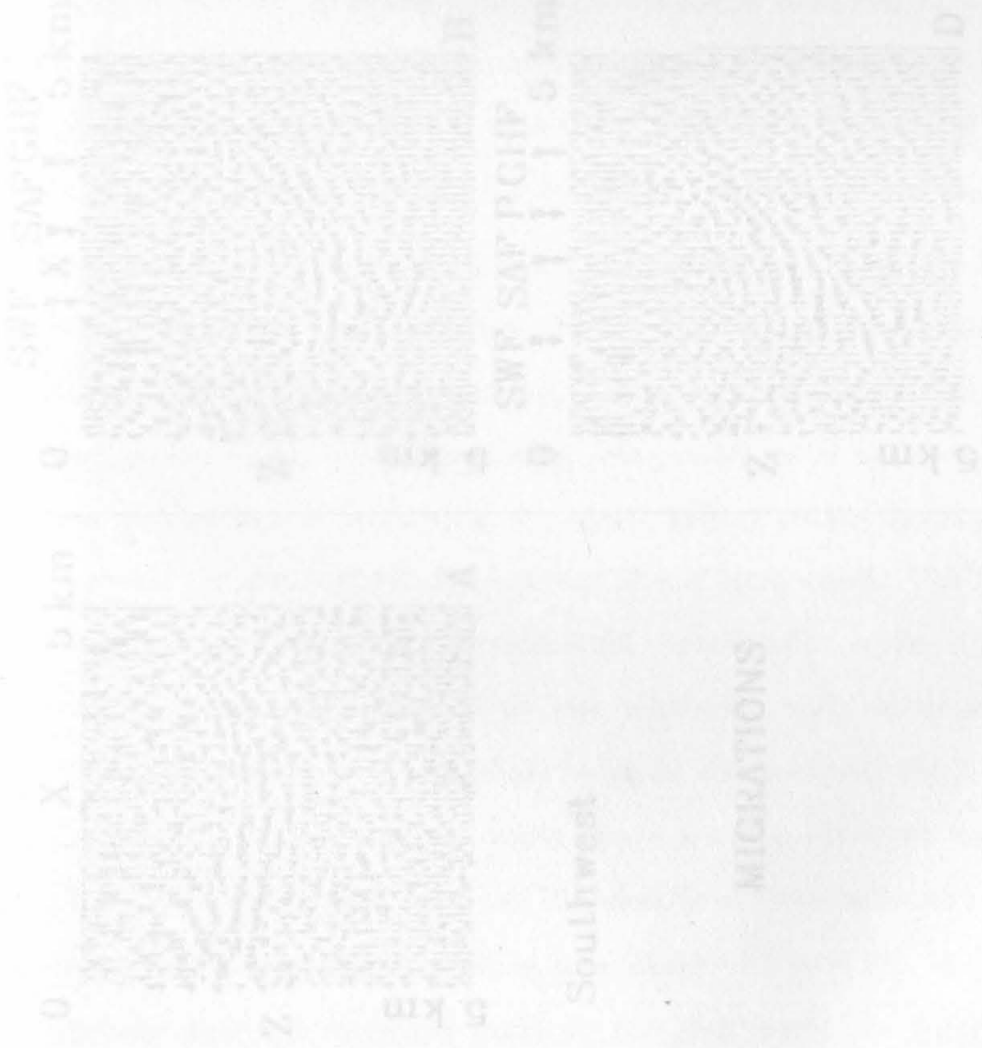
The reflection data are back projected into four depth sections, shown on Figure 1.13. The sections were located where there are heavier concentrations of midpoints, with B and D made parallel to test three-dimensional aspects of the image. All back projections were made using travel times calculated from the velocity profile in Figure 1.5, which is most appropriate for the region to the southwest of the San Andreas. In migrating all of the sections, except for C, only traces having both sources and receivers to the southwest of the Gold Hill fault were used. Section B was migrated both from traces having the first arrivals muted and from traces without any mutes. The two sections showed little difference, so all of the migrations were run on unmuted data. Ignoring the nearest offset traces, as done by McBride and Brown (1986), did improve the imaging.

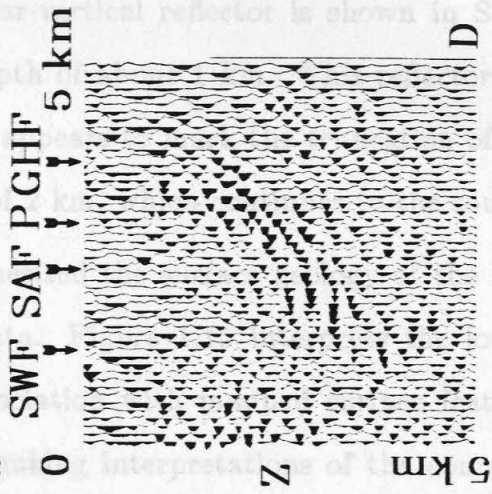
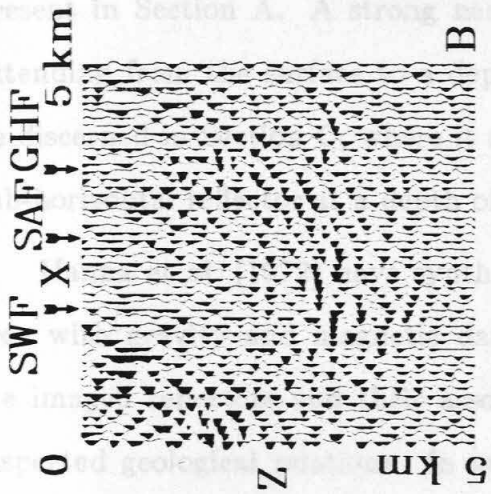
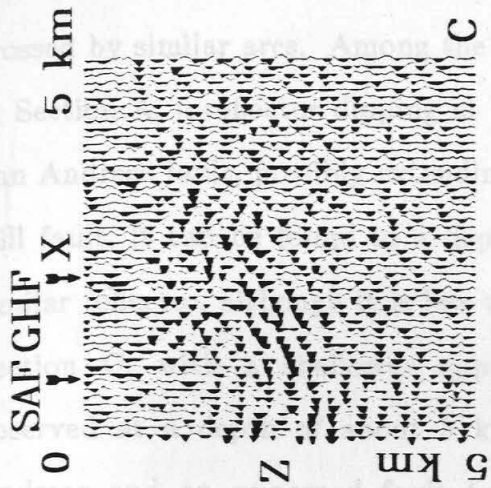
The back projected depth sections are shown in Figure 1.14. Many parts of these images are artifacts. Where the geometric coverage is poor, because of the layout of the line or the concentration of raypaths along refracting structures, the arching tails of the individual back-projected events may not be canceled. It is most useful to look for strong images that are at least



**Fig. 1.13:** Map of the vicinity of Parkfield showing the locations of the four depth sections migrated from the COCORP shot records. Each section is 5 km long by 5 km deep.

**Fig. 1.14:** Kirchhoff sum migrations of the COCORP shot records in the depth sections shown in Figure 1.13. The positions on the surface of the unnamed fault to the southwest of the San Andreas, SWF, the San Andreas fault, SAF, and the Gold Hill fault, GHF, are indicated by arrows.

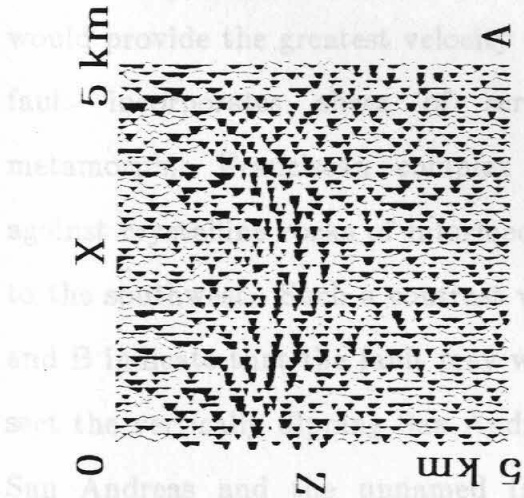




Northeast

Southwest

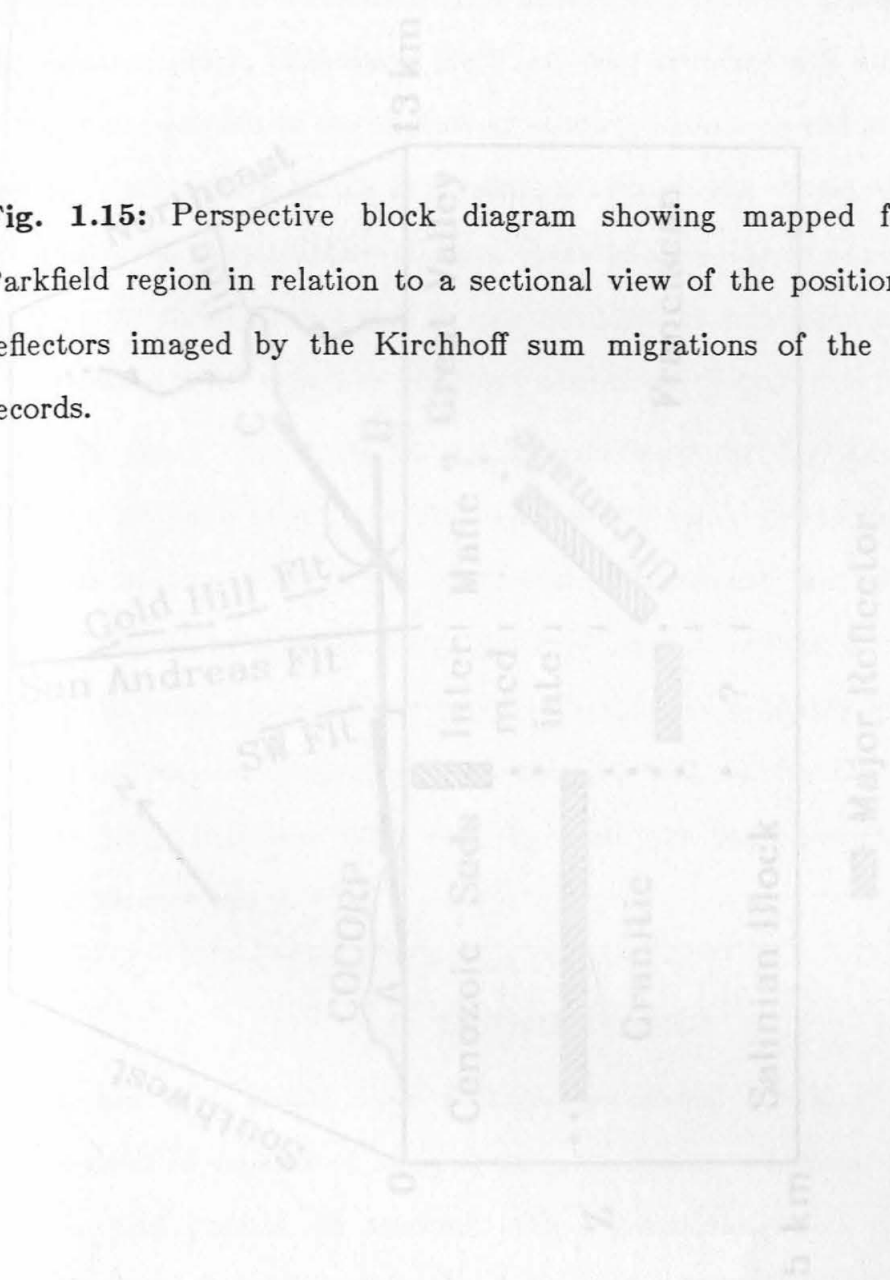
### MIGRATIONS

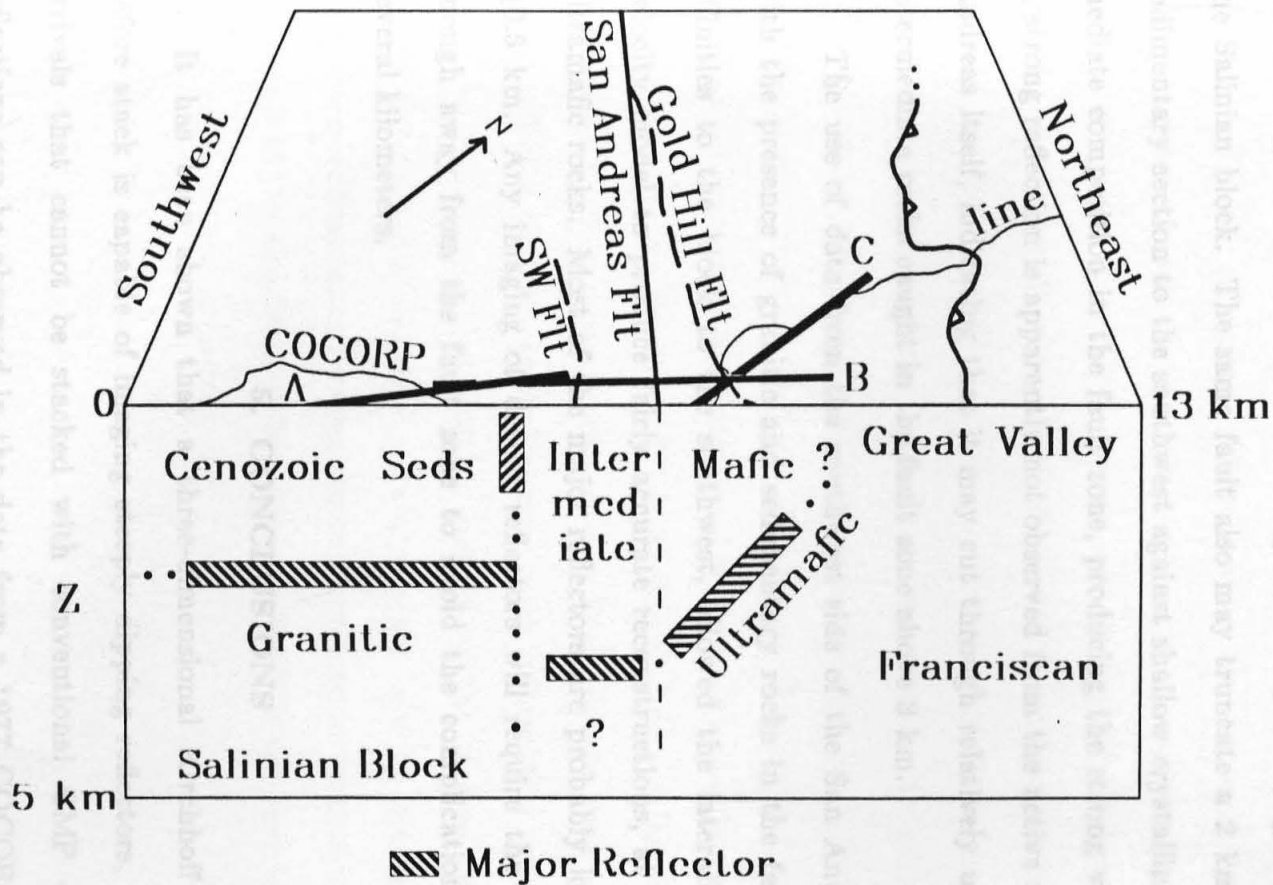


crossed by similar arcs. Among the images in which I have some confidence is, in Section A, a reflector dipping at least  $45^\circ$  to the southwest underneath the San Andreas fault, possibly extending to the surface near the trace of the Gold Hill fault. It can be found to a depth of at least 4 km. Section B contains a similar reflector, although it is less well defined. This reflector also appears on Section C, with a shallower apparent dip. A sub-horizontal reflector is observed at a depth of about 3 km between the surface traces of the San Andreas and an unnamed fault to the southwest. Such a reflector is also present in Section A. A strong near-vertical reflector is shown in Section B, extending from the surface to a depth of about 1 km. This reflector can also be discerned in Section C, where it appears to mark the truncation of a strong sub-horizontal reflector at a depth of 2 km, which continues to the southwest.

Hanna et al. (1972) have synthesized the surface geology of the Parkfield area with gravity and magnetic data. Figure 1.15 interprets the location of the imaged reflectors and their association with mapped surface features and suspected geological relations. In making interpretations of the connection of reflectors with geological boundaries, the most obvious, simple boundaries that would provide the greatest velocity contrast should be stressed. The Gold Hill fault incorporates slices of serpentized ultramafic rocks from the metamorphic Franciscan complex to the northeast and juxtaposes them against crystalline rocks of intermediate to mafic composition, which crop out to the southwest. Such a contrast would create a strong reflector. Sections A and B indicate that the fault may well dip steeply to the southwest and intersect the vertically dipping San Andreas at a depth of 3 to 4 km. Between the San Andreas and the unnamed fault to the southwest, the intermediate-

**Fig. 1.15:** Perspective block diagram showing mapped features of the Parkfield region in relation to a sectional view of the positions of the major reflectors imaged by the Kirchhoff sum migrations of the COCORP shot records.





ultramafic contact may be sub-horizontal at a depth of 3 km. It appears to be truncated by the southwestern fault against the possibly granitic basement of the Salinian block. The same fault also may truncate a 2 km thick Tertiary sedimentary section to the southwest against shallow crystalline rocks of intermediate composition in the fault zone, producing the strong vertical reflector. A strong reflection is apparently not observed from the active trace of the San Andreas itself, indicating that it may cut through relatively uniform mafic to intermediate rocks caught in the fault zone above 3 km.

The use of data from the southwest side of the San Andreas, combined with the presence of granitic and sedimentary rocks in the fault zone having affinities to the block to the southwest, allowed the laterally homogeneous velocity model to produce fairly accurate reconstructions, at least above the ultramafic rocks. Most of the major reflectors are probably located to within  $\pm 0.5$  km. Any imaging of deeper reflectors will require the use of data far enough away from the fault zone to avoid the complications in the upper several kilometers.

## 5. CONCLUSIONS

It has been shown that a three-dimensional Kirchhoff sum migration before stack is capable of imaging steeply dipping reflectors, which produced arrivals that cannot be stacked with conventional CMP methods. Such reflections can be observed in the data from a 1977 COCORP survey across the San Andreas fault near Parkfield, California. Previous workers, who used conventional methods, could not interpret the events, which arose from strong lateral heterogeneities. However, applying the Born, WKBJ, and far-field

approximations to the wave equation results in the simplification of the inversion of these reflections to a ray equation back-projection process very similar to Kirchhoff sum migration. This process can be easily implemented on unsorted data to back project reflector images into arbitrarily oriented depth sections of limited size. This process was verified by inversions of full wave acoustic synthetics incorporating the same geometric coverage limitations inherent in the COCORP survey. Although limited in accuracy by poor geometric coverage and the laterally inhomogeneous velocity structure, the method imaged reflectors around the San Andreas fault that are consistent with the known structural features of the area. The imaged relationships suggest that the fault zone has juxtaposed mafic to intermediate crystalline rocks against Cenozoic sediments on the southwest and serpentinized ultramafics on the northeast. The modern trace of the San Andreas does not form such a strong reflector that it can be imaged. Such information can prove useful in efforts to reconstruct the complex history of the motion of crustal blocks caught in the transform zone. Further work will be aimed at testing the method on additional structures where data become available, and at taking advantage of the amplitude information available in the multi-offset domain to further constrain the inversion.

## Chapter 2

### Seismic Acquisition Case History of the Calcrust Mojave-Sonoran Deep Crustal Survey

#### ABSTRACT

An extensive seismic reflection experiment was conducted by the Calcrust consortium of five California universities near the Colorado River in southeastern California in May and June of 1985. The geologic objective of the survey was to define the extensional history of an archetypical region of metamorphic core complexes. To reach this objective, both shallow, high-resolution and deep, long offset seismic reflection data had to be collected. Preliminary field experiments showed that the major geophysical acquisition problem to be solved was the poor penetration of seismic energy through a low-velocity surface layer covering certain areas. Its effects could be mitigated through special acquisition and processing techniques. Fortunately, speculative data obtained from industry showed that quality data could be obtained from areas having a deeper, older sedimentary cover, causing a redefinition of the geologic objectives. Preliminary field tests and constant monitoring of data quality and parameter adjustment allowed 108 km of excellent crustal data to be obtained. The preliminary experiments, industry data, and operational flexibility were crucial not just to acquisition success

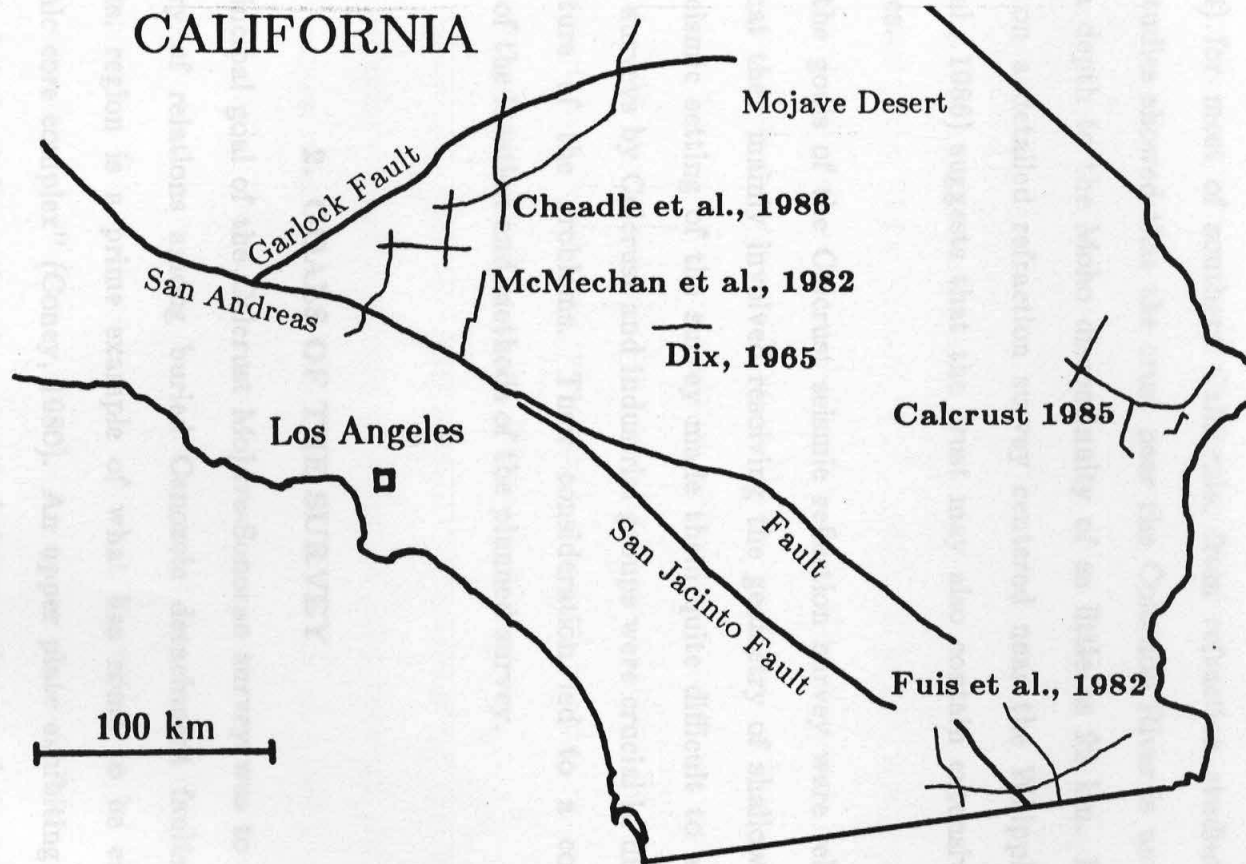
but also to proper interpretation. The interpretation of these data bears on both local and regional geological and geophysical problems.

## 1. INTRODUCTION

The California Consortium for Crustal Studies (Calcrust) is an effort involving geoscience departments at five universities: the University of Southern California, the California Institute of Technology, the San Diego State University, the University of California at Berkeley, and the University of California at Santa Barbara. Investigators within the consortium have diverse interests in the structure and evolution of continental crust, which cross the boundaries between geology, geophysics, and geochemistry. The group emphasizes the use of specialized seismic reflection studies coupled with strong surface geologic control to investigate both regional and local crustal phenomena. Cooperation with other seismic consortia, groups from the U. S. Geological Survey, and the petroleum and minerals industry is stressed.

The Calcrust consortium selects projects from a collection of proposals submitted by the member, and other, investigators. Funding support for Calcrust came from the National Science Foundation beginning in June, 1984, for a study to investigate crustal structures associated with metamorphic core complexes and adjacent detachment faults in the Mojave and Sonoran Deserts of southeastern California, near the Colorado River (Figure 2.1). This was the first detailed seismic investigation of the area. Seismic reflection surveys have been carried out in the central and western Mojave Desert by C. H. Dix (1965),

**Fig. 2.1:** Map of southern California showing major geographic and tectonic features in relation to the Calcrust Mojave-Sonoran project and previous seismic surveys.



and by COCORP (Cheadle et al., 1986). These established the presence of reflective structures at all levels of the crust in those areas. Constraints on overall crustal velocity structure were derived in the western Mojave by McMechan et al. (1982), near the Imperial Valley by Fuis et al. (1982), and by Hearn (1984) for most of southern California, from refraction studies. The latter two studies showed that the crust near the Colorado River is unusually thin, with a depth to the Moho discontinuity of as little as 22 km. Preliminary work on a detailed refraction survey centered near the Whipple Mts. (Wilson et al., 1986) suggests that the crust may also contain extensive low-velocity zones. (John, 1982; Howard et al., 1982). It is not, however, clear

While the goals of the Calcrust seismic reflection survey were relatively simple in that they mainly involved resolving the geometry of shallow structures, the seismic setting of the survey made them quite difficult to achieve. Preliminary surveys by Calcrust and industrial groups were crucial in discovering the nature of the problems. Their consideration led to a complete redefinition of the location and methods of the planned survey.

## 2. GOALS OF THE SURVEY

The principal goal of the Calcrust Mojave-Sonoran survey was to resolve the geometry of relations among buried Cenozoic detachment faults. The Whipple Mts. region is a prime example of what has come to be called a "metamorphic core complex" (Coney, 1980). An upper plate exhibiting extension through brittle deformation is separated from a lower plate extended through ductile processes by a low-angle detachment fault of possibly regional

extent (Davis et al., 1980). The upper plate is deformed by high-angle normal faults rooted in the detachment. The sense of motion on these faults is consistent with a northeast-to-southwest direction of regional extension. Dips and movement along these faults are consistent with the northeast-southwest regional extension direction. The lower plate is often marked by foliation and mylonitic fabrics.

Davis and others (1980) and Frost (1981) have detailed the geometry of the detachment faulting exposed in the Whipple Mountains. Similar structures are exposed in nearby ranges such as the Chemehuevi, immediately north of the Whipples (John, 1982; Howard et al., 1982). It is not, however, clear whether these structures and the detachment in the Whipples form one regional surface or are separate structures. If they are separate, hypotheses on their timing and the form of the regional deformation could be tested with knowledge of their geometric relationships. As these relations lie under the alluviated valleys between the ranges, seismic reflection imaging appeared to provide the best opportunity for testing different hypotheses.

In one hypothesis, the "breakaway zone" or headwall of the Whipple Mountains detachment fault has been proposed to exist between the Turtle and Mopah ranges, west of the Whipples by Davis et al. (1980), and by Howard et al. (1982). They also suggested that the headwall could be within the Ward Valley, farther west of the Turtle Mountains and east of the Old Woman Mountains. The headwall would mark the western limit of the area dissected by detachment faulting. Alternatively, buried detachment faults could exist west of the Turtles but lack any surface expression. This would suggest that such faulting could continue to the central Mojave detachment

terrane, studied by Dokka (1983).

Apart from the detachment, a distinguishing characteristic of metamorphic core complexes is a penetrative mylonitic foliation and lineation within the lower plate. A package of mylonites over 3.9 km thick is found in the antiformal core of the Whipple Mts. (Anderson and Rowley, 1980; Davis et al., 1982). These northeast-oriented simple shear mylonites have been recently dated to be of mid-Tertiary age (Wright et al., 1986). South of the Whipples, the Riverside Mountains are composed of imbricate stacks of Paleozoic and Mesozoic cratonal rocks, Precambrian crystalline rocks, and Mesozoic intrusive rocks, all of which have been deformed by late Mesozoic simple shear directed to the northeast (Hamilton, 1982; Lyle, 1982). The geometric relationships between Tertiary detachment faulting, Mesozoic thrusting, and their associated mylonitizations are not evident in surface exposures.

While the definition of the geometric relations between the shallow structures mentioned above helps resolve problems of the sequence and extent of detachment and core complex development, it leaves many questions on the mechanism of their formation. The fact that the crust is unusually thin near the belt of core complexes suggests that the extensional event affected the entire depth of the crust. The nature of the extensional mechanism should be evident if enough information on the middle and deep crust could be obtained. For this reason the imaging of deep structures became a major priority for the survey.

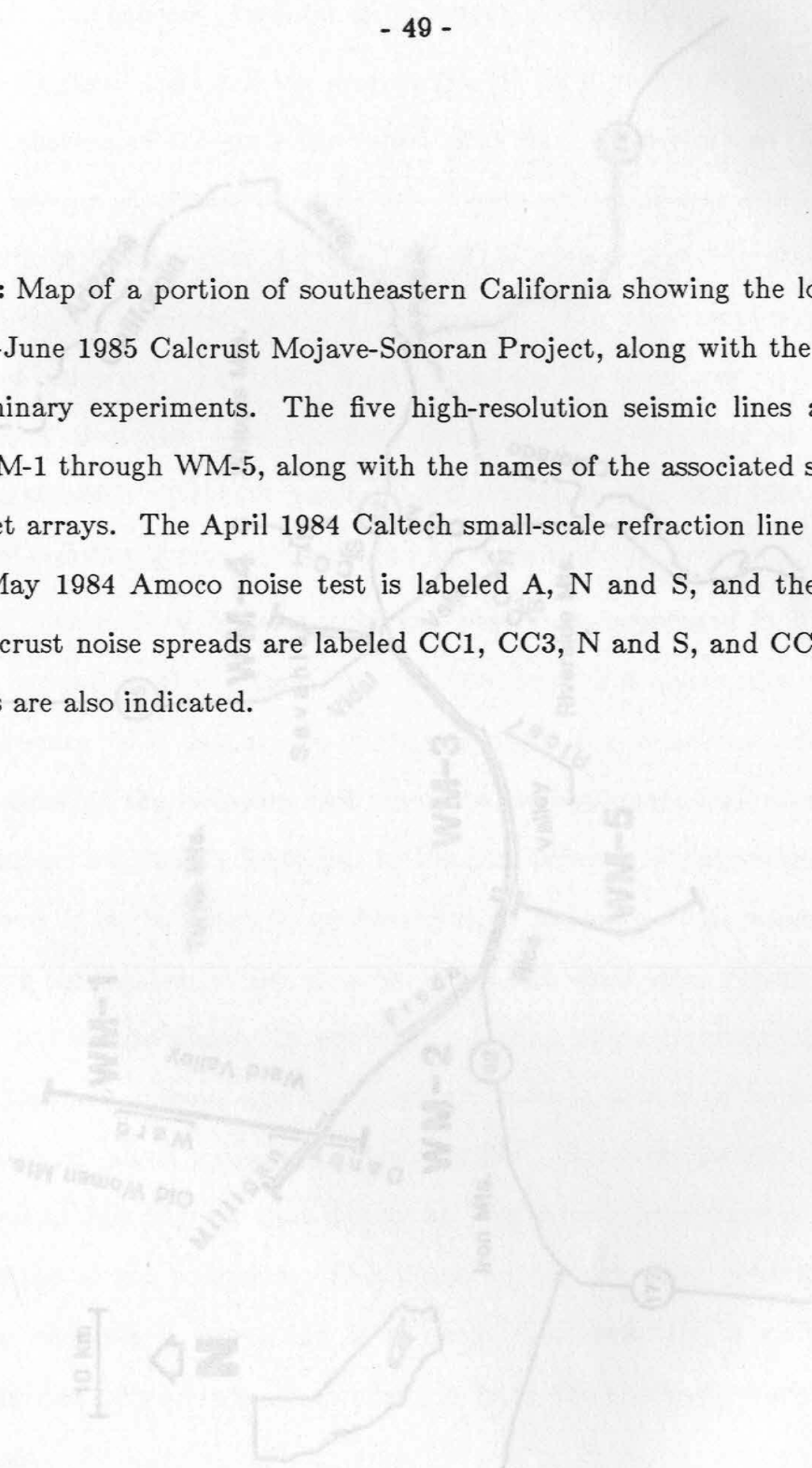
These geological objectives left the Mojave-Sonoran survey with two somewhat incompatible geophysical objectives. On one hand, the goal of resolving the geometric relations between weakly reflective detachment faults

at depths shallower than 5 km, and tracing these reflectors at extremely small depths to surface outcrop would require an intensive, high-resolution seismic survey. To fully address the question of detachment continuity between ranges, the survey would have to extend at least 60 km. On the other hand, to reliably detect and characterize deep crustal reflectors, a wide-ranging survey extensively employing long source-to-receiver offsets would be needed. Balancing these demanding objectives with the limitations of a \$350,000 budget and poor vehicle access would demand careful preparation and innovative acquisition techniques.

### 3. PRELIMINARY FIELD TESTS

Preparation for the Mojave-Sonoran survey began with an effort to determine, in the field, what the reflection character of a detachment fault might be. Shallow, short-line seismic refraction experiments were carried out across the surface exposure of the detachment in the southwestern Whipple Mountains in April 1984 by a group from Caltech. These experiments yielded information on the seismic characteristics of the area, which allowed realistic modeling to begin. A vibrator noise test was generously carried out nearby by AMOCO in May 1984. This test showed that special care would have to be taken to obtain interpretable data. The October 1984 Calcrust noise survey obtained additional information on seismic characteristics at later times and farther offsets, as well as in other areas of the Vidal Valley. Figure 2.2 shows the locations of these phases of field work. Finite difference modeling further clarified the measures necessary to successfully image the detachment.

**Fig. 2.2:** Map of a portion of southeastern California showing the location of the May-June 1985 Calcrust Mojave-Sonoran Project, along with the locations of preliminary experiments. The five high-resolution seismic lines are designated WM-1 through WM-5, along with the names of the associated stationary long-offset arrays. The April 1984 Caltech small-scale refraction line is labeled C, the May 1984 Amoco noise test is labeled A, N and S, and the October 1984 Calcrust noise spreads are labeled CC1, CC3, N and S, and CC2. Major highways are also indicated.



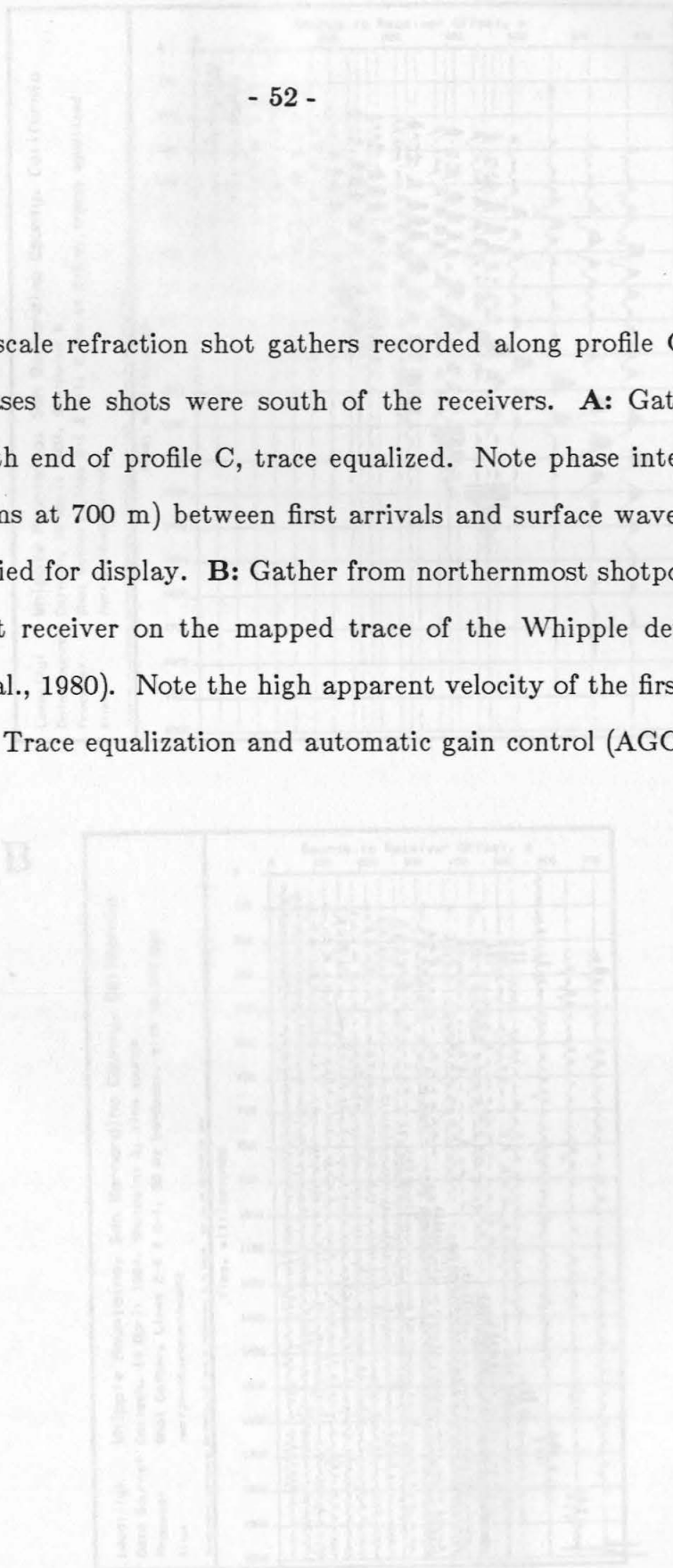


*Determining the seismic character of the target structure*

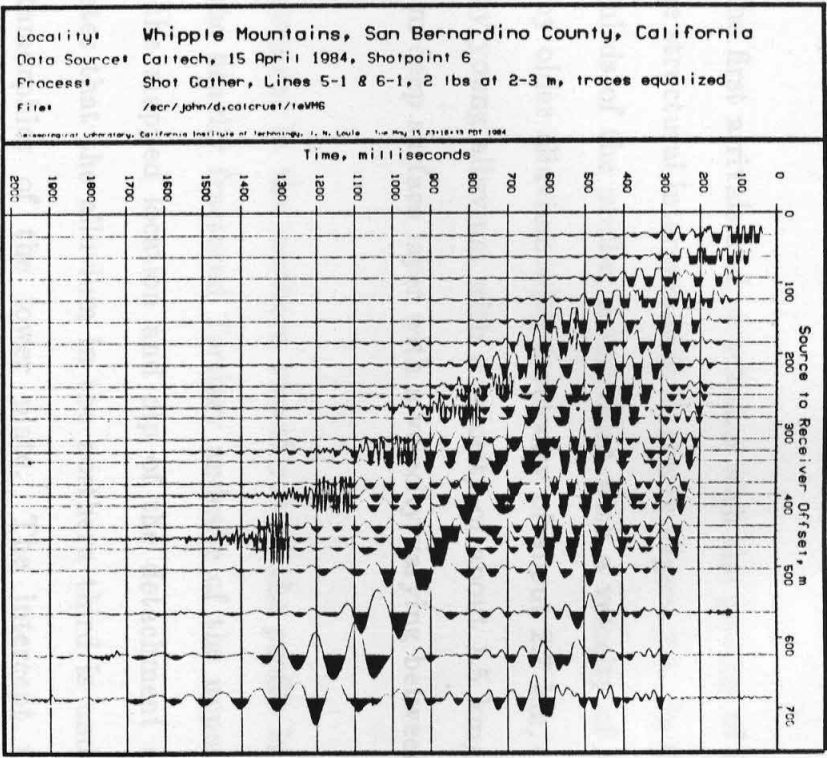
In early April 1984 a 2 km long profile (C on Figure 2.2) was shot using explosive charges of 0.5 to 3 kg buried at 1 to 2 m depth into lines of 12 clustered groups at offsets up to 700 m. The northernmost end of the profile was on a fault line scarp of the Whipple detachment mapped by Dickey et al. (1980). Vertical receivers were used, except for two lines employing four 3-component receivers. The eight lines of the profile were shot updip off the south end of each line, with the lines overlapping. In this way each receiver point was recorded with both nearer (0-300 m) and farther (300-700 m) offsets. Reciprocal sections approximating downdip shots could be produced.

Shot records from both ends of the profile are presented in Figure 2.3. The first arrivals in this dataset show the presence of 3 layers, the velocity of which increases with depth. No reflections from any interfaces below the 3 layers comprising the alluvium and basement are apparent, even after filtering out all energy not close in frequency to the first arrivals. Polarization information derived from the 3-component recordings indicates that, while the first arrivals are propagating in the plane of the profile, some later phases are arriving from out of the plane. In addition, a strong phase intermediate in time between the first arrivals and the Rayleigh wave is shown to be a vertically polarized shear wave propagating horizontally. However, its group velocity and intercept time suggest that it may be a refracted shear wave propagating along the top of the basement. This phase appears on other records recorded where the alluvium is more than 50 m deep. Unfortunately, it arrives at the same time and offset range as a reflection from the shallowly buried detachment might.

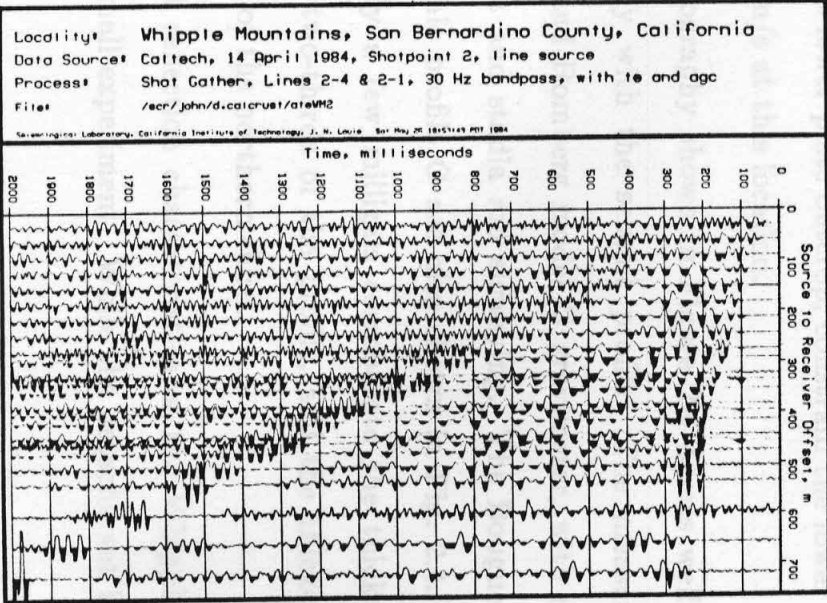
**Fig. 2.3:** Small-scale refraction shot gathers recorded along profile C (Figure 2.2). In both cases the shots were south of the receivers. **A:** Gather from shotpoint at south end of profile C, trace equalized. Note phase intermediate in time (at 600 ms at 700 m) between first arrivals and surface waves. Trace equalization applied for display. **B:** Gather from northernmost shotpoint, with the longest offset receiver on the mapped trace of the Whipple detachment fault (Dickey et al., 1980). Note the high apparent velocity of the first arrivals at 500 m offset. Trace equalization and automatic gain control (AGC) applied for display.



A



B



Analysis of the first arrivals and correlation with the geology of Dickey et al. (1980) yield the structural interpretation shown in Figure 2.4. In the southern and central thirds of the profile, a basement with a velocity of about 4.4 km/s is overlain by older alluvium with a velocity of about 2.7 km/s. This is overlain in turn by young alluvium with a velocity of about 1.5 km/s. There is also a 10 to 20 m deep surface layer with a velocity varying between 0.7 and 1.2 km/s.

While the basement in the southern two-thirds of the profile is likely to be composed of the heavily fractured Tertiary andesite of the upper plate of the detachment, the mapped location and dip of the detachment (WDF on Figure 2.4) indicates that the alluvium in the northern third is underlain by the granitic metamorphics of the lower plate. The intercept time and apparent velocity of the basement refraction in the northern third of the profile, and the adjacent lower plate outcrop, constrain the lower plate velocity to a maximum of 4.7 km/s at this location.

The basement topography shown in Figure 2.4 agrees well with gravity data taken concurrently with the seismic profile. The measurements were made with a LaCoste and Romberg model G gravimeter, with elevation control provided by transit and stadia rod surveying. The Bouguer anomaly at stations along the seismic profile C are also shown in Fig. 2.4. Decreases in Bouguer gravity of only a few milligals corroborate the thickening alluvial wedge in the southern two-thirds of the profile, and the thickened alluvium and high basement dips of the northern third.

Thus, the essential reflection characteristics of the Whipple detachment were revealed by this small experiment. While the detachment in that area is

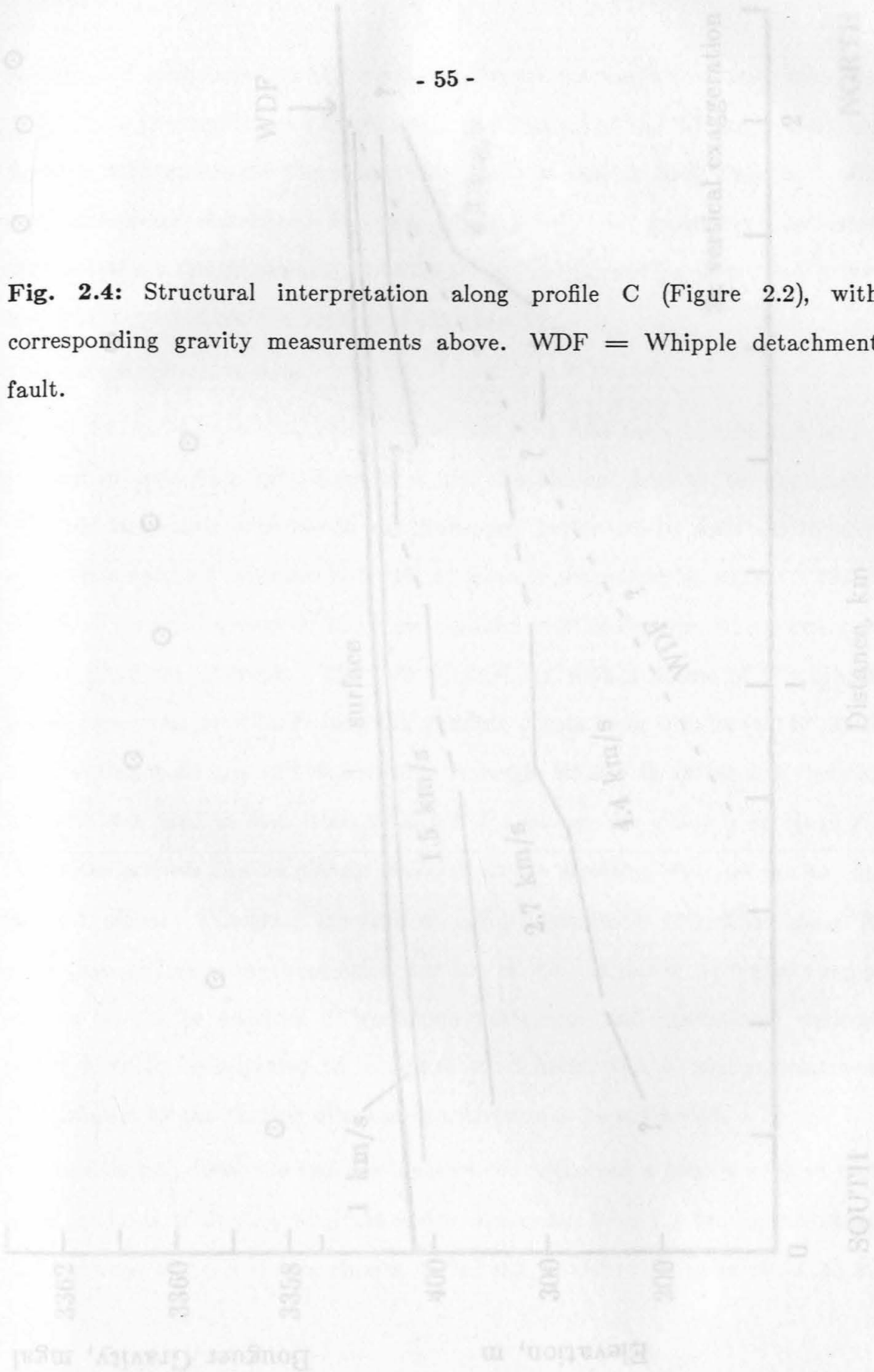
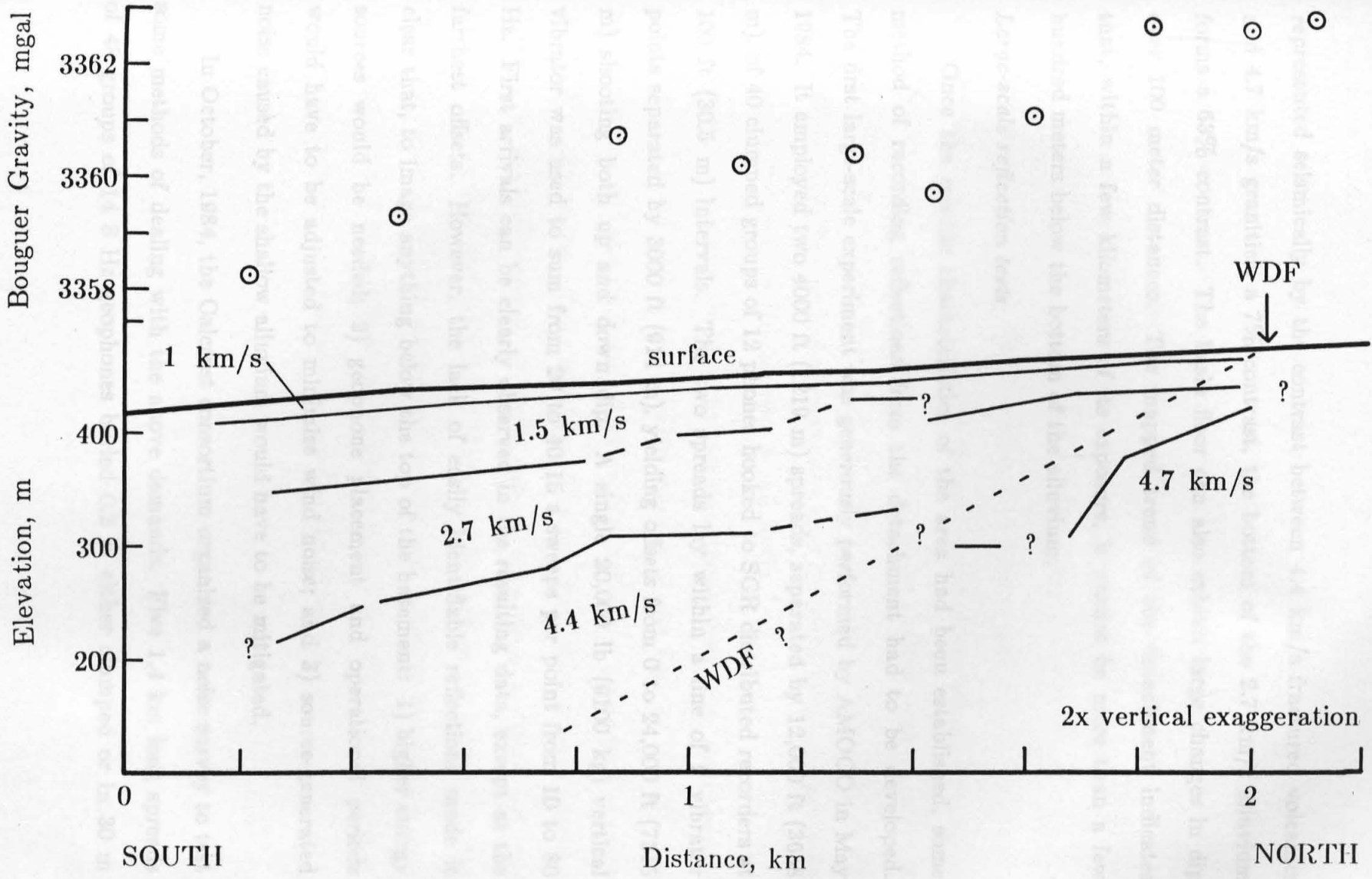


**Fig. 2.4:** Structural interpretation along profile C (Figure 2.2), with corresponding gravity measurements above. WDF = Whipple detachment fault.



represented seismically by the contrast between 4.4 km/s fractured volcanics and 4.7 km/s granitics, a 7% contrast, the bottom of the 2.7 km/s alluvium forms a 63% contrast. The basin floor can also exhibit large changes in dip over 100 meter distances. The mapped trend of the detachment indicates that, within a few kilometers of its exposure, it cannot be more than a few hundred meters below the bottom of the alluvium.

#### *Large-scale reflection tests*

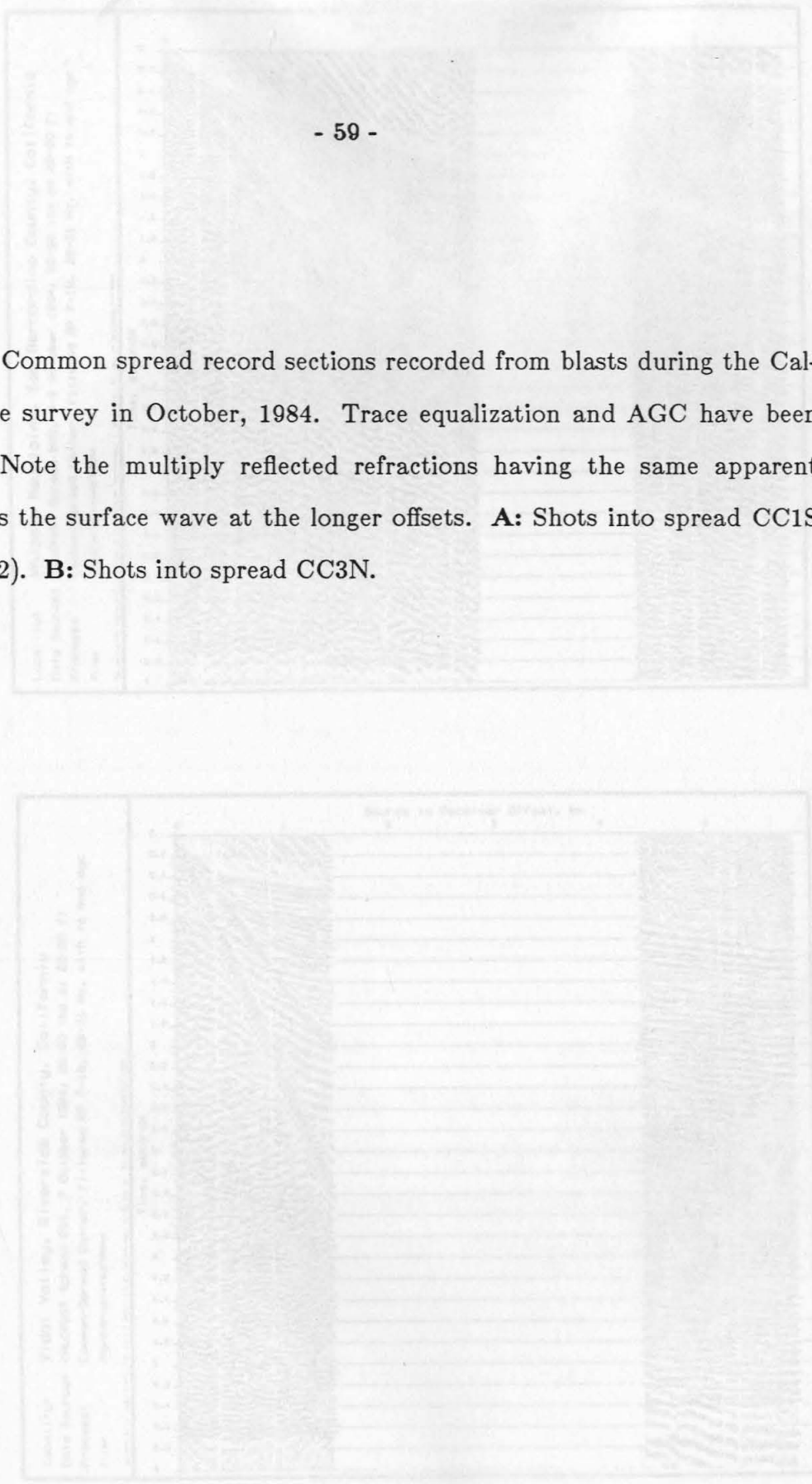
Once the seismic characteristics of the area had been established, some method of recording reflections from the detachment had to be developed. The first large-scale experiment was generously performed by AMOCO in May 1984. It employed two 4000 ft (1219 m) spreads, separated by 12,000 ft (3658 m), of 40 clumped groups of 12 phones hooked to SGR distributed recorders at 100 ft (30.5 m) intervals. The two spreads lay within a line of 9 vibrator points separated by 3000 ft (914 m), yielding offsets from 0 to 24,000 ft (7315 m) shooting both up and down dip. A single 20,000 lb (9100 kg) vertical vibrator was used to sum from 20 to 40 15 s sweeps per point from 10 to 80 Hz. First arrivals can be clearly observed in the resulting data, except at the farthest offsets. However, the lack of easily identifiable reflections made it clear that, to image anything below the top of the basement: 1) higher energy sources would be needed; 2) geophone placement and operational periods would have to be adjusted to minimize wind noise; and 3) source-generated noise caused by the shallow alluvium would have to be mitigated.

In October, 1984, the Calcrust consortium organized a noise survey to test some methods of dealing with the above demands. Five 1.4 km long spreads of 48 groups of 14 8 Hz geophones buried 0.2 m either clumped or in 30 m

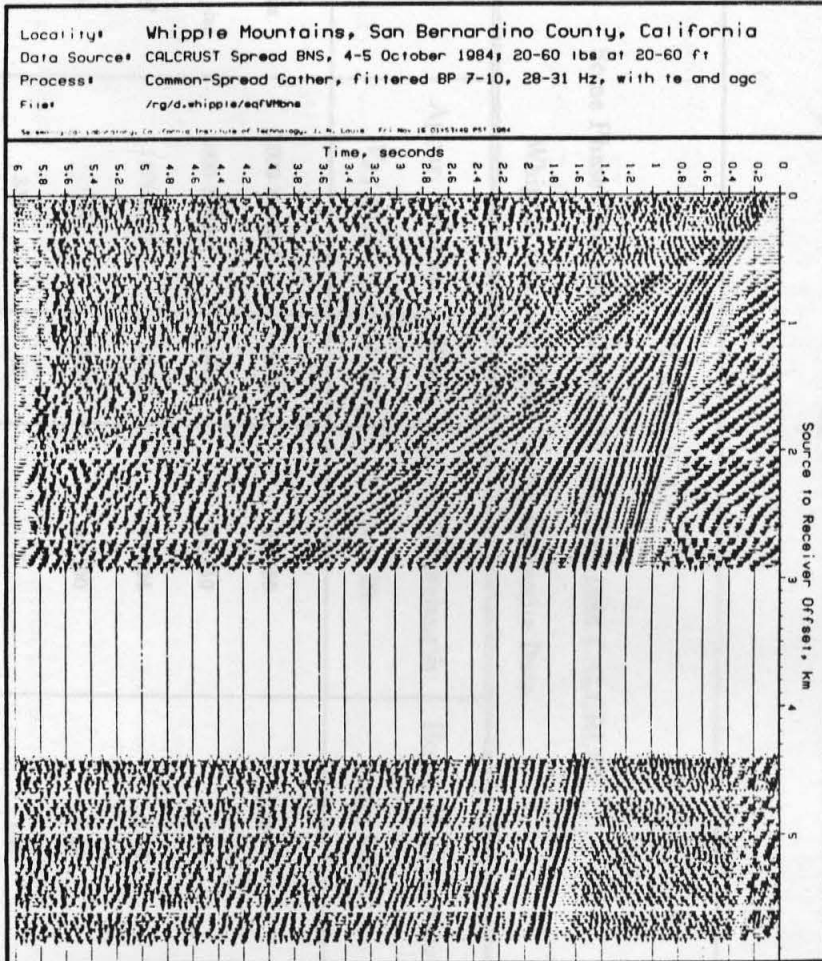
rectangular arrays were arranged into 3 lines, recorded by a DFS IV, on the southwestern flank of the Whipple Mountains, in the center of Vidal Valley, and on the northern flank of the Riverside Mountains. The variety of locations was tested to see how changes in the properties of the alluvium would affect the recording detachment reflections. The geophone burial and arrangement in small arrays were tested to reduce the effects of wind and small surface heterogeneities. Each line included 3 to 5 shot and vibrator points, to compare the energy of large explosive charges and multiple vibrator sweeps at offsets from 0 to 5.8 km. For the shots, 10 to 27 kg charges were placed in 20 m deep drillholes, near the bottom of the lowest velocity surface layer. A single 20,000 lb (9100 kg) vertical vibrator was used for 10 to 75 sweeps per point over varying frequency ranges between 8 and 60 Hz.

The record sections produced by this experiment show that, even towards the center of Vidal Valley, the velocity contrast at the base of the alluvium remains strong and sharp. Some of the profiles indicate a contrast of as much as 100% at the bottom of the alluvium. The principal effect of such a strong contrast is the development of basin bottom refractions multiply reflected between the surface and basin floor. These can be seen as the arrivals having the same apparent velocity as the first arrival, and following it up to 1 s later in the examples of blast data shown in Figure 2.5. Table 2.1 gives the characteristics of these and other phases recorded in the Vidal Valley.

**Fig. 2.5:** Common spread record sections recorded from blasts during the Calcrust noise survey in October, 1984. Trace equalization and AGC have been applied. Note the multiply reflected refractions having the same apparent velocity as the surface wave at the longer offsets. **A:** Shots into spread CC1S (Figure 2.2). **B:** Shots into spread CC3N.



A



B

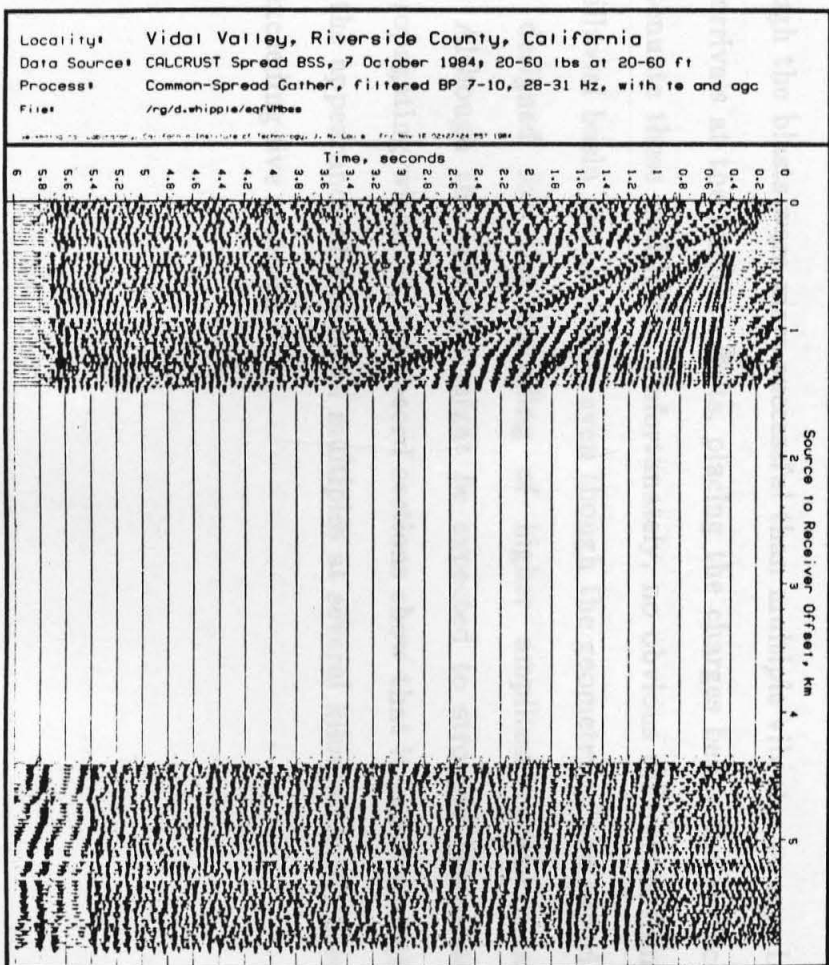


**Table 2.1**

Some Phase Characteristics of the October, 1984 CALCRUST  
Whipple Mts. and Vidal Valley Dynamite Data

Phase	Appar. Velocity $V_z$ , m/s	Freq. f, Hz	Horiz. Wavelength $\lambda_z$ , m	Horiz. Wavenumber $k_z$ , km <sup>-1</sup>
1st arrivals	3000-10000+	18-33	90-550	2-11
basin multiples	3000-10000+	18-33	90-550	2-11
reflections?	1475-2450	13-23	63-196	5-16
Rayleigh	≤ 950	5-27	35-190	5-29
air	330	50	7	150
refracted $S_v$	2200	12-14	163-190	5-6

Although the blasts were more successful than multiple vibrator sweeps in producing arrivals at the longest offsets, placing the charges below the surface did not attenuate these multiples. Unfortunately, no obvious reflections from below the alluvial basin are apparent, even though the geometry of the experiment was designed for the recording of higher amplitude post-critical reflections. Although the alluvium might be expected to strongly attenuate multiples propagating within it, the record sections show that it is not enough to prevent the appearance of the basin multiples at several kilometers of offset and times exceeding five seconds.

### *Finite difference modeling*

An initial effort at modeling intended to check the resolution of a number of features suggested to exist under the southwestern flank of the Whipple Mountains. Figure 2.6 shows the velocity model and zero offset seismograms generated by a 2-d finite difference solution of the acoustic wave equation, as described by Vidale and Helmberger (1987) and Frankel and Clayton (1986). The model velocities were calculated from guesses of the mineral composition and porosity of the units involved. They include granitic basement with an epidotized mylonite front, overlain by a detachment with volcanics, then overlain by an alluvial basin.

The two panels of zero offset seismograms represent, on the right, those recorded atop high-velocity volcanics, and on the left those recorded on low-velocity sediments. The hard rock recordings are seen to generate relatively clean reflections. The records from the sedimentary basin are harder to interpret. The only prominent reflection is from the floor of the alluvial basin. Even in this noise-free model, multiple reflections bouncing between the surface and the basin floor are obscuring the desired reflections.

With the information gained as a result of the small-scale surveys, more realistic modeling was undertaken. Figure 2.7A shows the velocity model obtained by simplifying the section in Figure 2.4 and including a projection of the Whipple detachment. Figure 2.7B shows the velocity model without the detachment. The corresponding record sections were generated by shooting up dip on the modeled structure, using offsets mimicking the April survey. The first arrivals of the model and the April data are quite similar. However, while the primary reflections from the interfaces with the older alluvium and the

6.3 km

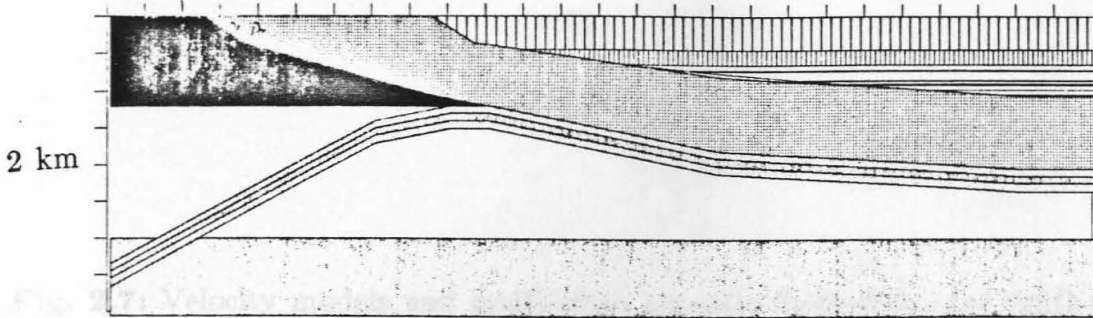
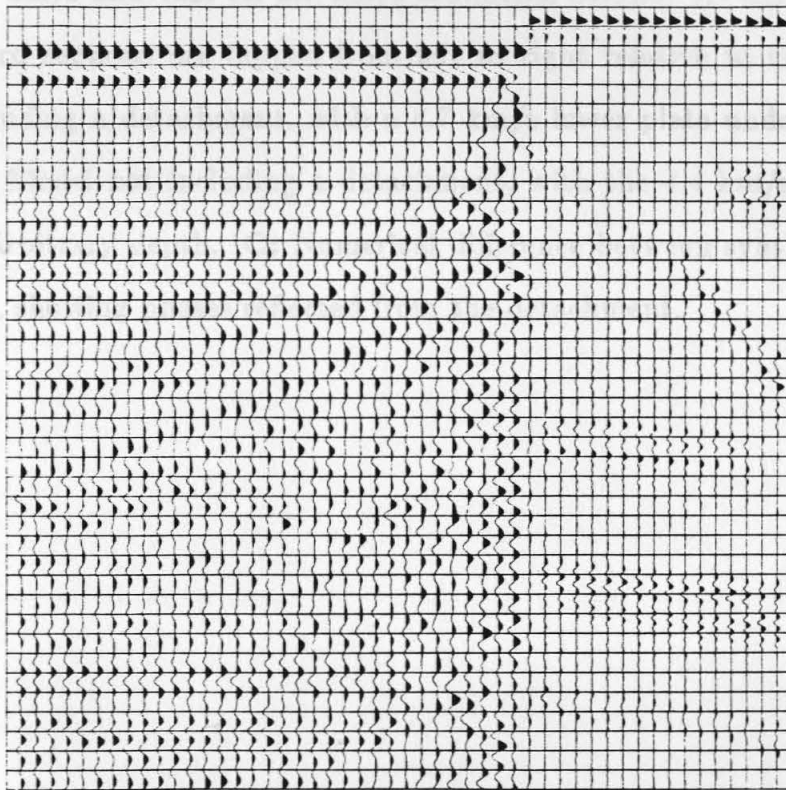
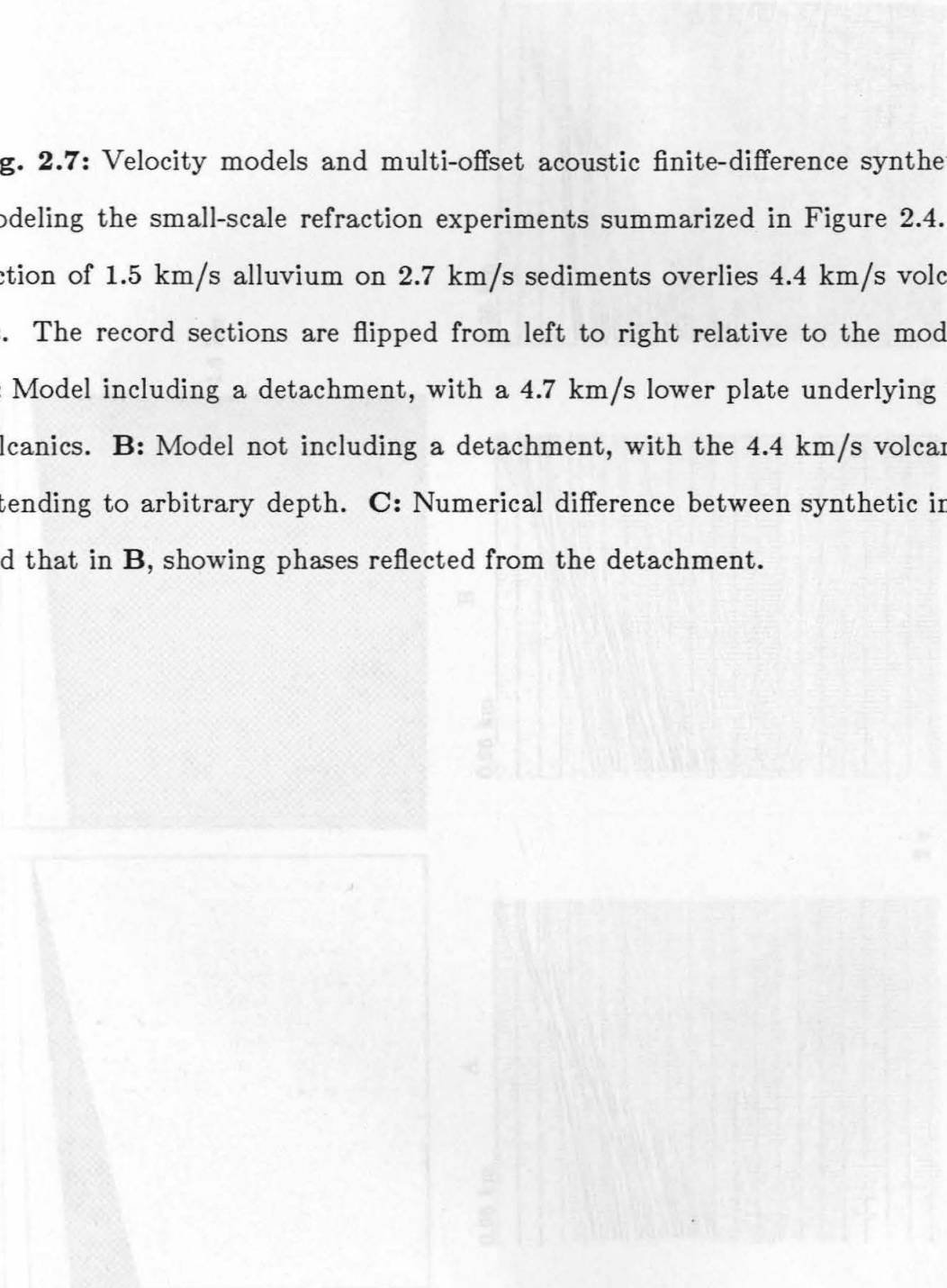


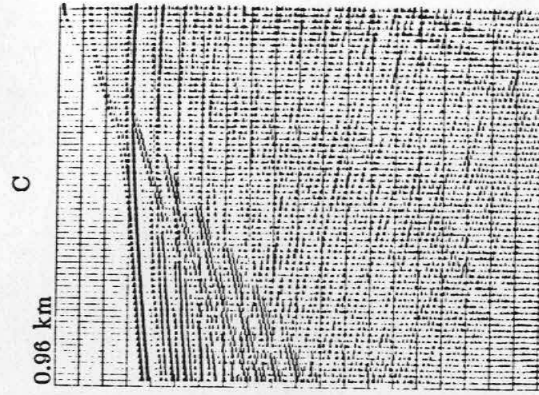
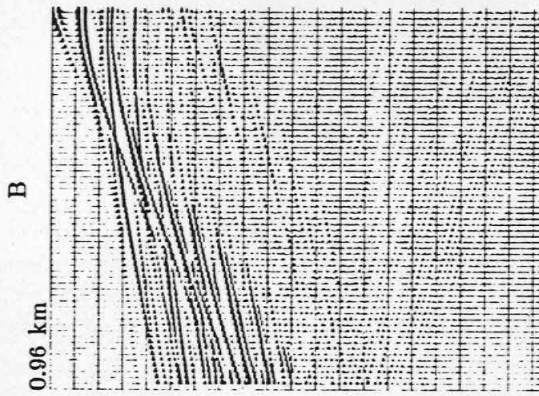
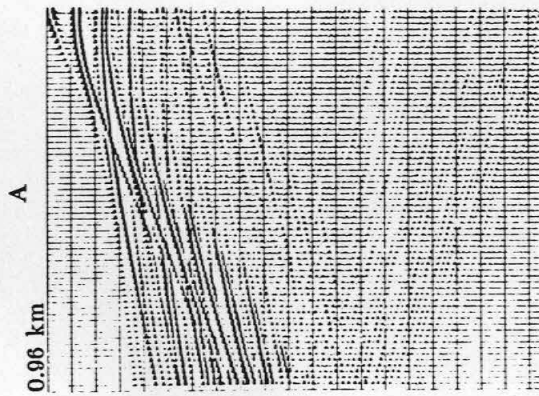
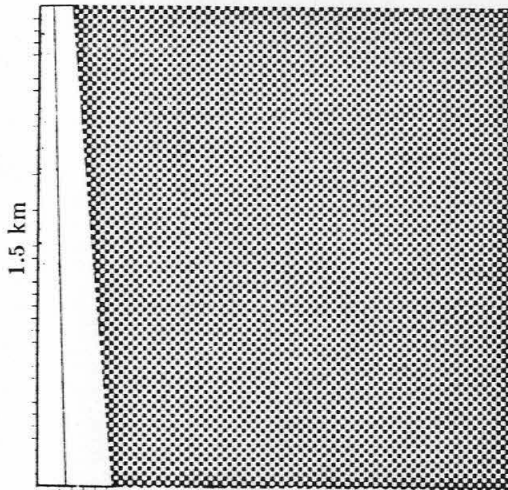
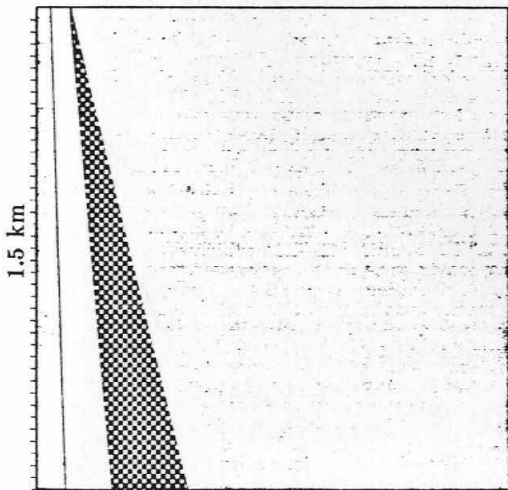
Fig. 2.6: Idealized velocity model of the southwestern flank of the Whipple Mts. and resulting zero-offset finite difference synthetics. The model contains an alluvial basin, floored by volcanics, separated from a granitic lower plate having a velocity gradient, by a detachment including a graded mylonite zone, diving into the lower plate. The acoustic seismograms are flipped from left to right relative to the model.

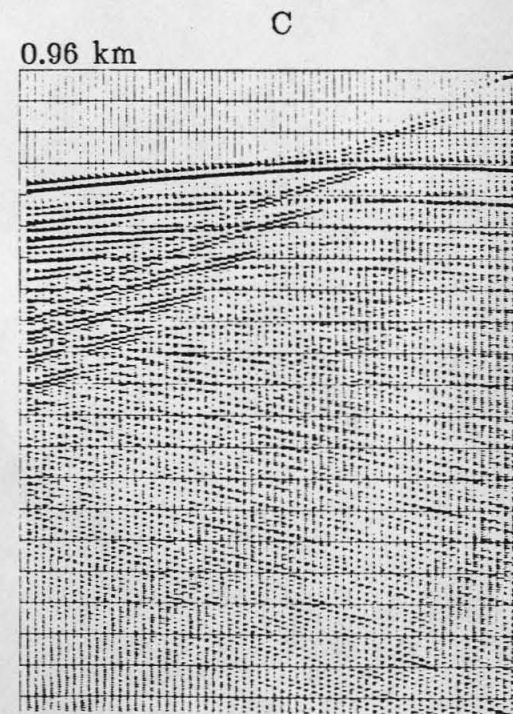
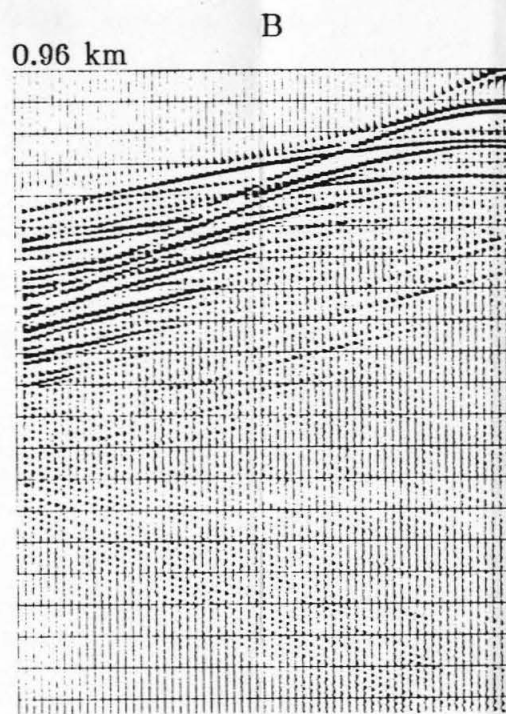
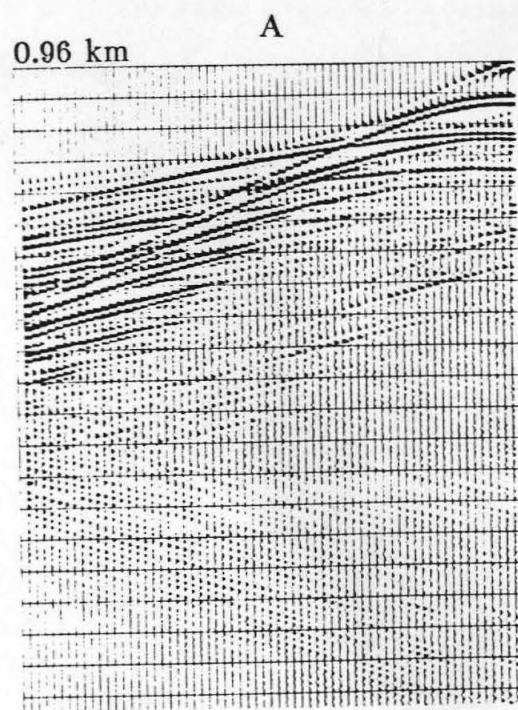
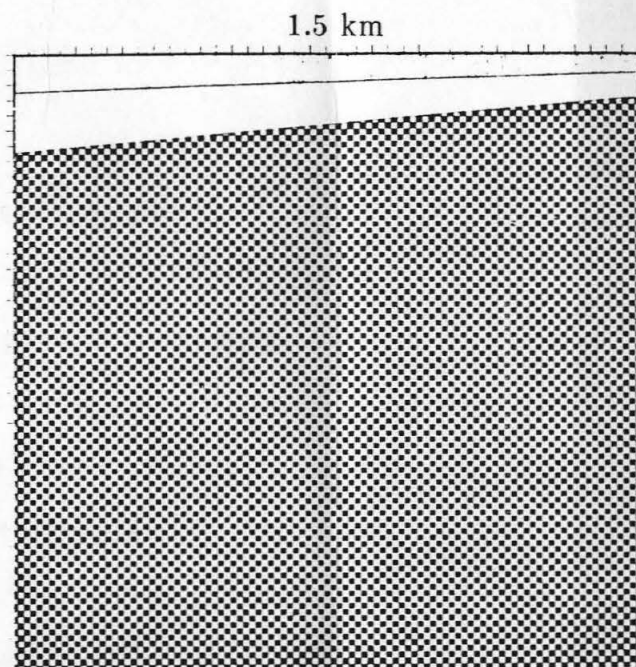
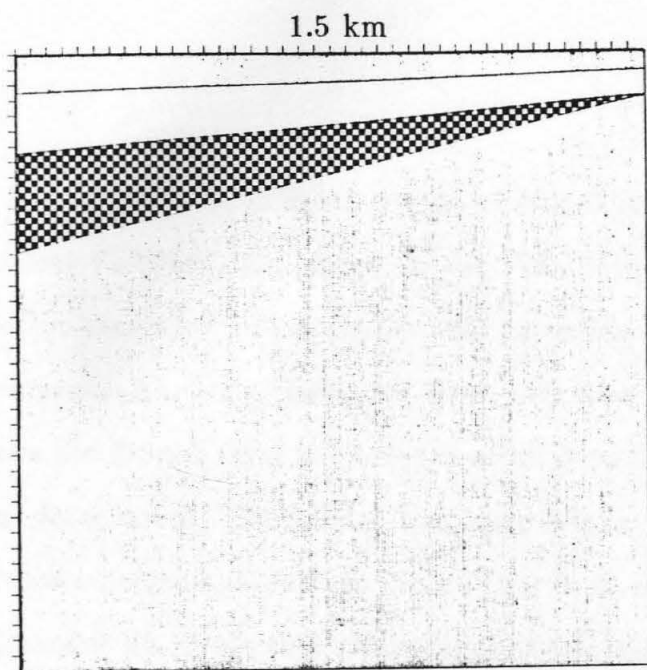


**Fig. 2.6:** Idealized velocity model of the southwestern flank of the Whipple Mts. and resulting zero-offset finite difference synthetics. The model contains an alluvial basin, floored by volcanics, separated from a granitic lower plate having a velocity gradient, by a detachment including a graded mylonite zone, diving into the lower plate. The acoustic seismograms are flipped from left to right relative to the model.

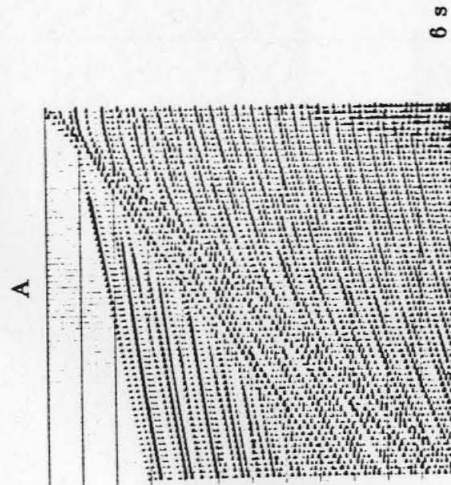
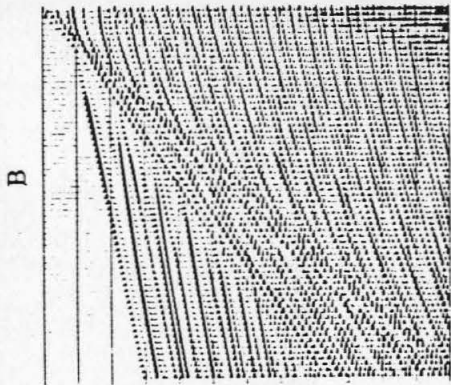
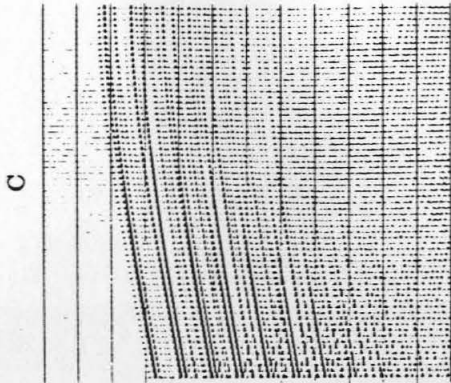
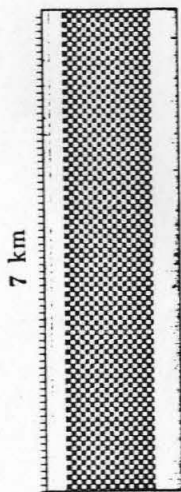
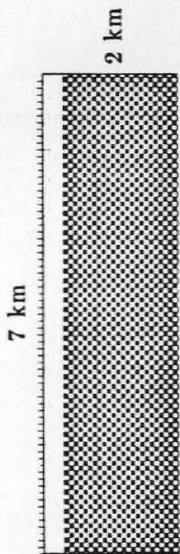
**Fig. 2.7:** Velocity models and multi-offset acoustic finite-difference synthetics modeling the small-scale refraction experiments summarized in Figure 2.4. A section of 1.5 km/s alluvium on 2.7 km/s sediments overlies 4.4 km/s volcanics. The record sections are flipped from left to right relative to the models. **A:** Model including a detachment, with a 4.7 km/s lower plate underlying the volcanics. **B:** Model not including a detachment, with the 4.4 km/s volcanics extending to arbitrary depth. **C:** Numerical difference between synthetic in **A** and that in **B**, showing phases reflected from the detachment.

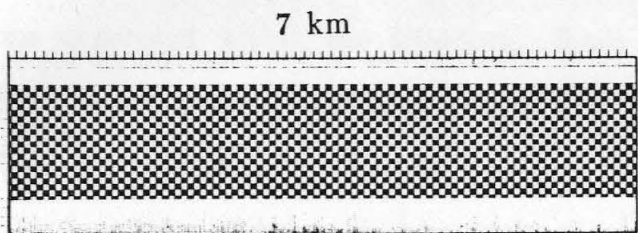




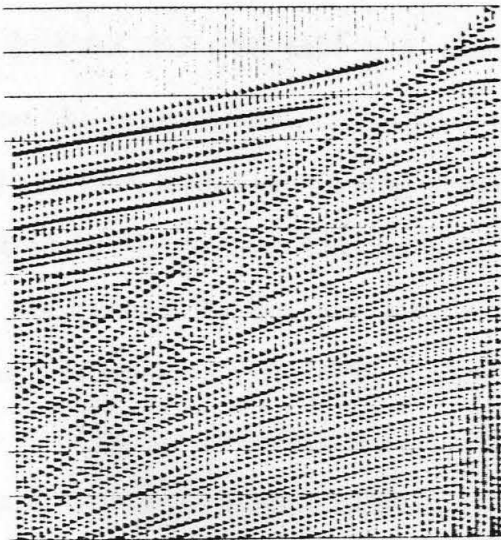


**Fig. 2.8:** Velocity models and acoustic finite-difference synthetics modeling the long offset Calcrust noise survey in the Vidal Valley (spread CC1S, Figure 2.2). A deeper, two-layer sedimentary section overlies upper and lower plates of the detachment. The units have the same velocities as in Figure 2.7. The record sections are flipped from left to right relative to the models. **A:** Model including a detachment. **B:** Model not including a detachment. **C:** Numerical difference between synthetic in **A** and that in **B**, showing phases reflected from the detachment. Note that the reflections are strongest at the farthest offsets, where they have the same apparent velocity as the multiply reflected basin bottom refractions.

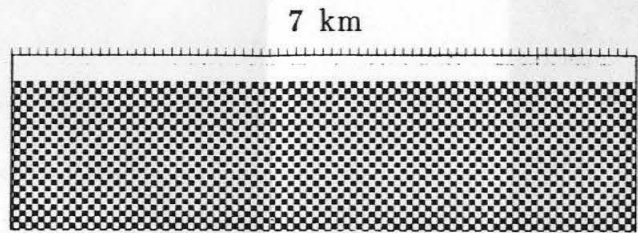




A

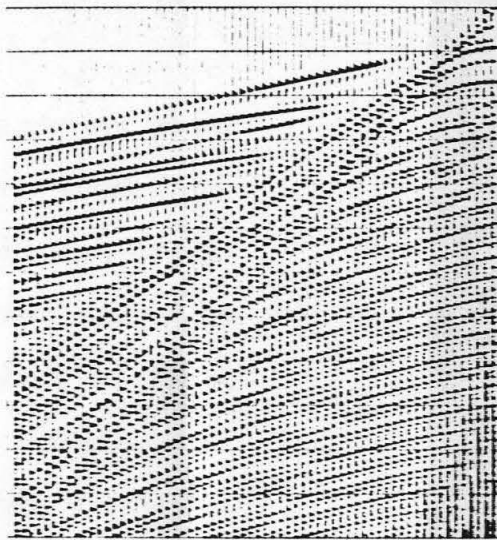


6 s



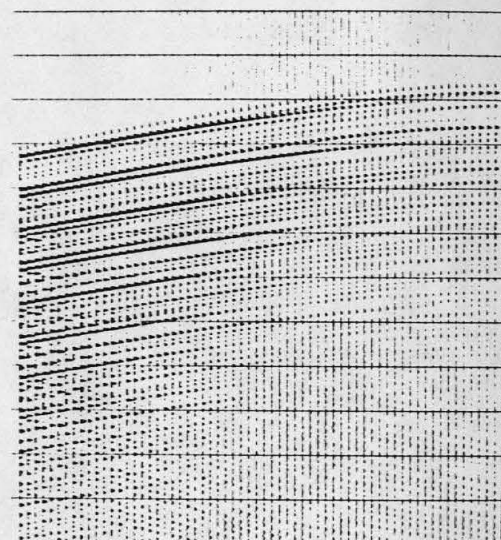
2 km

B



6 s

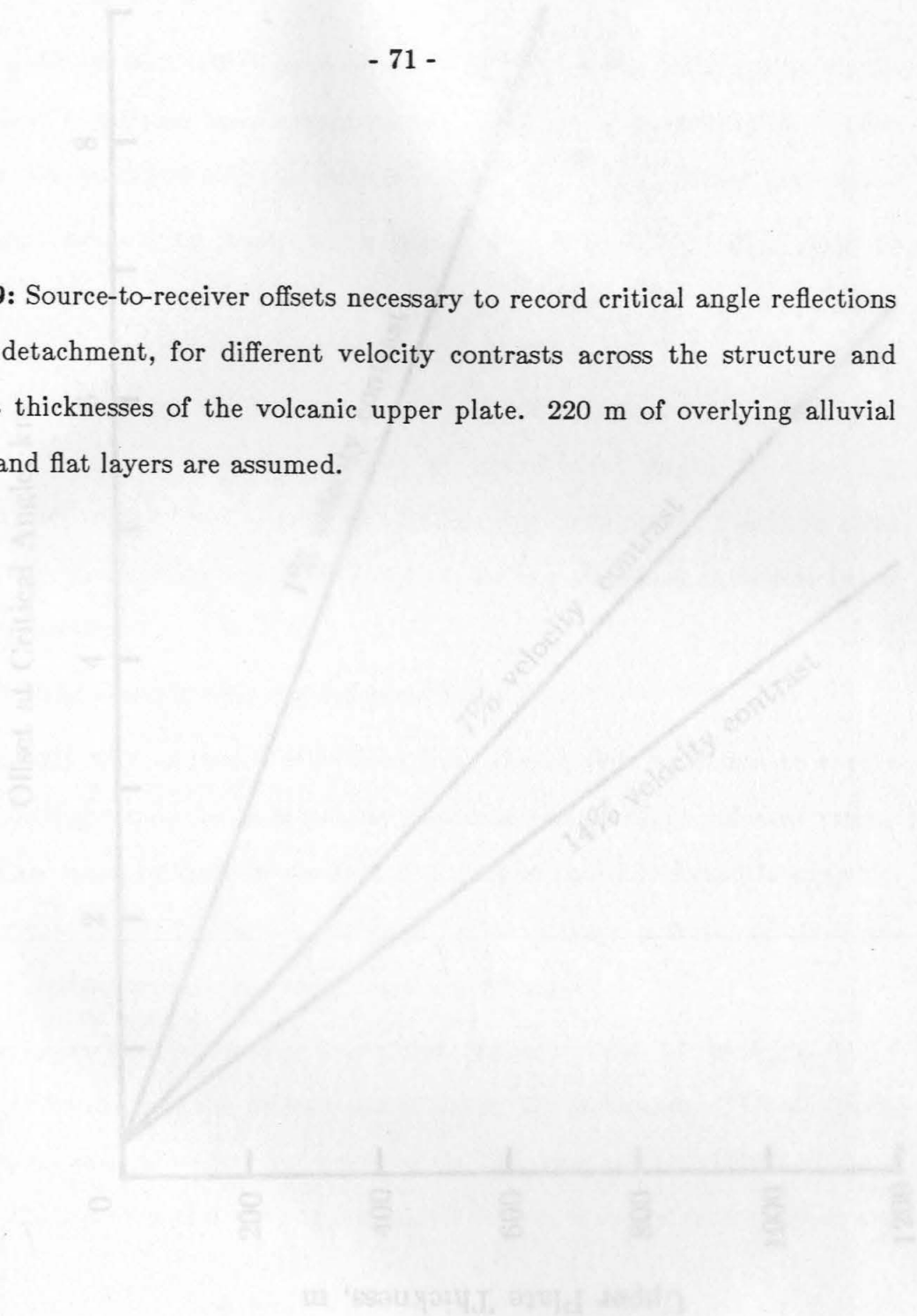
C

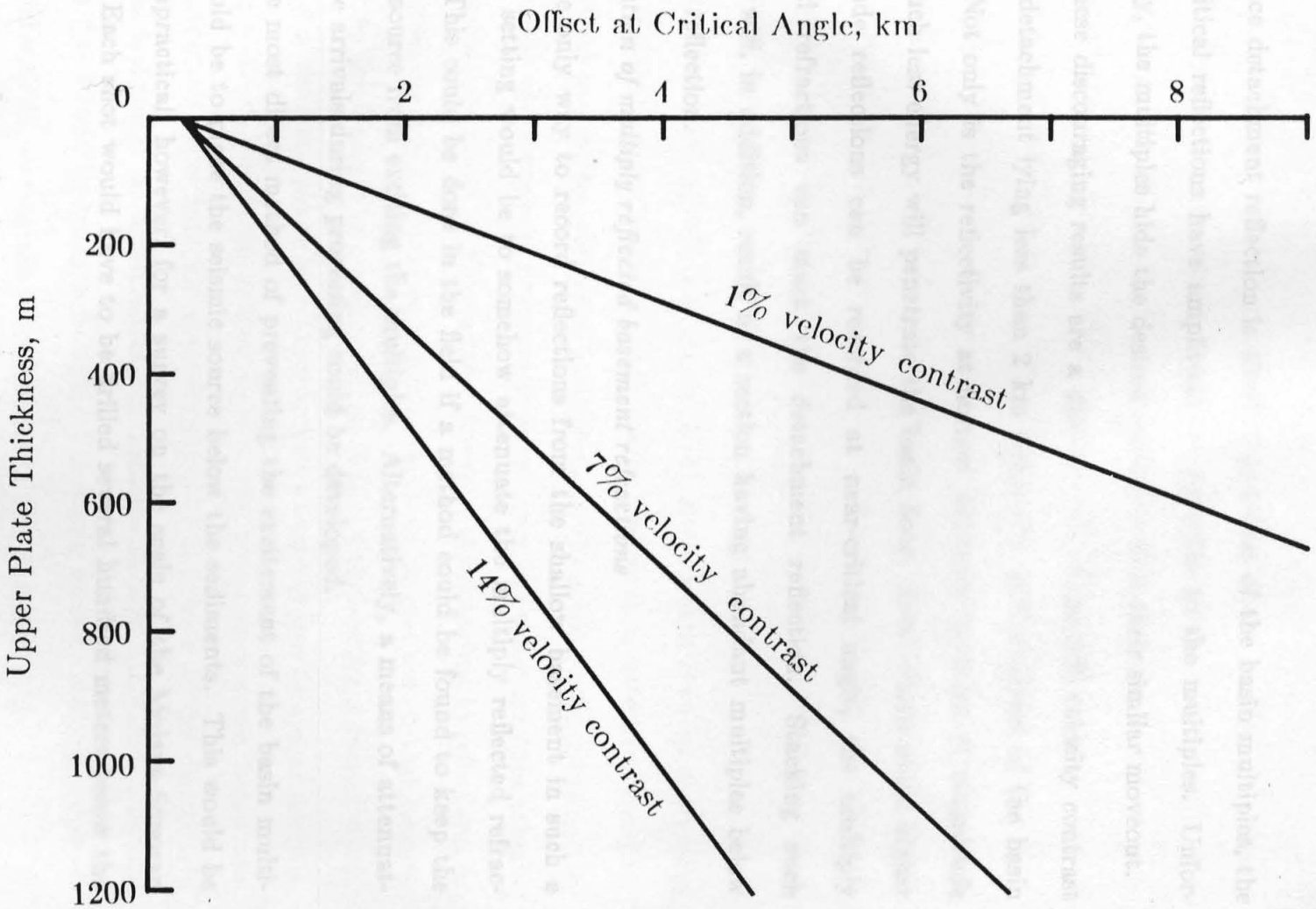


basement are clearly visible, comparing the sections from the models with and without the detachment shows that its reflection is invisible. Subtracting the section without the detachment from the section with it yields the record in Figure 2.7C, which shows where the desired reflection should appear in the section. It is, however, between 20 and 40 decibels weaker than the multiple reflections generated within the alluvium. Slant stacks of these synthetics show that the detachment reflection cannot be culled from the record on the basis of its moveout, either. Only at very high frequencies, almost ten times the 30 Hz frequency of these models, could the reflection be picked from in between the much larger wavelets of the basin multiples. This kind of procedure is of doubtful utility for field data, which include noise.

Based on the information gained from the longer offset surveys in the Vidal Valley, further models employing simple, flat layers were constructed. These are given in Figure 2.8. The model in Figure 2.8A includes a detachment at 1.3 km below a 0.3 km deep alluvial basin. The velocity contrast at the detachment is assumed to be 5%. Figure 2.8B shows a model that differs only in that it lacks the detachment. The synthetic acoustic record sections generated from these models are similar to the P phases recorded in the field. These records also show that the reflection from the detachment is not obvious among the basin multiples. The position of the reflection can, again, be seen by subtracting one section from another numerically, producing Figure 2.8C. This section shows that the detachment reflections do attain significant amplitudes at and beyond critical angle. Figure 2.9 shows what offsets must be used by a survey to record post-critical reflections from possible detachments below an area such as the Vidal Valley. While the amplitude of the near-normal

**Fig. 2.9:** Source-to-receiver offsets necessary to record critical angle reflections from a detachment, for different velocity contrasts across the structure and different thicknesses of the volcanic upper plate. 220 m of overlying alluvial section and flat layers are assumed.





incidence detachment reflection is 40 dB below that of the basin multiples, the post-critical reflections have amplitudes comparable to the multiples. Unfortunately, the multiples hide the desired reflection with their similar moveout.

These discouraging results are a direct result of the 5% velocity contrast of the detachment lying less than 2 km below the 63% contrast of the basin floor. Not only is the reflectivity at normal incidence an order of magnitude less; much less energy will penetrate the basin floor. Even where much higher amplitude reflections can be recorded at near-critical angle, the multiply reflected refractions can mask the detachment reflection. Stacking such records will, in addition, result in a section having abundant multiples below the real reflection.

#### *Attenuation of multiply reflected basement refractions*

The only way to record reflections from the shallow basement in such a difficult setting would be to somehow attenuate the multiply reflected refractions. This could be done in the field if a method could be found to keep the seismic source from exciting the multiples. Alternatively, a means of attenuating these arrivals during processing could be developed.

The most direct method of preventing the excitement of the basin multiples would be to place the seismic source below the sediments. This would be quite impractical, however, for a survey on the scale of the Mojave-Sonoran project. Each shot would have to be drilled several hundred meters below the surface.

To use surface seismic sources in this area, it is necessary to get some of their energy to propagate below the basin bottom. In Vidal Valley, the preliminary experiments showed that any energy propagating down from the

surface at an angle greater than about  $12^\circ$  from vertical would be critically reflected off the basement interface, creating the multiples. More steeply propagating energy can still be bent by the basin bottom interface to reflect post-critically off the detachment. This observation indicated that some type of source arraying could attenuate the multiples. Three types of arrays were tested with acoustic finite difference synthetics (Figure 2.10): 1) an array wherein all of the sources initiate simultaneously; 2) an array wherein the initiation of the sources is linearly phased with distance to produce a wave having a constant horizontal velocity; and 3) an array having a nonlinear phasing that can produce a curved wavefront.

In the first case, synthetics (Figure 2.11) showed that even an extremely long simultaneous array leaked enough energy propagating at more than  $12^\circ$  from vertical to produce obscuring multiples. In the second case, phasing the array so that the wavefront propagates *away* from the receivers does attenuate the multiples caused by the source. However, the detachment reflection, as it propagates back up into the sediments, produces its own set of basin multiples. In the third case, the phasing can be designed to produce a curved wavefront having the same shape as a hypothetical wavefront due to a source below the sediments. A wavefront shaped in this way propagates down below the basin bottom to focus into an approximation of a source in the basement. Even this technique, however, could not provide enough attenuation of the multiples due to the up-going reflection. The basin bottom velocity contrast was too extreme to prevent the source from exciting the multiples.

A method of semblance filtering may be capable of attenuating these multiples during the processing of the data. Although the post-critical

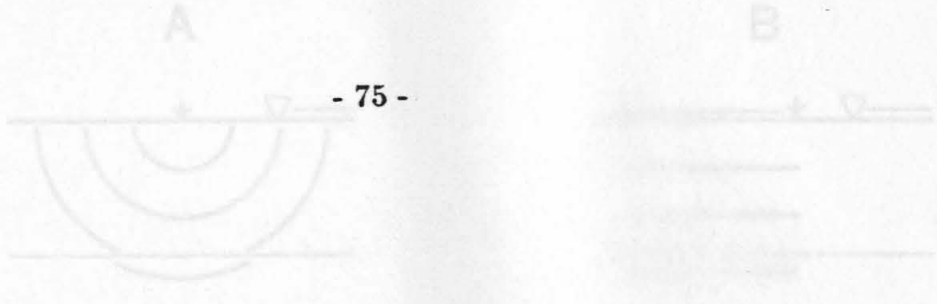


**Fig. 2.10:** Schematic representation of source array concepts designed to increase the amount of energy penetrating the alluvial basin bottom. The cross sections show the wavefronts resulting from the vibrator positions indicated by arrows, with respect to the receivers indicated by triangles. **A:** A single vibrator. **B:** A 290 m long array of 30 simultaneous vibrators, each separated by 10 m. **C:** The same array of vibrators, except that the initiation of each vibrator is delayed from the previous one by  $1/600$  of a second to produce a linear wavefront moving *toward* the receivers with a horizontal apparent velocity of 6 km/s. **D:** The same source array as **C**, with the same delays, except that the wavefront has an apparent velocity of 6 km/s *away* from the receivers. **E:** The same source array, except that a varying, non-linear delay between the subsequent vibrator initiations is introduced to produce a curved wavefront calculated to converge to an approximate point source at a depth just below the modeled basin bottom, and using only that part of the wavefront that propagates away from the receivers.

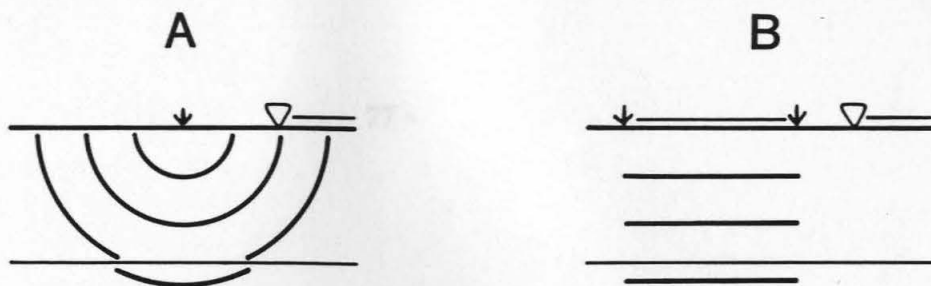
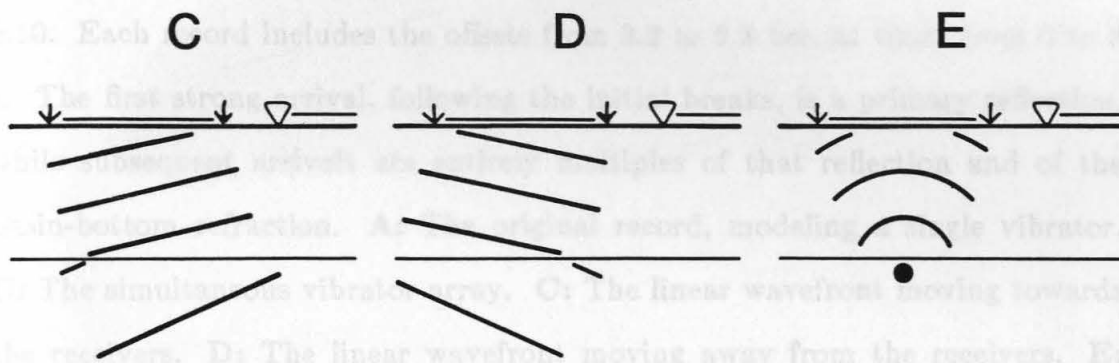
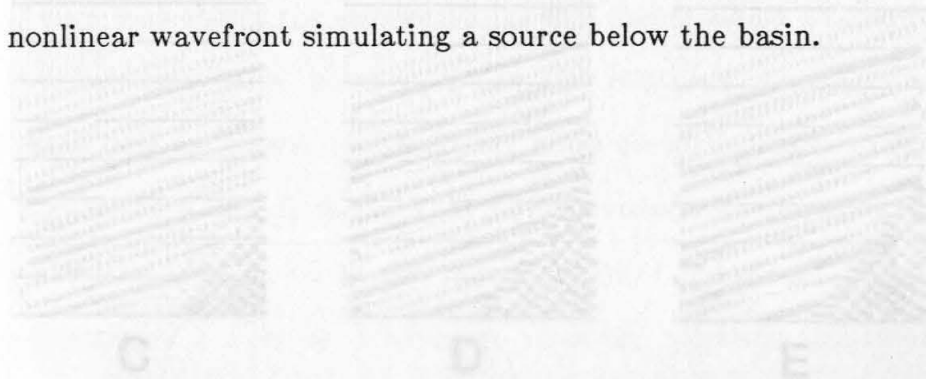


Fig. 2.11: The far offset portion of the synthetic seismogram shown in Fig. 2.8A modified to model different types of wave motion (see Fig. 2.10). Each record includes the offset 2.2 to 2.3 sec. at the top of the



The nonlinear wavefront simulating a source below the basin.

**Fig. 2.11:** The far offset portion of the synthetic record section shown in Figure 2.8A modified to model different types of source arrays given in Figure 2.10. Each record includes the offsets from 3.2 to 6.3 km, at times from 0 to 3 s. The first strong arrival, following the initial breaks, is a primary reflection, while subsequent arrivals are entirely multiples of that reflection and of the basin-bottom refraction. **A:** The original record, modeling a single vibrator. **B:** The simultaneous vibrator array. **C:** The linear wavefront moving towards the receivers. **D:** The linear wavefront moving away from the receivers. **E:** The nonlinear wavefront simulating a source below the basin.





detachment reflections and the basin multiples have virtually the same moveout at large offsets, they do differ in another aspect. The multiples generally show a constant moveout with offset, whereas the apparent velocity of the detachment reflection should decrease as the offset increases, because of its hyperbolic shape. The methods of Harlan et al. (1984) can be used to distinguish events on the basis of their shape. Their methods make use of Bayesian estimations of what parts of a seismic section have been focused by a particular linear transformation. For example, a slant stack should focus straight lines, while a velocity semblance focuses reflection hyperbolae. The method picks out or rejects the focused parts of the transformed section and inverts it to obtain a version of the record in which the shape of event focused by the transform has been enhanced or attenuated.

Figure 2.12 shows the application of this technique to a blast record from the October 1984 noise survey. When the relatively straight first arrivals, basin multiples,  $S_v$  phase, and Rayleigh wave are attenuated by rejecting the most focused part of a slant stack, hyperbolic reflections appear, at least in the nearer offsets. These reflections can be further enhanced by selecting the focused parts of a velocity semblance, although selecting too strongly introduces many artifacts. This method is preferable to simple dip filtering in this situation, since the desired reflections have moveouts similar to the basin multiples. Where dip filtering would find only the reflections at near offsets where they have a very high moveout, the semblance method has some chance of revealing the reflection at all offsets.

The preliminary field experiments showed that the seismic character of the Whipple Mountain detachment is a 5% velocity contrast below the 60-

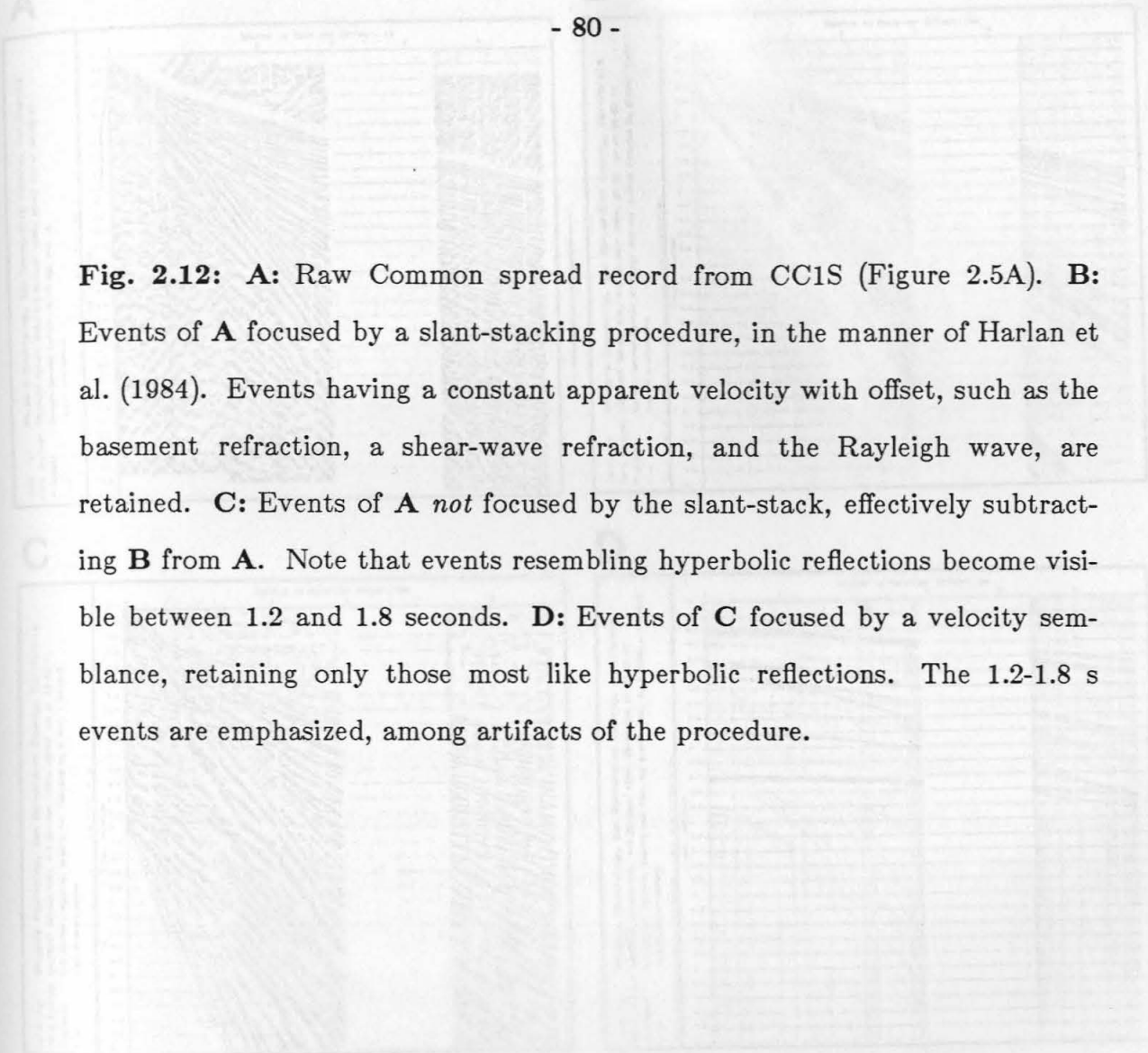
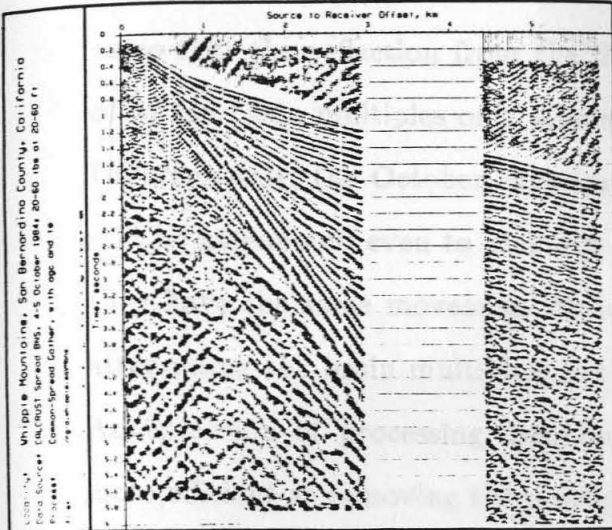
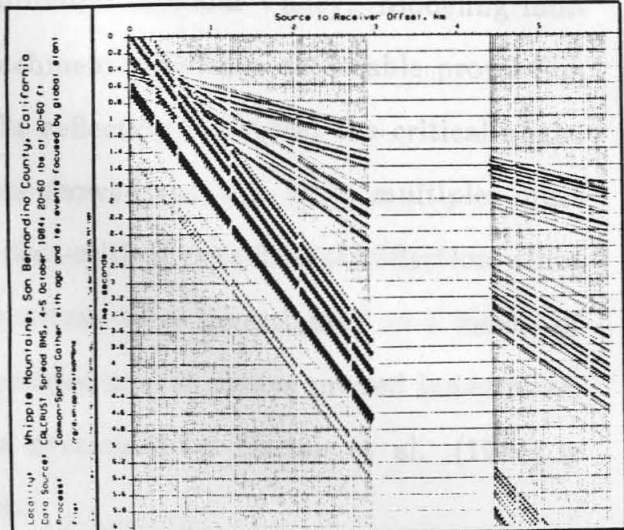


**Fig. 2.12:** **A:** Raw Common spread record from CC1S (Figure 2.5A). **B:** Events of **A** focused by a slant-stacking procedure, in the manner of Harlan et al. (1984). Events having a constant apparent velocity with offset, such as the basement refraction, a shear-wave refraction, and the Rayleigh wave, are retained. **C:** Events of **A** *not* focused by the slant-stack, effectively subtracting **B** from **A**. Note that events resembling hyperbolic reflections become visible between 1.2 and 1.8 seconds. **D:** Events of **C** focused by a velocity semblance, retaining only those most like hyperbolic reflections. The 1.2-1.8 s events are emphasized, among artifacts of the procedure.

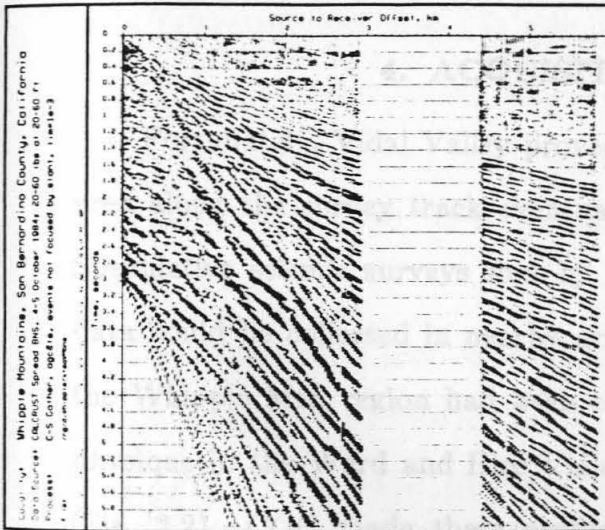
A



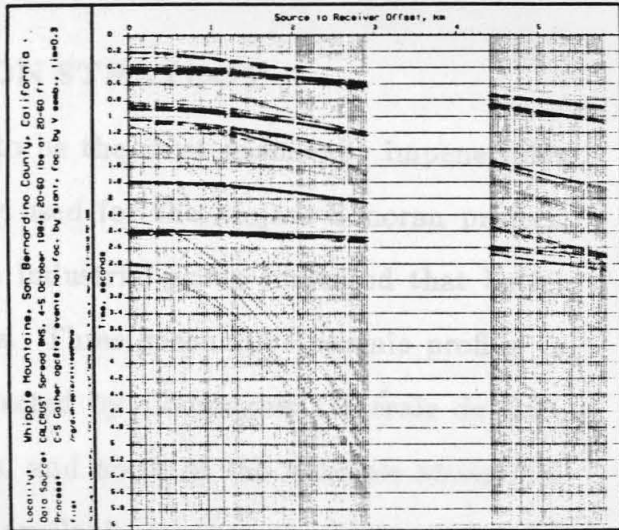
B



C



D



acquisition parameters could be compared to those being used by industry for concrete profiles.

The acquisition parameters used by CCG were the conventional parameters used by speculative industry surveys. They employed a 96 channel symmetric split spread with a receiver group spacing of 33 m, four 20,000 lb (9100 kg) vibrators performing eight 8 to 80 Hz, 12 s sweeps at every record center

100% contrast at the bottom of the alluvium in Vidal Valley. Modeling indicates that the reflection from the detachment reaches a detectable proportion of the basin multiples only where the reflection is beyond the critical angle. Unfortunately, the October experiments showed that the basin multiples must still be attenuated even to pick out a post-critical detachment reflection, since they have the same moveouts. Source arrays were investigated as a means of attenuating the basin multiples, but modeled source arrays proved inadequate. An extension of processing techniques developed by Harlan et al. (1984) is more efficient at removing the multiples.

#### 4. ACQUISITION STRATEGY

Fortunately, Vidal Valley proved to be the most seismically impenetrable area along the survey track eventually used for the Mojave-Sonoran project. Speculative seismic surveys shot by an industrial group indicated that better data could be collected in nearby areas. Three speculative seismic profiles in the Whipple Mts. region had been collected by Compagnie Générale de Géophysique in the Ward and Rice Valleys, and north of the Whipple Mountains (Fig. 2.2). CGG made these profiles available so that the results of CGG acquisition parameters could be compared to those being considered for the Calcrust profiles.

The acquisition parameters used by CGG were the conventional parameters used by speculative industry surveys. They employed a 96 channel symmetric split spread with a receiver group spacing of 33 m, four 20,000 lb (9100 kg) vibrators performing eight 8 to 80 Hz, 12 s sweeps at every second receiver

point. Significantly, the linear geophone arrays were not buried.

Extensive reprocessing of the CGG profiles at Lawrence Berkeley Laboratories (LBL) by David Okaya during early 1985 led to an improvement in the quality of the stacked sections. As was seen in the previous noise surveys, prominent multiply reflected refractions permeated the field gathers. Fourier domain dip filtering to remove the multiples did allow some of the weaker near-offset reflections to stack coherently.

The reprocessed profiles suggested that high quality data might be collected in certain areas near the Whipple Mountains with essentially conventional industry parameters. Frequency analysis of the unstacked and stacked data indicated that only the lower frequency portion of the 8-80 Hz sweep energy was reflected to any significant degree. Surface waves dominated at the inner offset receivers and were spatially aliased at 30 m group intervals. This source generated noise was similar to that recorded in Vidal Valley (Table 2.1).

The reprocessed profiles revealed strong events that could, in Chemehuevi Valley, be correlated with detachment fault exposures in the northern Whipples. (Figure 2.2). The geometry of these events, if they were assumed to arise from detachment surfaces at two levels, suggested that the breakaway zone of the fault could be located as far west as the Old Woman Mountains. This suggestion led the Calcrust consortium to design a survey route that could provide some three dimensional coverage of such structures to the west of the Turtle Mountains.

The geophysical objectives of the Mojave-Sonoran survey, together with the problems of recording in young alluvial basins, demanded that Calcrust

develop an innovative seismic acquisition strategy. Since basement reflections had been recorded in the deeper, older Ward and Rice Valleys by CGG, the consortium decided to realign the survey route to pass through those areas. This path could track shallow detachments exposed in the Old Woman and Whipple Mountains, where they are buried beneath the intervening valleys and the Turtle Mountains (Figure 2.2). At the ends of the route, the survey would approach the surface outcrop of the detachments. The geographic coordinates of the endpoints of the survey lines are given in the Appendix, Table A-1, to an accuracy of 30 m.

Where the detachments are shallow, the alluvium is young and relatively thin, causing the most problems for the preliminary experiments. In these areas a high-resolution survey would be necessary. Close source and receiver spacing would help to resolve surface statics, aid in processing to mitigate source generated noise, and provide high fold for effective stacking. A split spread would be used, since structural dips were expected to vary tremendously. While downdip shooting provides deeper penetration of the refracted arrivals, which are critical for accurate velocity determination, updip shooting would assist in the penetration of energy below the basin bottom and provide more recordings of high amplitude reflections near critical angle. Therefore, both were used, thus demanding a large number of receiver channels so that offsets could be kept relatively long while maintaining a tight receiver spacing. Initial vibrator and receiver geometries and parameters would be taken directly from the previously successful CGG surveys. This would be the main survey, which would roll along the entire route.

At the same time, the detection and characterization of deep crustal reflections require the use of both high fold and long offsets. While the main survey could have been extended to provide tightly spaced receivers out to offsets of 10 km or so, this would have required more recording channels than the budget would allow. As a compromise, the consortium decided to record high fold, long offset deep crustal information from only about one-third of the survey path. Stationary receiver spreads several km long would be set at each end of the three main lines. As the vibrators and the main roll along spreads began working one end of the line, the stationary spread would be laid out at the other end. As the vibrators approached the center of the line, the stationary spread would be relocated at the other end (Figure 2.13). This technique would produce a stretch of midpoints near the center of the line having extremely high fold, reversed recordings with offsets from near 0 to almost 20 km. While this concept would provide unusually high-density deep crustal information, it would cost very little extra, since a separate truck would be used to record the stationary spread. The spread itself, for the three main lines, would have to be planted and moved only six times.

A very important part of the acquisition strategy would be the continuous monitoring of the progress of the survey in the field by Calcrust research seismologists. Each day's records would be displayed and brute stacked within 24 hours of recording, allowing the monitors to change the spread, vibrator, or recording parameters at will, in response to unforeseen problems. Parameters could also be changed rapidly to take advantage of any unexpected opportunities.

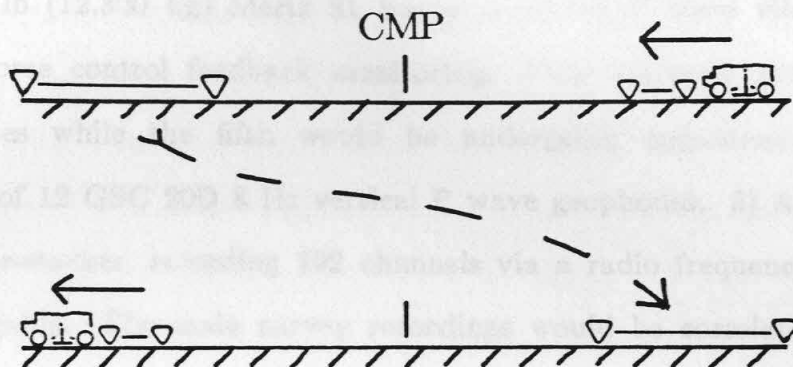


**Fig. 2.13:** Recording spread concept for main and secondary surveys. The vibrator and the receivers rolling along with them (triangles) start on one end of a line, while a stationary spread is placed at the other end of the line. As the roll-along survey reaches the center of the line, the stationary spread is taken up and planted at the other end of the line. This provides reversed, long offset range coverage of a limited interval near the center of the line.

Companie Général de Géophysique, the same contractor that ran the speculative lines in the Ward, Chemehuevi, and Rice Valleys, was selected by the consortium to run the Mojave-Sonoran survey. CGG sent a crew for that main survey that was equipped with: 1) Four 42,000 lb (19,100 kg) Mertz 18 and one 27,000 lb (12,300 kg) Mertz 21 buggy mounted P wave vibrators, equipped with force control feedback monitoring. Four vibrators would be used at all times while the fifth would be undergoing maintenance. 2) Receiver groups of 12 GSC 20D 8 Hz vertical P wave geophones. 3) A Sercel SN-348 correlator-stacker, recording 192 channels via a radio frequency two-wire telemetric cable. The main survey recordings would be correlated and summed prior to being written on the field tape. 4) A Raytheon 500 computer running CGG's Geomax seismic processing system would be within a 1.5 hour drive of every point on the survey. Record sections would be displayed on a 24 inch Gould electrostatic plotter.

The secondary long offset recordings would be made by a Sercel SN-338 stacker. It would be connected to 96 groups of 14 GSC 8 Hz vertical P wave geophones. The 338 would sum but not correlate vibrator sweeps onto the field tape. Further processing would be done on the Digicon DISCO system running on a VAX 11/780 at the Center for Computational Seismology at LBL. All field tapes would be demultiplexed there prior to distribution.

## 5. VIBRATOR SYSTEM FIELD TESTS

Fieldwork began on May 18, 1985. The initial task was to find an adequate set of acquisition parameters for the main high-resolution survey. Several tests were performed at the northernmost end of line WM-1 (Figure 2.2), where the CGG speculative Ward Valley line intersects WM-1. The tests began using the same parameters as the CGG survey, and focused on varying the sweep frequencies, length, and number per record. All sweeps tested were in the range of 8 to 56 Hz, since explosion data recorded by Dix (1965), the Calcrust noise survey, and CGG's speculative work, showed that arrivals returning from below the alluvial section rarely contained substantial energy above 40 Hz. Higher frequencies tended to be incoherently scattered by the rapidly variable young alluvium. In addition, to avoid spatial aliasing of higher frequencies in the extremely slow 1 km/s surface material, the receiver spacing would have to have been decreased to much less than 25 m. This was impractical given budget constraints and the need to record at offsets beyond 1 km to pick up near-critical angle reflections.

The initial tests gave two results. First, lowering the high-frequency end of the sweep to 36 Hz eliminated a substantial amount of the air wave from the correlation without detracting from the frequency content of the arrivals from the upper basement. Second, an intensive effort had to be made to mitigate correlation harmonic ghosts. These harmonics mimic the first arrivals and are nearly as strong, wiping out any reflections from the deeper basement. They were caused by the decoupling of the vibrator pads at low frequencies, particularly at about 18 Hz. When operating at that frequency, the pads could be observed shaking abnormally from side to side.

A number of strategies were investigated to control these harmonics. First, the harmonics were pushed down the record to below 10 s by lengthening the sweep to the hardware maximum of 31 s. Thus the vibrators passed 18 Hz 11.1 s after beginning the sweep, so noise from the decoupling did not correlate with the 8 Hz fundamental of the first arrivals until 10 s into the record. Figure 2.14 shows how previously invisible deep crustal reflections appeared once the 31 s sweep was used. However, second-order harmonics can still be observed throughout the record. The next strategy was to attempt to increase vibrator coupling by operating at one-half drive level, limiting the lowest frequency part of the sweep, or by not moving the vibrators up between sweeps on the same vibrator point, to pack the surface more firmly.

Limiting the lowest frequency drive levels with a 3 s cosine taper, eliminating most energy below 10 Hz, did prove effective in cleaning up some of the harmonics. It also eliminated the usefulness of the force control feedback, which was turned off for the entire project. Otherwise, the only factor that showed any improvement was the variation of the material on the surface at the vibrator points. Most of the survey routes in the Ward Valley are underlain by fine windblown loess. Due to the aridity of the region, the loess has extremely little cohesion. It was often observed billowing out from under a vibrator pad in operation. Better records were obtained when the vibrator point was in a sandy wash.

The loess layer also contributed to the extremely low 1 km/s velocity of the surface alluvial layer. First breaks on the records show that this layer undergoes a sharp transition to somewhat older alluvium at a depth of 50 to 100 m. The underlying material often has a velocity more than twice that of

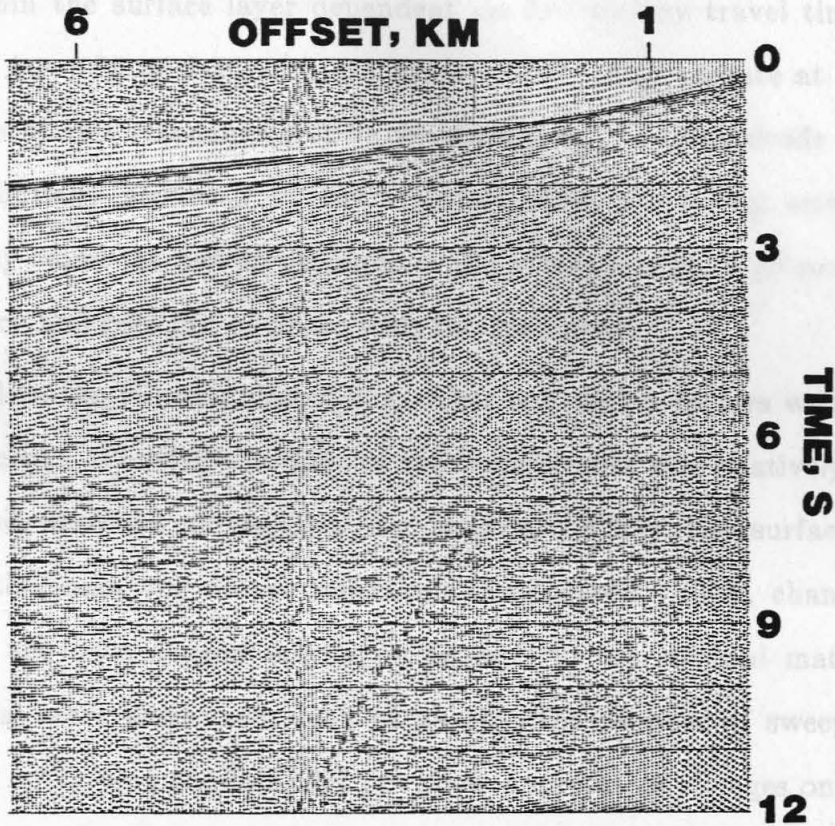


**Fig. 2.14:** Field shot record from the northern end of line WM-5. For this line the receivers are off end to the south of the vibrators. Trace equalization and AGC applied for display. Note the multiply reflected refraction within 1 to 2 s of the first arrival, prominent middle and deep crust reflections between 5 and 11 s and 1 to 6.5 km offset, and vibrator correlation harmonics below 10 s at the nearest offsets.

Once some control over the vibrator stacking problem had been established, the survey proceeded over all of the lines. The line number (Figure 2.5) reflects the order in which each line was vibrated. While survey

the surface layer, forming a reflector with a normal incidence reflection coefficient of more than 30%. This strong near-surface reflector generates resonance within the surface layer dependent on its two-way travel time. In fact, a surface layer 85 m deep with a 1 km/s velocity will resonate at 18 Hz. The amplitude of this resonance will be within an order of magnitude of the displacement initially produced by the vibrator. This continuing motion of the surface may cause the pad to decouple as the vibrator tries to proceed to a higher frequency and goes out of phase with the resonance.

Compared to the vibrator decoupling, other acquisition factors were relatively insignificant. Where the surface of the survey route was relatively firm, reflections were observed throughout the records. Where the surface was covered with the loess, the deeper reflections disappeared. Thus, changes in the quality of the data depend mostly on changes in the surficial materials. Other tests that were performed, such as varying the number of sweeps per vibrator point, or varying the fold, did not show appreciable changes on brute stacks prepared in the field, nor on those prepared at LBL. Therefore, it was decided to keep those parameters at the maximum level of effort that would still allow the project to complete the necessary line mileage within the budget.

## 6. ACQUISITION PARAMETERS

Once some control over the vibrator decoupling problem had been established, the survey proceeded over all of the lines. The line number (Figure 2.2) reflects the order in which each line was vibrated. While survey

production was under way, quality control monitoring by Calcrust personnel was concentrated into two efforts. First, continuing attention had to be kept on geophone plants. In most areas, the loose nature of the surface materials and the occasional winds demanded that each geophone be buried under several cm of sand, with the lead wires also clamped down by piles of sand. A few areas were covered by a clay hardpan, which made the use of picks necessary to make holes for the geophone spikes. The jugs then had to be buried in addition.

The second effort was continuous monitoring of the data quality, using the field processing center. Representative field records were displayed daily on the electrostatic plotter. Each day's production was also added to a growing brute stack of the line, usually within 24 hours of recording. This monitoring assured us that, insofar as the decoupling problem would allow, data quality did not decrease from other causes. It also allowed us to increase the station spacing on lines WM-2 and WM-5 to gain mileage, while observing that the resolution of complex shallow structures did not decline unacceptably. In all, 108 km of seismic data were collected on the main lines between May 18 and June 14, 1985. The Appendix gives detailed information on the acquisition parameters used during different phases of the survey.

The sizes of source and receiver arrays were kept to a minimum to try to take advantage of the relatively close station spacing. Horizontally propagating source-generated noise could have been filtered out by employing arrays a few hundred meters long. However, such a strategy would have canceled the gain in horizontal resolution derived from the close spacing. Arrays were made only as long as necessary for efficient field operations. Another advantage of

relatively short source and receiver arrays is the cancellation of some of the random noise caused by wind and rapid variations in the properties of the surface layer.

The stationary long offset arrays were deployed around the centers of three lines to provide the densely spaced, wide offset range data needed for analysis of deep crustal reflections. The Ward and Danby arrays provided coverage over line WM-1, the Milligan and Freda arrays for WM-2, and the Rice and Savahia arrays for WM-3. Merging the main and long offset data would provide about 10 km of midpoints spaced between 75 and 100 m apart, each with a gather often exceeding 100 or 200 fold having reversed offsets to beyond 20 km. At a minimum, first arrivals were recorded on every trace of the long offset data.

The Rice array was also used to good advantage in a unique survey of midpoints within Rice Valley, between the Rice array and line WM-5. It was recorded as the vibrators were working both on the westernmost part of WM-3, and on WM-5. Using sources on both sides of the valley provided many midpoints in the center with recordings of deep reflections at a number of different azimuths. Variations in amplitude or arrival time as a function of azimuth may be resolvable into constraints on anisotropy within the lower crust.

The long offset recordings from the 338 had to be extended correlated to yield 12 s records to match those from the main 348 recorder, as done by Okaya (1985). This process resulted in a gradual loss of the highest sweep frequencies in the parts of records beyond 9 s, with 33.3 to 36 Hz energy being lost at 12 s. This loss is not significant, however, since little energy was

returned from below the alluvial section in that frequency range.

To image reflections above 5 seconds two-way travel time, special pre-stack processing had to be undertaken both in the field processing center and at LBL. While a frequency-wavenumber domain dip filter is not effective in distinguishing near-critical angle reflections from the multiply reflected basement refractions (or basin multiples), because of their similar moveout, it is able to attenuate the multiples while leaving the stronger reflections at near normal angles. This allowed the upper crustal part of the survey to be stacked, showing the strongest of the reflections arriving at less than 5 s. This upper dip filtered stack was combined with a conventional stack of the lower crustal data, again, both in the field center and at LBL.

## 7. DESCRIPTION OF THE DATA

The field record from line WM-5 in Figure 2.14 is demonstrative of several features of the data from all the main high resolution lines. Picking the first arrivals on many gathers reveals that the survey is generally underlain by a three-layer sedimentary section up to 2 km thick, including the very slow 1 km/s surface layer 50-120 m deep. The underlying sedimentary units have velocities from 2 to 4 km/s. Basin bottom refractions show basement velocities between 5.2 and 5.8 km/s. The basin bottom contrast creates the strong multiply reflected refractions parallel to the first arrival that can be seen above 5 s. These remain even in the data from the deeper basins because the extremely low surface velocity, and conservation of ray parameter, cause any energy propagating down from the vibrators at more than 12° from vertical to

be critically reflected at the basin floor.

The vibrator decoupling correlation harmonics, possibly due to the resonance in the slow surface layer, appear below 10 s time on Figure 2.14, mimicking the first arrival. The surface layer resonance has an important effect on the frequency content of all reflections in the data. Essentially, the power spectrum of any arrival is multiplied by a raised cosine, the frequency periodicity of which depends on the travel time through the surface layer. The resulting peakedness of the spectra limits the frequency content of any particular reflection to a band as narrow as 5 Hz. This band limiting manifests itself on the records in the extended, multi-cycle character of many of the reflections. While the multi-cycle character could be due to structure at the reflector, the similar character of the first arrivals indicates that the cause is more likely in the surface layer.

The above phenomena, demonstrated in the field records, have important effects on the stacked sections. The basin multiples and vibrator harmonics weaken the stacks where they are present, causing some areas above 5 s and below 10 s to stack without showing appreciable reflections. The boundaries between these apparent "reflective" and "transparent" zones are due almost entirely to the limits of contamination by source-generated noise. Further, most of the stacked reflections have a multi-cycle character, because of the surface layer resonance.

These effects can be demonstrated in the stack of the high-resolution data from line WM-1, in Figure 2.15. The most prominent events are the top of a Tertiary volcanic section above 2 s two-way travel time, and basal crustal events between 8 and 10 s. The basal events seem to form a double zone near

**Fig. 2.15:** Brute stack of the high-resolution roll-along data from line WM-1. Prominent reflections include the top of a Tertiary volcanic section above 2 s two-way travel time, middle crustal events between 5 and 7.5 s, and the basal crustal events near 9 s.



-97-

the center of the stack, pinching down to a single reflection near the sides. This feature underlies the thickest part of the sedimentary basin, suggesting that the double zone may be a multiple within the basin. However, the time between the basal events is not equal to the time of the basin bottom reflection. Further, other mid-crustal events do not show the same doubling.

The region below the basal events appears to lack reflections. This is, however, simply a result of stacking over the harmonics below 10 s. A few field records with less strong harmonics do show the presence of events within this interval. The region below the basin bottom reflection, above about 5 s is similar. Here the presence of the multiply reflected refractions have allowed only the strongest reflections to stack in at a few places. Thus, while there may appear to be sharp break between the non-reflective and reflective crust at a time just below 5 s, this is surely an artifact.

Almost all of the events in Figure 2.15 have a multi-cycle character. This is true even for those events observed to have just a single cycle on the CMP gathers. Lateral velocity heterogeneities have deformed the multi-offset hyperbolae of the reflections to the point that the same events at different offsets will stack in at slightly different times. This effect is aggravated by the resonance in the surface layer, which severely limits the bandwidth of the reflections. The deep events show the effects of this the most. Thus, whether an event has a single or multi-cycle character in this stack is primarily dependent on factors not at all related to the nature of the reflector itself.

The best advantage of the data from the stationary, long offset arrays can be taken by sorting them into common midpoint (CMP) gathers along with the data from the main high-resolution survey. Figure 2.16 shows the stacking

**Fig. 2.16:** Stacking diagram for the merged main high resolution and the stationary long offset experiments from line WM-1. VP-101 is the northern terminus of WM-1 (Figure 2.2). The light dots indicate receiver positions; the heavy dots show midpoint locations. Common midpoints line up vertically in this representation.

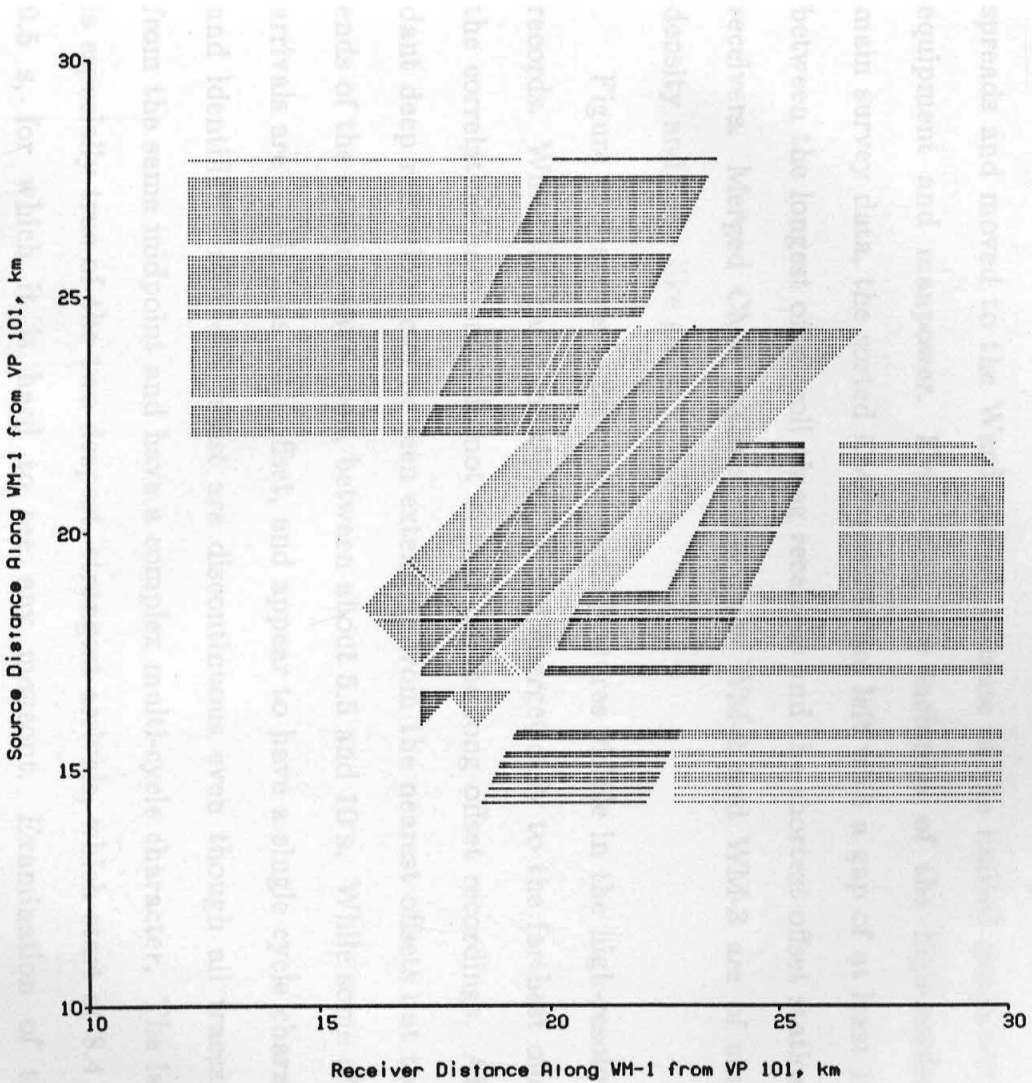
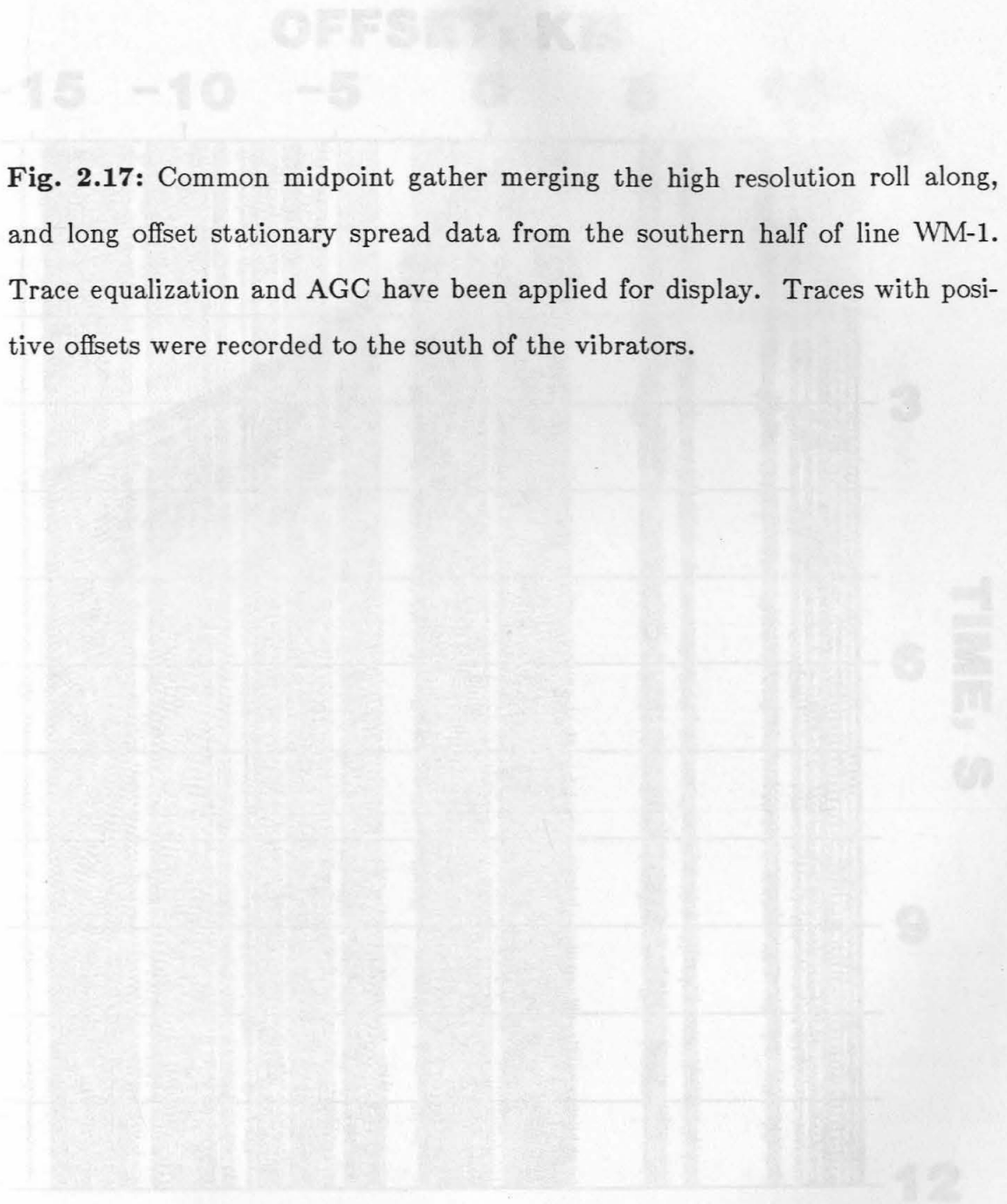


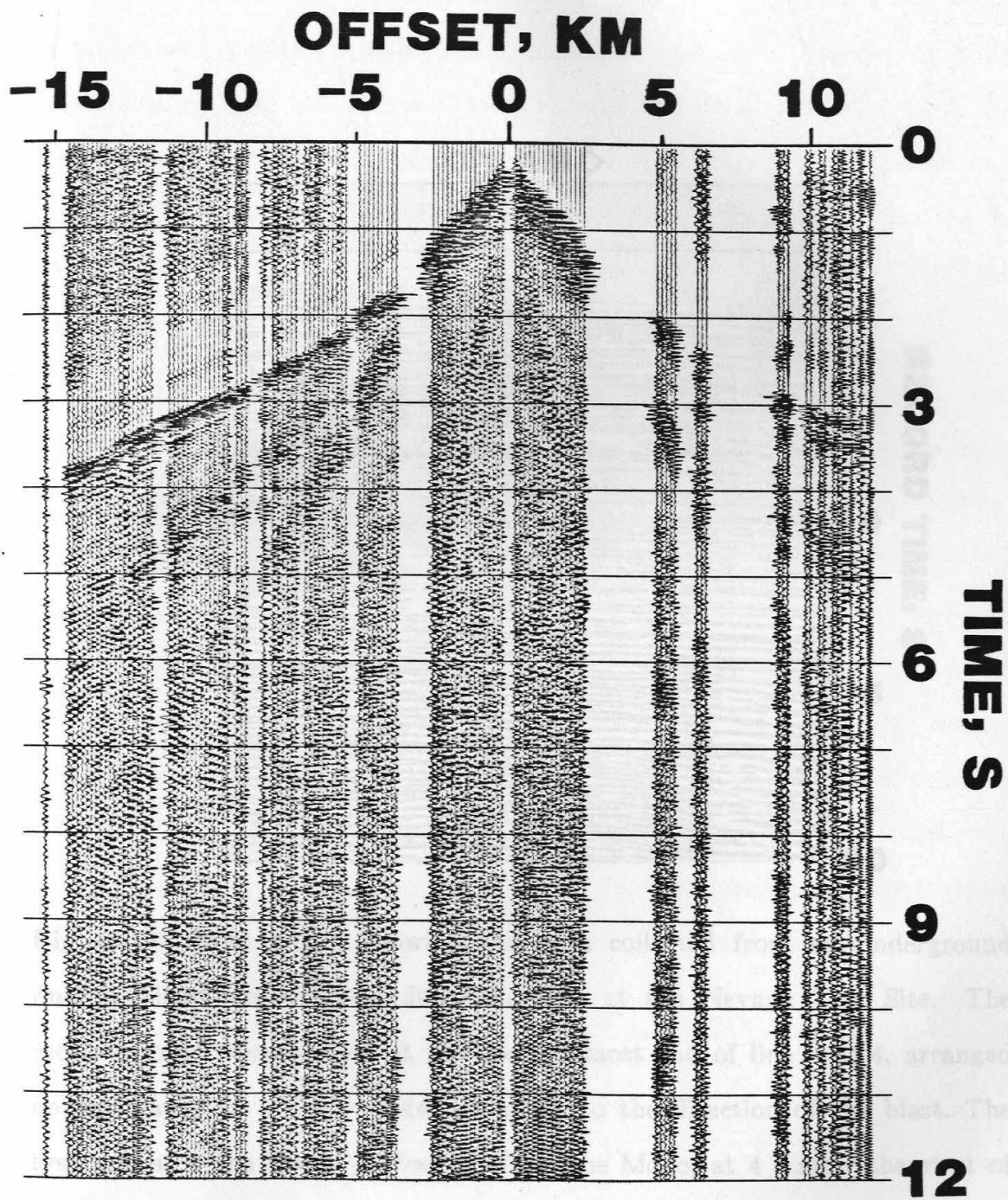
Figure 1. Scatter plot of source distance versus receiver distance for stations along WM-1. The plot shows a strong positive correlation between source and receiver distances, indicating that stations closer to the source also tend to be closer to the receiver. The axes range from 10 to 30 km.

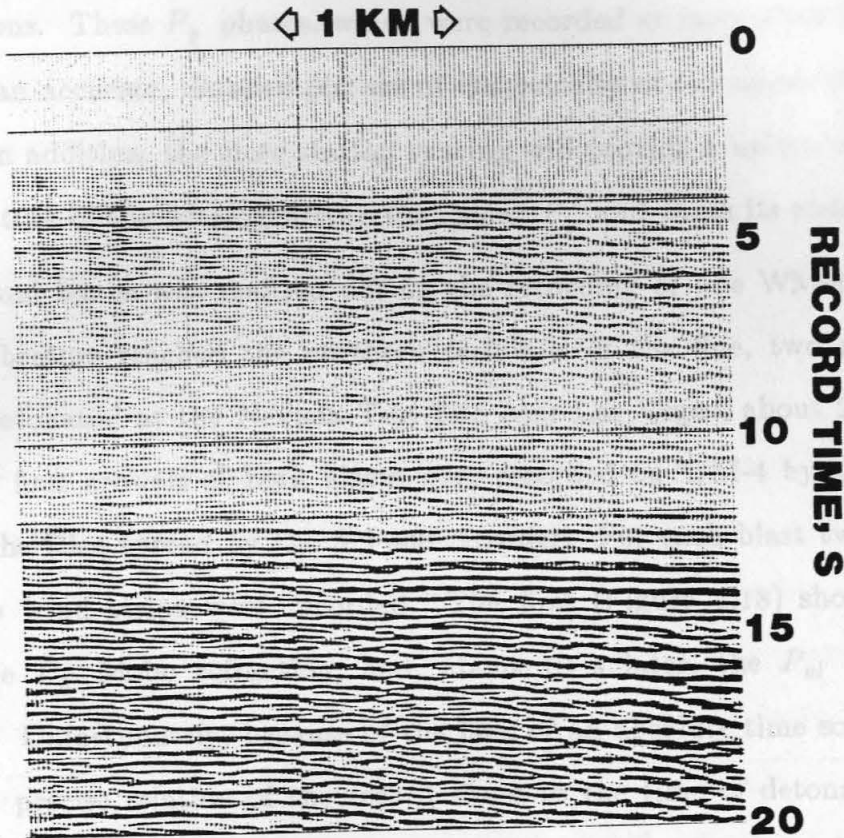
diagram resulting from this process for the short and long offset data from line WM-1. One of more than 80 of these gathers that have more than 100 fold, from the southern half of WM-1, is shown in Figure 2.17. The gaps in offset resulted from VPs missed by the secondary SN-338 recorder due to instrument or radio problems. The northern half of the Danby spread was removed before the vibrators reached the midpoint of the Danby and Ward spreads and moved to the Ward spread, because of the limited availability of equipment and manpower. Even with the inclusion of the high-resolution main survey data, the sorted CMP records are left with a gap of at least 1 km between the longest offset roll along receivers and the shortest offset stationary receivers. Merged CMP gathers from lines WM-2 and WM-3 are of similar density and have like gaps.

Figure 2.17 shows some of the same features visible in the high-resolution records. While the basin multiples extend energetically to the farthest offsets, the correlation harmonics do not appear on the long offset recordings. Abundant deep reflections can be seen extending from the nearest offsets out to the ends of the surface wave coda, between about 5.5 and 10 s. While some of the arrivals are continuous with offset, and appear to have a single cycle character and identifiable moveout, most are discontinuous even though all traces are from the same midpoint and have a complex multi-cycle character. The latter is especially true of the two deepest, strongest arrivals, which start at 8.4 and 9.5 s, for which it is hard to see any moveout. Examination of these reflections in many gathers reveal that apparent static offsets of the upper reflection do not appear in the lower reflection. Such a feature could result only from either rapid structural variations or from strong lateral velocity



**Fig. 2.17:** Common midpoint gather merging the high resolution roll along, and long offset stationary spread data from the southern half of line WM-1. Trace equalization and AGC have been applied for display. Traces with positive offsets were recorded to the south of the vibrators.





**Fig. 2.18:** Field record showing the data collected from an underground nuclear blast detonated on June 12, 1985 at the Nevada Test Site. The receivers used were located at the northernmost end of line WM-4, arranged approximately in a line oriented obliquely to the direction of the blast. The first arrival is the P-wave refraction from the Moho, at 4 s after the start of the record, more than 60 s after detonation.

inhomogeneities just above the upper reflector.

The merged long and short offset data have refractions from the upper basement as their most prominent first arrivals. The reason a stationary array was placed at each end of the three lines was to provide reversed offsets for these refractions. These  $P_g$  phases, which were recorded at more than 20 km, should allow an accurate, detailed picture of the velocity of the upper crust to be derived. In addition, the close station spacing will provide a unique evaluation of the nature of the heterogeneities that affect  $P_g$  and cause its coda.

An unusual bonus was realized during the recording of line WM-4. Just before the vibrators reached the northern terminus of the line, two nuclear blasts were detonated at the Nevada Test Site near Las Vegas, about 200 km distant. The first arrivals of both blasts were recorded on WM-4 by the SN-348 and on the Rice spread by the SN-338 recorder. For each blast two consecutive 50 s wind strips were recorded. The first (Figure 2.18) shows the arrival of the  $P_n$  Moho refraction, and, about 10 s later, the  $P_{ni}$  crustal guided wave. Unfortunately, because of the lack of an absolute time source in the field, the precise relation of the record times to the time of detonation is not known. However, the primary interest in these recordings lies in their uniquely dense spacing, compared to conventional seismograms of regional phases.

surface outcrops. Detachment reflections would, even under ideal conditions, have to be imaged at frequencies close to 300 Hz where the structures are shallow. Given the highly heterogeneous nature of the overlying volcanics and alluvium, using such high frequencies would have been impossible. Therefore, the objectives of the survey had to be redefined to the imaging of detachment relations beneath the deeper basins, and the characterization of deeper

## 8. CONCLUSIONS

As has been discussed above, the principal geophysical problem encountered by the Calcrust Mojave-Sonoran project was to find a method that would allow energy to penetrate below the low-velocity alluvial layers. The surface velocity was so slow, about 1 km/s as measured during the preliminary experiments, that any energy propagating down from the vibrators at more than  $12^\circ$  from vertical would critically reflect at the bottom of the sedimentary section. Since ray parameter is conserved, this is true even for the deeper sedimentary basins that do not have such a sharp contrast at the bottom. Thus, the largest proportion of energy from the source and from the up going reflections is trapped within the alluvium as multiples.

Such a low-velocity surface layer could be expected to cause similar effects in any arid region covered by aeolian sediment to some degree. Synthetic seismograms showed that, for pre-critical reflections from the target detachment surfaces, the reflection arrivals would be 40 dB below the multiples in amplitude. Even post-critical reflections, having an amplitude similar to the multiples, would still be invisible because of their similar moveout.

It was these relative amplitude considerations that made it impossible for the Mojave-Sonoran survey to truly trace the detachments in seismic sections to their surface outcrops. Detachment reflections would, even under ideal conditions, have to be imaged at frequencies close to 300 Hz where the structures are shallow. Given the highly heterogeneous nature of the overlying volcanics and alluvium, using such high frequencies would have been impossible. Therefore, the objectives of the survey had to be redefined to the imaging of detachment relations beneath the deeper basins, and the characterization of deeper

structures. In the process of defining new objectives, speculative industry data proved invaluable.

Calcrust's problems with the slow surface layer point out the need to pay close attention to the geophysical nature of the shallowest part of the geological section in the planning of a deep crustal survey. The effects of shallow layers are quite site-specific and demand the constant attention of geophysicists in the field, backed up by careful preliminary seismic experiments and wave equation modeling. The ability to alter acquisition parameters during a survey can be crucial both to the successful detection of reflections and to their correct interpretation.

The above points are demonstrated by three effects in the Mojave-Sonoran data. First, reverberation within the surface layer due to the doubling of velocity at its base caused the vibrators to decouple at particular frequencies. If the field processing system had not been available to allow identification of the problem, and the vibrator sweep had not been lengthened, the survey's results would have been poor indeed. Second, the stacks show "reflective" and "transparent" zones that, more often than not, have more to do with the presence in the unstacked data of source-generated noise. Only with careful analysis, such as Harlan's (1984) semblance techniques, can the absence of reflections within a particular interval be established. Third, the reflections that are imaged are fundamentally affected by the shallow layers. The narrowing of reflection bandwidth by the reverberation in the surface layer gave many of the reflections a multi-cycle character that has nothing to do with the reflector itself. Characterization of the reflectors can be accomplished only through the interpretation of effects in the multi-offset data that

must arise within the deep structure.

The need to make reflector interpretations from multi-offset data made it necessary to put receivers at long offsets. While the offsets in the main high resolution survey were long enough for the interpretation of reflectors to a few km depth, a strategy had to be developed to record inexpensively at much longer offsets. The use of stationary spreads at each end of three of the lines proved effective in providing limited areas with dense, high fold, reversed mid-point coverage at offsets to 20 km. Both  $P_g$  refractions and deep reflections were recorded at all offsets, which will allow the development of better upper crustal velocity models along with the determination of constraints on the nature of deep crustal structures.

While the Mojave-Sonoran survey cost several times per kilometer what a standard reconnaissance deep crustal survey would have, the expense of both the greater amount of scientific effort and of the high-resolution recording were well justified. It is doubtful that such a standard survey could have imaged any significant reflections in this area. Further, an understanding of the seismic nature of the area is crucial to the proper interpretation of the imaged reflections. Ignorance of the details of the shallowest section could have led to erroneous interpretations of the deepest structures.

### Chapter 3

## Constraints on the Physical Nature of Deep Crustal Structures in the Mojave Desert, California

### ABSTRACT

Understanding crustal processes hinges on knowledge of the physical nature of the deep crust. Rock properties and physical condition can be constrained through analyses of reflection waveforms at multiple offsets prior to stacking. This analysis proceeds in two steps. First, an increase in reflection peak frequency with offset is indicative of a thinly layered reflector. The thickness and velocity contrast of the layering, calculated from the spectral dispersion, can be used to discriminate between structures resulting from broad scale or local effects. Second, the amplitude effects at different offsets of high frequency P-P scattering from weak elastic heterogeneities indicate whether the signs of the changes in density, rigidity, and Lamé's parameter at the reflector agree or are opposed. The effects of reflection generation and propagation in a heterogeneous, anisotropic crust are contained by the design of the reflection experiment and the simplicity of the observed amplitude and frequency trends.

Three available datasets from the Mojave Desert incorporate wide offsets sufficient for the lower crust. A 100 km COCORP line in the western Mojave, a 1962 shot gather recorded by C. H.

Dix, and the 1985 Calcrust Ward Valley survey share clear deep crustal records but differ in geometric coverage. Multi-offset spectra and amplitude trend stacks suggest that the most reflective structures in the middle crust are strong Poisson's ratio contrasts. Porous zones or the juxtaposition of units of mutually distant origin are indicated. Heterogeneities in Poisson's ratio increase towards the top of a basal crustal zone, which may be stable at  $\sim 22$  km depth. The transition to the basal zone and to the mantle include increases in Poisson's ratio. The Moho consists of at least one layer  $\sim 400$  m thick, having a velocity higher than that of the uppermost mantle. The configuration of the Moho is constant over the Mojave despite 5 km of crustal thinning near the Colorado River. This indicates that Miocene extension there either thinned just the basal zone, or that the basal zone developed regionally after the extensional event.

## 1. INTRODUCTION

The purpose of the work presented here is to begin to understand the physical nature of reflectors in the deep crust. While the geometries of such structures have been adequately imaged by several projects, their geological interpretation has been guided only by indirect evidence. Our approach is to analyze the reflected energy in detail at varying angles of incidence in order to constrain possible lithologic models.

Reflections from structures deep below the Mojave desert were first recognized by Dix in 1965. His careful fieldwork allowed him to define the strikes and dips of many mid crustal reflectors and the Mohorovicic (Moho) discontinuity within a small area of the central Mojave. The multiplicity and strength of the reflections he recorded led him to believe that the velocity of the crust could oscillate as a function of depth, rather than increase monotonically. The much more extensive COCORP survey across the western Mojave (Figure 3.1) succeeded in imaging the geometry of several deep crustal reflectors over a wide area (Cheadle et al., 1986). With the exception of one reflection which they believe can be traced to surface exposures, their geologic interpretation of the middle and deep crustal reflections was guided solely by their geometry. They consider all of the major reflectors to be detachment fault structures. Not included in their interpretation is the possibility, proposed by Kosminskaya in 1964, that crustal velocity discontinuities can be viewed as the effect of physical conditions such as pressure or temperature.

Both of the above surveys made use only of the arrival time and "character" of the recorded reflections in their interpretations. The character of the reflections evaluated is their average character (i.e. of stacked traces) over the entire source-to-receiver offset range of the experiment. However, much more information is available in the multi-offset seismograms, which can constrain the physical properties of the reflector, such as the changes in compressional and shear velocity and density. I will separate the problem of inverting the seismograms for such properties into two parts. The first-order problem is whether the reflector constitutes an abrupt change in these properties (a step discontinuity); is a more gradual variation over some depth range (a gradient);

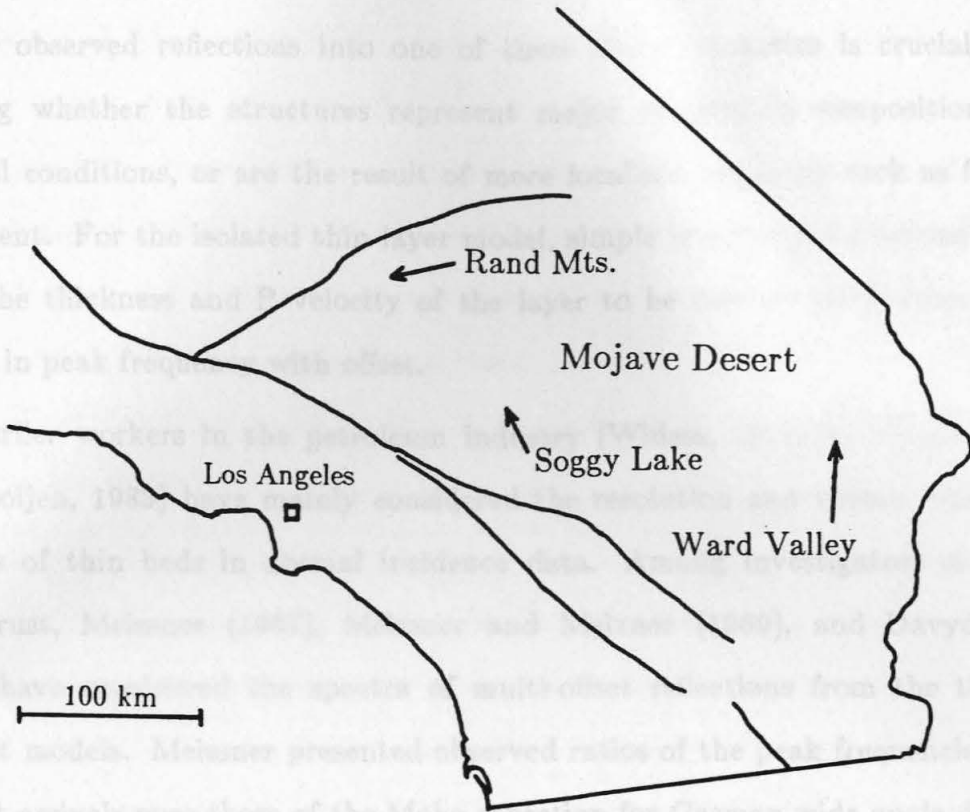


**Fig. 3.1:** Map of southern California giving the locations of deep crustal reflection surveys in the Mojave Desert. Major faults are also shown.

or is composed of layers having thicknesses on the same scale as the seismic wavelength, the simplest case of which is an isolated thin layer. The ability to classify observed reflections into one of these three categories is crucial for deciding whether the structures represent major changes in composition or physical conditions, or are the result of more localized processes such as fault movement. For the isolated thin layer model, simple interference relations will allow the thickness and P velocity of the layer to be derived solely from the change in peak frequency with offset.

Earlier workers in the petroleum industry (Widess, 1973; de Voogd and den Rooijen, 1983) have mainly considered the resolution and seismic characteristics of thin beds in normal incidence data. Among investigators of the deep crust, Meissner (1967), Meissner and Meixner (1969), and Davydova (1972) have considered the spectra of multi-offset reflections from the three different models. Meissner presented observed ratios of the peak frequencies of the first arrivals over those of the Moho reflection for German wide angle data, which showed that the reflection peak frequency decreases at critical angle. Meissner and Meixners' reports of sample calculations for thin layers did not mention any distinguishing effects at pre-critical angles. Davydova, and Mikhota (1972) found their most convincing evidence for layering in the spectral variations between pre- and post-critical reflections. Mair and Lyons (1976) did, however, suggest that deep layering would produce sufficient changes in the frequency of reflections, at the wider pre-critical angles, to interfere with the stacking process. Fuchs (1969) also made complex reflectivity synthetics of the reflections resulting from layered structures that show an increase in frequency as offset increases over the subcritical range.

The spectra of normal incidence reflections were used to support the concept of a layered Moho and to derive layer thicknesses on the order of 100 m by Clowes and Kanasewich (1970), and Meissner (1973). Later workers (Hale and Thompson, 1982; Jones and Nur, 1984; Jones, 1985) combined these ideas with laboratory measurements of candidate rock types for deep crustal reflectors and the Moho to support the thin layer model as the cause of high-amplitude normal incidence reflections observed on deep seismic reflection sections. A straightforward extension of these concepts (Figure 3.2) allows more detailed interpretations to be made of the reflections observed in deep crustal data from the Mojave.

The second-order problem in discovering the physical properties of a reflector is to use the variation of reflection amplitude with offset to yield information on the relative changes in the velocities and density. Such information is needed to decide whether the structures represent changes in mineralogy or are due to changes in physical properties such as porosity or anisotropy. By applying these two types of analysis to the observed reflections, a direct evaluation of differing geologic models for the history of the crust in southern California will be possible.

The effects of different contrasts in physical properties on reflection amplitudes as a function of offset can be calculated from the solutions of the Zoeppritz equations for plane waves incident on a plane reflector as given by Aki and Richards (1980, p. 150). The reflection power is, however, a complicated function of several variables, even at pre-critical angles. Approximations of the solutions to the Zoeppritz equations, such as those given by Shuey (1985) and Wu and Aki (1985), can help to simplify the inversion of an observed

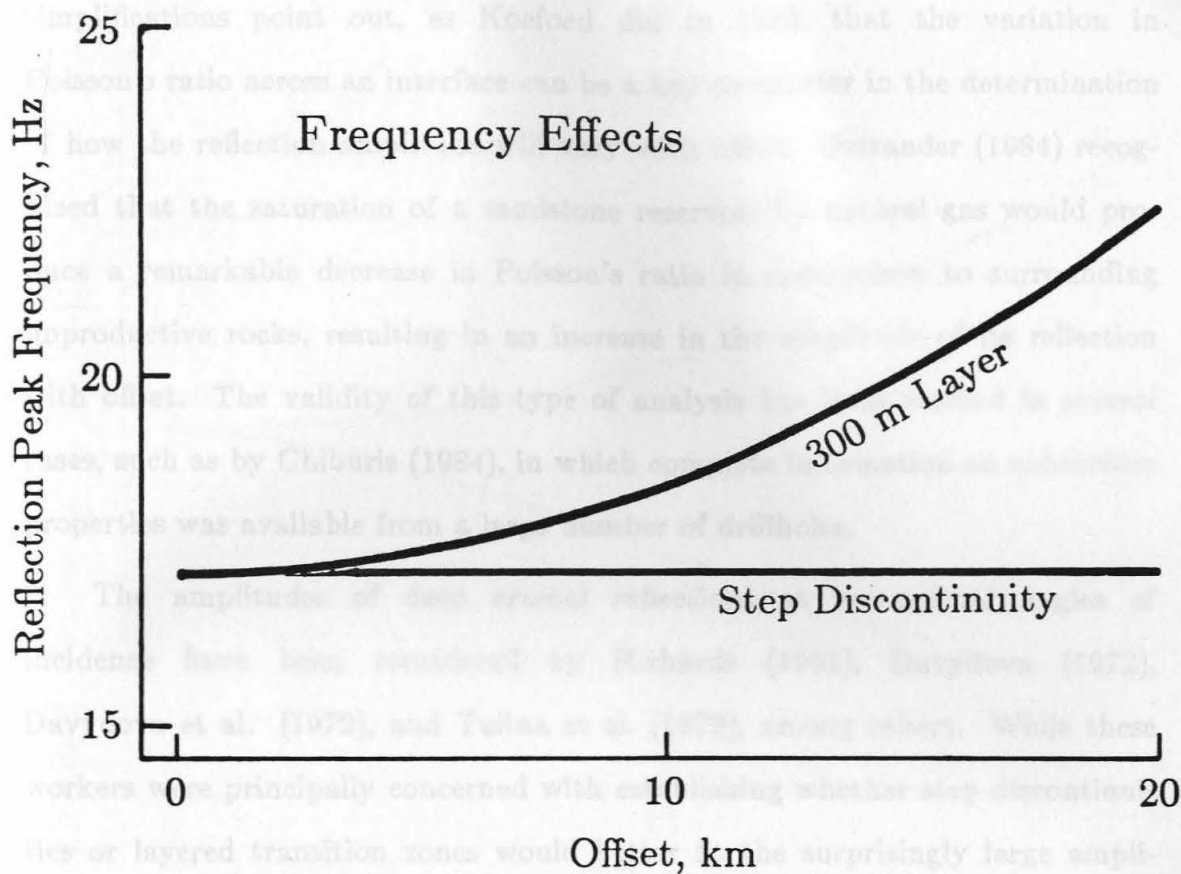


**Fig. 3.2:** Comparison of the reflection peak frequency at different offsets from a thin layer and step discontinuity at 15 km depth. The angle of incidence was calculated from the offset using the low velocity granitic layer model of Table 3.2.

In order to analyze the physical properties at depth, one must find the variations of amplitude with angle of incidence of the reflector. Unfortunately,

amplitude-offset relation to a physical property contrast. Shuey's simplifications point out, as Koefoed did in 1955, that the variation in Poisson's ratio across an interface can be a key parameter in the determination of how the reflection amplitude will vary with offset. Ostrander (1984) recognized that the saturation of a sandstone reservoir by natural gas would produce a remarkable decrease in Poisson's ratio in comparison to surrounding unproductive rocks, resulting in an increase in the amplitude of its reflection with offset. The validity of this type of analysis has been verified in several cases, such as by Chiburis (1984), in which complete information on subsurface properties was available from a large number of drillholes.

The amplitudes of deep crustal reflections at non-normal angles of incidence have been considered by Richards (1961), Davydova (1972), Davydova et al. (1972), and Tulina et al. (1972), among others. While these workers were principally concerned with establishing whether step discontinuities or layered transition zones would better fit the surprisingly large amplitudes observed for crustal and Moho reflections, they did not consider the possibility that variations in Poisson's ratio might also produce these effects. However, for a large set of likely contrasts in the deep crust, which follow Koefoed's simplifying assumptions, the gross relation of amplitude to offset can be ascribed to changes in Poisson's ratio. Where Poisson's ratio increases with depth more strongly than density varies, the reflection power will increase as offset lengthens. Conversely, where Poisson's ratio decreases or density changes drastically, the reflection power will decrease with offset (Figure 3.3).

In order to analyze the physical properties at depth, one must find the variations of amplitude with angle of incidence *at the reflector*. Unfortunately,

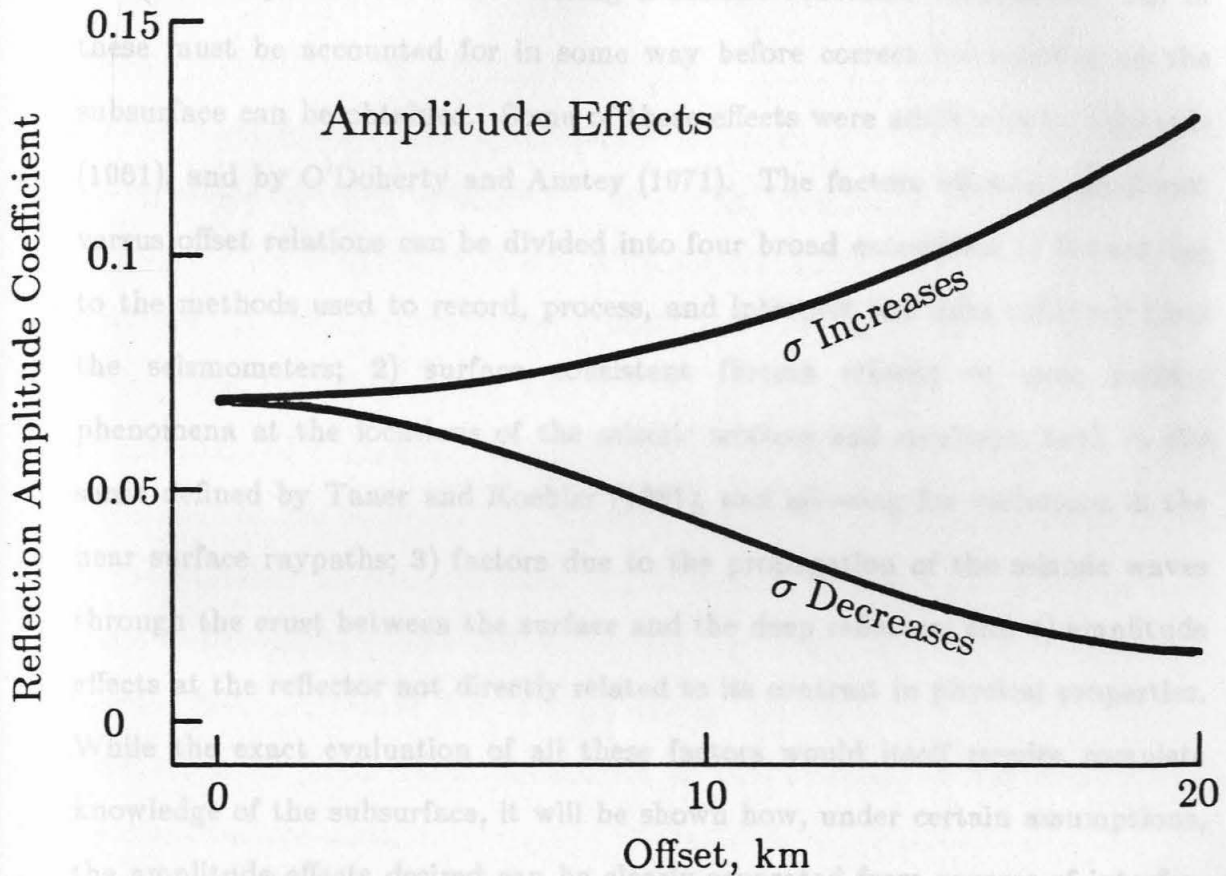


**Fig. 3.3:** Comparison of reflection amplitudes at different offsets from an increase in Poisson's ratio from 0.347 to 0.392 and from a decrease from 0.347 to 0.292 at 12 km depth. The angle of incidence was calculated from the offset using the low velocity granitic layer model of Table 3.2.

there are many factors not related to the deep reflectors that often interfere with the amplitudes recorded during a seismic reflection experiment. All of these must be accounted for in some way before correct information on the subsurface can be obtained. Some of these effects were addressed by Richards (1961), and by O'Doherty and Anstey (1971). The factors affecting amplitude versus offset relations can be divided into four broad categories: 1) factors due to the methods used to record, process, and interpret the data collected from the seismometers; 2) surface consistent factors related to near surface phenomena at the locations of the seismic sources and receivers, both in the sense defined by Taner and Koehler (1981), and allowing for variations in the near surface raypaths; 3) factors due to the propagation of the seismic waves through the crust between the surface and the deep reflector; and 4) amplitude effects at the reflector not directly related to its contrast in physical properties. While the exact evaluation of all these factors would itself require complete knowledge of the subsurface, it will be shown how, under certain assumptions, the amplitude effects desired can be clearly separated from sources of interference.

With this in mind, I should point out that this study will not attempt to invert a measured relationship of reflection amplitude to offset for the exact physical property contrasts. The data from the Mojave Desert are contaminated with a variety of effects that preclude the measurement of the precise amplitude responses of the reflectors. It is often advantageous to be able to examine the seismic data in as raw a form as possible, as done by Mazzotti (1984), in order to keep the physical phenomena surrounding the seismic experiment firmly in mind. The most simple analysis techniques, such the

basic determination of whether reflection amplitudes increase or decrease with offset performed by Long and Richgels (1985), can often yield the most information on fundamental crustal phenomena.

It is important to find questions on the nature of the deep crust that may be answered through examination of strong, diagnostic phenomena. Such basic issues as whether, or where, metamorphic fluids may exist at depth, as proposed by Welder and Nur (1984), can be addressed through these phenomena. Far from being simply an academic exercise, the identification and location of changes in the physical condition of the crust can have broad implications. For example, Sibson (1984) proposed that the location and shape of the boundary marking the onset of greenschist facies metamorphism in fault zones could control the nucleation and size of earthquakes. Simple amplitude versus offset analysis of deep crustal seismic reflection data in active regions may serve to locate these boundaries so fundamental to the history and mechanics of the crust.

iment that resulted in reversed, high fold common mid-point (CMP) records with offsets to 15 km over a substantial portion of three lines. Chapter 2 of this thesis describes the setting, acquisition, and initial processing of this dataset. This paper will begin with an analysis of the highest quality data, recorded on line WM-1. The results from this experiment have prompted the recording of a new dataset by Calcrust in Apple Valley in the central Mojave, close to Dix's profile, in December, 1986. The results from this survey will be reported in the future.

## 2. DATASETS USED

Four datasets exist from the Mojave desert that include reflections from reasonably far offsets. C. H. Dix's survey between Soggy and Melville Lakes in the central Mojave (Dix, 1965, Figure 3.1) produced essentially one high fold shot gather with offsets to 13 km. These records of deep reflections are, even to this day, unusually good. The COCORP Mojave survey (Cheadle et al., 1985, 1986) recorded several lines in the western Mojave. The longest line (line 3) totaled 92 km with offsets to 10 km.

The Calcrust consortium of California universities collected a total of 108 km of seismic reflection profiling in May and June of 1985. The survey was located along five lines in the Ward, Rice, and Vidal Valleys of the eastern Mojave Desert, southeastern California (Figure 3.4). While the main objective of the survey was to collect high-resolution seismic reflection data from the shallow part of the crust, the consortium was able to augment the main survey with a secondary experiment that resulted in reversed, high fold common midpoint (CMP) records with offsets to 15 km over a substantial portion of three lines. Chapter 2 of this thesis describes the setting, acquisition, and initial processing of this dataset. This paper will begin with an analysis of the highest quality data, recorded on line WM-1. The results from this experiment have prompted the recording of a new dataset by Calcrust in Apple Valley in the central Mojave, close to Dix's profile, in December, 1986. The results from this survey will be reported in the future.

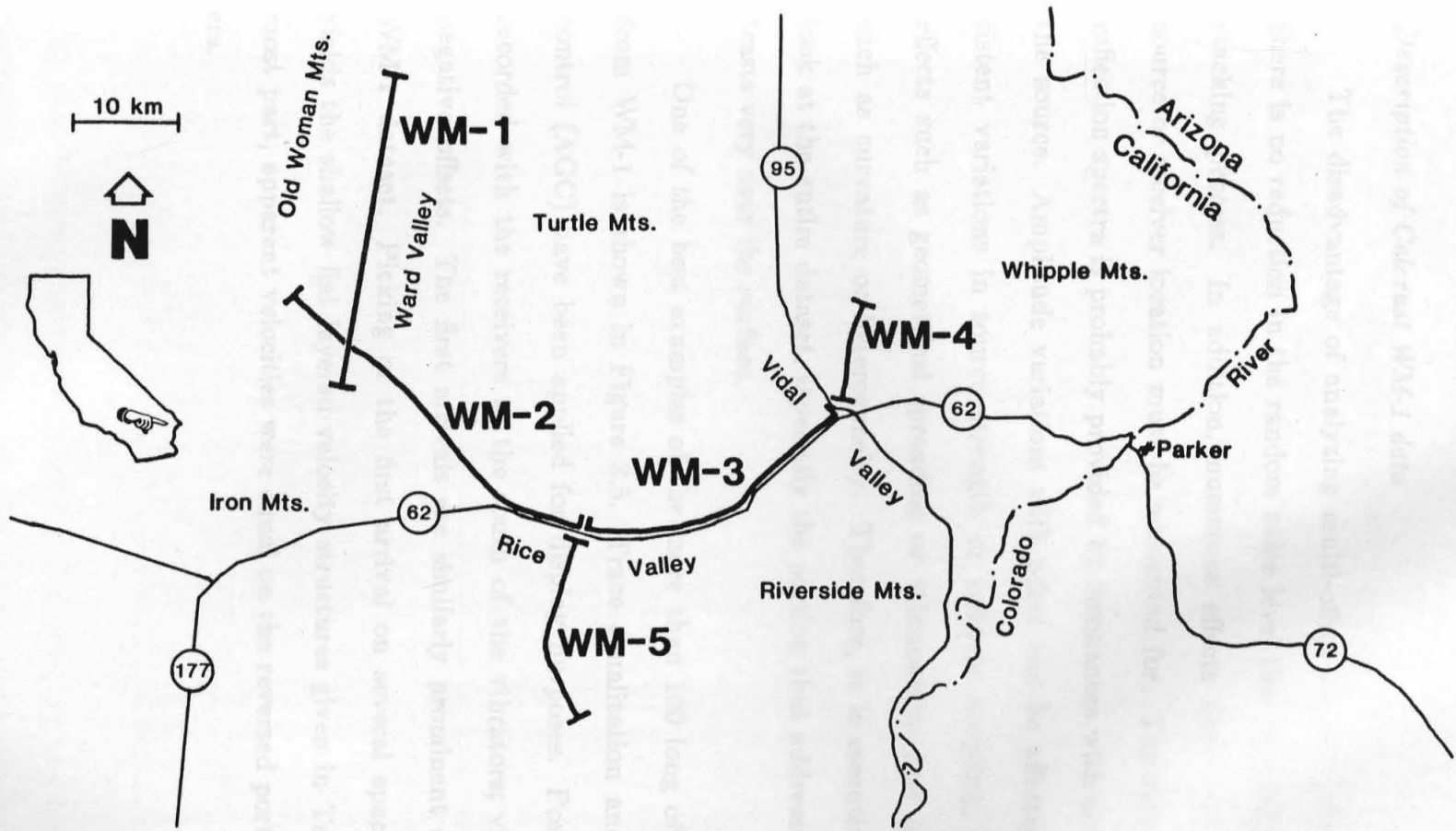


**Fig. 3.4:** Map of a portion of southeastern California showing the location of the May-June 1985 Calcrust Mojave-Sonoran project. The five high-resolution seismic reflection lines are designated WM-1 through WM-5. Major highways are also indicated.

### *Description of Calcrust WM-1 data*

The disadvantage of analyzing multi-offset seismic reflection data is that there is no reduction in the random noise level that is usually provided by the stacking process. In addition, numerous effects that vary with offset, and source or receiver location must be accounted for. The largest interference in reflection spectra is probably provided by resonances with shallow layers below the source. Amplitude variations with offset can be affected by surface consistent variations in source strength or receiver coupling, propagation path effects such as geometrical spreading or attenuation, and by reflector effects such as curvature or heterogeneity. Therefore, it is essential to take a close look at the entire dataset, especially the portion that addresses the strong contrasts very near the surface.

One of the best examples of the more than 100 long offset CMP gathers from WM-1 is shown in Figure 3.5. Trace equalization and automatic gain control (AGC) have been applied for display purposes. Positive offsets were recorded with the receivers to the south of the vibrators; vice versa, for the negative offsets. The first arrivals are similarly prominent over most of the WM-1 dataset. Picking of the first arrival on several spaced CMP gathers yields the shallow flat layered velocity structures given in Table 3.1. For the most part, apparent velocities were equal on the reversed portions of the gathers.

Fig. 3.5: Common midpoint (CMP) gather merging the high resolution and long offset data from the southern half of line WM-1. Trace equalization and automatic gain control (AGC) have been applied for display.

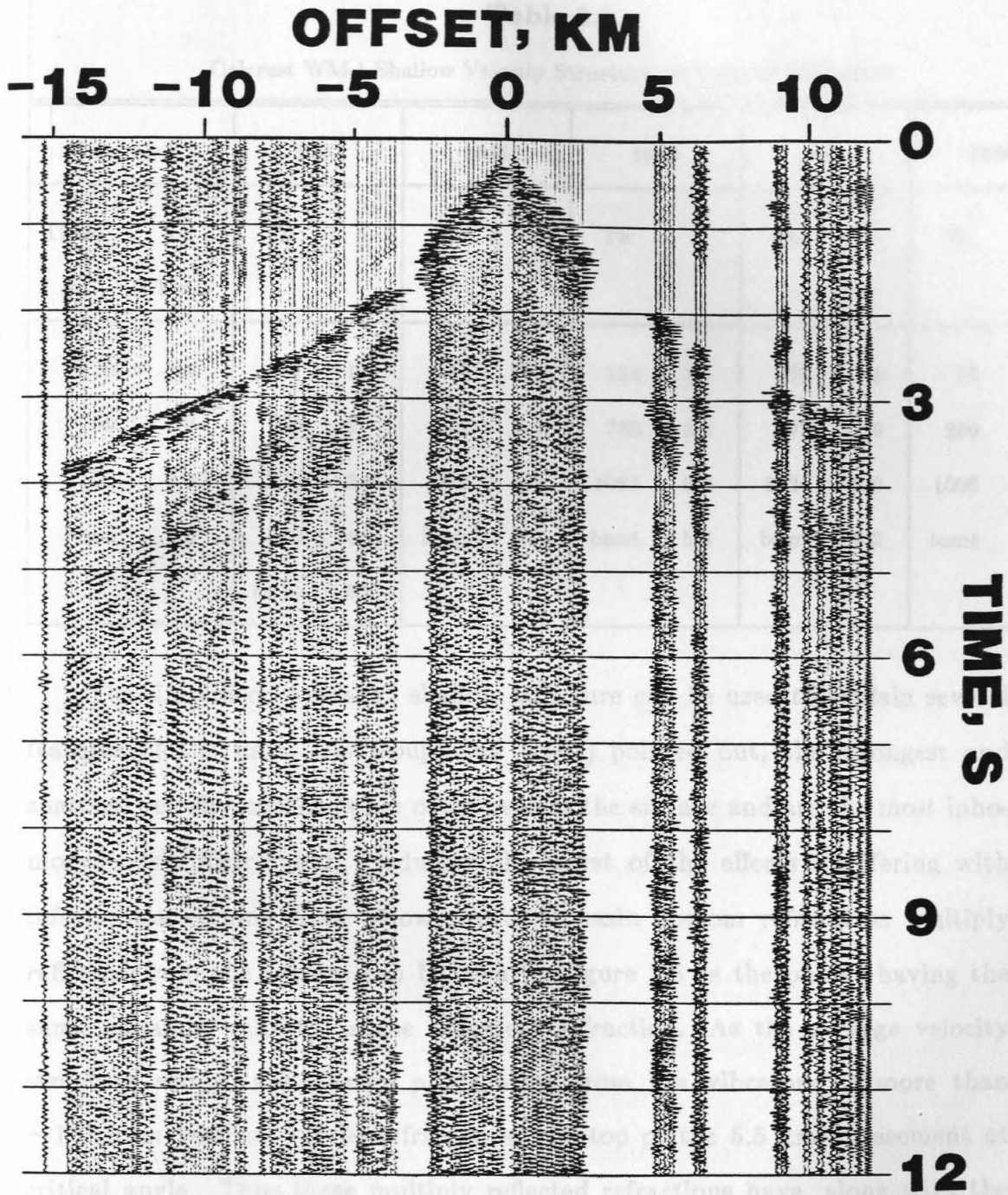


Fig. 3.5: Common midpoint (CMP) gather merging the high resolution and long offset data from the southern half of line WM-1. Trace equalization and automatic gain control (AGC) have been applied for display.

**Table 3.1**

Calcrust WM-1 Shallow Velocity Structures at Selected Midpoints

"average"		1590		1644		1653		1665		1686	
Thick., m	Vel., km/s	Th	V								
120	1.1	87	1	51	0.9	124	1.1	67	1.1	75	1
750	2.4	240	2	342	1.9	750	2.4	297	1.9	260	2
1100	3.8	840	2.8	1376	2.9	1082	3.8	1324	2.9	1006	2.4
bsmt	5.5	1110	4.1	bsmt	5.8	bsmt	5.4	bsmt	5.3	bsmt	5.2
		bsmt	5.8								

The simplified "average" shallow structure can be used to explain several features of the data. As Goupillaud (1961) pointed out, the strongest and sharpest velocity contrasts are often nearest the surface and are the most inhomogeneously distributed, producing the worst of the effects interfering with information coming from below. Alluvial basin bottom refractions multiply reflected from the surface can be seen in Figure 3.5 as the phases having the same apparent velocity as the basement refraction. As the average velocity structure shows, any energy propagating from the vibrators at more than  $\sim 12^\circ$  from vertical will be refracted at the top of the 5.5 km/s basement at critical angle. Thus these multiply reflected refractions have, along with the surface waves, contained most of the seismic energy within the shallow sedimentary section.

The low velocity of the surface layer also provides an important advantage for multi-offset analyses. Since no energy propagates below the basin bottom that was incident at more than  $12^\circ$  from vertical, even wide-angle reflections from deep structures propagate nearly vertically immediately beneath the source and receiver. For this reason the effects of source and receiver array size, angle dependent sensitivity of the vertical geophones, and angle dependent radiation from the vibrators are all negligible. This fortuitous situation can also be found in the datasets from the central and western Mojave.

Another prominent feature of the gather in Figure 3.5 is the presence of vibrator correlation harmonics below 10 s on the offsets of less than 3 km. These were caused by the decoupling of the vibrator pads from the ground as the sweep passed between 18 and 19 Hz, a phenomenon that was consistently observed in the field. It was this feature that made the use of the long 31 s sweep necessary, to push the 18-19 Hz harmonics of the first arrival down to 10 s below the start of the sweep. The moveout of the first arrival takes the harmonics down below 12 s on the long offset traces, so they are not a problem there.

The decoupling of the vibrators at 18-19 Hz may have been caused by resonance within the low velocity surface layer. The velocity increases so sharply at the bottom of the layer that the reflection coefficient at normal incidence would be more than 30%, even assuming there is no density variation. This will produce strong resonances at particular frequencies proportional to the travel time through the surface layer. Perhaps the vibrators caused a resonance that peaked at just under 18 Hz and then went out of

phase with the still strongly resonating ground surface as the sweep progressed through 18 and 19 Hz, resulting in decoupling that produced the harmonics. This is a topic of active research within the Calcrust consortium.

The resonance of the surface layer has an important effect on the frequency content of the seismic waves that propagate downward to impinge on the reflectors of interest. We can call these waves resulting from the resonance triggered by the vibrators the "source" waves. At the surface, the source wave  $s(t)$  can be described as the wave produced by the vibrators  $v(t)$  plus the normal incidence reflection from the bottom of the surface layer:

$$s(t) = v(t) + R_0 v(t - \tau_0) , \quad [3.1]$$

where  $R_0$  is the normal incidence reflection coefficient at the bottom of the surface layer, and  $\tau_0 = 2h_0/v_0$  is the two-way travel time through a surface layer of thickness  $h_0$  and velocity  $v_0$ . The power spectrum  $S_s(f)$  of the source wave is then given by:

$$S_s(f) = S_v(f) (1 + R_0^2 + 2R_0 \cos 2\pi\tau_0 f) , \quad [3.2]$$

where  $S_v(f)$  is the power spectrum of the vibrator input, and  $f$  is the frequency. Thus, the spectrum of the source wave traveling down out of the surface layer will be the spectrum of the vibrator input multiplied, for the very low velocity surface layer present in Ward Valley, by an only slightly raised cosine. Essentially the same result is found by Shugart (1944), who also considered multiple reflections. Dix (1965) thought that this resonance contributed to the narrow frequency range of the deep reflections he observed in the central Mojave. The effect of such a source on the reflection spectra will be seen in a section below.

The gather in Figure 3.5 shows good examples of the reflections that are examined in this work. Abundant deep reflections can be seen extending from the nearest offsets out to the bottom of the surface wave, between about 5.5 and 10 s. While some of the arrivals are continuous with offset, appear to have a single cycle character and identifiable moveout, most are discontinuous and have a complex multi-cycle character, even though all traces are from the same midpoint. The latter is especially true of the two deepest, strongest arrivals, which start at 8.4 and 9.5 s, for which it is difficult to see any moveout.

Figure 3.6 is a stack of all the merged CMP gathers from the primary and secondary experiments on line WM-1. It includes only the reflections from below 5 s two-way travel time, or about 12.4 km. The method used to calculate it will be discussed in the section on amplitude analysis below. The discontinuous nature of most of the deep crustal reflections allows them to be imaged well over some range of high stacking velocities. Several short, though prominent, reflections are apparent between 5 and 8 s. Some appear to dip to the north. The strong double arrivals are present between 8.5 and 10.2 s, although they may pinch down into one towards the south. The second arrival is not a sedimentary basin multiple of the first; stacks of the shallow high-resolution data for all of WM-1 show that the separation between the two is not in general equal to the two-way travel time to the basement. In addition, the two arrivals do not pinch down into one at the places where the sediments thin. If the second arrival were a multiple of the 8.5 s arrival, one would also expect to see multiples of the strong mid crustal reflections, which are not present. In general, the stack shows that a large number of target

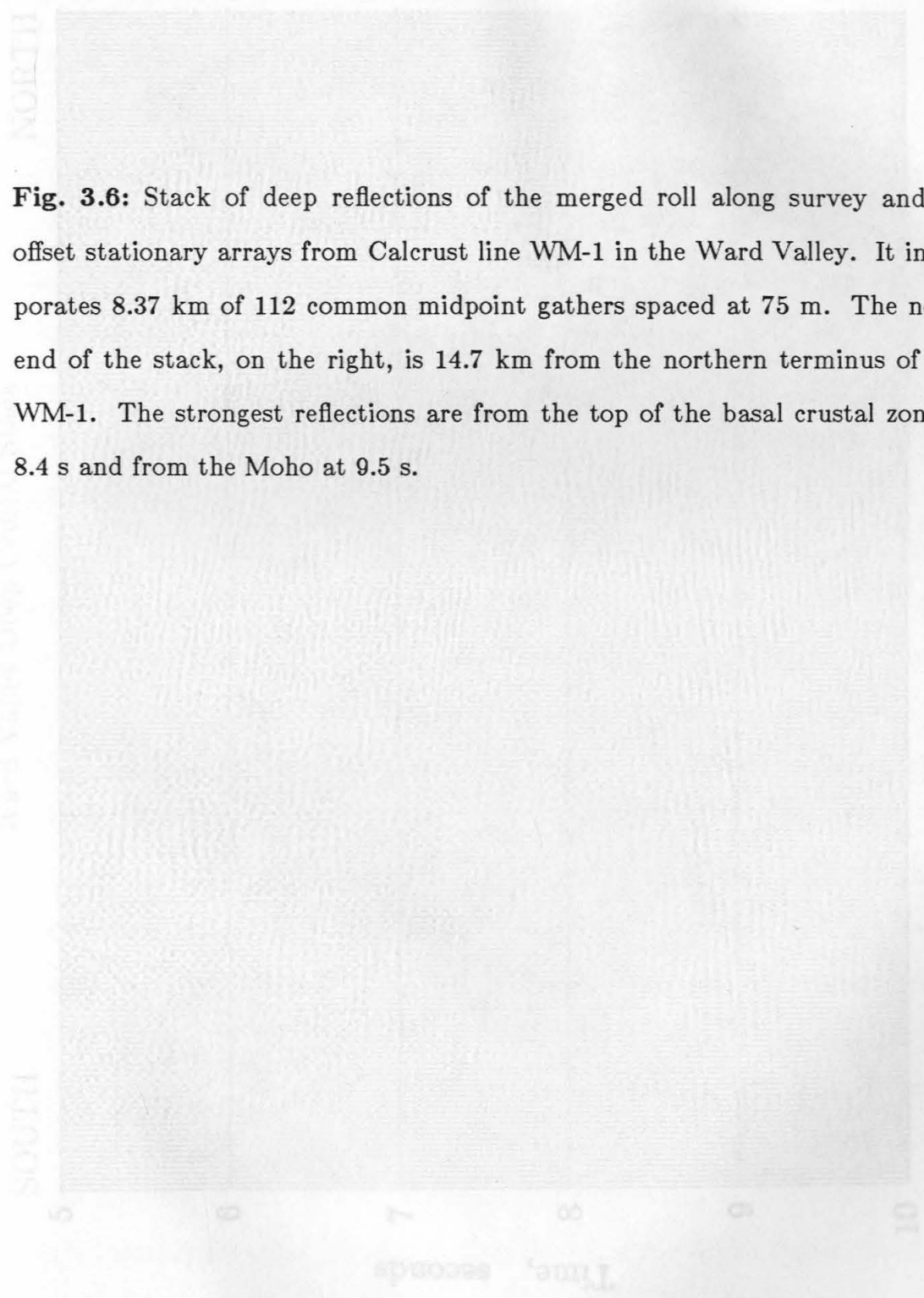
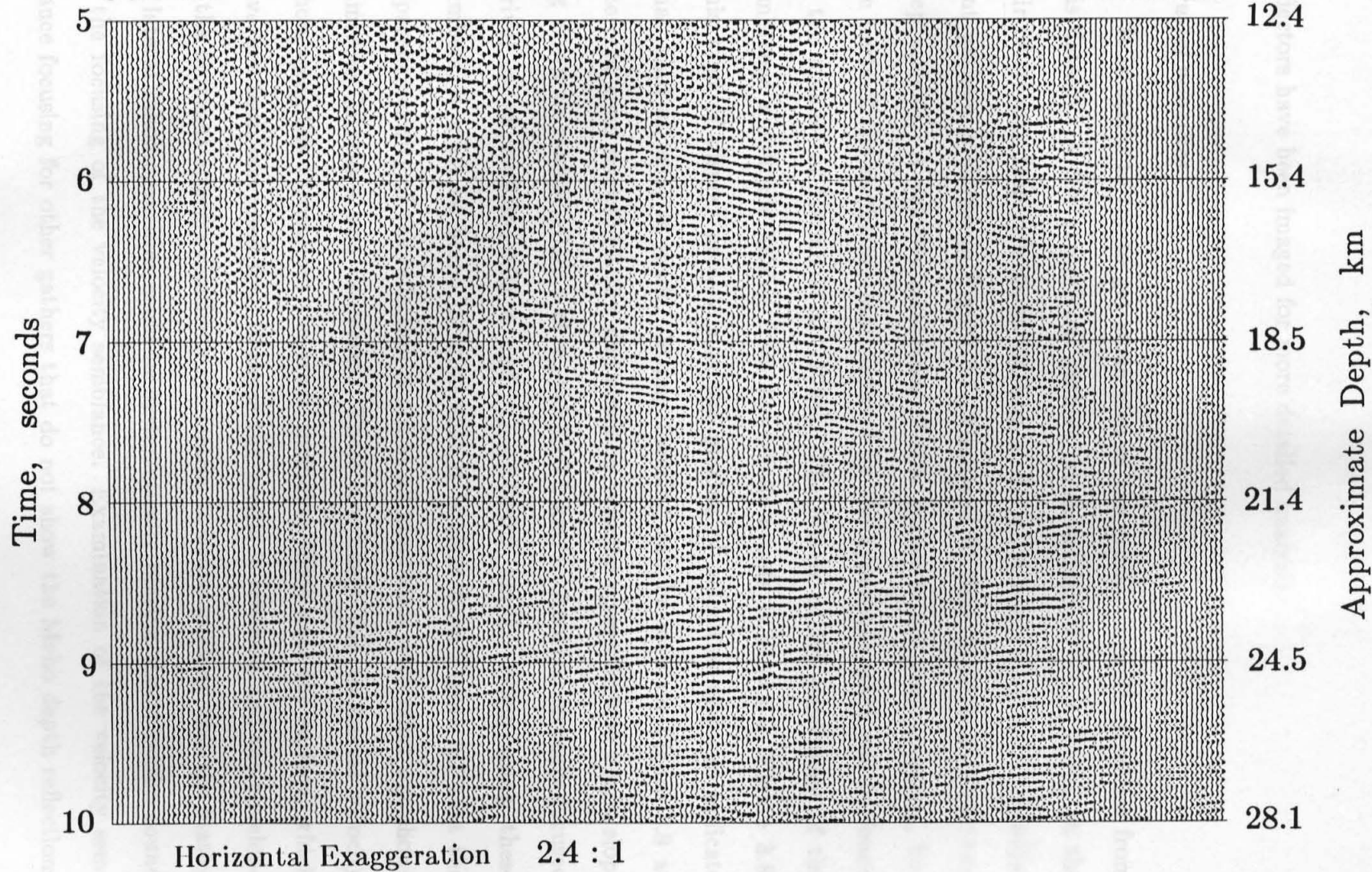


**Fig. 3.6:** Stack of deep reflections of the merged roll along survey and far offset stationary arrays from Calcrust line WM-1 in the Ward Valley. It incorporates 8.37 km of 112 common midpoint gathers spaced at 75 m. The north end of the stack, on the right, is 14.7 km from the northern terminus of line WM-1. The strongest reflections are from the top of the basal crustal zone at 8.4 s and from the Moho at 9.5 s.

Ward Valley Deep Crustal Stack

SOUTH

NORTH



reflectors have been imaged for more detailed analysis.

### *Crustal velocities*

It is useful to try to get some idea of the crustal velocity structure from this dataset. A few exceptional gathers do show identifiable moveout on the pair of strong, deep reflections starting at 8.4 s. A composite of 3 such adjacent gathers is shown in Figure 3.7, windowed in time to show just the two deep arrivals. A velocity semblance of this gather is not very revealing, but the parts of the semblance most focused by the hyperbolic stack can be found in the manner of Harlan et al. (1984). The matrix of the percentage of the semblance amplitude arising from hyperbolic events is shown in Figure 3.8. This kind of display greatly aids the picking of velocities and can indicate what kind of error is made. Strong focusing can be seen on Figure 3.8 at intercept time  $\tau=8.45\pm 0.02$  s and stacking velocity  $v_{st}=4.6\pm 0.05$  km/s, sloping down to  $\tau=8.57\pm 0.02$  s at  $v_{st}=5.5\pm 0.1$  km/s. Another strongly focused arrival is at  $\tau=9.36\pm 0.03$  s and  $v_{st}=5.6\pm 0.2$  km/s. When using these numbers, it must be borne in mind that it is clear from Figure 3.7 that the apparent velocity of the reflection is not at all monotonic with offset but shows numerous increases and decreases. These are likely due to lateral velocity inhomogeneities throughout the crust, including those near the surface, which have not been corrected for. Because the profile is reversed and the envelope of the moveout appears relatively symmetric, it seems unlikely that the statics or lateral inhomogeneities could be systematically biasing the velocities found in the focusing of the velocity semblance. Examination of the velocity semblance focusing for other gathers that do not show the Moho depth reflections



quite as well indicate stacking velocities similar to those given above in about half of the cases, and slightly higher in the remainder.

Detailed refraction information is not yet available for this area of the Mojave Desert. Kanamori and Hadley (1975) present a velocity model for the western and central Mojave that is generally used for earthquake location work. Hearn (1984), and Hearn and Clayton (1986) analyzed the travel times of Moho refractions between local earthquakes and the stations of the southern California seismic network. Some of his raypaths do cross underneath the Ward Valley, where he derives a crustal thickness of close to 25 km. This is 10 km thinner than the crustal thickness of other parts of the Mojave as found by Kanamori and Hadley. The best survey to date was carried out by the U.S. Geological Survey as part of the Pacific-Arizona Crustal Experiment (PACE). It consists of two crossing, 120 km-long refraction lines centered near WM-4 (Figure 3.1), employing several shots per line and a 1 km receiver spacing. A preliminary interpretation by Wilson et al. (1986) indicates upper crustal velocities similar to Kanamori and Hadley's model and a crustal thickness close to Hearn's. However, they find extensive zones of radically lower velocities in the middle and lower crust indicated by the data from the line running northeast to southwest. Curiously, low-velocity zones were not indicated for the same areas by the crossing, northwest-to-southeast trending line. Resolving this conflict between the two profiles may involve recognizing that the apparent effects of a low-velocity zone could actually be due to lateral heterogeneity in the upper crust.

Until the two interpretations of the PACE profiles can be reconciled, it is safer, for the purposes here, to build the simplest possible model that explains

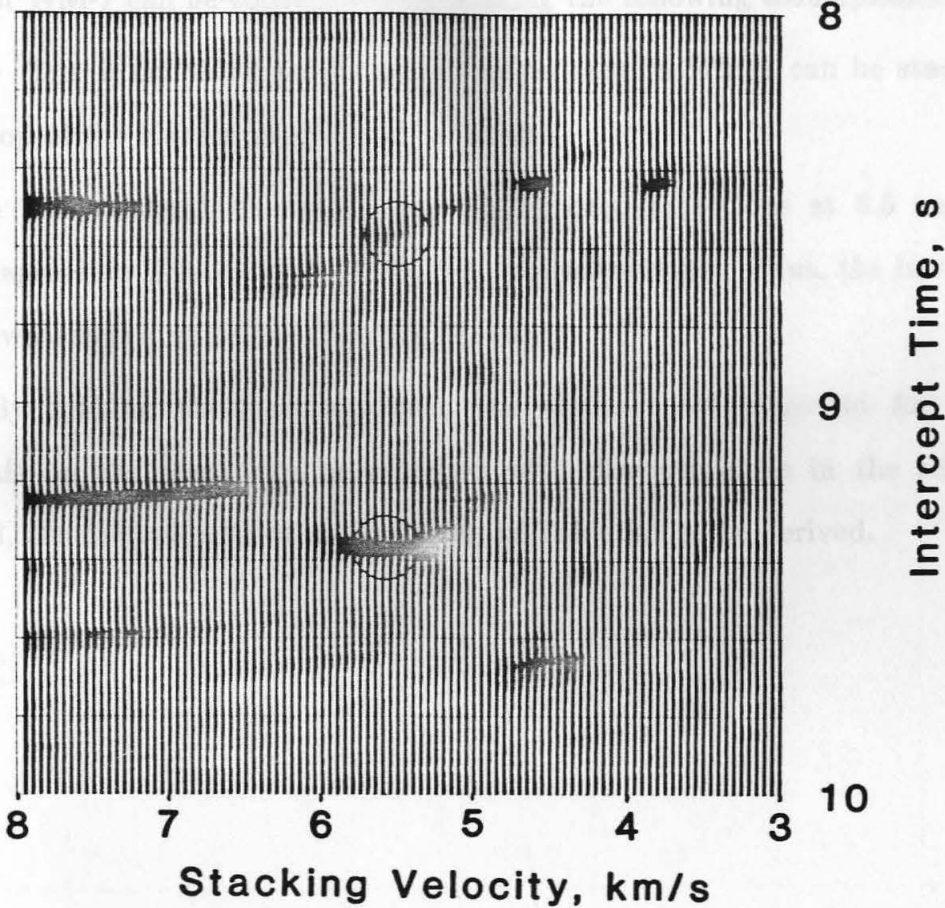


**Fig. 3.8:** Matrix indicating the proportion of hyperbolic "signal" in the Moho depth reflections of Figure 3.7, for each point of a velocity semblance, using the techniques of Harlan et al. (1984). Where a high percentage of the semblance amplitude is due to hyperbolic events having the indicated intercept time and stacking velocity, a dark area is formed. The stacking velocity picks used are circled.

the gross features seen by Kanamori and Hadley (1975), Hearn (1984), Wilson et al. (1986), and in Calcrust line WM-1. A reasonable starting model for the area of WM-1 can be constructed by making the following assumptions:

- The 2 km thick sedimentary section seen in WM-1 can be stacked on top of the Kanamori and Hadley model.
- The region between the two strong deep reflections at 8.5 and 9.4 s represents Kanamori and Hadley's subcrustal layer. Thus, the later of the two arrivals would be from the Moho.

By making these assumptions, the travel times observed for specific arrivals on the stack can be matched with discontinuities in the refraction model, the first velocity structure given in Table 3.2 to be derived.

Low-Velocity	2	3.0	1.1	2.0
Granitic	4	5.5	2.57	4.77
Layer	17.4	5.8	3.37	5.5
	2.0	6.0	3.36	5.0
Forecast	2	3.0	1.1	2.0
5.2 km/s	14.9	5.5	6.5	6.29
Granitic	8.4	6.3	3.57	6.5
Layer	2.5	6.0	3.36	5.0

Assuming that the root-mean-squared (rms) velocity is a good approximation of the stacking velocity for the structures and offsets in question here, it is obvious that the rms velocities to the top of the subcrust and the Moho for the modified Kanamori and Hadley model are recognizably higher than would be indicated by the velocity semblance focusing of Figure 3.3. A model that fits

**Table 3.2**  
Alternative Crustal Velocity Models

Model	Layer Thickness, km	Interval Velocity, km/s	2 way time to base, s	$v_{rms}$ to base, km/s
Modified	2	3.6	1.1	3.6
Kanamori	4	5.5	2.57	4.77
& Hadley	18.4	6.3	8.4	5.88
(1975)	3.5	6.8	9.4	5.98
Low-Velocity	2	3.6	1.1	3.6
Granitic	4	5.5	2.57	4.77
Layer	17.4	5.8	8.57	5.5
	2.6	6.6	9.36	5.6
Forced	2	3.6	1.1	3.6
6.3 km/s	14.9	5.5	6.5	5.23
Granitic	6.4	6.3	8.57	5.5
Layer	2.6	6.6	9.36	5.6

Assuming that the root-mean-squared (rms) velocity is a good approximation of the stacking velocity for the structures and offsets in question here, it is obvious that the rms velocities to the top of the subcrust and the Moho for the modified Kanamori and Hadley model are recognizably higher than would be indicated by the velocity semblance focusing of Figure 3.8. A model that fits

both the  $\sim 25$  km Moho of Hearn, and Wilson et al., and the observed moveouts must have a lower average crustal velocity than was found farther west in the Mojave. If this is so, then the WM-1 Moho reflection moveouts may be another line of evidence to support the existence of low-velocity zones as proposed by Wilson et al.

With the available data, a unique model cannot be defined. However, two end members can be suggested. On one hand, the velocity of the granitic layer can be decreased to match the observed stacking velocity at its base. This procedure yields a velocity of  $5.78 \pm 0.1$  km/s for the granitic layer. Alternatively, the thickness of the 5.5 km/s shallow basement layer could be increased at the expense of the thickness of the 6.3 km/s granite layer. To match the observed rms velocities, the 5.5 km/s layer would have to be 14.9 km thick, leaving a 6.4 km thick 6.3 km/s layer just above the subcrust. A look at Figure 3.6 shows that there could be an interface at the indicated two-way time of 6.5 s for the bottom of the 5.5 km/s layer, but it is certainly not as strong nor as continuous as the top of the sub-crust or the Moho. Pending further analysis of these datasets, I will, for the moment, make use of the model having a lower velocity granitic layer.

The stacking velocities found in the semblance focusing (Figure 3.8) can also be used to derive the interval velocity of the subcrustal layer. The Dix formula gives a velocity of  $6.6 \pm 2$  km/s, including the uncertainties in the velocity and intercept time picks. The subcrust would thus have a thickness of 2.6 km. This velocity is no more uncertain than the 6.8 km/s velocity derived by Kanamori and Hadley (1975), which was based on wide-angle reflection amplitudes. With these values for the subcrust, a total crustal

thickness of about 26 km is obtained, which agrees well with the work of Hearn (1954), and of Wilson et al. (1986).

The conclusions given above provide some of the basic information necessary for more detailed analysis of the deep reflections. As more of the Calcrust dataset is analyzed, some of these conclusions will undoubtedly have to be adjusted.

While one expects the reflection frequency response of a step discontinuity to be white, Polheima and Ziolkowski (1985) showed that the spectral response of a sequence of layers is non-white at pre-critical angles. In order to discover the nature of differences in the frequency behavior of the three reflector models, a fourth order finite difference solution of the two-dimensional elastic wave equation was used to calculate synthetic seismograms. The methods for source disposition and the boundary conditions are explained by Frankel and Clayton (1985).

Three of the models calculated are shown in Figure 3.9. Each models an isotropic explosion in a constant velocity half-space impinging upon a flat reflector having no density variation, with the vertical component of the particle velocity being recorded in the half space at the same level as the source. The gradient and thin layer reflectors were given a thickness near half of the dominant wavelength of the source pulse. The synthetic shot gathers are also shown, along with the spectra of the reflections windowed out of the individual traces of the gathers. It is clear from the spectra that: 1) the step discontinuity does not affect the frequency content of the reflection as a function of the angle of incidence; 2) the gradient shows a slight increase in peak frequency as incident angle increases; and 3) the thin layer shows a pronounced

### 3. REFLECTION SPECTRAL ANALYSIS

#### *Thin layer reflection spectra at multi-offset*

Following Davydova (1972) and Mair and Lyons (1976), the changes in reflection frequency content with offset will be examined to see if reflectors can be distinguished as step discontinuities, gradients, or thin layers. While one expects the reflection frequency response of a step discontinuity to be white, Fokhema and Ziolkowski (1985) showed that the spectral response of a sequence of layers is non-white at pre-critical angles. In order to discover the nature of difference in the frequency behavior of the three reflector models, a fourth order finite difference solution of the two-dimensional elastic wave equation was used to calculate synthetic seismograms. The methods for source imposition and the boundary conditions are explained by Frankel and Clayton (1986).

Three of the models calculated are shown in Figure 3.9. Each models an isotropic explosion in a constant velocity half-space impinging upon a flat reflector having no density variation, with the vertical component of the particle velocity being recorded in the half space at the same level as the source. The gradient and thin layer reflectors were given a thickness near half of the dominant wavelength of the source pulse. The synthetic shot gathers are also shown, along with the spectra of the reflections windowed out of the individual traces of the gathers. It is clear from the spectra that: 1) the step discontinuity does not affect the frequency content of the reflection as a function of the angle of incidence; 2) the gradient shows a slight increase in peak frequency as incident angle increases; and 3) the thin layer shows a pronounced

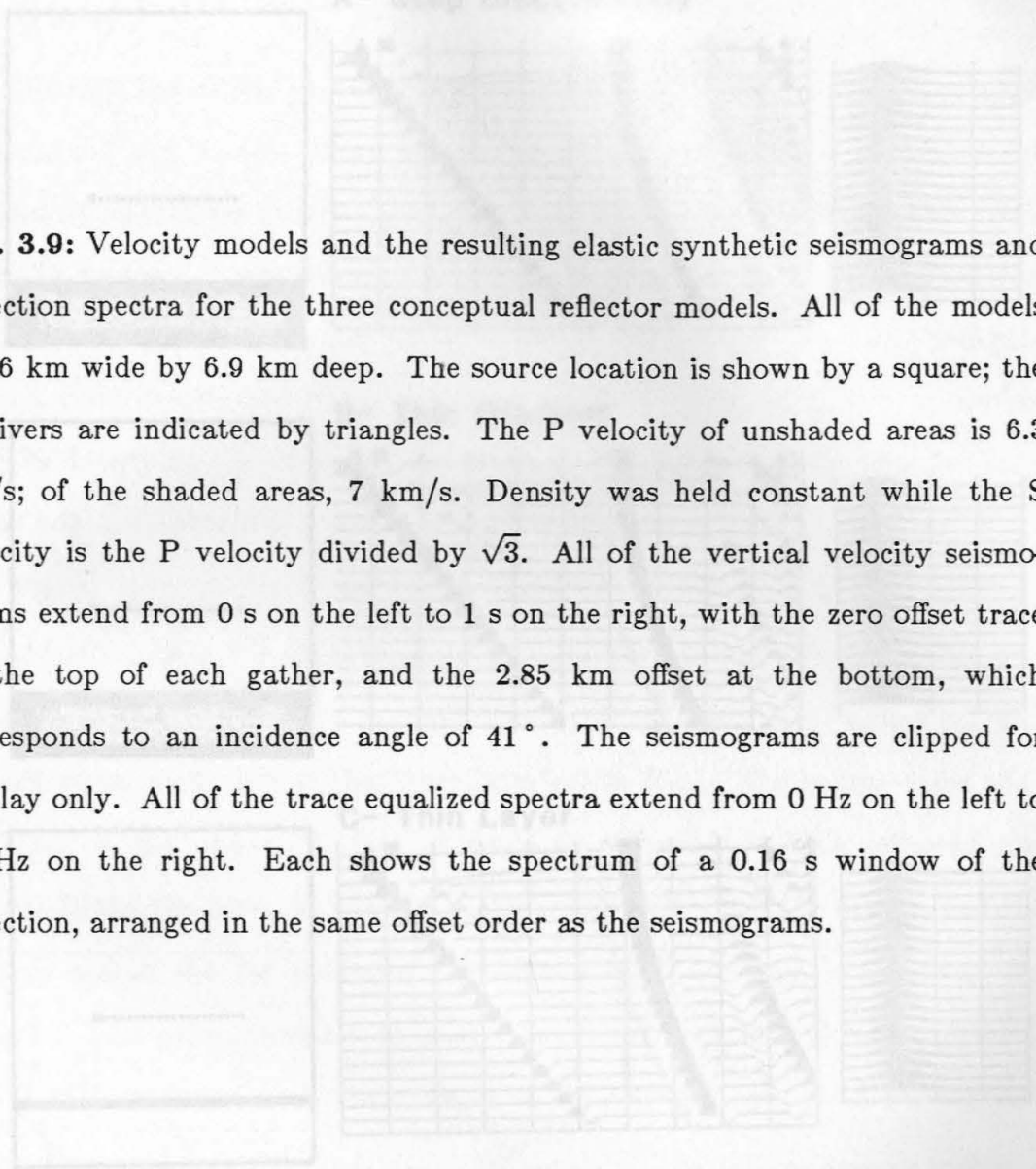
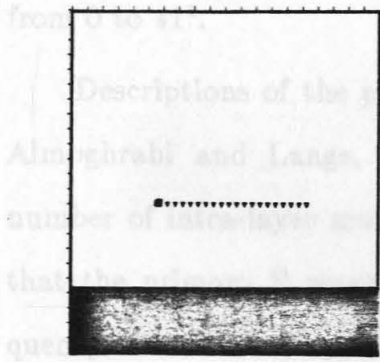
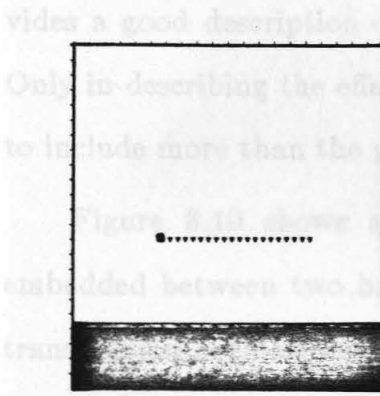
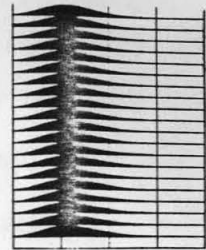
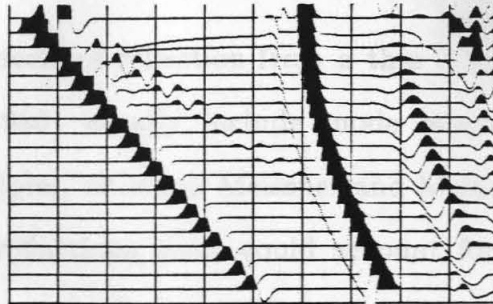


**Fig. 3.9:** Velocity models and the resulting elastic synthetic seismograms and reflection spectra for the three conceptual reflector models. All of the models are 6 km wide by 6.9 km deep. The source location is shown by a square; the receivers are indicated by triangles. The P velocity of unshaded areas is 6.3 km/s; of the shaded areas, 7 km/s. Density was held constant while the S velocity is the P velocity divided by  $\sqrt{3}$ . All of the vertical velocity seismograms extend from 0 s on the left to 1 s on the right, with the zero offset trace at the top of each gather, and the 2.85 km offset at the bottom, which corresponds to an incidence angle of  $41^\circ$ . The seismograms are clipped for display only. All of the trace equalized spectra extend from 0 Hz on the left to 40 Hz on the right. Each shows the spectrum of a 0.16 s window of the reflection, arranged in the same offset order as the seismograms.

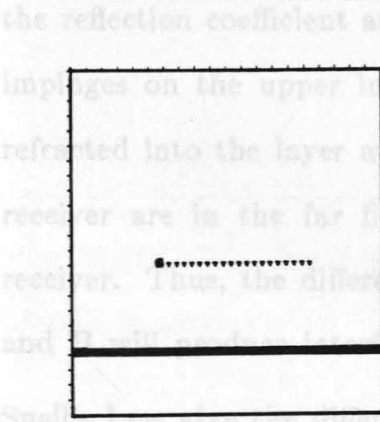
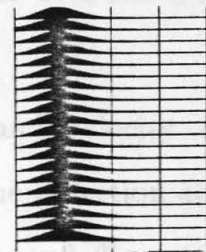
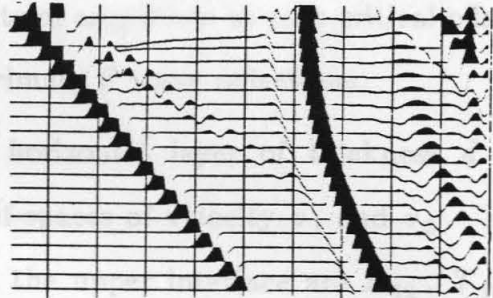
increase in peak frequency with increasing incidence angle. The wave number  $k$  is



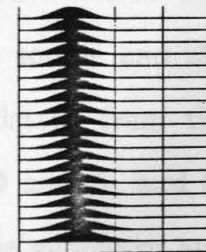
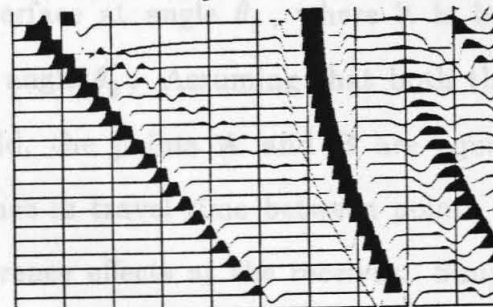
**A- Step Discontinuity**



**B- Thin Gradient**



**C- Thin Layer**



Snell's law give the angle as  $\tau_1 = \frac{v_1}{v_2} \sin \theta_2$ . The reflected wave recorded at the receiver,  $s(t)$ , will in the simplest case be the reflection off the upper interface of the source wave  $s(t)$  plus the reflection off the lower interface:

$$s(t) = R_{12} s(t) + T_{12} R_{23} T_{21} s(t - \tau) \quad [9.3]$$

The spectrum  $S_s(f)$  of the reflection is, assuming  $R_{12} = R_{23} = T_{12}$  and  $T_{21}$

increase in peak frequency with increasing incidence angle, more than 2 Hz from 0 to 41°.

Descriptions of the process of reflection from a thin layer (Mikhota, 1972; Almoghrabi and Lange, 1986) usually include mode conversions and some number of intra-layer multiples, although Meissner and Meixner (1969) showed that the primary P wave reflections alone could account for most of the frequency effects. A simple analysis of the interference within the thin layer provides a good description of the frequency increase observed in the synthetics. Only in describing the effects of amplitude at post-critical offsets does one have to include more than the primary P wave reflections.

Figure 3.10 shows a horizontal layer of thickness  $d$  and velocity  $v_2$  embedded between two half-spaces of velocity  $v_1$  and  $v_3$ . The reflection and transmission coefficients at the upper interface are  $R_{12}$ ,  $T_{12}$ , and  $T_{21}$ , and the reflection coefficient at the lower interface is  $R_{23}$ . The source wave  $s(t)$  impinges on the upper interface at angle  $\theta_1$ , where it is both reflected and refracted into the layer at angle  $\theta_2$ . Assuming that both the source and the receiver are in the far field, the points **A** and **B** are equidistant from the receiver. Thus, the difference in travel time between points **O** and **A**, and **O** and **B** will produce interference effects at the receiver. Simple geometry and Snell's Law give the difference as  $\tau_l = \frac{2d}{v_2} \cos\theta_2$ . The reflected wave recorded at the receiver,  $d(t)$ , will in the simplest case be the reflection off the upper interface of the source wave  $s(t)$  plus the reflection off the lower interface:

$$d(t) = R_{12} s(t) + T_{12} R_{23} T_{21} s(t - \tau_l) . \quad [3.3]$$

The spectrum  $S_d(f)$  of the reflection is, assuming  $R_{12}$ ,  $R_{23}$ ,  $T_{12}$ , and  $T_{21}$

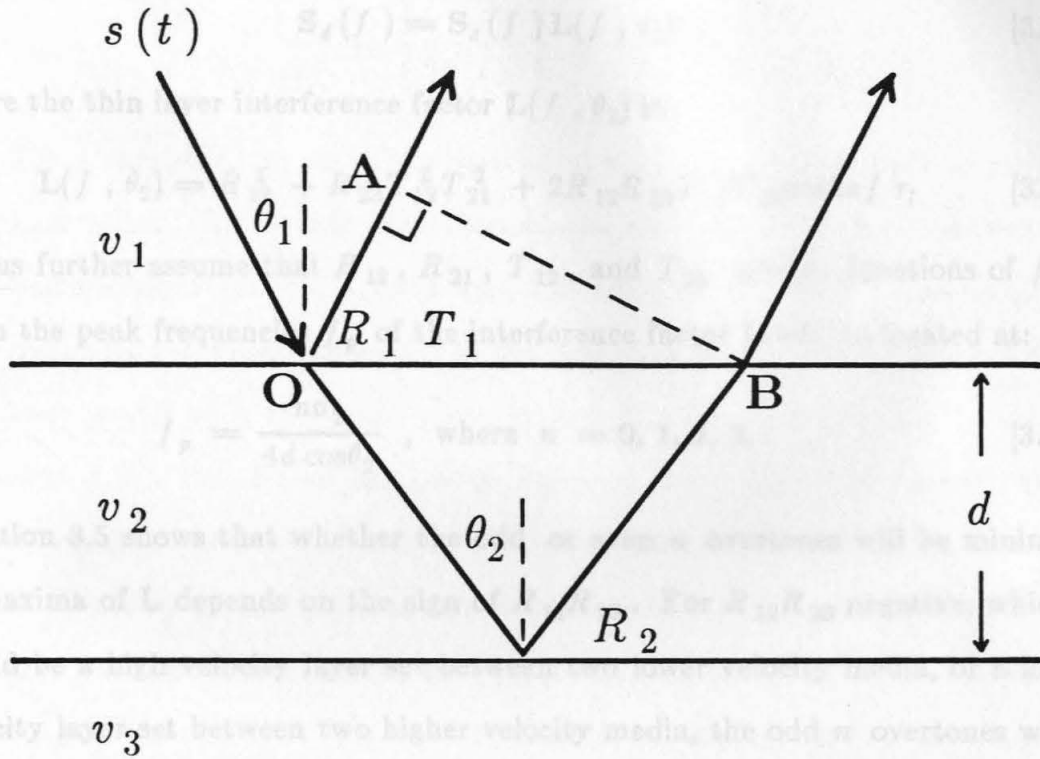


**Fig. 3.10:** Thin layer geometry for the calculation of interference effects (details in text).

It is further straightforward to show that, if a change in peak frequency of  $L$  with offset,  $dL_p/d\theta_1$ , is observed at a particular offset, the angle of incidence on the layer  $\theta_1$  can be found for that offset, and the velocity above the layer  $v_1$  is known, then the thickness  $d$  and velocity  $v_2$  of the layer can be calculated from:

$$d = \frac{v_1}{4} \left[ \frac{v_1}{L_p \sin^2 \theta_1 \cos \theta_1} \frac{dL_p}{d\theta_1} \right]^{1/2} \quad [3.5]$$

to be real:

$$\mathbf{S}_d(f) = \mathbf{S}_s(f) \mathbf{L}(f, \theta_2), \quad [3.4]$$

where the thin layer interference factor  $\mathbf{L}(f, \theta_2)$  is:

$$\mathbf{L}(f, \theta_2) = R_{12}^2 + R_{23}^2 T_{12}^2 T_{21}^2 + 2R_{12}R_{23}T_{12}T_{21}\cos 2\pi f \tau_l \quad [3.5]$$

Let us further assume that  $R_{12}$ ,  $R_{21}$ ,  $T_{12}$ , and  $T_{21}$  are not functions of  $f$ .

Then the peak frequencies  $f_p$  of the interference factor  $\mathbf{L}$  will be located at:

$$f_p = \frac{nv_2}{4d \cos\theta_2}, \quad \text{where } n = 0, 1, 2, 3, \dots \quad [3.6]$$

equation 3.5 shows that whether the odd or even  $n$  overtones will be minima or maxima of  $\mathbf{L}$  depends on the sign of  $R_{12}R_{23}$ . For  $R_{12}R_{23}$  negative, which would be a high velocity layer set between two lower velocity media, or a low velocity layer set between two higher velocity media, the odd  $n$  overtones will be the maxima of  $\mathbf{L}$ . This case can be called an "isolated thin layer." For  $R_{12}R_{23}$  positive, in other words, the velocity increasing or decreasing in the same direction across both interfaces, the even  $n$  overtones will be the maxima of  $\mathbf{L}$ . This case will be called a "boundary layer." In both cases, equation 3.6 shows that as the angle of incidence  $\theta_2$  increases, the peak frequency  $f_p$  also increases.

It is further straightforward to show that, if a change in peak frequency of  $\mathbf{L}$  with offset,  $df_p/d\theta_1$ , is observed at a particular offset, the angle of incidence on the layer  $\theta_1$  can be found for that offset, and the velocity above the layer  $v_1$  is known, then the thickness  $d$  and velocity  $v_2$  of the layer can be calculated from:

$$d = \frac{v_1}{4} \left[ \frac{n}{f_p^3 \sin\theta_1 \cos\theta_1} \frac{df_p}{d\theta_1} \right]^{\frac{1}{2}} \quad [3.7]$$

and:

$$\frac{1}{v_2^2} = \left[ \frac{n}{4d f_p} \right]^2 + \frac{\sin^2 \theta_1}{v_1^2} \quad [3.8]$$

The assumptions made in the derivation above essentially apply to acoustic plane waves. Since only peak frequencies are being considered, however, these assumptions provide a good approximation of the elastic case. Figure 3.11 compares the peak frequencies of the reflection spectra of the elastic finite difference model with the peaks given by the thin layer interference factor  $L$  (equation 3.5). The dotted line shows the peak frequency of the  $n=1$  overtone of equation 3.6 for the model. The interference factor must then be multiplied by the spectrum of the source wavelet, which in the case of the model is a broad Gaussian with a peak near 12 Hz. Thus, the slope of the Gaussian source spectrum above 12 Hz, when multiplied by the interference factor, will shift the peaks of the reflected wave down in frequency. The peaks of the product are shown as the open squares. The peak frequencies of the finite difference seismograms are plotted as the filled circles. The close correspondence of the two shows that assuming an acoustic medium without multiples is a reasonable approximation to the full elastic case.

The shifting of the peak frequencies by the source spectrum would seem to be a problem in applying equations 3.7 and 3.8. Fortunately, however, the source spectra which resulted from the resonance in the low velocity surface layer in the Ward Valley, as discussed previously, are amenable to this analysis. Figure 3.12 shows the factor in equation 3.2 for the surface layer in the average shallow velocity model (Table 3.1) multiplied by the thin layer interference factor for the finite difference model. It can be seen that, if one is

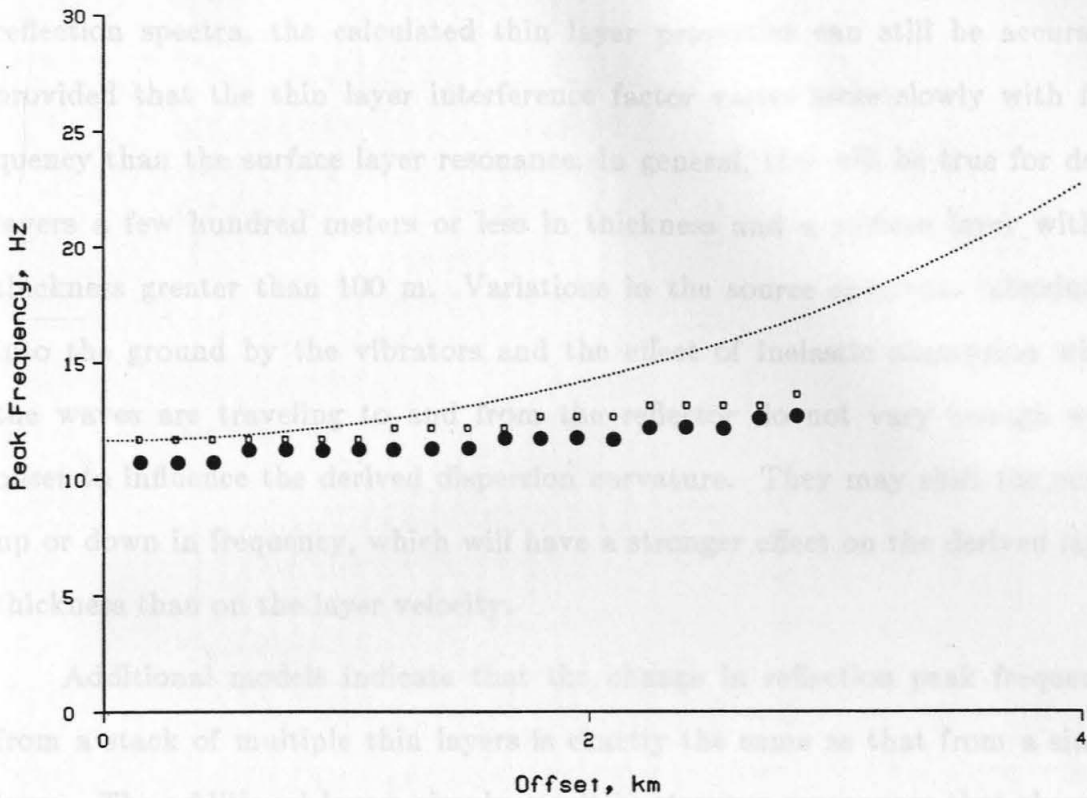


**Fig. 3.11:** Diagram of reflection peak frequency dispersion with offset for the thin layer model of Figure 3.9C. The dotted line shows the peak frequency of the  $n=1$  overtone for the model (equation 3.6). The open squares show the automatically picked peaks of the product of the interference factor (equation 3.5) and the model source spectrum. The filled circles show the automatically picked peaks of the synthetic reflection spectra, from Figure 3.9C, of the same model.

willing to fit a curve through a cloud of points picked from the peaks of reflection spectra, the calculated thin layer properties can still be accurate, provided that the thin layer interference factor varies more slowly with frequency than the surface layer resonance. In general, this will be true for deep layers a few hundred meters or less in thickness and a surface layer with a thickness greater than 100 m. Variations in the source spectrum introduced into the ground by the vibrators and the effect of inelastic absorption while the waves are traveling to and from the reflector do not vary enough with offset to influence the derived dispersion curvature. They may shift the curve up or down in frequency, which will have a stronger effect on the derived layer thickness than on the layer velocity.

Additional models indicate that the change in reflection peak frequency from a stack of multiple thin layers is exactly the same as that from a single layer. The additional layers simply result in stronger resonances that sharpen the spectral peaks. Therefore, whether the reflection has a simple, single cycle character, or is complex and consists of many cycles, may be more useful than the spectra to decide whether a thin layer reflector is composed of one or many layers.

The spectral effects of the gradient model cannot be so handily defined. However, as shown by Gupta (1966), and modeling of gradients of different thickness, a band limited source such as a vibrator produces a strong reflection only if the thickness of the gradient is close to or smaller than the principal wavelength of the source. In the case of such a thin gradient, however, the response is almost identical to that of a thin boundary layer having a velocity intermediate between those of the media above and below. All of the analysis

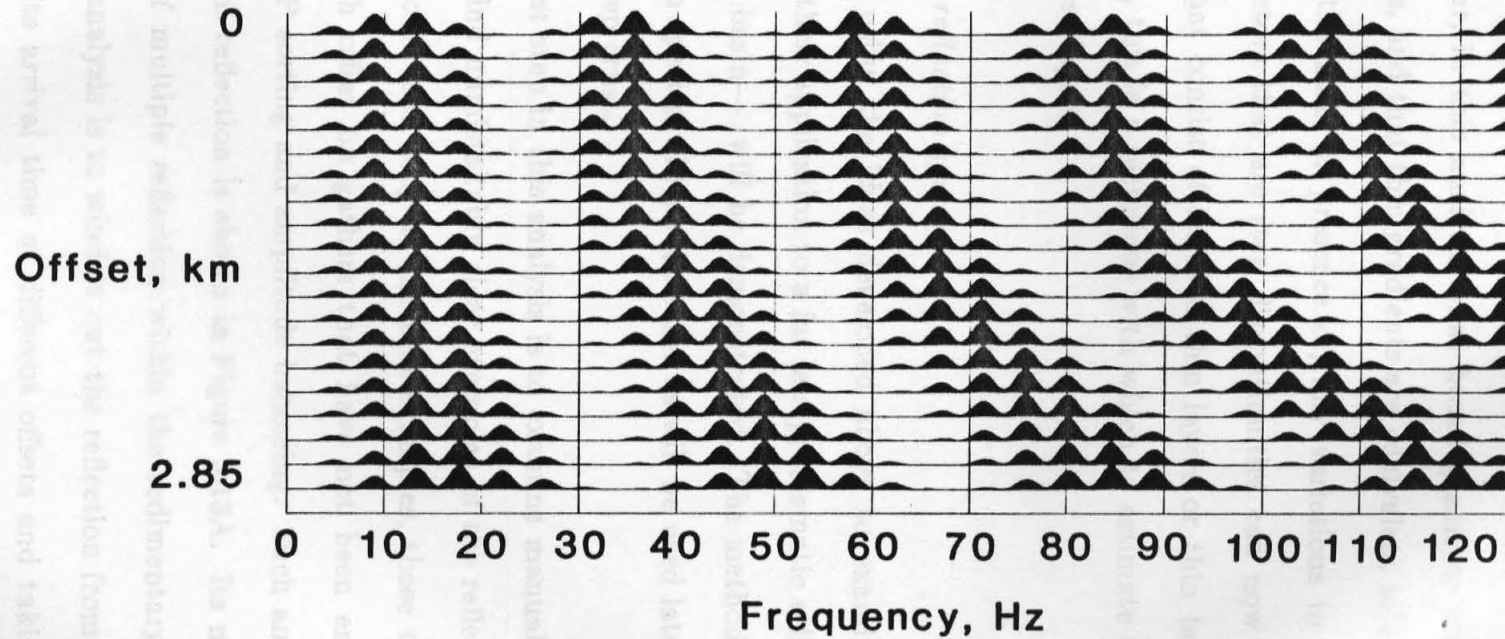


**Fig. 3.12:** Product of the surface layer resonance factor (equation 3.2) and the thin layer interference factor (equation 3.5) for a 120 m thick, 1.1 km/s surface layer and and a 7 km/s, 150 m thick layer 1.65 km deep in a 6.3 km/s medium, for the offsets of the finite difference model.

above will apply, with the overtone  $n$  of equation 3.6 being even. Therefore, I will consider, in this analysis, that broad gradients are invisible to reflection experiments, and that thin gradients are equivalent to thin boundary layers.

From the lack, or presence of, any variations in reflection spectra with offset, reflectors that are step discontinuities can now be discriminated from reflectors that consist of isolated thin layers or thin boundary layers. In the latter cases, this is a technique with which to estimate the thickness and velocities of these layers.

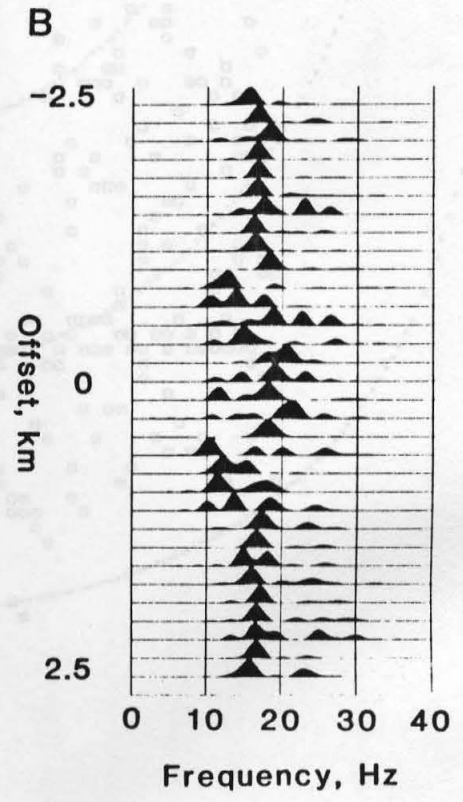
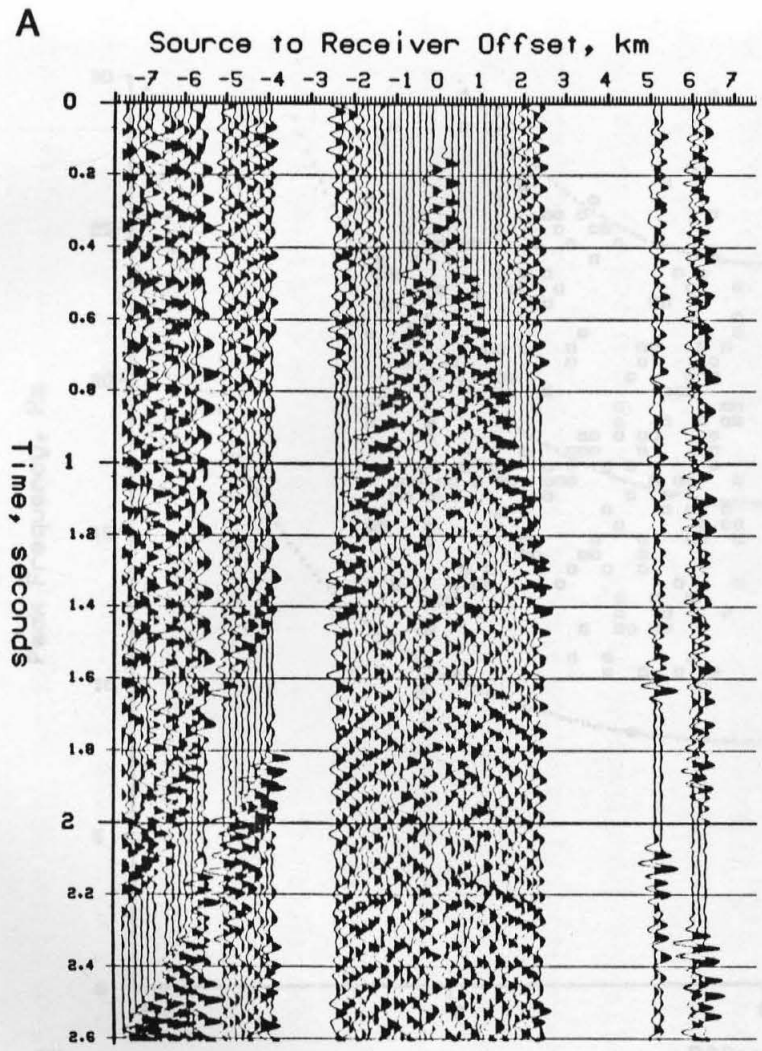
#### *Analysis of reflection spectra*

Before using the ideas developed above to examine the nature of deep reflections, their application to a far less problematic reflector— the bottom of the alluvial basin— will be demonstrated. The methods developed to analyze its reflection spectra will be the same as will be used later to look at reflections from the deep crust.

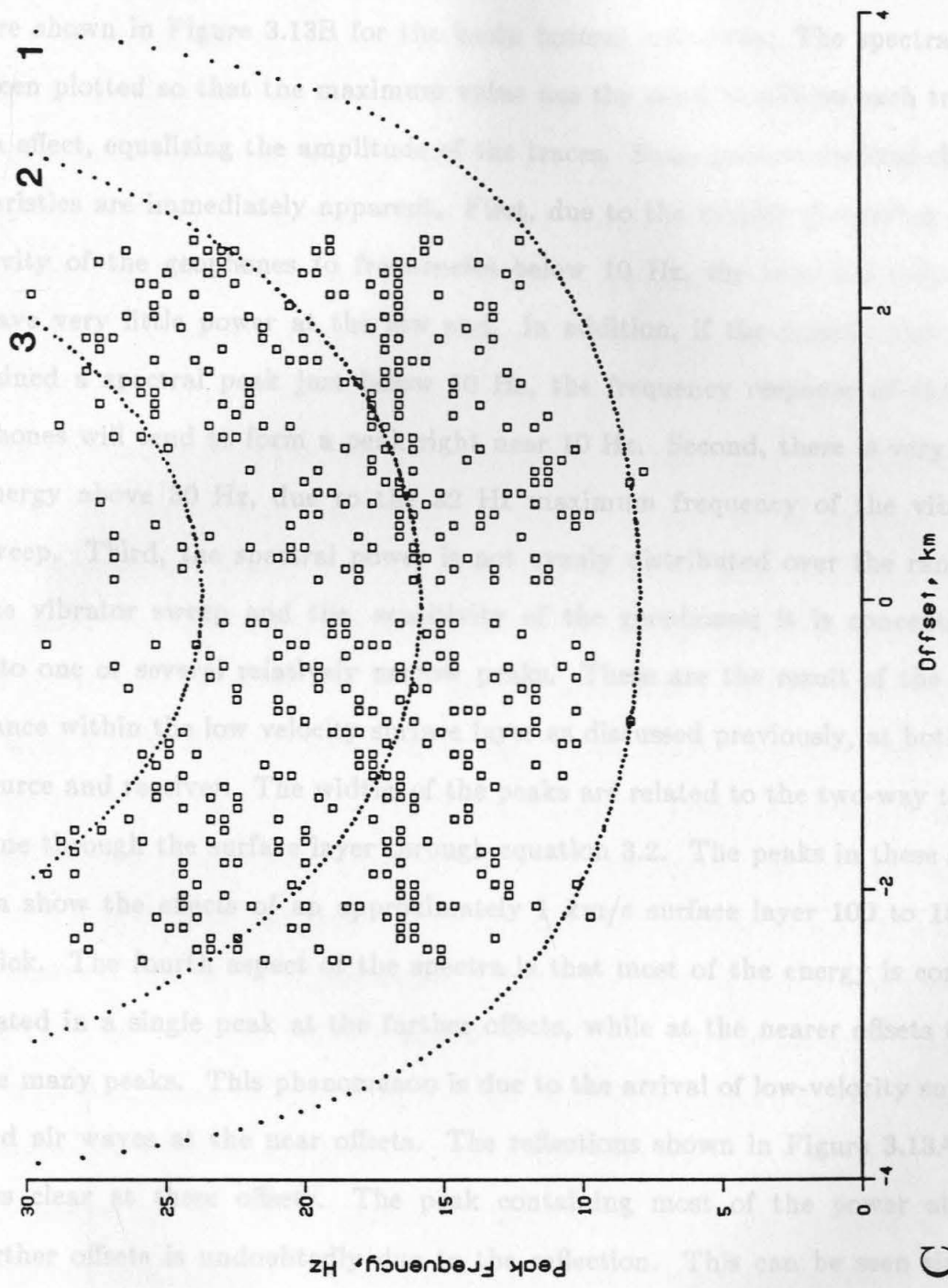
The first step in this analysis is to examine manually the dataset of CMP gathers to find unmistakably clear examples of the reflections needed. At this stage we should look only at the best examples, those that are clear and continuous with offset on gathers that have not been enhanced by processing beyond CMP sorting and amplitude balancing. Such an example of a shallow, basin bottom reflection is shown in Figure 3.13A. Its multi-cycle character is the result of multiple reflection within the sedimentary section. The second step of the analysis is to window out the reflection from the rest of the gather by picking its arrival time at different offsets and taking, in this case, 0.4 s (100 time points) of data around the reflection from each trace. The power

**Fig. 3.13:** **A:** Portion of a merged CMP gather from WM-1 showing the sedimentary basin bottom reflection, at a zero offset time of 1.6 s. Trace equalization and AGC have been applied. **B:** Power spectra of 0.4 s windows of each trace centered around the basin bottom reflections of A. **C:** Automatically picked peaks of the spectra in B, plus the reflection spectra of 4 adjacent gathers, plotted as open squares. For each spectrum, the locations of the three highest peaks are plotted. Note the concentration of peaks near 16.5 Hz for all offsets. The dotted lines show the dispersion, from equation 3.6 for the indicated values of  $n$  and the average shallow velocity model of Table 3.1, due to an imaginary 6.3 km/s layer 200 m thick at a depth of 2.5 km.





spectrum of each of these windows is calculated. These are shown in Figure 3.13B for the same traces. The spectra have been plotted so that the maximum value for the spectra in each trace—in effect, equalizing the amplitude of the traces. Some characteristic features are immediately apparent. First, due to the nature of the sweep, the frequency of the vibrator sweep is 10 Hz. The spectra are divided into one octave bands. Second, there is a very distinct peak at 10 Hz. This is the result of the resonance within the low velocity surface layer 100 to 150 m thick. The spectra show that most of the energy is concentrated in a single peak at the further offsets, while at the nearer offsets there are many peaks. This phenomenon is due to the arrival of low-velocity surface and air waves. The reflections shown in Figure 3.13A are very clear at the near offsets. The peak containing most of the energy at the further offsets is undoubtedly a reflection. This can be seen by measuring the period of the raw reflection of the seismograms in Figure 3.13A. It corresponds very closely with the peak frequency shown on Figure



spectrum of each of these windowed reflection traces is then calculated. These are shown in Figure 3.13B for the basin bottom reflection. The spectra have been plotted so that the maximum value has the same height on each trace—in effect, equalizing the amplitude of the traces. Some general spectral characteristics are immediately apparent. First, due to the rapidly decreasing sensitivity of the geophones to frequencies below 10 Hz, the recorded reflections have very little power at the low end. In addition, if the seismic wave contained a spectral peak just below 10 Hz, the frequency response of the geophones will tend to form a peak right near 10 Hz. Second, there is very little energy above 30 Hz, due to the 32 Hz maximum frequency of the vibrator sweep. Third, the spectral power is not evenly distributed over the range of the vibrator sweep and the sensitivity of the geophones; it is concentrated into one or several relatively narrow peaks. These are the result of the resonance within the low velocity surface layer as discussed previously, at both the source and receiver. The widths of the peaks are related to the two-way travel time through the surface layer through equation 3.2. The peaks in these spectra show the effects of an approximately 1 km/s surface layer 100 to 150 m thick. The fourth aspect of the spectra is that most of the energy is concentrated in a single peak at the farther offsets, while at the nearer offsets there are many peaks. This phenomenon is due to the arrival of low-velocity surface and air waves at the near offsets. The reflections shown in Figure 3.13A are less clear at these offsets. The peak containing most of the power at the farther offsets is undoubtedly due to the reflection. This can be seen simply by measuring the period of the raw reflection off the seismograms in Figure 3.13A. It corresponds very closely with the peak frequency shown on Figure

3.13B, 16.5 Hz.

The third step in the analysis is to automatically pick the peaks of the spectra of the individual traces and plot their frequency as a function of offset. Figure 3.13C shows this plot for the spectra of Figure 3.13B plus the spectra of the same reflection from four adjacent CMP gathers. For each trace spectrum the three highest peaks are plotted. The peaks plot at discrete frequencies because of the discretization of the spectra. While many scattered peaks can be seen, a grouping of the reflection peaks at 16.5 Hz for all offsets is obvious. This grouping reflects the nearly constant 16.5 Hz peaks in the spectra of Figure 3.13B. Since a step discontinuity is a good reflector model for the bottom of a sedimentary basin, it is not surprising that the peak frequency of the reflection does not increase with offset. In fact, it appears to decrease about 0.5 Hz at close to 2.5 km offset which, the larger offset traces of these gathers (Figure 3.13A) show, is approaching the critical angle. A similar effect was observed by Meissner (1967). For comparison, the lowest 3 overtones of the peak frequency, calculated from equation 3.6, are plotted for the interference from a hypothetical thin layer at this depth with a velocity of 6.3 km/s and a thickness of 200 m. The calculation includes the bending of the rays through the "average" shallow velocity structure of Table 3.1 but assumes that the layer is horizontal. If such a layer were causing the observed reflection, the spectral peaks would have to show some dispersion.

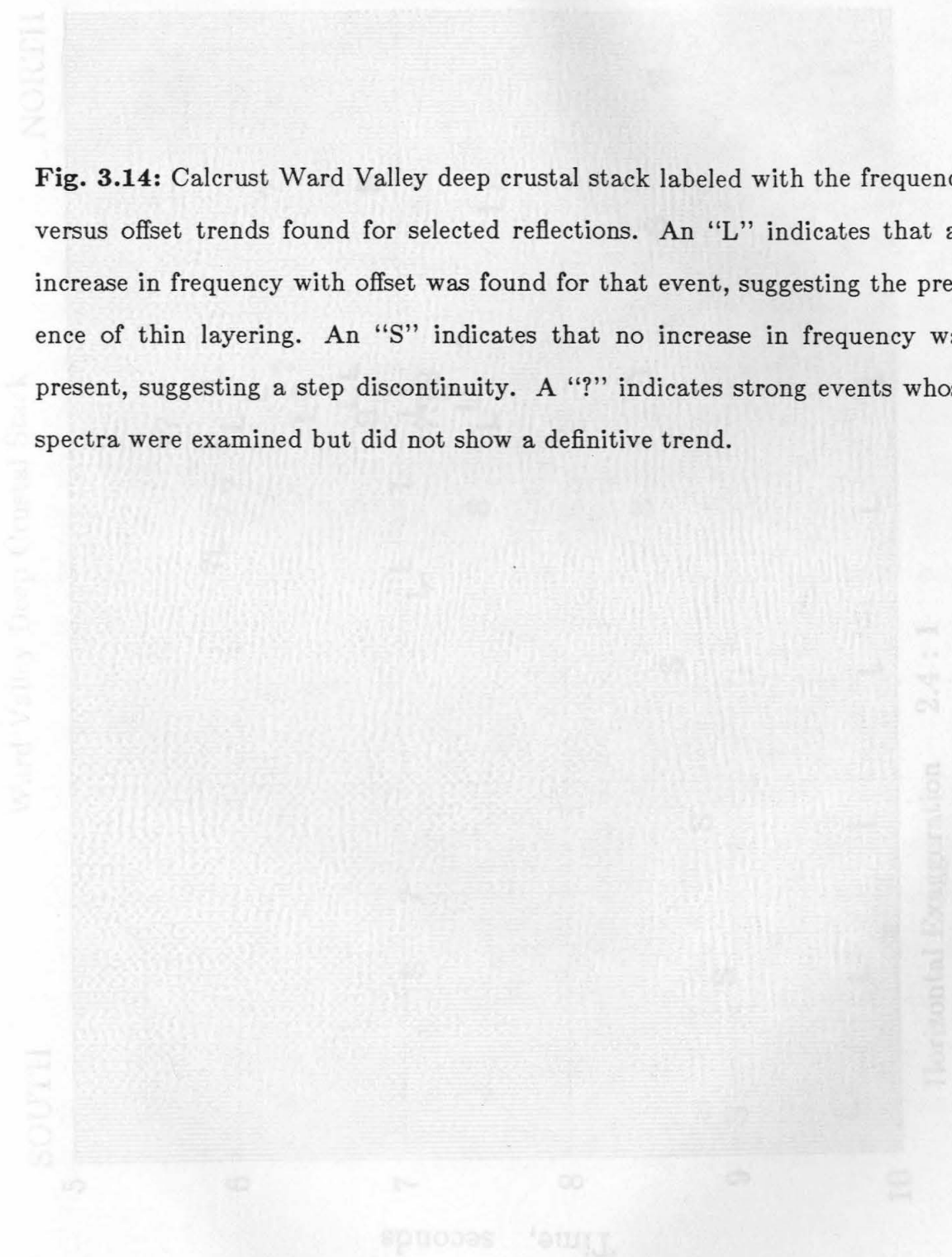
Essentially the same procedures were applied in the analysis of the reflections from within the middle and deep crust of the Calcrust Ward Valley dataset. The other datasets discussed in this paper could not be used for definitive analysis of frequency with offset. Dix's (1965) profile from the

central Mojave, because it is essentially a single shot gather, lacks the multiplicity needed for definitive analysis. The COCORP profiles in the western Mojave (Cheadle et al., 1985, 1986) lack offsets beyond 10 km.

All of the Ward Valley long offset CMP gathers were inspected manually to find the best examples of reflections that have some prominence and continuity across all available offsets. Thirty-five such examples were selected from the more than 200 CMP gathers. These do not include some of the more prominent reflections in the stack (Figure 3.6), such as the one at 5.3 s, near CMP 1830. That particular reflection is quite strong on the limited far offsets available, but cannot be traced to the near offsets. Even the best examples do not continue across a large range of midpoints, as the discontinuous nature of the reflections in the stack would suggest. In addition, the examples are concentrated at midpoints having the highest fold CMP gathers. Figure 3.15 shows the reflections selected from the particularly good CMP gather 1614. Clear reflections can be seen at intercept times of 5.5, 6.0, 6.7, 7.1, 7.2, and 7.4 s.

A first look at the frequency variation with offset was provided by calculating the power spectra of the windowed reflections from the individual traces, and then summing the spectra for the near and far ranges of offset. Figure 3.16 (bottom) shows the sum of the spectra over the offset ranges of -2.5 to 2.5 and -8.2 to -3.7 km, along with the spectra of the windows from the individual traces at all offsets, for the 7.4 s reflection from CMP gather 1614. The summed spectra show 2 peaks. One is at 11 Hz on both offset ranges; it represents surface wave coda limited by the 10 Hz lower frequency cutoff of the geophones. The other peak is at 16 Hz on the near offsets and 19 Hz on

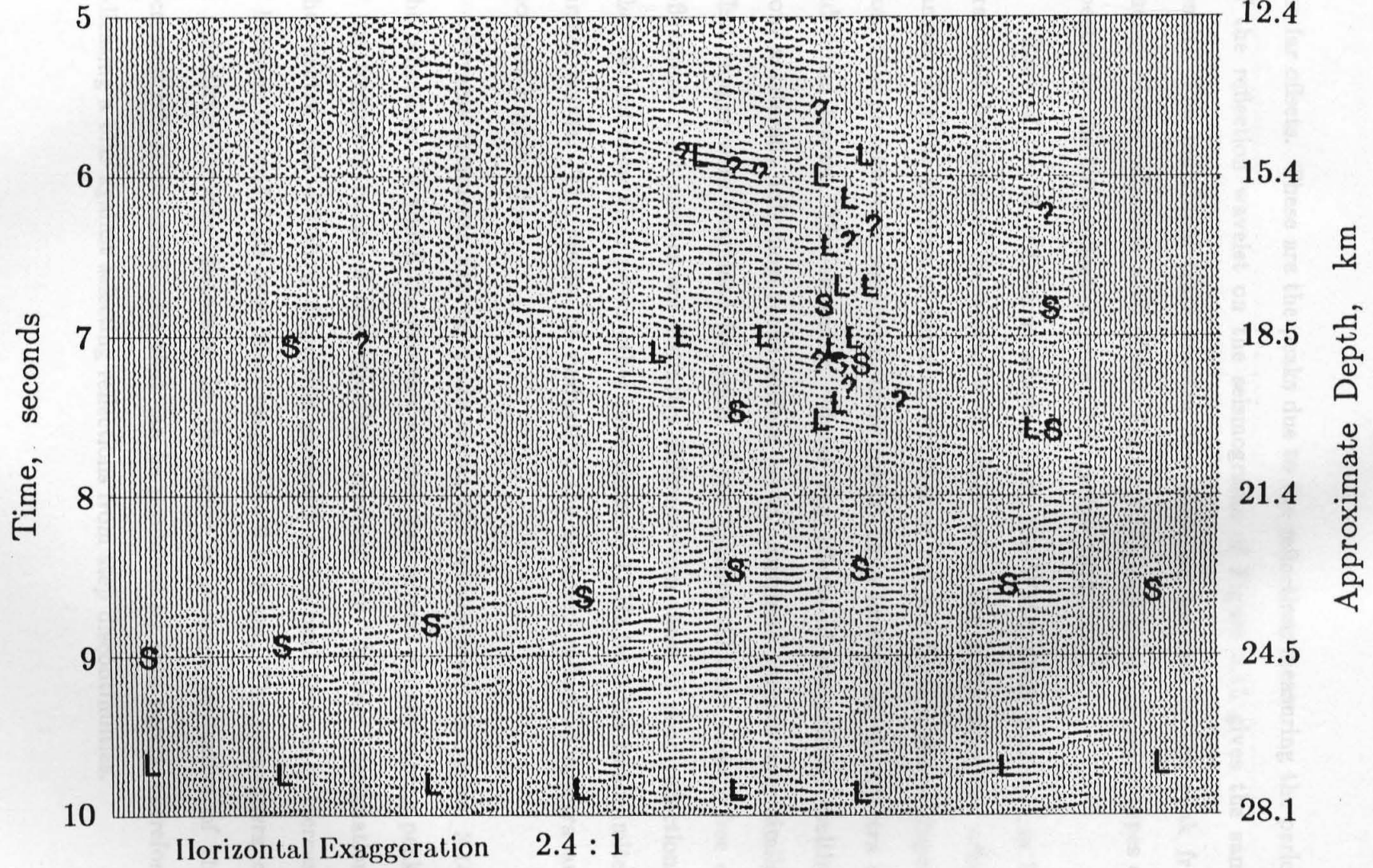
**Fig. 3.14:** Calcrust Ward Valley deep crustal stack labeled with the frequency versus offset trends found for selected reflections. An "L" indicates that an increase in frequency with offset was found for that event, suggesting the presence of thin layering. An "S" indicates that no increase in frequency was present, suggesting a step discontinuity. A "?" indicates strong events whose spectra were examined but did not show a definitive trend.



Ward Valley Deep Crustal Stack

SOUTH

NORTH



the far offsets. These are the peaks due to the reflection; measuring the period of the reflection wavelet on the seismograms of Figure 3.15 gives the same result. The individual trace spectra also show an increase in the peak frequency of the reflection with offset. Figure 3.16 (top) gives the same types of spectra for the 6.0 s reflection from CMP gather 1617.

Each of the 35 reflections selected from the WM-1 CMP gathers can be examined for spectral dispersion with offset using the sums over two offset ranges. For the purpose of deciding whether or not a reflection shows dispersion, this procedure is somewhat more robust than looking at the spectra of individual traces. The summing reduces the effects of resonances resulting from a laterally inhomogeneous surface layer. Summed spectra over similar offset ranges were examined for areas of the gathers that are clearly free of reflections. Such spectra are distinctly different from those of good reflections. They do not show clear peaks other than those at 11 Hz from the band-limited surface waves. The results of evaluating the summed reflection spectra are shown in Figure 3.14.

Several comments can be made about the results given in Figure 3.14. The reflections for which the summed spectra had several equally strong peaks in the frequency range of the reflections received the "unclear" designation. The spectra that did show dispersion generally had a peak frequency increase of between 0.5 and 3 Hz over offset ranges like 0 to 8 km. The preponderance of reflections showing dispersion in the figure is perhaps indicative of the increased reflection amplitudes that can be produced by thin layers, therefore indicating a bias against selecting reflections from step discontinuities.

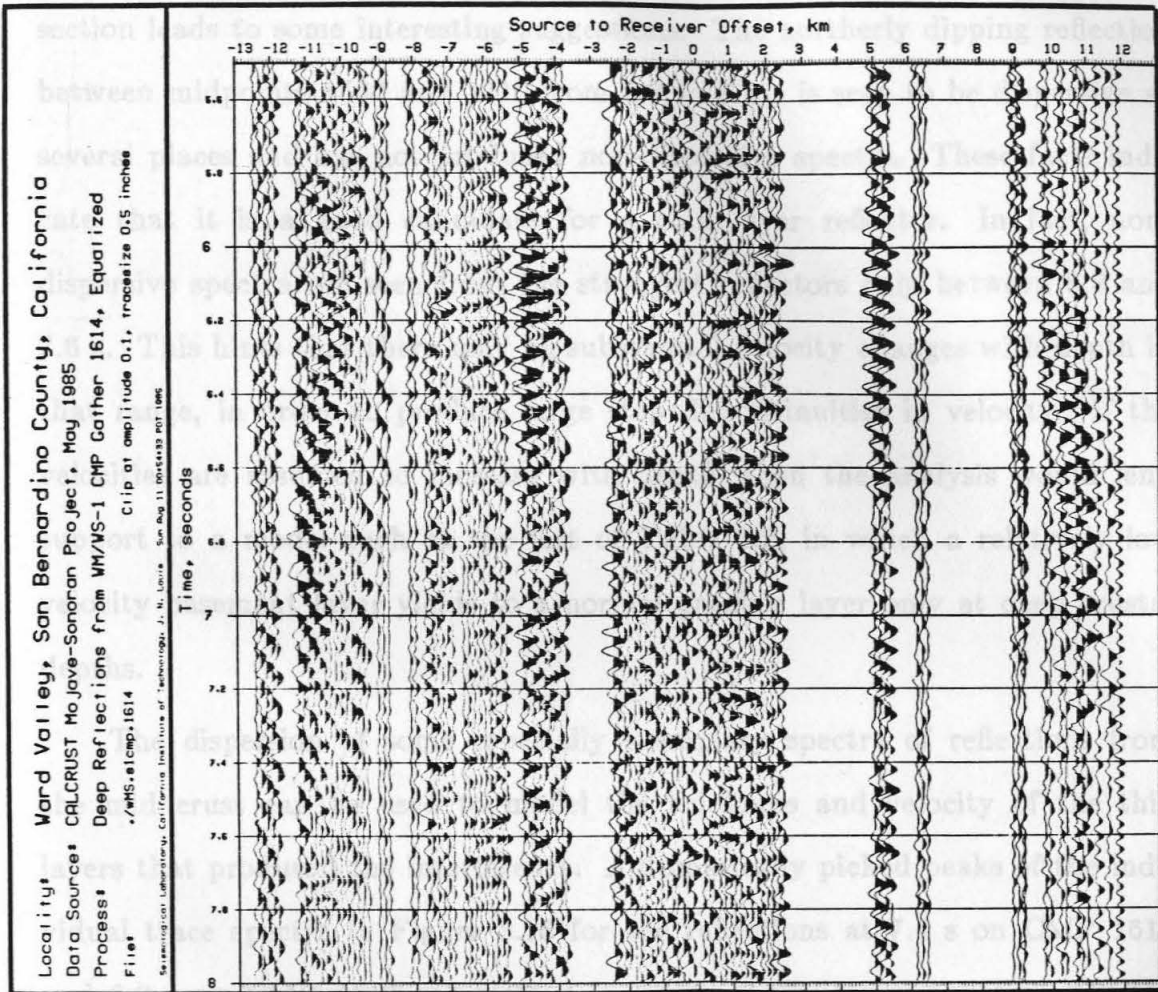


**Fig. 3.15:** Portion of CMP gather 1614, centered 17.8 km south of the northern terminus of line WM-1. The seismograms are shown between 5.5 and 8 s. Trace equalization and AGC have been applied.

The distribution of offset dependent frequency phenomena on the stacked section leads to some interesting suggestions. The northerly dipping reflection between midpoints 1530 and 1710 from 5.9 to 6.4 s is seen to be dispersive at several places and has not produced non-dispersive spectra. These facts indicate that it is a good candidate for a thin layer reflector. In fact, non-dispersive spectra are seen from the strongest reflectors only between 6.8 and 7.6 s. This hints that there may be substantial velocity changes with depth in that range, in order to produce large step discontinuities in velocity. If the velocities are assumed to increase with depth, then the analysis would lend support to a model such as the last of Table 3.2, in which a relatively low velocity basement layer yields to a normal granitic layer only at deep crustal depths.

The dispersion of some especially exemplary spectra of reflections from the mid crust can be used to model the thickness and velocity of the thin layers that produced the interference. Automatically picked peaks of the individual trace spectra in Figure 3.16 for the reflections at 7.4 s on CMP 1614 and 6.0 s on CMP 1617 are plotted in Figure 3.17. Using equation 3.6, the peak frequency dispersion curves of hypothetical thin horizontal layers can be superimposed on the plots of peak frequency. A velocity model such as one of the last two in Table 3.2 must also be assumed. An evaluation of such models for the 6.0 s reflection results in a suggestive fit of the  $n=3$  overtone for a 6.3 km/s layer 275 m thick at a depth of 15 km. While the  $n=1$  overtone could be expected to be strong, it arises at frequencies below the sensitivity of the geophones. The 7.4 s reflection spectral peaks suggest a fit to the  $n=5$  overtone from a 6.9 km/s layer 450 m thick at 19.1 km depth. The  $n=3$  overtone

**Fig. 3.16:** Spectra from the 6.0 s event at on CMP gather 1617 (top) and the 7.4 s event on gather 1614 (bottom). The two sums over the indicated offset ranges are on the left; the spectra from individual traces are on the right. All spectra have been plotted with their maxima at the same height.

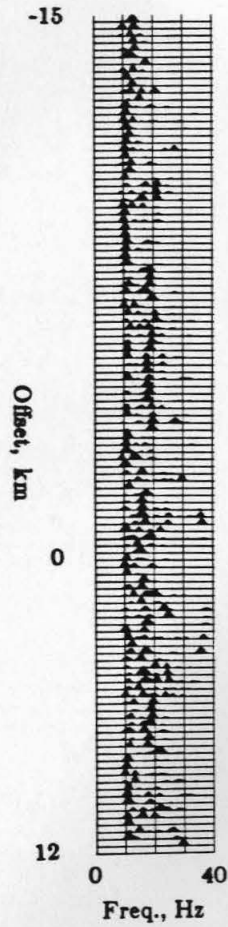
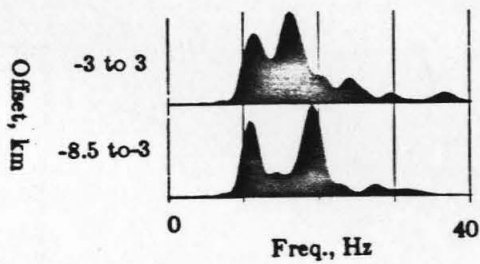
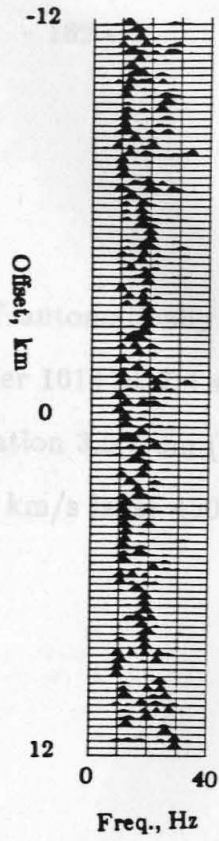
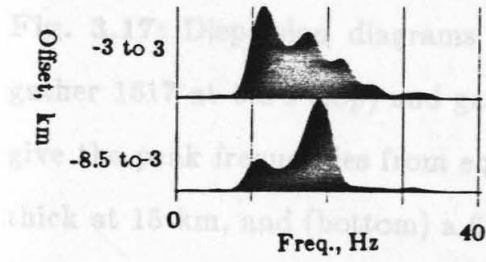
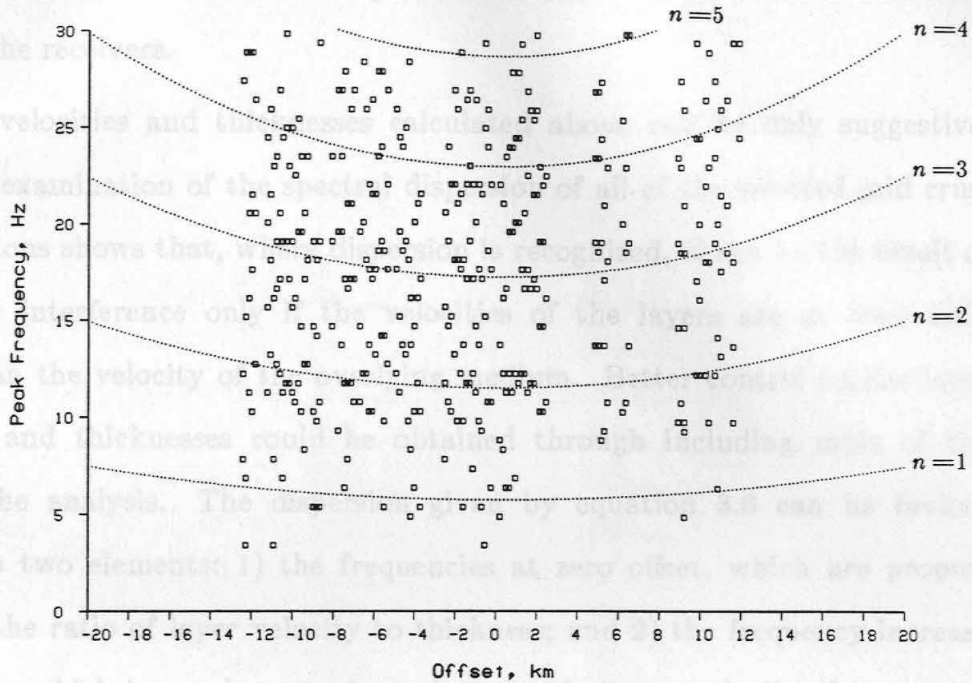


**Fig. 3.17:** Dispersion diagrams of automatically picked spectral peaks from gather 1617 at 6.0 s (top) and gather 1614 at 7.4 s (bottom). The dotted lines give the peak frequencies from equation 3.6 from (top) a 6.3 km/s layer 275 m thick at 15 km, and (bottom) a 6.9 km/s layer 450 m thick at 19.1 km, for the indicated  $n$  overtones.



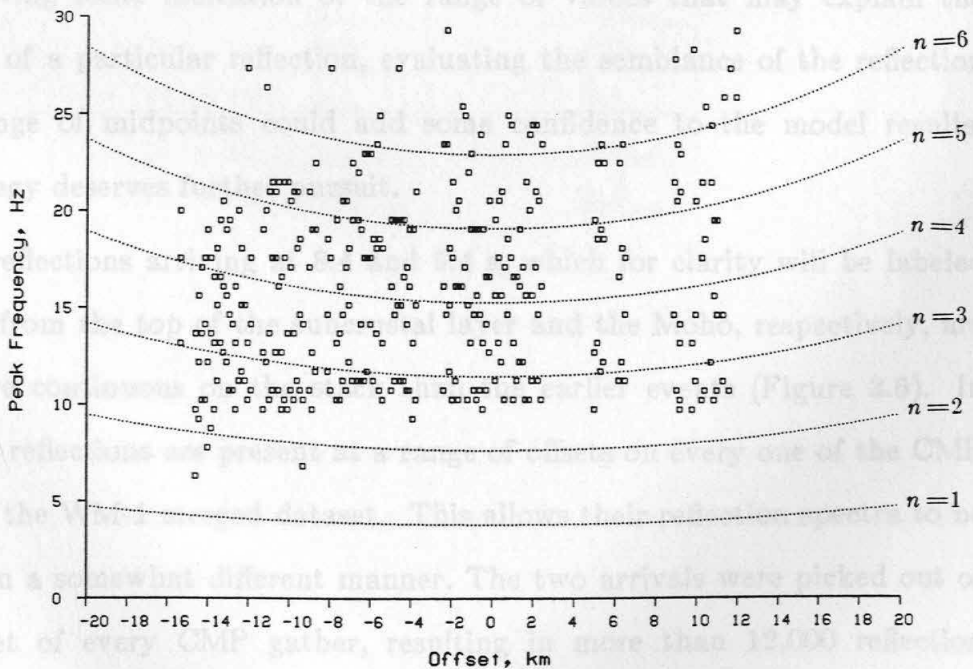
WM/S-1 CMP Gather 1617 at 6 s, 4 highest peaks

Calculated dispersion of lowest 3 modes, Model vmod.nmo1698 Vd=5.8 Vlay=6.3 depth=15 thick=0.275  
Source numbers 0 to 100000



WM/S-1 CMP Gather 1614 at 7.4 s, 3 highest peaks

Calculated dispersion of lowest 3 modes, Model vmodKH.nmo1606 Vd=6.3 Vlay=6.92 depth=19.1 thick=0.454  
Source numbers 0 to 100000



may be buried in the surface wave peak, while the  $n = 1$  overtone is below the range of the receivers.

The velocities and thicknesses calculated above can be only suggestive. However, examination of the spectral dispersion of all of the selected mid crustal reflections shows that, where dispersion is recognized, it can be the result of thin layer interference only if the velocities of the layers are at least 10% higher than the velocity of the overlying medium. Better control on the layer velocities and thicknesses could be obtained through including more of the data in the analysis. The dispersion given by equation 3.6 can be broken down into two elements: 1) the frequencies at zero offset, which are proportional to the ratio of layer velocity to thickness; and 2) the frequency increase with offset, which is much more dependent on the layer velocity than on the thickness. Thus, a semblance of the spectra can be calculated over a field of thicknesses and velocities, in a manner similar to a velocity semblance. Besides giving some indication of the range of values that may explain the dispersion of a particular reflection, evaluating the semblance of the reflection over a range of midpoints could add some confidence to the model results. This strategy deserves further pursuit.

The reflections arriving at 8.4 and 9.4 s, which for clarity will be labeled as arising from the top of the subcrustal layer and the Moho, respectively, are much more continuous on the stack than the earlier events (Figure 3.6). In fact, these reflections are present at a range of offsets on every one of the CMP gathers in the WM-1 merged dataset. This allows their reflection spectra to be analyzed in a somewhat different manner. The two arrivals were picked out of every offset of every CMP gather, resulting in more than 12,000 reflection

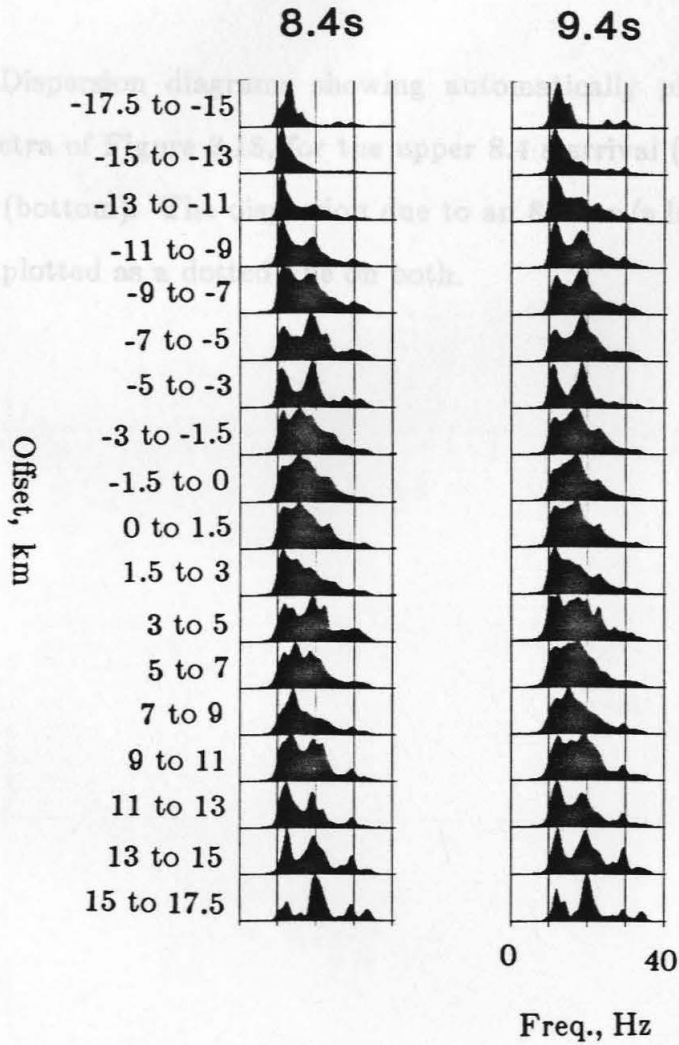
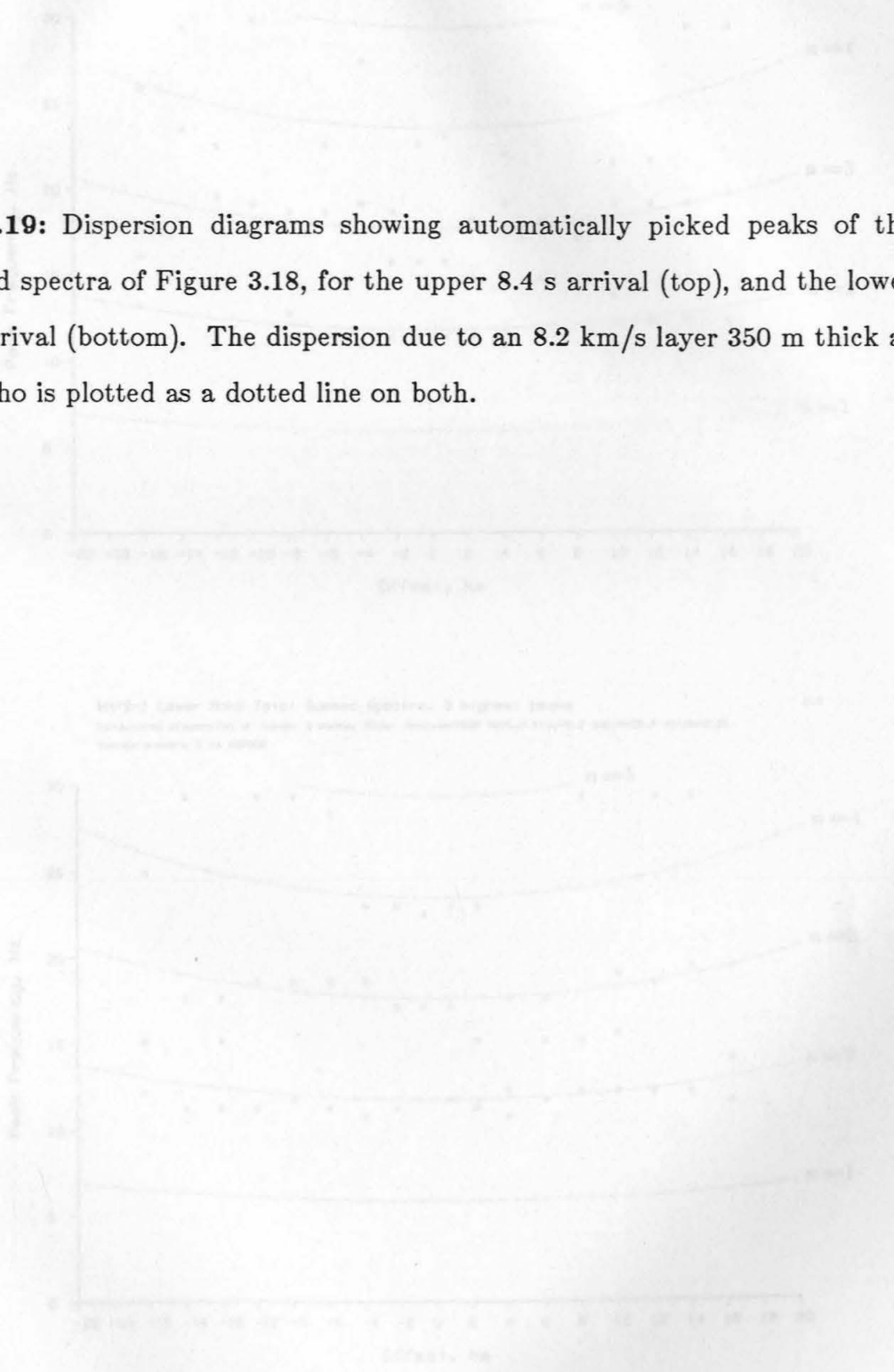


**Fig. 3.18:** Spectra summed over the indicated ranges of offset from the more than 12,000 spectra calculated from windowed Moho depth reflections near 8.4 s (left) and 9.4 s (right).

**Fig. 3.19:** Dispersion diagrams showing automatically picked peaks of the summed spectra of Figure 3.18, for the upper 8.4 s arrival (top), and the lower 9.4 s arrival (bottom). The dispersion due to an 8.2 km/s layer 350 m thick at the Moho is plotted as a dotted line on both.



WM/S-1 Upper Moho Total Summed Spectra, 3 highest peaks  
Calculated dispersion of lowest 3 modes, Model vmad.nao1698 Vd=6.6 Vray=8.2 depth=25.7 thick=0.35  
Source numbers 0 to 100000

2.5

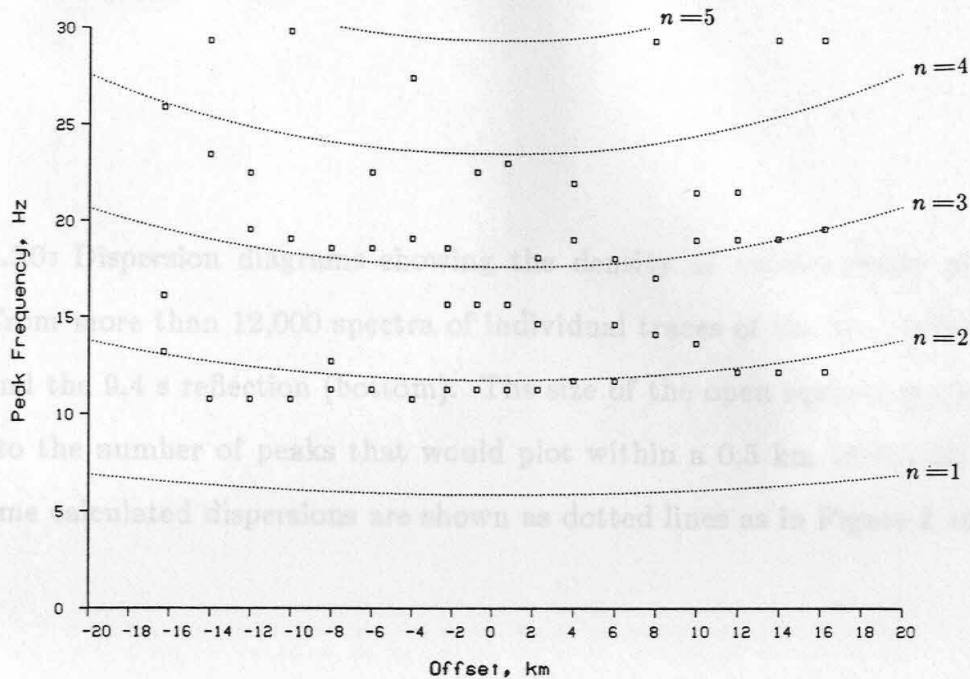
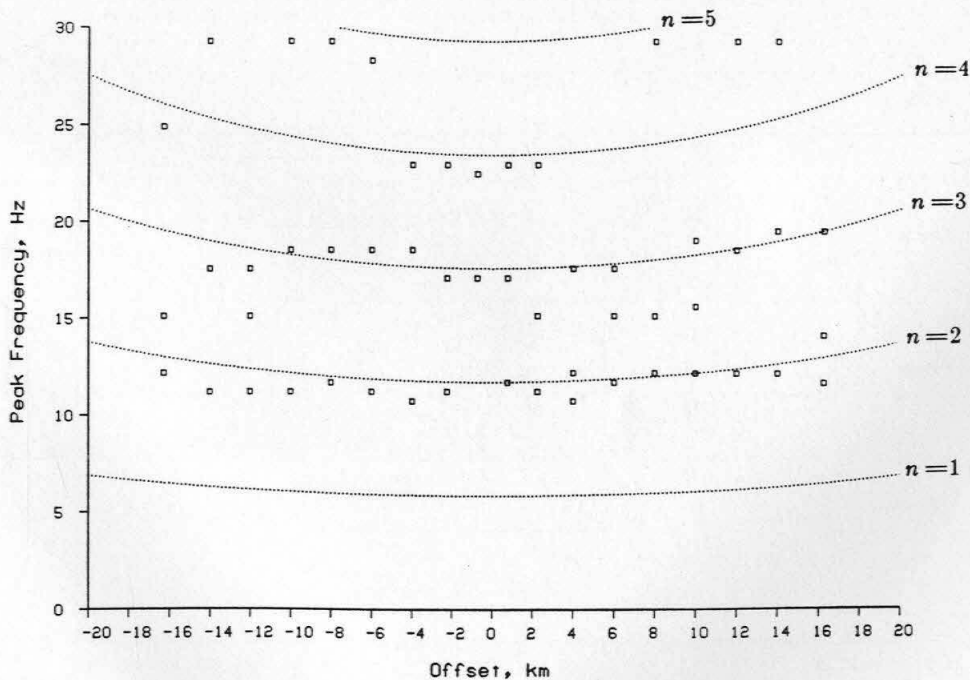
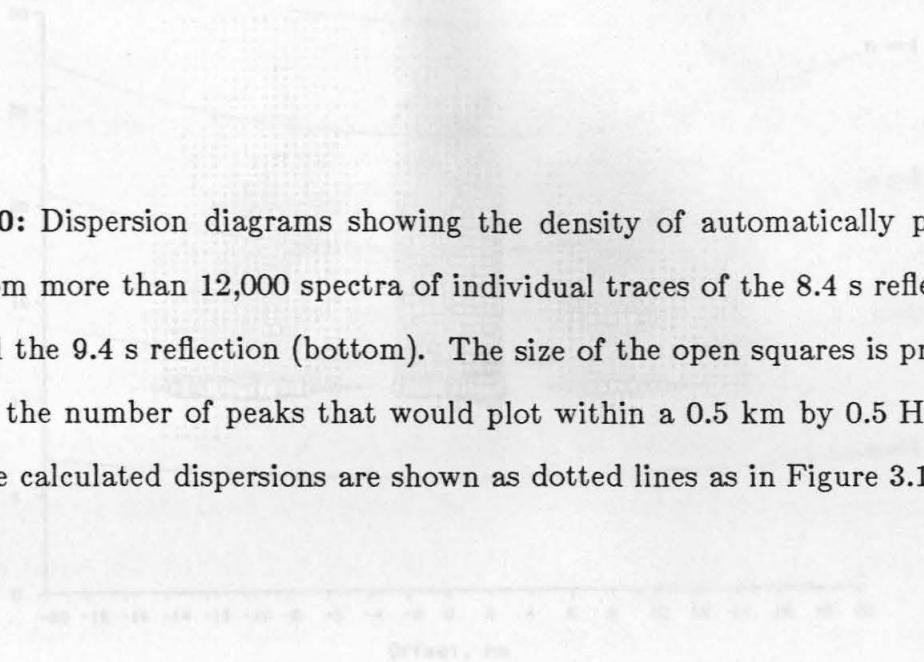


Fig. 3. Calculated dispersion of lowest 3 modes, Model vmad.nao1698 Vd=6.6 Vray=8.2 depth=25.7 thick=0.35  
peaks from more than 12,000 spectra of individual traces of  
(top) and the 9.4 s reflection (bottom) of the data set  
tional to the number of peaks that would plot within a 0.5 km  
The same calculated dispersions are shown as dotted lines as in Figure 2.

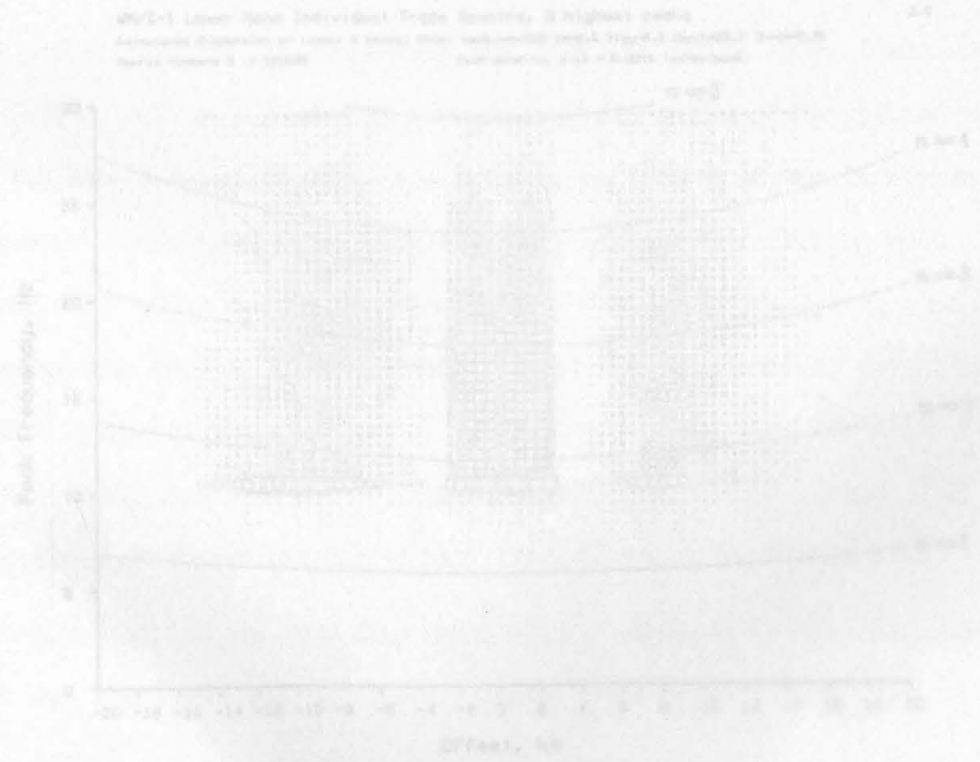
WM/S-1 Lower Moho Total Summed Spectra, 3 highest peaks  
Calculated dispersion of lowest 3 modes, Model vmad.nao1698 Vd=6.6 Vray=8.2 depth=25.7 thick=0.35  
Source numbers 0 to 100000

2.5



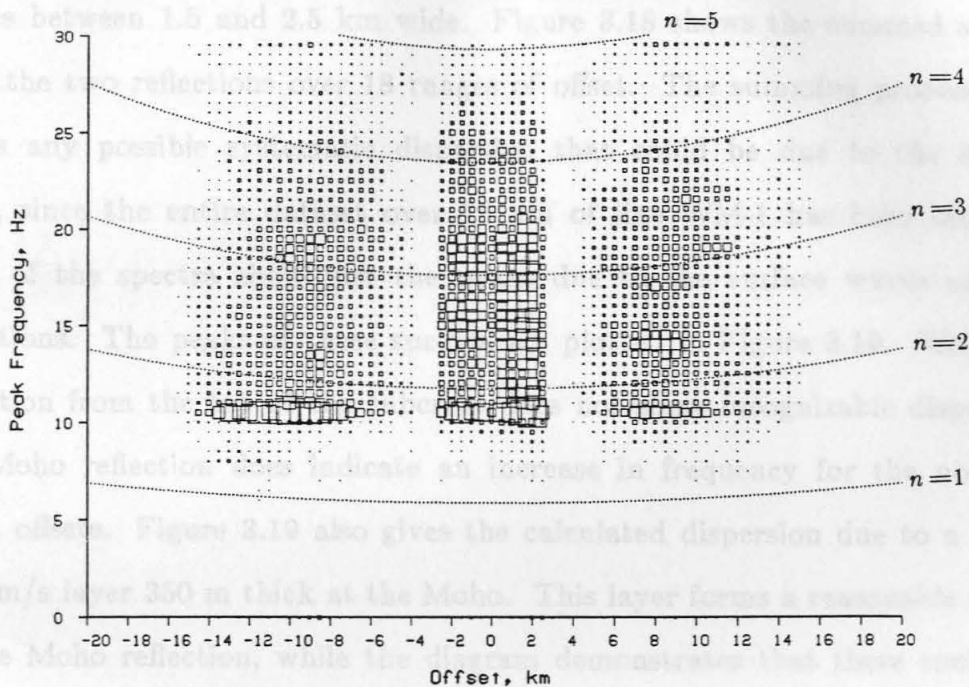


**Fig. 3.20:** Dispersion diagrams showing the density of automatically picked peaks from more than 12,000 spectra of individual traces of the 8.4 s reflection (top) and the 9.4 s reflection (bottom). The size of the open squares is proportional to the number of peaks that would plot within a 0.5 km by 0.5 Hz bin. The same calculated dispersions are shown as dotted lines as in Figure 3.19.



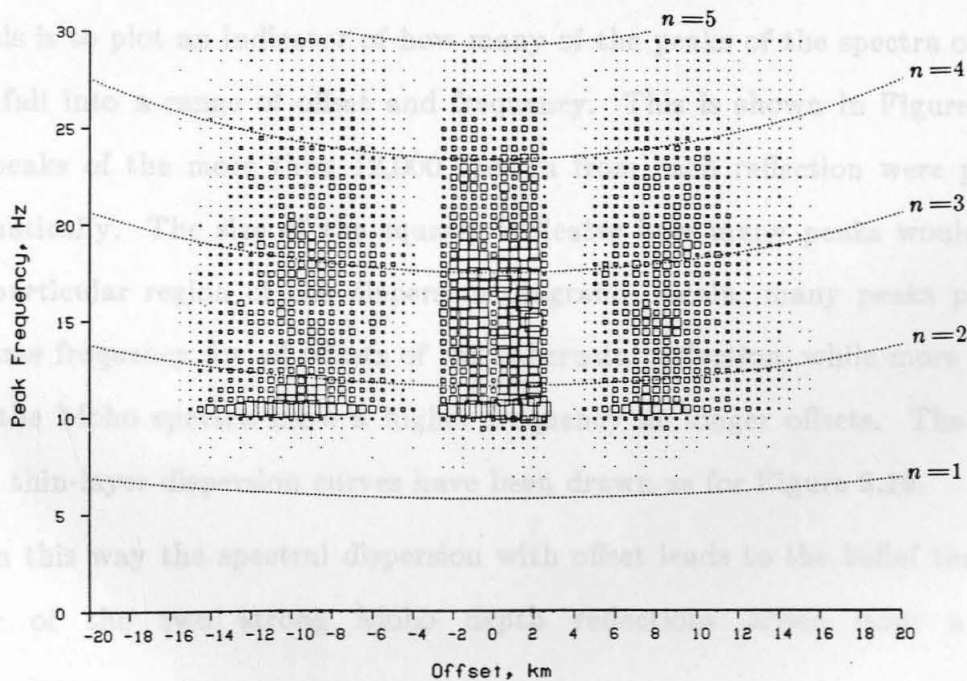
WM/S-1 Upper Moho Individual Trace Spectra, 3 highest peaks  
Calculated dispersion of lowest 3 modes, Model vmod.nmo1698 Vd=6.6 Vlay=8.2 depth=25.7 thick=0.35  
Source numbers 0 to 100000 Peak density, size = 0.0019 inches/peak

2.5



WM/S-1 Lower Moho Individual Trace Spectra, 3 highest peaks  
Calculated dispersion of lowest 3 modes, Model vmod.nmo1698 Vd=6.6 Vlay=8.2 depth=25.7 thick=0.35  
Source numbers 0 to 100000 Peak density, size = 0.0019 inches/peak

2.5



spectra from each interface. These spectra were then summed over offset ranges between 1.5 and 2.5 km wide. Figure 3.18 shows the summed spectra from the two reflections over 18 ranges of offset. The summing process eliminates any possible systematic dispersion that could be due to the surface layer, since the entire dataset over 18 km of line WM-1 has been included. Most of the spectra show just the peaks due to the surface waves and the reflections. The peaks of these spectra are plotted in Figure 3.19. While the reflection from the top of the subcrust does not show recognizable dispersion, the Moho reflection does indicate an increase in frequency for the north to south offsets. Figure 3.19 also gives the calculated dispersion due to a model 8.2 km/s layer 350 m thick at the Moho. This layer forms a reasonable match to the Moho reflection, while the diagram demonstrates that there could not be enough dispersion in the subcrustal reflection for it to have resulted from such a layer.

Another method of displaying the spectral peaks from these deepest arrivals is to plot an indicator of how many of the peaks of the spectra of each trace fall into a range of offset and frequency. This is shown in Figure 3.20. The peaks of the more than 12,000 spectra from each reflection were picked automatically. The size of the squares indicates how many peaks would plot in a particular region of the dispersion diagram. Again, many peaks plot at the same frequency for all offsets of the subcrustal reflection, while more peaks from the Moho spectra have a higher frequency at longer offsets. The same model thin-layer dispersion curves have been drawn as for Figure 3.19.

In this way the spectral dispersion with offset leads to the belief that the earlier of the two strong Moho depth reflections arises from a step

discontinuity in velocity. If this reflector is envisioned to be the interface between the granitic layer and a higher-velocity subcrust, then this interpretation would be quite consistent. The later of the two reflections exhibits a definite increase in frequency with offset, which can be seen over the entire merged WM-1 dataset. The amount of dispersion indicates that the Moho may contain one or more layers a few hundred meters thick, having a very high velocity, probably greater than the velocity of the uppermost mantle.

Assuming that the variations in the density  $\rho$ , Lamé's parameter  $\lambda$ , and rigidity  $\mu$  at a point scatterer are small, they derive a system of equivalent forces for each reflected phase from each of the three types of scatterer. These effects are linear; the forces will simply add if physical properties are combined.

As shown in Figure 3.21, an incident plane compressional wave produces, at the scatterer, the same effect as a point force in the case of a variation in  $\rho$ , a point explosion for a  $\lambda$  variation, and a point couple for a  $\mu$  variation. Thus, under Wu and Aki's assumptions, reflection amplitude can only decrease as incidence angle increases over a pure  $\rho$  or  $\mu$  variation, while the amplitude does not vary with angle over a pure  $\lambda$  variation. Since the forces can be added algebraically, one can see that an inhomogeneity incorporating any combination of  $+\delta\rho$ ,  $+\delta\lambda$ , or  $+\delta\mu$  will produce a decrease in amplitude with angle. The same is true for a combination of  $-\delta\rho$ ,  $-\delta\lambda$ , or  $-\delta\mu$ , since the absolute value of the reflection amplitude is being measured, not its phase.

Suppose, however, that the inhomogeneity incorporates  $+\delta\lambda$  and  $-\delta\mu$  variations. In this case the algebraic sum of the equivalent forces will produce an increase in the absolute value of the reflection amplitude as incidence angle

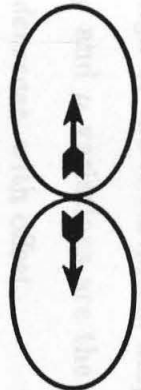
#### 4. REFLECTION AMPLITUDE ANALYSIS

The second step in this analysis is to determine what aspects of the physical nature of the reflectors can be constrained by the multi-offset amplitude information within the datasets. Perhaps the most direct approach to the problem of inverting an observed amplitude versus offset relation for the properties of the reflector is to refer to the simplifications of Wu and Aki (1985). Assuming that the variations in the density  $\rho$ , Lamé's parameter  $\lambda$ , and rigidity  $\mu$  at a point scatterer are small, they derive a system of equivalent forces for each reflected phase from each of the three types of scatterer. These effects are linear; the forces will simply add if physical properties are combined.

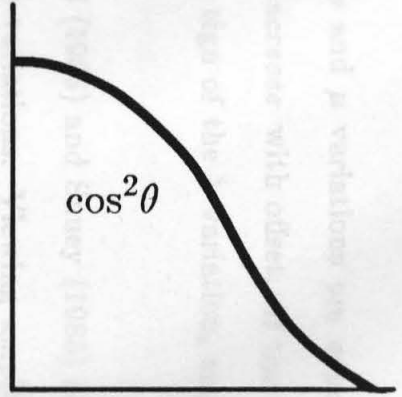
As shown in Figure 3.21, an incident plane compressional wave produces, at the scatterer, the same effect as a point force in the case of a variation in  $\rho$ , a point explosion for a  $\lambda$  variation, and a point couple for a  $\mu$  variation. Thus, under Wu and Aki's assumptions, reflection amplitude can only decrease as incidence angle increases over a pure  $\rho$  or  $\mu$  variation, while the amplitude does not vary with angle over a pure  $\lambda$  variation. Since the forces can be added algebraically, one can see that an inhomogeneity incorporating any combination of  $+\delta\rho$ ,  $+\delta\lambda$ , or  $+\delta\mu$  will produce a decrease in amplitude with angle. The same is true for a combination of  $-\delta\rho$ ,  $-\delta\lambda$ , or  $-\delta\mu$ , since the absolute value of the reflection amplitude is being measured, not its phase.

Suppose, however, that the inhomogeneity incorporates  $+\delta\lambda$  and  $-\delta\mu$  variations. In this case the algebraic sum of the equivalent forces will produce an increase in the absolute value of the reflection amplitude as incidence angle

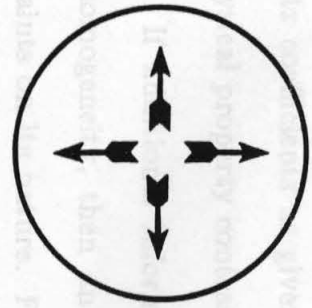
**Fig. 3.21:** Equivalent forces and their directivity for P-P reflections arising from the impingement of plane waves on small inhomogeneities of the density  $\rho$ , Lamé's parameter  $\lambda$ , and rigidity  $\mu$ , observed at any scattered angle. The incident wavefront is horizontal. The bottom three graphs show reflection amplitudes as a function of offsets corresponding to angles less than  $90^\circ$ . Adapted from Wu and Aki, 1985a.



$+\delta\mu$



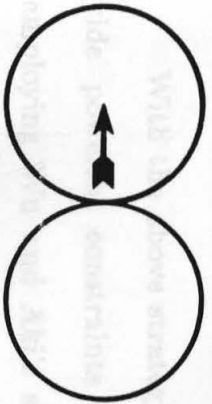
Offset



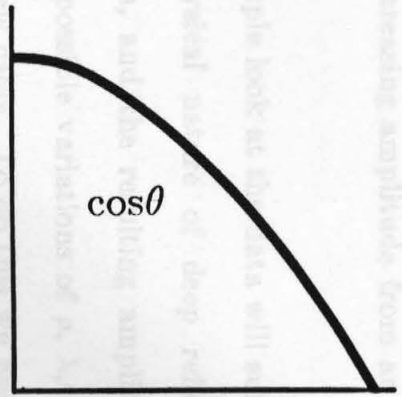
$+\delta\lambda$



Offset



$+\delta\rho$



Offset

After Wu and Aki, 1985

increases. In fact, if the signs of the  $\rho$  and  $\mu$  variations are *opposed* to the sign of the  $\lambda$  variation, amplitude will *increase* with offset. If the signs of the  $\rho$  and  $\mu$  variations are the *same* as the sign of the  $\lambda$  variation, amplitude will *decrease* with offset.

The assumptions made by Koefoed (1955) and Shuey (1985) are a narrow special case of the above set of possible variations. Viewing amplitude effects as resulting from differences between the sign of  $\delta\rho$ ,  $\delta\mu$ , and the sign of  $\delta\lambda$  gives a more complete picture. Less traditional variations in the crust can be considered. These relations have been verified by simply calculating the Zoeppritz coefficients as given in Aki and Richards (1980) at subcritical angles for physical property contrasts of up to 10%.

If additional information can be brought to bear on the nature of the inhomogeneity, then an amplitude versus offset trend can yield strong constraints on its nature. For example, if a reflector is known to be a  $+\delta\lambda$  variation, then the above relations indicate that increasing amplitude with offset results from an increase in Poisson's ratio  $\sigma$ , and decreasing amplitude would be from a decrease in  $\sigma$ . Conversely, a  $-\delta\lambda$  variation would show increasing amplitude from a decrease in  $\sigma$  and decreasing amplitude from an increase in  $\sigma$ .

With the above strategy a very simple look at the data will suffice to provide powerful constraints on the physical nature of deep reflectors. By employing Wu and Aki's simplification, and the resulting amplitude versus offset relations given above, the set of possible variations of  $\rho$ ,  $\lambda$ , and  $\mu$  at a particular reflector can be limited to a few cases. To do this we need only discern whether the amplitude increases or decreases with offset, in the manner of

Long and Richgels (1985). It is not even necessary to look for variations between the amplitudes at three ranges of offset, as done by Onstott et al. (1984). The ability to look for such a simple, distinguishable phenomenon makes this method practical for deep crustal datasets.

### *Effects on seismic amplitudes*

Before the desired relation of reflection amplitude to incidence angle can be derived from the observed relation of amplitude to offset, a number of factors that could corrupt the observations need to be taken into account. Some are listed by Ostrander (1984). These, and additional factors, can be divided into four categories based on where they arise in the process of a seismic experiment. Each of the factors is explained below, along with strategies for mitigating their effects.

#### *a) Recording and processing effects*

This category includes factors arising from the recording and processing of the data collected by the seismometers. The most obvious factor in obtaining a correct trend of amplitude versus offset is the calibration of the seismic sources and receivers. A seismic reflection experiment usually lacks calibration of the geophones, and the power output by the blasts or vibrators is unknown. The most robust strategy is to apply a constant gain to the seismogram obtained by any particular source-receiver pair, the level of which is determined by amplitude level of a quantile within the spectrum of amplitude levels within a certain interval of the seismogram. In the manner of Wiggins et al. (1985), each seismogram of a dataset is multiplied by a factor such that the value at some percentile of the amplitude range of the time samples in the

seismogram always has the same numerical value. The assumption made is that values below about the 70th percentile represent "background noise," which can be environmental noise, source-generated noise, or very weak reflections. The amplitudes above the quantile thus represent the reflections in question. Little functional difference can be detected between the use of percentile values from 50 and 90% (Wiggins, personal communication). This procedure does establish a consistent calibration for the source-receiver combination, provided that the data are not contaminated by strong source-generated noise in the interval used to evaluate the quantile (Yu, 1985).

In considering the effects of source-generated noise, it is important to find a way to derive amplitude-offset trends from the data while assuring that only direct compressional wave reflection phases are being analyzed. The relations between amplitude versus offset trends and reflector properties are not valid for any other phases. In addition, one would like to mitigate the effects of reflections coming from out of the plane of the survey line, which can produce spurious arrivals from a structure as simple as a hemispherical basin (Cohen and Bleistein, 1983). Choosing the areas for such detailed analysis, and adding a few special procedures to a normal processing sequence can help to avoid misidentified phases.

The most direct way to analyze amplitude versus offset trends is to incorporate the analysis into the stacking process. In this way, if the assumptions inherent in stacking are not violated, the effects of phases other than direct compressional reflections, and out-of-plane reflectors, can be minimized. Therefore, this analysis will concentrate on the more horizontal, laterally continuous reflections, which can be shown to best obey the assumptions of the

stacking process.

Stacking is a limited part of the linear transformation commonly known as "velocity stack" or as finding a "velocity spectrum" (Thorson and Claerbout, 1985). For such transformations Harlan et al. (1984) developed a method to calculate how well any particular result of the transform fit the objective assumptions of the transform. Using their procedure, for each sample of the stacked trace the percentage of hyperbolic "signal" within the multi-offset gather can be calculated, as opposed to the "noise" of the gather with trace-to-trace coherency destroyed by changing the signs of random traces. This distribution of signal content is used to weight the stack itself, emphasizing those events best fitting the hyperbolae defined by the stacking velocities, and therefore closest to the stacking assumptions. Out-of-plane events and non-direct compressional reflection phases are suppressed by this procedure.

The amplitude versus offset trends are found by a similar operation. For each point of the stacked trace, a linear regression of the rms amplitude of a window along the stacking hyperbola against offset is performed. The linear trends of amplitude thus found are plotted as a section similar to the stacked section, in the manner of Long and Richgels (1985), which we can call an "amplitude trend stack."

The process of calculating the linear regressions of amplitude against offset can be corrupted by the presence of source-generated noise in the gathers. Yu (1985) pointed out how multiple reflections could falsely bias the linear trends. Air and surface waves could also be sources of interference. I will, however, look for the more rapid variations of trend with respect to

intercept time on the amplitude trend stack. Source-generated noise, as it has a much slower apparent velocity across the gather than the reflections, will produce a broad bias in the amplitude trend section that will not vary rapidly with respect to intercept time. The trends of the direct reflections will stand out against this background and can be evaluated relative to it.

*b) Surface consistent effects*

This category includes factors that depend only upon the location and characteristics of the sources and receivers, and factors arising within a few wavelengths of them. These factors are both surface consistent in the sense defined by Taner and Koehler (1981), and offset dependent in that I will consider near-surface effects arising out of differences in travel path near the surface. A factor related to source and receiver calibration as discussed above is the relative efficiency of mechanical coupling between the sources and receivers and the ground. While this can be affected by differences in the physical properties of the surface, the effects should not extend deeper than the length scale of the vibrators or of the geophones, both of which are much smaller than the seismic wavelengths of deep crustal experiments. Such frequencies are also well below the usual limits on the frequency response of a geophone plant (Krohn, 1984). These effects can be considered to be surface consistent in the strictest sense, not variable with raypath to the transducer. As far as the coupling affects the rms amplitude of the recorded reflections, the quantile-based trace equalization should mitigate its effects.

A factor not as strictly surface consistent concerns the directivity inherent in the use of vertical vibrators and geophones. Both devices produce and detect compressional waves most strongly at vertical angles of incidence on the

surface, especially when they are deployed in arrays (Miller and Pursey, 1954; Tan, 1985). Thus, the amplitude efficiency of a source-receiver pair will decrease as offset, and incidence angle, increase. Kahler and Meissner (1983) and Safar (1984) point out that the directivity patterns can vary appreciably because of variations in the Poisson's ratio of the surface materials. Unconsolidated surface rocks often show large, rapid variations in Poisson's ratio. Fortunately, however, changes in Poisson's ratio have very little effect on the directivity of vertical sources and receivers for compressional waves, as long as Sv phases can be avoided.

In the case of the Ward Valley dataset, as described above, the velocities at the surface are so low compared to the velocities at the depths of interest that any pre-critically reflected rays are bent to near-vertical incidence at the surface— less than  $12^\circ$  from vertical. This phenomenon will hold true for almost any dataset in the Mojave Desert, as they are generally recorded over arid alluvial deposits at least one wavelength thick. In fact, curvature of reflected rays is likely to occur in most deep crustal experiments, as the velocities at reflector depths are at least three times the surface velocity. With so little variation in the ray angle at the surface of a deep reflection at any pre-critical offset, the source and receiver directivities can be ignored.

A more serious problem within this category is the effect of near-surface lateral heterogeneities. Goupillaud (1961) cautioned that the velocity contrasts near the surface are likely to be sharper and more inhomogeneously distributed than anywhere else in the crust. The shallow section, even if it is laterally homogeneous, or contains the simplest lateral variations, can still corrupt the reflections to the point that they seriously violate the stacking assumptions

(Honeyman, 1983; Pullan and Hunter, 1985). Repeating a seismic experiment identically, but at a location just a wavelength or so away, can greatly change the character of the recorded reflections (Savit, 1950).

The multiplicity and reciprocity available from a high-density seismic reflection experiment are relied on to address this problem. Each reflector in question should be imaged at many different depth points, and each depth point should be imaged from sources and receivers at many locations on the surface. At the least, this calls for long offset surveys such as those described in Chapter 2, where a large number of widely distributed sources are recorded into a large number of widely distributed receivers. A short, fixed spread such as the one used by Wen and McMechan (1985) during the COCORP Wind River survey will always suffer from doubts about the effects of lateral heterogeneities. An experiment organized to provide common midpoint gathers will benefit from increased multiplicity at the surface and from crossing raypaths in the subsurface, especially at the longer offsets (Mayne, 1962). Given enough lateral continuity at the reflector, the midpoint gathers can be combined over limited ranges to provide a finer sampling of the offset range (Yu, 1985). Such multiplicity allows the amplitude effects of lateral heterogeneities to be averaged out during the linear regression process.

The assumption of source and receiver reciprocity, as defined by Knopoff and Gangi (1959), aids in producing a multiplicity of depth points and travel paths. It has, however, been shown to break down for "propagating modes," e.g., surface waves and multiply reflected refractions, in the presence of near receiver inhomogeneity (Balachandran, 1974). Fortunately, Fenati and Rocca (1984) were able to suggest from field experiments that the reciprocity of more

vertically propagating energy, at longer offsets and later arrival times, is preserved. It is just this type of energy that is analyzed from a deep crustal experiment, so reciprocity should hold.

*c) Propagation effects*

The effects of the propagation of the seismic wave through the crust between the source and the reflector, and back up to the receiver, are included in this category. The most obvious effect on amplitudes is that of geometric spreading. Its effect can be removed from the amplitudes of a seismic gather if the amount of divergence can be calculated, which is related to the length of the travel path from the source to the receiver. In the flat layer case, the correction can be made with a formula given by Newman (1973). Its use requires, however, knowledge of the thicknesses and interval velocities of all the layers above the reflector in question. Newman proposes a simpler correction, which relies only on knowing the stacking velocity above the reflector, velocity at the surface, and the travel time of the reflection.

The main difficulty with calculating the geometric spreading correction is in finding the length of the travel path through an often highly heterogeneous crust, while knowing only the reflection travel time and possibly the stacking velocity. If the medium above the reflector can be thought of as having a constant velocity equal to the stacking velocity, then the geometric spreading correction is obviously  $G_t = tV_{stack}$ , where  $G_t$  is the length of the travel path from the source,  $t$  is the two-way travel time of the reflection, and  $V_{stack}$  is the stacking velocity. Newman (1973) derives a similar formula,  $G_{t0} = tV_{stack}^2/v_0$ , where  $v_0$  is the surface velocity, for a multi-layered

medium at offset distances near zero, as a specific case of the multi-offset formula.

In the Mojave desert, the main deviation of any geometric spreading correction, accounting for vertical heterogeneity, from one that simply assumes a constant velocity should arise at the interface between the sedimentary fill and the underlying basement, where there is a large velocity contrast. Figure 3.22 shows four different geometric spreading corrections calculated from a model having a 2 km thick 3.6 km/s basin overlying a 6 km/s constant velocity crustal section 20 km thick, for the range of experimental offsets. It is clear that Newman's zero offset formulation  $G_{t_0}$ , the travel time and stacking velocity product  $G_t$ , and the actual path length  $G_R$  will all correct the far offsets relative to the near offsets with the same proportion. Newman's multi-offset formulation  $G_x$  will boost the far offset amplitudes to a greater degree. Given the nearly equal slope of  $G_{t_0}$  and  $G_t$ , the very close correspondence of  $G_t$  to the actual path length  $G_R$ , and the fact that  $G_t$  intersects  $G_x$  while  $G_{t_0}$  does not, the simple  $G_t$  correction appears to be more robust. Therefore, the datasets will be corrected for geometric spreading by multiplying the amplitude of each point of the seismograms by the arrival time and by the stacking velocity.

The fact that we are looking for rapid variations of reflector amplitude versus offset trend with respect to intercept time will mitigate any errors in the calculated geometric spreading correction. Any under or over correction of this effect will simply result in a broad bias of the traces within the amplitude trend stack. Further, as Figure 3.22 shows, the corrections for the far offsets will not be greater than three times those for the near offsets. This is unlikely

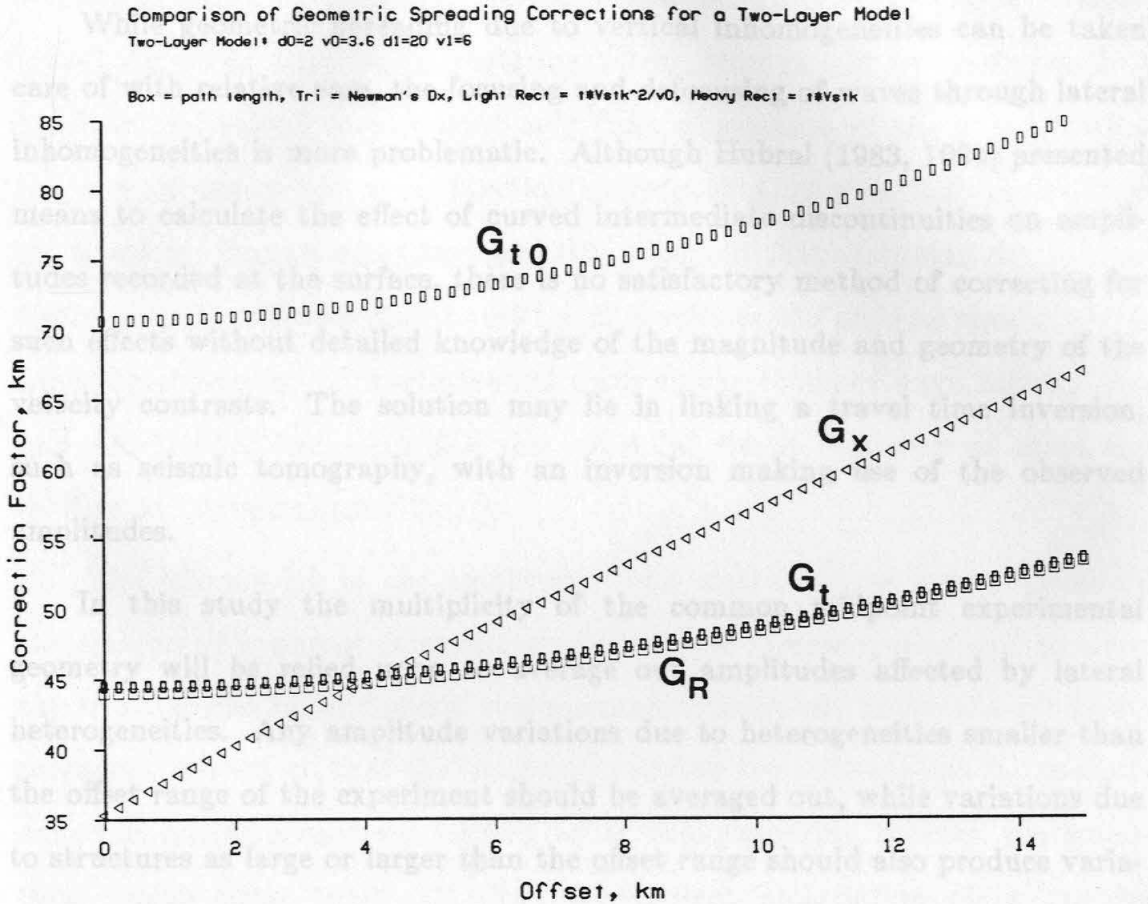


**Fig. 3.22:** Comparison of Newman's (1973) multi-offset and zero offset geometric spreading corrections,  $G_x$  and  $G_{t0}$ , respectively, with the actual path length  $G_R$  and the product of the arrival time and stacking velocity  $G_t$ . The corrections were calculated for a reflection from a structure overlain by 20 km of 6 km/s crust, topped by a 2 km thick 3.6 km/s sedimentary section.

to affect the gross amplitude versus offset trends, which are the objective here.

While geometric spreading due to vertical inhomogeneities can be taken care of with relative ease, the focusing and defocusing of waves through lateral inhomogeneities is more problematic. Although Hubral (1983, 1984) presented means to calculate the effect of curved intermediate discontinuities on amplitudes recorded at the surface, there is no satisfactory method of correcting for such effects without detailed knowledge of the magnitude and geometry of the velocity contrasts. The solution may lie in linking a travel time inversion, such as seismic tomography, with an inversion making use of the observed amplitudes.

In this study the multiplicity of the common midpoint experimental geometry will be relied upon to average out amplitudes affected by lateral heterogeneities. Any amplitude variations due to heterogeneities smaller than the offset range of the experiment should be averaged out, while variations due to structures as large or larger than the offset range should also produce variations in the travel times that will not allow the reflection to be stacked at a normal velocity. Heterogeneities that escape that criterion should cause lateral changes in the apparent amplitude trend of the reflector imaged. This will be another reason to look for reflectors showing laterally continuous trends.

A second effect on reflection amplitudes due to propagation between the surface and the reflector is attenuation. The apparent attenuation that can be measured by a seismic experiment has two causes. The first is the scattering and loss of energy from heterogeneities along the travel path, while the second is the energy dissipated as heat from the intrinsic non-linearity of the propagation of seismic waves. Schoenberger and Levin (1978) showed that up to half of

the observed apparent attenuation in well logs could be explained by the scattering produced in a flat layered model as intrabed multiples. Dainty (1984) suggested that while scattering attenuation should be observed, in a band limited seismic experiment, only from a sequence of sharp boundaries, the loss of amplitude as a function of frequency mimics that of intrinsic attenuation. Frankel and Clayton (1986) point out that scattering due to relatively smooth randomly distributed inhomogeneities will produce similar effects from the conversion of compressional wave energy to shear wave energy. Wu and Aki (1985b) had quantified this effect for elastic scatterers of finite size relative to the seismic wavelength.

The information in the amplitude trend stacks can be used to evaluate the amount of apparent attenuation affecting the seismic section and to allow the trend stacks to be thereby compensated. Assuming, as for the geometric spreading correction, that the medium overlying the reflector can be approximated as having a constant velocity equal to the stacking velocity, the amplitude versus offset trend  $T_Q$  due to apparent attenuation alone can be evaluated at different intercept times by:

$$T_Q(\tau) = \frac{A_s}{h} \left[ e^{-\frac{\pi f}{Q_{ap}} \sqrt{\tau^2 + h^2/V_{stack}^2}} - e^{-\frac{\pi f}{Q_{ap}} \tau} \right] \quad [3.9]$$

Here  $\tau$  is the intercept time,  $A_s$  is the amplitude of the wave at the source,  $h$  is the offset range of the experiment,  $f$  is the frequency,  $V_{stack}$  is the stacking velocity at time  $\tau$ , and  $Q_{ap}$  is the apparent quality factor. Calculations made, varying  $h$ ,  $f$ , and  $V_{stack}$  within reasonable ranges for the experiments in the Mojave Desert, show that the shape of  $T_Q$  as a function of  $\tau$  is sensitive almost exclusively to  $Q_{ap}$ . This will allow  $Q_{ap}$  to be determined from the

amplitude trend stacks.

Given the extreme heterogeneity of the near-surface section in the Mojave Desert, it will not be surprising to discover quite low values for  $Q_{ap}$  at the frequencies used in seismic reflection. Frankel and Clayton (1986) suggested that values less than 200 would show the effect of scattering. Evaluations of  $Q_{ap}$  from spectral ratios in a wide variety of settings have yielded low values from inhomogeneous materials. Small-scale measurements of materials such as tuff, aa lava, and limestone by De Bremaecker et al. (1966) gave values as low as 5 to 75. A value of 25 was obtained by vertical seismic profiling (VSP) measurements at 1.5 to 2 km depth below the North Sea in calcareous shale by Stainsby and Worthington (1985). Over larger offsets, Carpenter and Sanford (1985) showed apparent  $Q$  values of less than 50 within 2 km of the surface in the Rio Grande rift, and as low as 10 near the surface even at relatively homogeneous hard rock receiver sites.

Workers who possessed enough information to derive estimates of the intrinsic attenuation from observed apparent attenuation have also given low  $Q$  values. Ganley and Kanasewich (1980), after modeling scattered waves using borehole information, derived intrinsic values of 40 to 70 at 0.5 to 1.3 km depth below the Beaufort Sea. In Paleozoic sediments, Newman and Worthington (1982) found values of 4 to 25 during a VSP experiment at less than 0.2 km depth. Even at much lower frequencies, in the Basin and Range near the Mojave Desert Patton and Taylor (1984) found that the intrinsic shear wave  $Q$  did not exceed 175 anywhere in the crust. Thus, it should not be surprising to find  $Q_{ap}$  to be less than 100 for compressional wave reflections recorded on the surface through highly inhomogeneous sedimentary materials.

In a section below it will be shown that an evaluation of  $Q_{ap}$  across an extensive amplitude trend stack will indicate lateral heterogeneities in scattering and intrinsic attenuation, probably from changes in the degree of heterogeneity and intrinsic  $Q$  near the surface. As for spherical divergence, however,  $Q_{ap}$  heterogeneities can produce differences only in the overall biases of the trend stacks, which will vary far more slowly in  $\tau$  than the trends due to reflections.

Scattering from structures along the propagation path can be more problematic if the scattered energy reaches the receivers in consort with the direct reflection, rather than being delayed or radiated elsewhere. O'Doherty and Anstey (1971) warned that while transmission through layered sequences would not be a problem if the layer boundaries were not abrupt, sharp interfaces would cause internal multiple reflections with poorly understood effects. The effects of transmission through intermediate interfaces at different angles of incidence were shown to have an order of magnitude larger effect on amplitude versus offset trends than the properties of the objective reflectors by Gassaway (1984). This effect can reverse the apparent linear amplitude trend.

In examples given below it will be demonstrated that the confusion introduced by transmission through intermediate layering can be controlled. An intermediate layer with strong offset dependent transmission effects produces a bias on the amplitude trend stack of all reflections below it. This allows such intervals to be easily identified from breaks in the lateral continuity of the amplitude trends of the underlying structures. Further, for deep crustal work, the curvature of the rays due to the strong increases in velocity below the sedimentary section will make the range of incidence angles on an intermediate

layer less than that on the objective reflector.

Given such a large degree of vertical heterogeneity, it would not be surprising for the intermediate layering to produce apparent anisotropy dependent on incidence angle (Helbig, 1984). This anisotropy may further distort the relation between offset and incidence angle at the reflector, which is already poorly known because of the lack of information on crustal velocity distributions. However, this distortion should have little effect on the determination of gross amplitude versus offset trends at obviously pre-critical angles.

#### *d) Reflector effects*

Even if all of the effects of the recording, processing, surface, and propagation on reflection amplitudes can be accounted for, there are a number of phenomena arising at the reflector that can influence amplitude versus offset trends. These must be accounted for before one may interpret the trends in terms of physical property variations.

Variations in anisotropy may be important in producing reflective structures. Jones and Nur (1984) found that, while the anisotropy of shear zones at depth may not consistently produce much variability against the surrounding rock, a contrast having a maximum 7% anisotropy could produce detectable deep reflections. A reflector including such a contrast in anisotropy can interfere with the interpretation of amplitude trends. Wright (1984) presented physical and numerical models indicating that the inclusion of anisotropy can reverse an amplitude versus offset trend. However, Daley and Hron (1977) gave calculations indicating that, for a physical property contrast including anisotropy, increasing the anisotropy up to a maximum of 20% mainly affects

the position of the critical angle. While the critical angle may change by up to  $15^\circ$ , reflected amplitudes will change by less than 25% within the pre-critical range. Such changes should not affect the interpretation of reflector properties from overall amplitude trends.

Details of the geometric configuration of the reflector will also influence amplitude trends independently of the physical property contrasts. The frequency effects of a thinly layered reflector have been extensively developed in previous sections. Fisher and Gardner (1984) have suggested that reflector layering, as well, can invert the amplitude trends expected from considering the physical property contrasts of a step discontinuity.

To test this, the bounds on the thin layer spectral interference factor  $L$  (equation 3.5) were calculated for a variety of canonical physical contrasts. The bounds on  $L$  are independent of the thickness of the layer and of the frequency of the waves. Calculations, using the coefficients given by Aki and Richards (1980), to compare these bounds for an isolated thin layer with the reflection coefficient of a step discontinuity having the same properties, were made for contrasts of up to 10% for the ten cases of  $\pm\rho$ ,  $\pm\alpha$ ,  $\pm\beta$ , and  $\pm\alpha\pm\beta$ .  $\alpha$  and  $\beta$  are the compressional and shear velocities. Figure 3.23 shows the calculation for the  $+\alpha-\beta$  case, which is also an increase in  $\sigma$ . The two types of structures exhibit the same trend as a function of offset, while the thin layer reflection has a lower amplitude overall. In all cases the envelope of  $L$  exhibits the same trend as the coefficient for a step discontinuity. Severely band-limited data may show a different trend over small ranges of offset, but combining a reasonable range with some bandwidth should remove that effect.

This page intentionally left blank.

Homogeneous, Isotropic Plane Wave P-P Amplitude Thin Layer Reflection Coefficients

Calculated Coefficient with Model vmod.nao1698 depth=15  
p1=6 s1=3.5 rho1=2.5 imp1=15 pois1=0.242105  
p2=6.5 s2=3.15 rho2=2.5 imp2=16.25 pois2=0.346532

Box = step, Tri = layer spectral response range

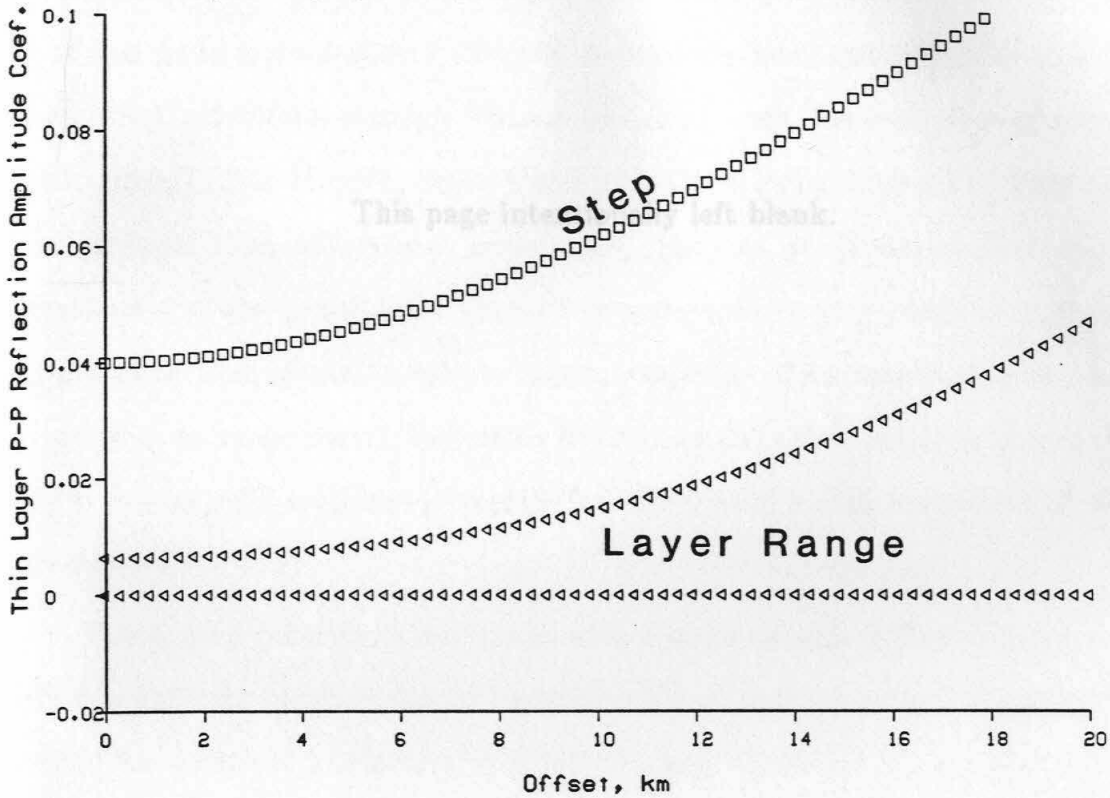


Fig. 3.23: Comparison of the bounds on the thin layer interference factor  $L$  (equation 3.5), dots, with the plane wave P-P reflection coefficient for a step discontinuity, boxes. The medium above the reflector has  $\alpha=6$  km/s,  $\beta=3.5$  km/s, and  $\sigma=0.242$ . For the isolated thin layer and for the medium below the step discontinuity,  $\alpha=6.5$  km/s,  $\beta=3.15$  km/s, and  $\sigma=0.347$ .  $\rho$  is constant at  $2.5 \text{ g/cm}^3$ . The low velocity granitic layer model of Table 3.2 was used to convert incidence angle to offset, with the reflector at a depth of 15 km.

This page intentionally left blank.

Lateral as well as vertical reflector heterogeneity also plays a roll in determining amplitude trends. Reflector curvature is a type of lateral heterogeneity that can have serious effects. Several researchers have quantified its effect on zero offset reflections through various high-frequency, far-field approximations (Hilterman, 1975; Hubral, 1983; Ursin 1986). In general, syncline reflections are stronger than those from anticlines. Shuey et al. (1984) derived similar relations for the multi-offset case. For reflectors having radii of curvature larger than their depth, synclines will increase far offset amplitudes and anticlines will decrease them. Reflectors having, on the other hand, radii less than their depths will produce decreased far offset amplitudes regardless of their orientation. The critical angle can be decreased by as much as 15°.

For a deep reflector, a curvature with a large enough radius to cause a far offset amplitude increase should be observable as such on a stacked section. It would have several kilometers of relief. A deep reflector with a radius of curvature so small that its depth variations cannot be observed on a stack can attenuate only far offset amplitudes. Thus, it appears that a flat reflector bounded above by other events not showing lateral discontinuities on the amplitude trend stack and exhibiting increasing amplitude with offset itself, should have an amplitude trend resulting only from its contrast in physical properties. The deep crust can be derived from that information alone. Next is

One possibility for a lateral variation in the properties of a reflector is a change in its thickness. Through modeling thickness variations constrained by drilling and VSP work, Balch et al. (1981) were able to verify the effects of thickness changes on reflection amplitudes observed in stacked sections. Hale and Thompson (1982), among others, have proposed that the discontinuous

nature of deep crustal reflections results from truncated layering at depth. Savit (1950) believed that relocating a seismic experiment by less than a wavelength of distance caused sharp changes in the reflections that were due to lateral variation of the reflector. While looking for laterally continuous reflector effects, it is important not to dismiss automatically every lateral discontinuity as an artifact.

To consider contrasts in physical properties from multi-offset amplitudes, the range of validity of the Zoeppritz equations should be kept in mind. Krail and Brysk (1983) showed that the multi-offset reflection coefficients for *spherical* waves can vary more strongly and more complexly than the coefficients for plane waves. The critical angle can be decreased by as much as  $15^\circ$ . Consideration of spherical waves should not, however, be necessary in high frequency seismic reflection work. For the deep crust, the reflector is removed from the source by hundreds of wavelengths.

From considering the above factors that interfere with seismic amplitudes, it is apparent that there are a few crucial techniques that enable meaningful amplitude versus offset trends to be derived. Foremost is the ability to consider just the gross trend at pre-critical offsets. Useful constraints on the nature of the deep crust can be derived from that information alone. Next is the collection of a dataset, which has not only sufficient multiplicity and areal coverage, but also succeeds in imaging simple, flat reflections that closely obey the assumptions of the stacking process. Third is the ability to separate the trends from these reflections, which vary rapidly with intercept time from the much broader trends introduced by divergence, attenuation, and source

generated noise. Finally, the amplitude trend stack itself can indicate, from a reflection's relations to the trends of surrounding events, whether a trend can be considered to be the effect of physical property contrasts alone. The following sections will demonstrate the application of these principles to datasets from three areas of the Mojave Desert.

### *Multi-offset reflection amplitudes from the Mojave Desert*

Despite the influence of the above interference factors, the reflection amplitude trends are much less subtle than the frequency trends. It will be possible to derive information on the physical property contrasts of reflectors imaged by each of the three datasets considered here. While all three show reflections from the deep crust and the Moho, each has advantages and disadvantages. In the eastern Mojave (Figure 3.1), the 1985 Calcrust dataset was specifically designed to acquire multi-offset information on deep crustal reflectors. The areas of such coverage are limited, however, to sections of the lines less than 10 km long. Dix's (1965) dataset at Soggy Lake in the central Mojave, although it consists of just one shot gather, was designed and ideally located for the recording of deep reflections through minimally complex surficial materials. The COCORP survey (Cheadle et al., 1985, 1986) covers hundreds of kilometers of the western Mojave with fair multiplicity. Unfortunately, this coverage takes it through quite a wide variety of surface related geophysical settings. Taking these three data sets together, it is possible to assemble a picture of the nature of the major reflectors beneath the Mojave Desert.

*Eastern Mojave—*

The 1985 Calcrust experiment in Ward Valley yielded a section of line 8.3 km long with 110 common midpoint gathers spaced at 75 m intervals. These gathers were constructed by merging together a 192 channel roll-along survey with offsets to 2.5 km and two reversing stationary spreads with offsets to 15 km (Chapter 2). Thus, the CMP gathers show large variations in fold, from 7 to 120, and in offset coverage along the 8.3 km length of WM-1. This analysis of the gathers concentrates on the deep crustal section of WM-1, from intercept times of 5 to 10 s.

To stack the gathers, each trace was first culled for binary value errors and labeled with information on its source and receiver positions and offset. Then trace equalization, on the 70th percentile of the amplitude levels, and the spherical divergence correction,  $G_t$ , were applied as discussed in the previous section. Each trace was filtered to pass the band between 13 and 26 Hz to mitigate the effects of the air waves and surface wave coda present on the gathers at deep crustal arrival times. Where the horizontally propagating energy was too strong to filter, it was muted out.

Stacking velocities for these gathers were evaluated by calculating a suite of constant velocity stacks of the entire set of gathers. The constant velocity stacks were weighted by the percentage of hyperbolic signal calculated using the method of Harlan et al. (1984). The constant velocity stacks gave clear indications of the velocities that resulted in the best images of many different reflections throughout the stack, allowing the velocity spectra to be picked for 19 different midpoint intervals. Velocities were picked only to yield a well-focused stack. While the resulting interval velocities were often unreasonable,

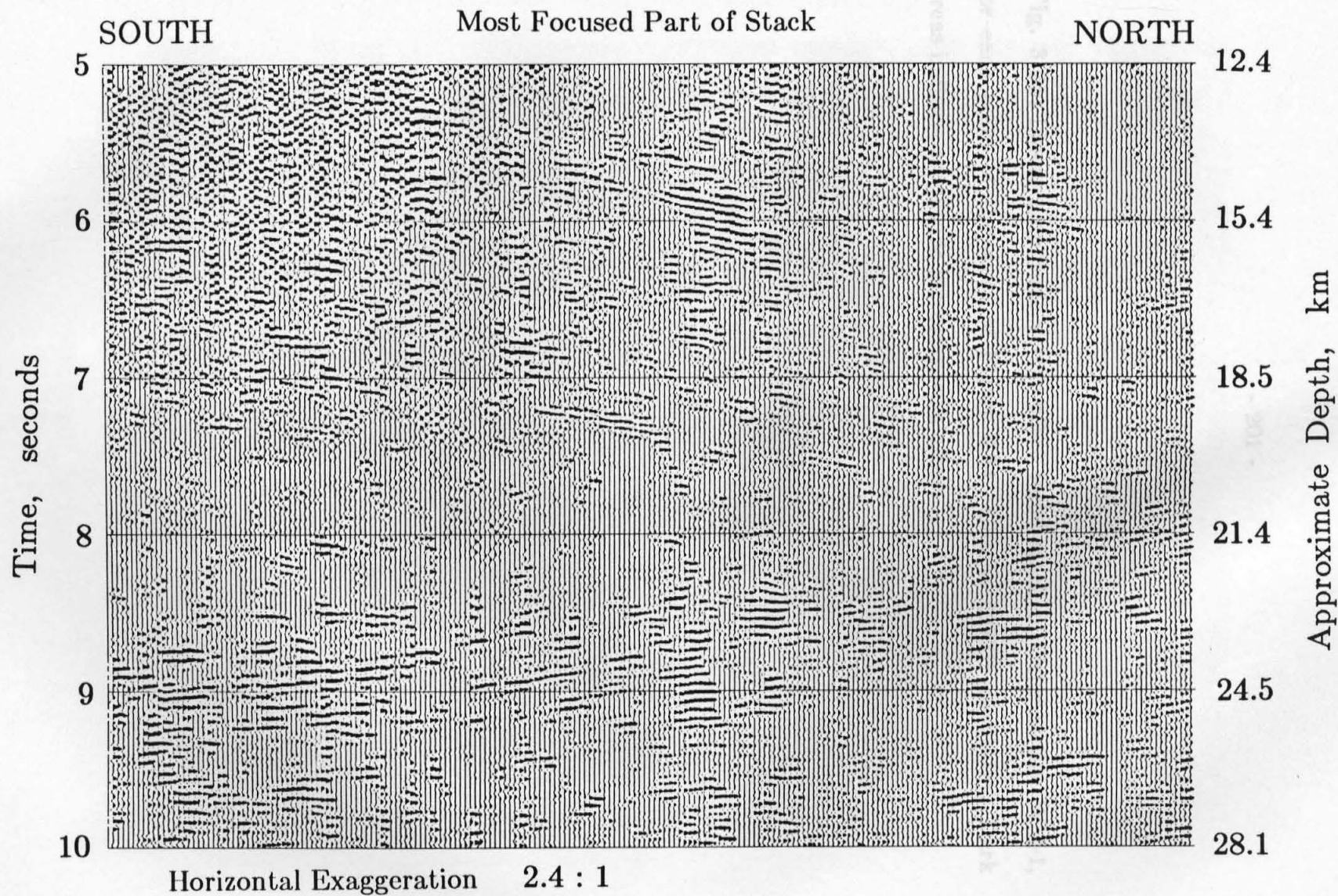
this simply reflects the degree of lateral heterogeneity present below Ward Valley.

After recalculating the spherical divergence corrections with the picked stacking velocities, the gathers were stacked into the deep crustal time section presented in Figure 3.6. This stack, representing a section of the deep crust from about 12 to 28 km depth, and 8.3 km in extent, clearly shows the north dipping mid crustal reflections and the double basal crustal reflections, as discussed above and in Chapter 2. These features are made clearer by weighting this stack with the calculated hyperbolic signal percentages, producing the stack in Figure 3.24. In this image the strongest deep reflections that best fit the assumptions of the stacking process stand out as "bright spots." Of the reflections seen on the unweighted stack, certain portions of the mid crustal events stand out clearly, as do most of the basal crustal events. The strongest, most continuous reflection is, in fact, the top of the basal crustal zone, at about 23 to 24.5 km depth.

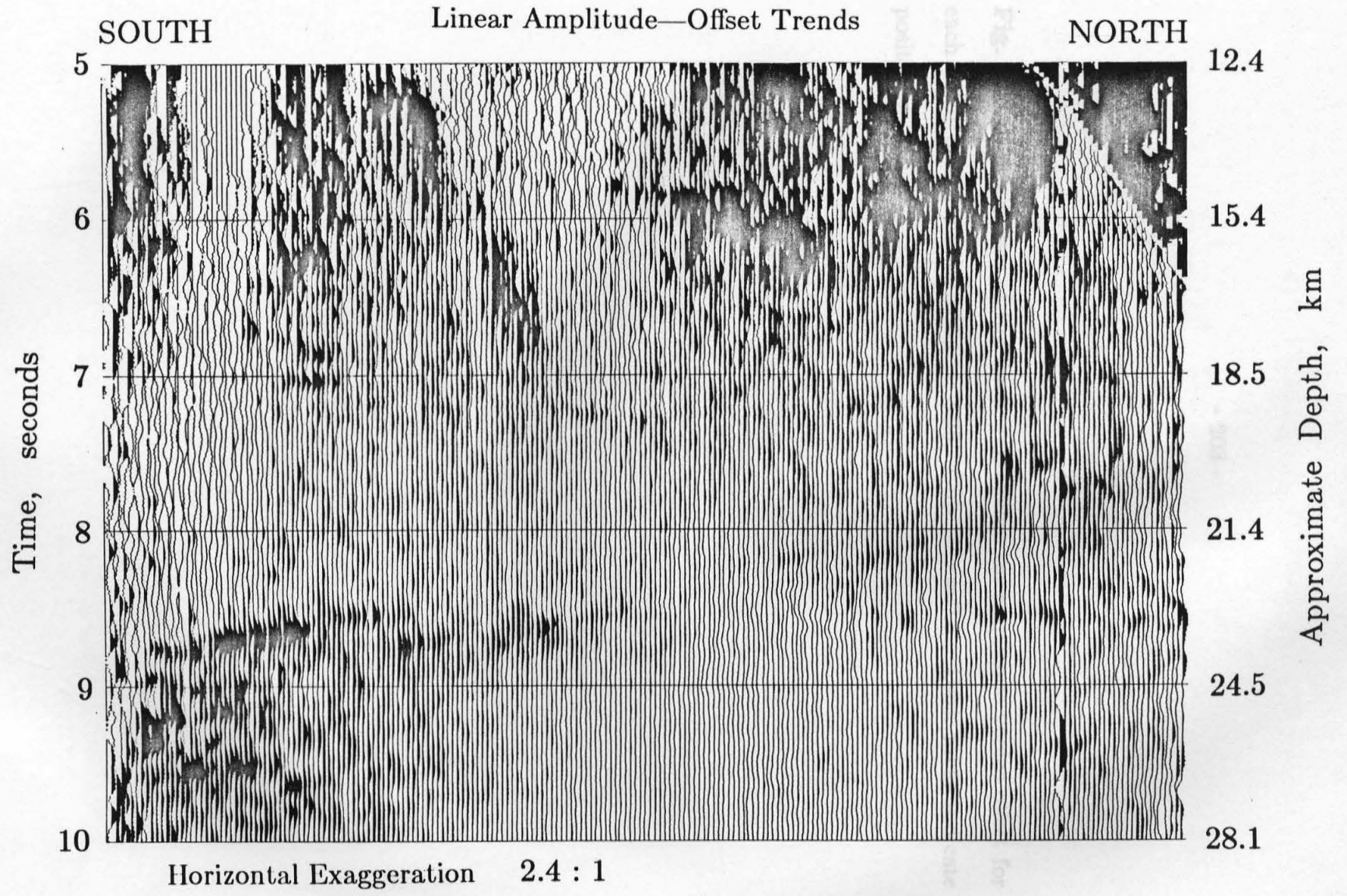
The next step in the analysis of reflection amplitude with offset is to plot the amplitude trend stack, in the manner of Long and Richgels (1985). The stacking algorithm collects statistics on the root mean-squared amplitude of a 0.08 s window of each offset trace centered about the normal moveout time at each intercept time point of each stacked trace. These statistics are reduced by simple linear regressions to yield the linear trend of amplitude with offset at each intercept time point. The correlations of each regression are also found.

The amplitude trend stack and the amplitude trend correlation stack can be plotted separately. Figure 3.26 gives the correlation stack, while Figure 3.25 gives the trend stack. Comparing these two derived sections with the

**Fig. 3.24:** Calcrust line WM-1 deep crustal stack of Figure 3.6 after weighting by the proportion of hyperbolic signal in the common midpoint gathers, in the manner of Harlan et al. (1984).



**Fig. 3.25:** Linear amplitude versus offset trend stack of Calcrust line WM-1, for each point of the stack of Figure 3.24. Clip at 0.0001 counts/m. Dark areas indicate amplitude increases with offset.



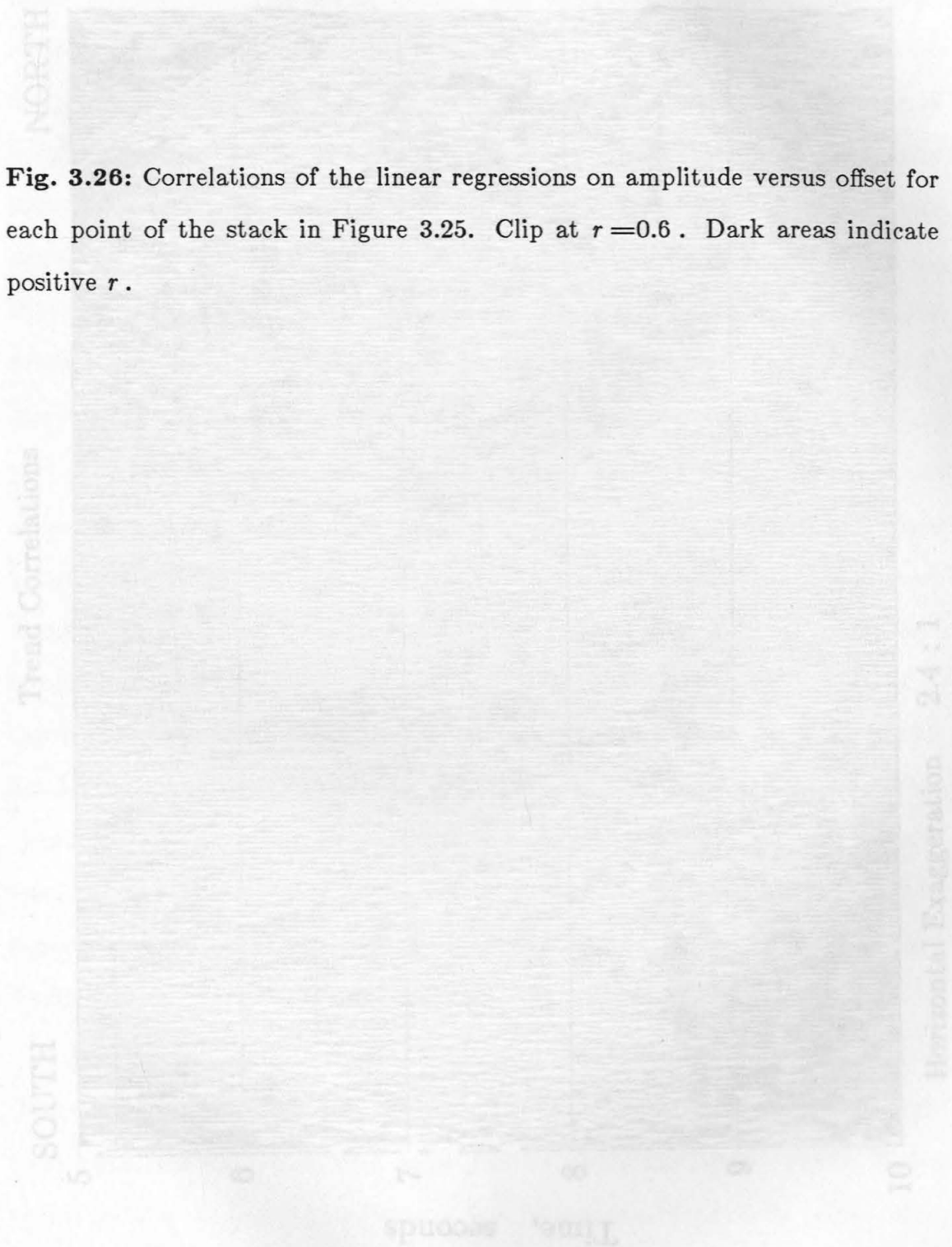
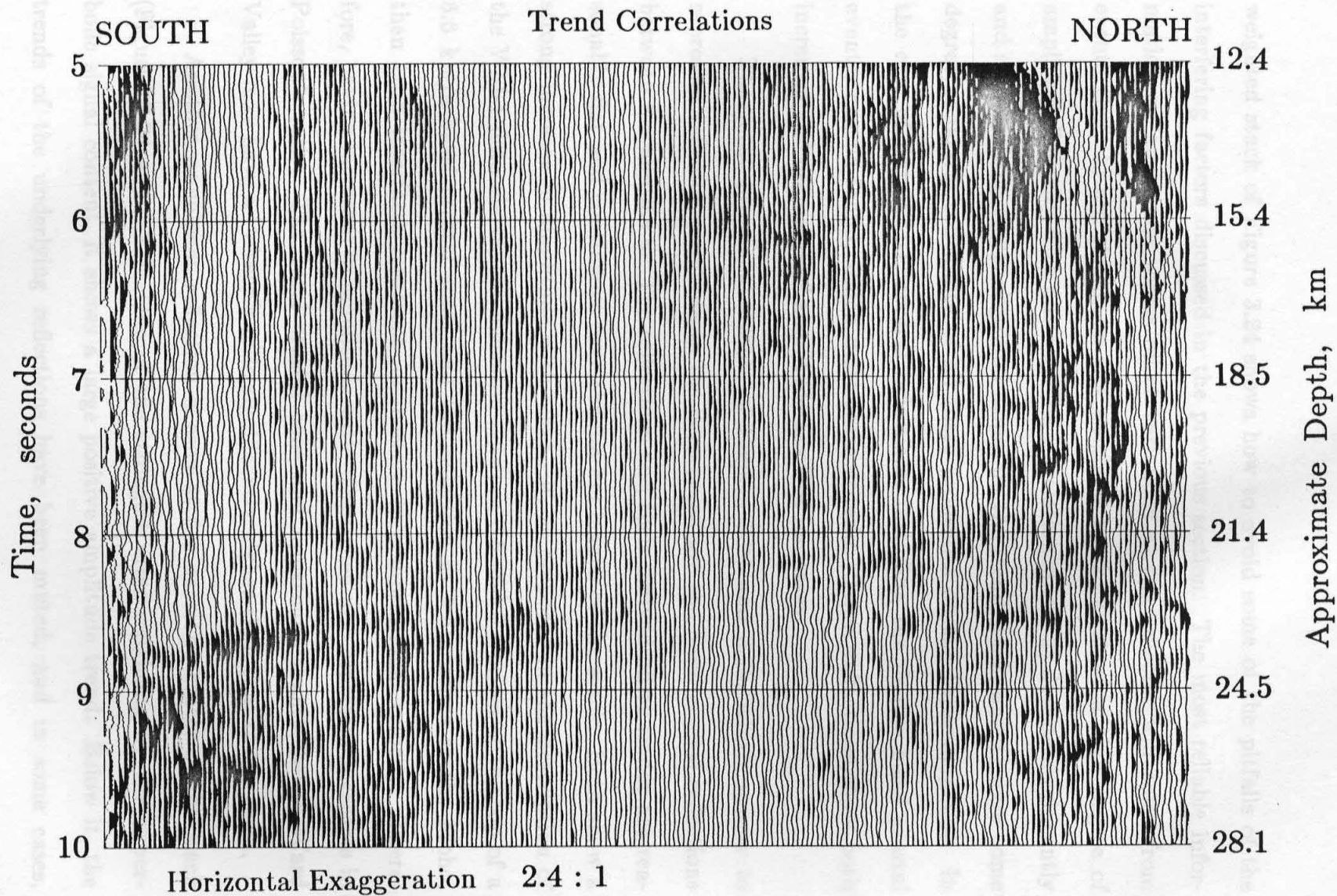


**Fig. 3.26:** Correlations of the linear regressions on amplitude versus offset for each point of the stack in Figure 3.25. Clip at  $r=0.6$ . Dark areas indicate positive  $r$ .



weighted stack of Figure 3.24 shows how to avoid some of the pitfalls of the interfering factors discussed in the previous section. The most reliable information on amplitude versus offset variations at the reflector will come from events that: 1) are strong on the weighted stack, 2) show a high degree of amplitude linearity with offset on the correlation stack, 3) deviate significantly and sharply from the background slopes on the trend stack, and 4) show some degree of lateral continuity of all these properties on the three diagrams. In the case of line WM-1, several reflections, including the double basal crustal events, can be found, which meet these criteria. These reflections show both increases and decreases of amplitude as offset increases.

The most prominent events of Figures 3.24 and 3.25, which appear to represent reflector variations in the deep crust, are the basal crustal reflections between 8.5 and 9.5 s. The reflections and their derived offset trends are reasonably flat and continuous over the 8.3 km length of the stack. Both show a strong increase in amplitude with offset. If, as proposed in the description of the WM-1 data above, the reflection between 8.5 and 9 s arises at the top of a 6.6 km/s basal crustal zone, and the reflection at 9.5 s arises at the Moho, then both interfaces represent an increase in compressional velocity. Therefore, having increases in amplitude with offset, they also represent increases in Poisson's ratio. The basal crustal zone and uppermost mantle below Ward Valley may have a Poisson's ratio significantly higher than that of the crust.

Another prominent reflection is seen at 6 s near the center of the stack (Figures 3.24 and 3.25). One of the strongest after weighting by the hyperbolic signal content, it shows a large positive amplitude trend. Below it, the trends of the underlying reflections have been muted, and in some cases,

reversed. This is a fine example of how the transmission through a strong reflector can affect the apparent trends of the underlying reflections, as suggested by Gassaway (1984). Since the stack was constructed from common midpoint gathers, the strong 6 s event adds a negative bias only to the events immediately below it. This is the effect that disrupts the continuity of the basal crustal reflections. The negative bias may be useful, since it shows that the reflector produces increased reflection, and decreased transmission, amplitudes at larger pre-critical incidence angles.

The section does have other strong, well-stacked events that show a decrease in amplitude with offset. Principal among these, on the northern half of Figures 3.24 and 3.25, are a reflection that dips south at 8 to 8.5 s into the top of the basal crustal events, and a flat reflection at 5.8 s. Examination of the individual trace amplitudes of these and the surrounding positively trending events confirms that their amplitude versus offset trends are clearly different. To produce these strong reflections just above the top of the basal zone, there must be large, sharp variations in physical properties, especially Poisson's ratio.

The strong 6 s reflection was identified in the section on frequency analysis as producing an increase in reflection frequency with offset. This indicated that it consists of a thin layer about 300 m thick, having a compressional velocity at least 10% above that of the overlying medium. Again, this indicates that its positive amplitude trend results from an increase in Poisson's ratio. This event is one of a suite of such north dipping, positive trend reflections in the middle crust below Ward Valley. If these reflectors are the result of tectonic motion, then the motions proposed must be large enough to

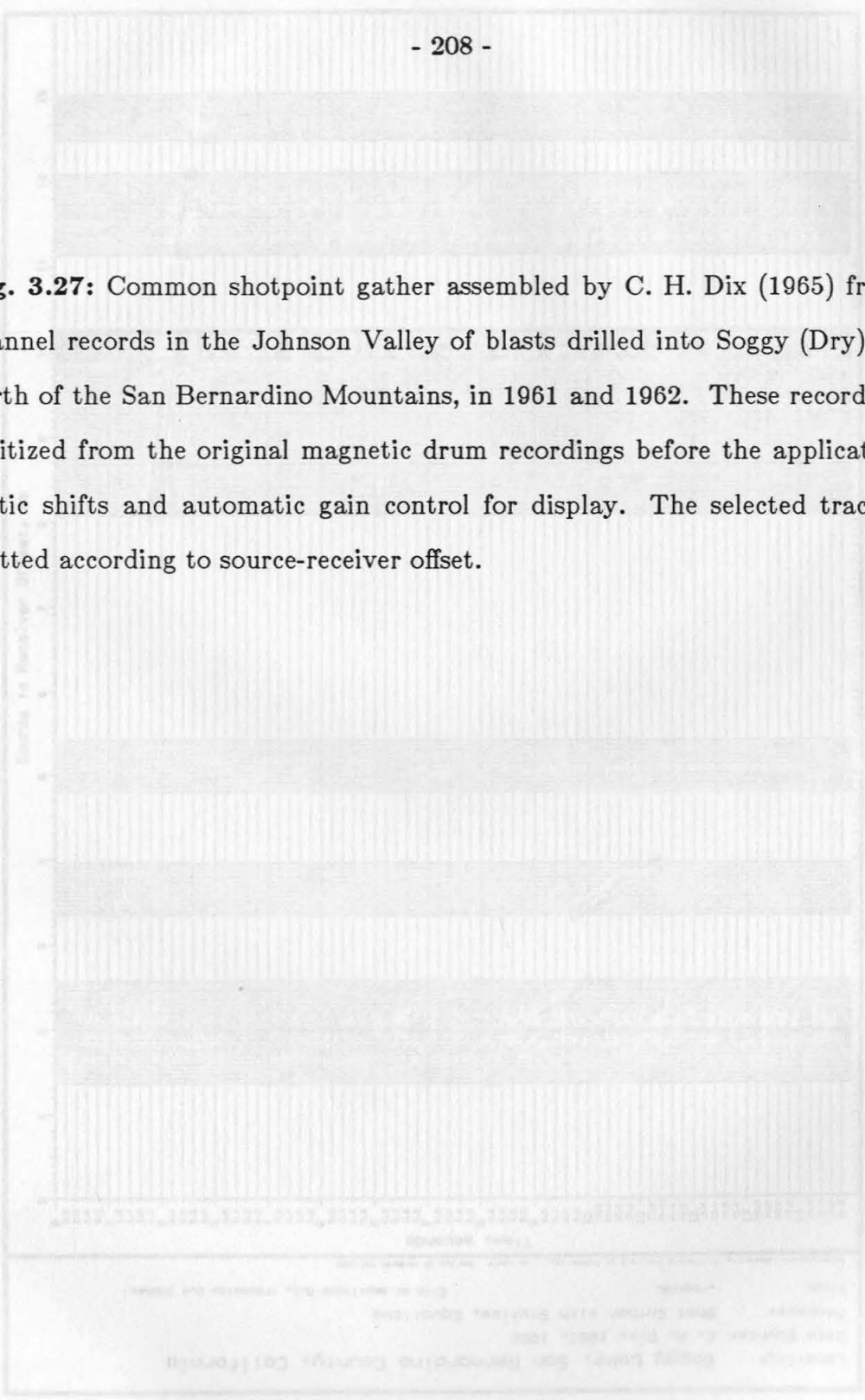
produce either the juxtaposition of such radically different rocks, or to form a thick shear zone with a heavily metamorphosed mineralogy compared to the country rock.

The Calcrust 1985 Ward Valley dataset demonstrates well both the techniques of multi-offset analysis and important properties of an extended lower crust. The merging of a high-resolution roll along survey with stationary, long offset spreads yielded a dataset covering the deep crust at a useful range of offsets with a high degree of multiplicity. This dataset exhibits flat, continuous reflections, which can be demonstrated to show changes in frequency and amplitude with incidence angle. These changes suggest that the middle crust contains north dipping, finely layered structures having elevated compressional velocities and Poisson's ratios. The base of the crust is marked by a sharp step discontinuity to a zone of high velocity and Poisson's ratio, overlain by highly heterogeneous dipping structures. The crust is floored by a layered Moho exhibiting a transition to a still higher Poisson's ratio.

#### *Central Mojave—*

The deep crustal profile acquired by C. H. Dix (1965) consists of a number of 12 channel recordings of blasts drilled into the dry bed of Soggy Lake in the central Mojave just north of the San Bernardino Mountains (Figure 3.1). These recordings form a single, long-offset common shot gather, which is shown in Figure 3.27. The gather shows, as interpreted by Dix, a full set of deep crustal reflections. The strongest are at about 5, 8, and 10 s. The 8 s event is especially strong in that it can be identified over the full range of offsets, even at near-normal incidence.

**Fig. 3.27:** Common shotpoint gather assembled by C. H. Dix (1965) from 12 channel records in the Johnson Valley of blasts drilled into Soggy (Dry) Lake, north of the San Bernardino Mountains, in 1961 and 1962. These records were digitized from the original magnetic drum recordings before the application of static shifts and automatic gain control for display. The selected traces are plotted according to source-receiver offset.



Locality: Soggy Lake, San Bernardino County, California

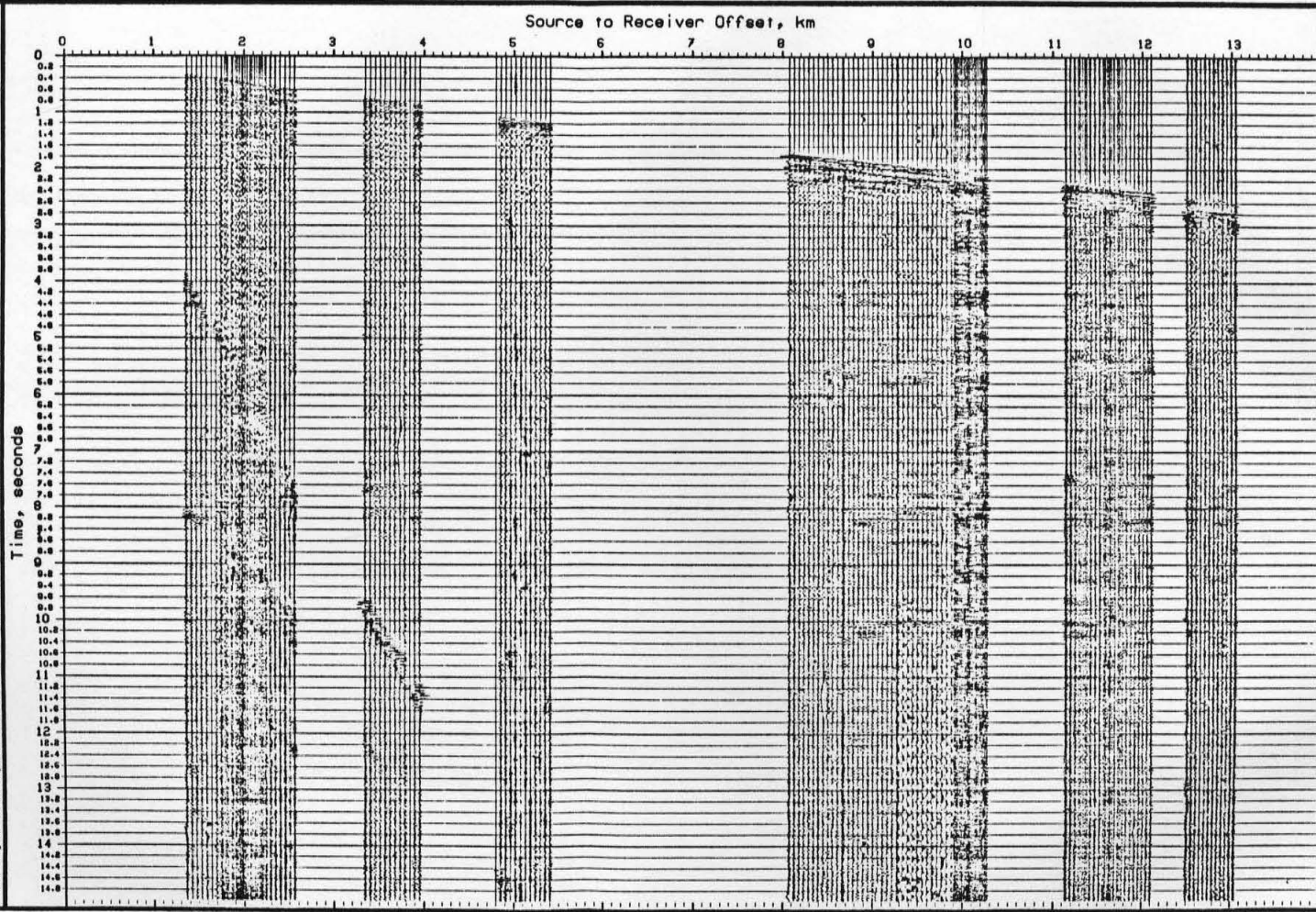
Data Source: C. H. Dix, 1961, 1962

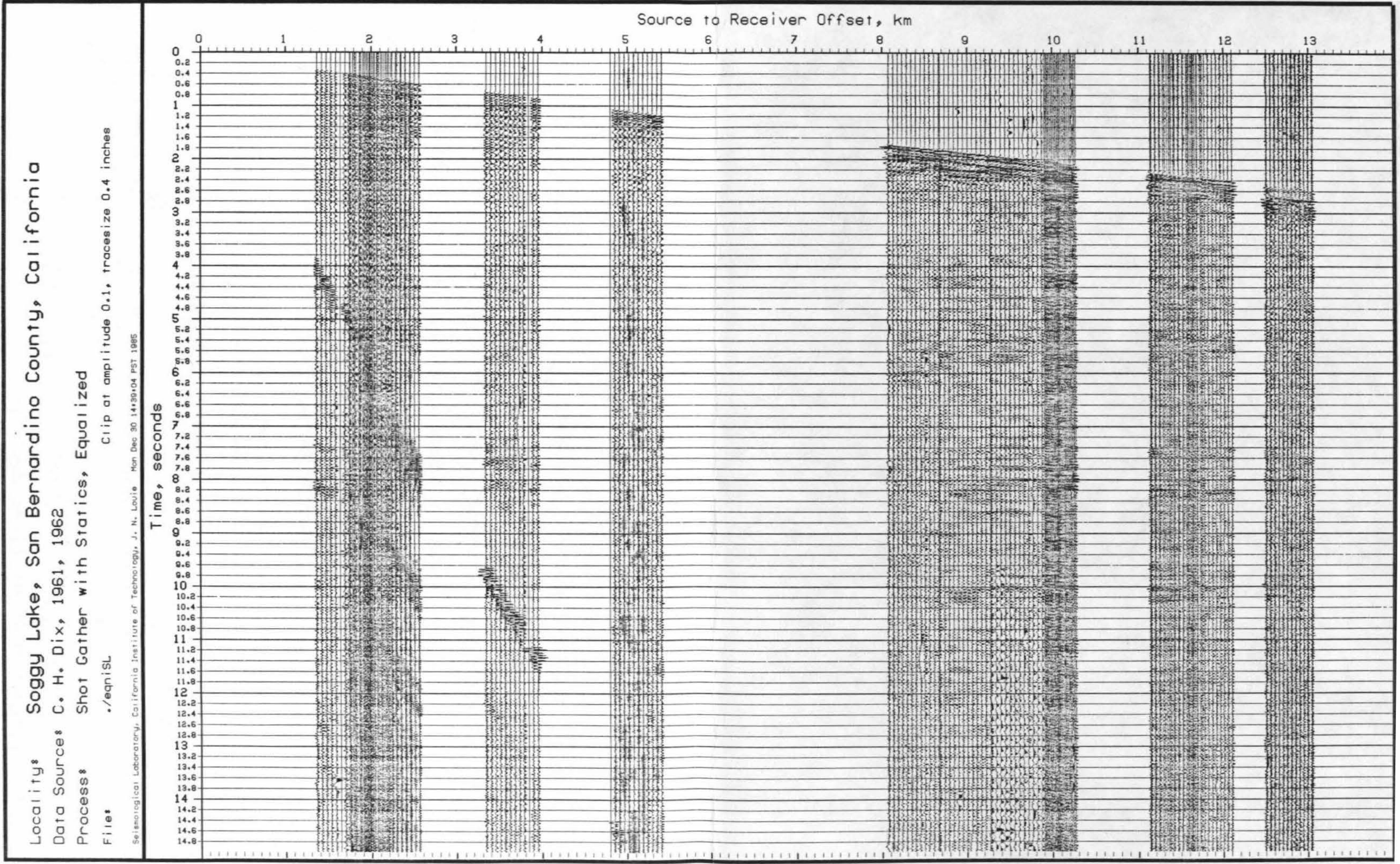
Process: Shot Gather with Statics, Equalized

File: ./eqn15L

Clip at amplitude 0.1, trace size 0.4 inches

Seismology Laboratory, California Institute of Technology, J. N. Louie, San Diego 30, 1443004, 8/1/65





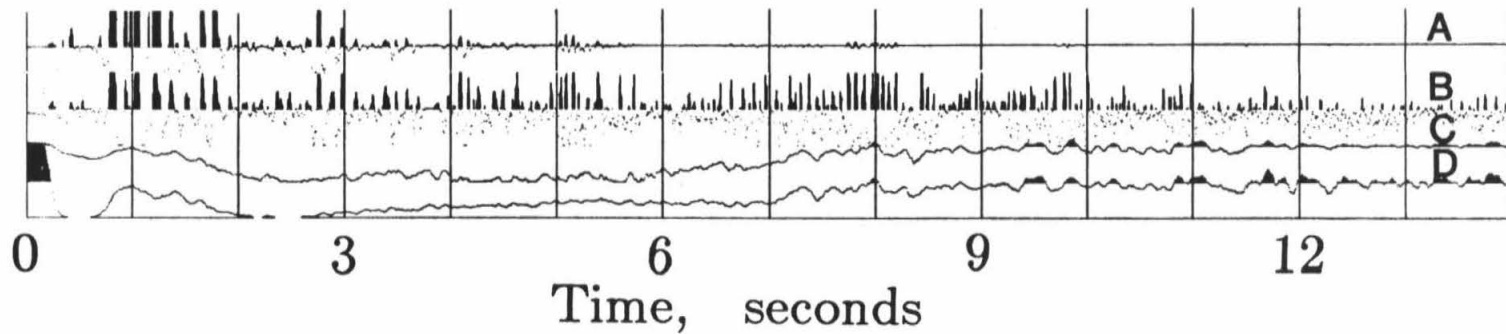


**Fig. 3.28:** **A:** Stacked trace of the gather of Figure 3.27, after trace equalization at the 70% amplitude quantile, but without correction for spherical divergence; weighted by the hyperbolic signal content. **B:** Stacked, weighted trace of the gather including spherical divergence correction. Clip at  $8 \times 10^{10}$  counts. **C:** Linear amplitude versus offset trend for each point of the stack above. Clip at 9.3 counts/m. Dark areas where amplitude increases with offset. **D:** Correlation of the regressions used to find the trends above. Clip at  $r = 0.6$ . Dark areas where  $r$  is positive.

Despite the obvious lack of multiplicity in this dataset, the same methods as those used on the Calcrust dataset can still be applied. Under the assumption of flat layering, which actually was contradicted by Dix's own analysis, a shot gather can be stacked in the same manner as a midpoint gather. A velocity semblance was run and weighted by the proportion of hyperbolic signal, as done above. The stacking velocities indicated are similar to those found for Ward Valley, except that the minimum velocity near the surface is 5.2 km/s. The Soggy Lake area is uniformly underlain by granitic bedrock topped by a thin veneer of alluvium; it lacks a thick, low-velocity sedimentary section. The trace amplitudes were corrected for the amplitude of the 70% quantile in the same manner as the Calcrust dataset, but were not filtered.

Stacking the gather with the derived velocity spectrum produced the trace given in Figure 3.28A, after weighting by the hyperbolic signal content. The three reflections are still prominent. If the stacked trace is made after correcting for spherical divergence, Figure 3.28B, the strongest events do not stand out as clearly, although more events are visible. Figures 3.28C and 3.28D show the linear amplitude trends and the amplitude trend correlations, respectively. Above 3 s intercept time, the algorithm was finding the trend of the refracted waves. At larger times, the trends should be valid. They show a slowly varying negative bias, which becomes smaller with time. This bias could be due to some combination of an incorrect adjustment for spherical divergence and the effective attenuation. Whatever the source of the bias, it does not prevent rapidly varying trends, arising from reflections, from standing out.

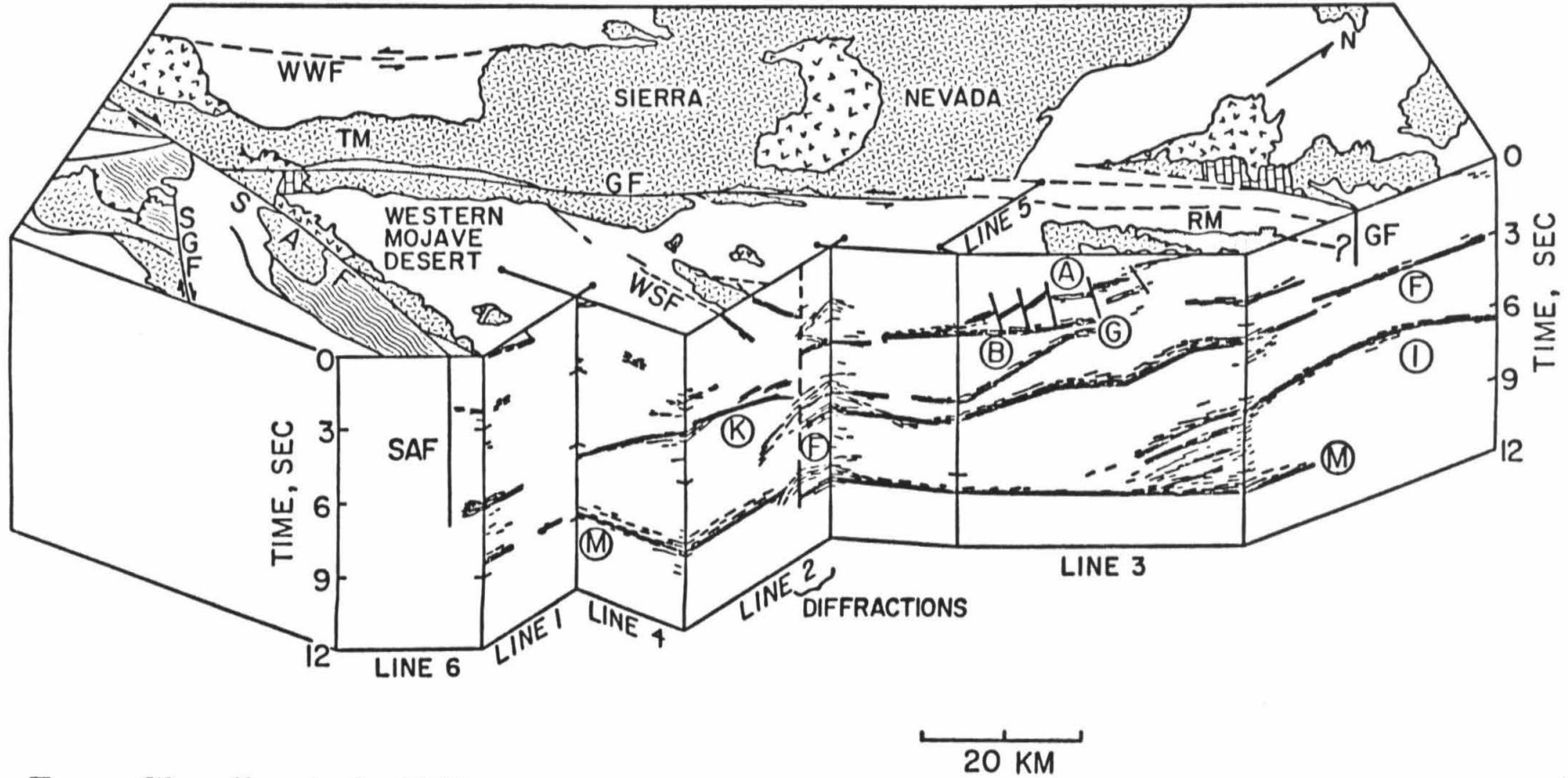
The trend stack suggests that the 5 s reflection has a decrease in amplitude with offset, while the 8 and 10 s events have increases. In addition, the spectra of the 10 s reflection indicate the presence of layering very similar to that at the base of the crust below Ward Valley. There is no multiplicity in this dataset to protect the analysis from the effects of lateral heterogeneities in the propagation paths or at the reflectors. However, the gather is of such high quality (Figure 3.27) that these results must be kept for comparison with other datasets, especially the new 1986 Calcrust survey in Apple Valley.

*Western Mojave—*

In the western Mojave Desert, an extensive COCORP dataset is available (Figure 3.1). It consists of six overlapping lines spanning the wedge of the Mojave between the Garlock and San Andreas faults, and spanning the faults themselves. Cheadle et al. (1985, 1986) identified several shallowly dipping, regional reflections, all of which appear to be cut by the San Andreas fault but not by the Garlock (Figure 3.29). They interpreted these reflections as arising from horizontal shear zones, with several models available for their ages and sense of motion.

The data from line 3, as indicated on Figure 3.29, will be considered here. This line contains the most well-imaged reflections and was the basis for the geometric interpretation of Cheadle et al. (1985). The data were recorded using off end spreads with 96 offsets of from 0.4 to 10 km. While the offsets are unreversed, the coverage of the offset range is continuous. This will allow the effects of at least the mid crustal reflectors to be analyzed. Filtering of the surface and air waves was not required, since the survey employed 200 m long

**Fig. 3.29:** Cutaway view of the western Mojave Desert, looking northwest, showing line drawings of the major deep reflections in the stacks of the COCORP Mojave lines. Taken from Cheadle et al., 1985.



From Cheadle *et al.*, 1986

receiver arrays. Because of the 900 megabyte size of the multi-offset dataset and limits on the capabilities of the computer available, the gathers were not sorted into common midpoint form before stacking. Instead, common shot-point gathers were used. While the dataset retains the advantages of multiplicity, the analysis of shot gathers will force additional assumptions about the lateral homogeneity of the reflectors. However, making a comparison of the shot gather stack derived here with the full midpoint stack of Cheadle et al. will show that the differences are few enough to suggest that lateral reflector homogeneity on the scale of a few kilometers is not an unreasonable assumption.

For an initial analysis, a small area of line 3 directly beneath the Rand Mountains, indicated on Figure 3.29, was selected for an evaluation of stacking velocities. As before, reasonable stacking velocities could be picked from a set of constant velocity stacks weighted by the hyperbolic signal content in the manner of Harlan et al. (1984). However, these stacks of shot gathers actually served to point out phenomena that could not be observed on stacks of midpoint gathers. At different stacking velocities, different interfaces having different dips would be emphasized. This is due to the one-sided nature of the receiver spreads, which gave the reflections apparent velocities having one-to-one correspondences with the best stacking velocities. Such reflections could be observed throughout the crust but were most prominent above 3 s. For any particular point of the stack, one stacking velocity capable of imaging reflectors of different dip cannot be found. With stacks of shot gathers, at least, their presence can be established.

The stacking velocities were selected to emphasize the strongest, flat-lying reflections. For this dataset, the trace amplitude equalization was set to the 75th quantile. Spherical divergence and air and surface wave mutes were applied as before. The shot gather stack of the small area of line 3 is shown by Figure 3.30, and by Figure 3.31 after weighting by the hyperbolic signal content. The stack shows an impressively strong reflection between 5 and 6 s, at about 16 km depth. There are also indications of a reflection from the Moho between 10 and 11 s, at about 32 km depth. The lack of offsets of less than 400 m forced the direct wave mute to eliminate all data in the stack from less than 0.9 s. The variation in trace strengths on the weighted stack (Figure 3.31) is due directly to the presence of heterogeneities that emphasize a particular reflection or attenuate all of them. This effect would have been compensated by the reciprocity provided by true source to receiver reversals, if they had been available.

During stacking, the amplitude versus offset trends were tracked within 0.2 s windows surrounding the stacking hyperbolae. The larger window compensates for the lower-frequency character of the reflections from this dataset. The amplitude trend stack and amplitude trend correlations are shown in Figures 3.32 and 3.33. Several features are at once apparent. First, the trends exhibit a broad negative bias across the section that increases strongly at the shallower times. This feature is due to the apparent attenuation of the waves during propagation. Second, the trends begin to lose coherency below 6 or 7 seconds. It seems that, at greater times, no reflections were recorded that showed enough amplitude change, within the 10 km offset range of this survey, to stand out from the background noise level. With such a limited range of

**Fig. 3.30:** Stack of 94 selected shot gathers of the COCORP Mojave line 3 survey between vibrator points 466 and 562, within the Rand Mountains.

SW

# Rand Mountains Crustal Shot Stack

NE

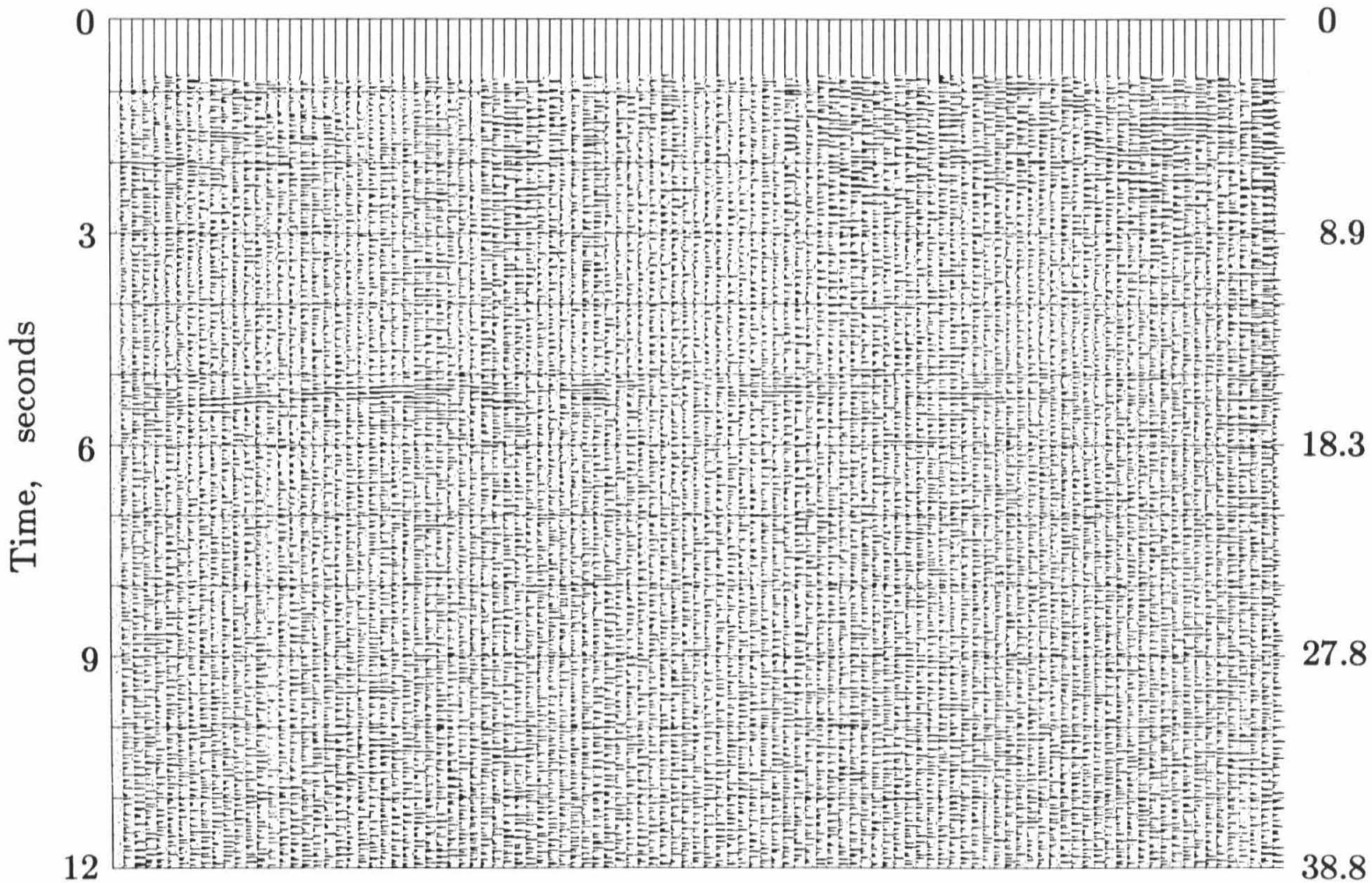


**Fig. 3.31:** COCORP Mojave line 3 shot gather stack for the Rand Mountains of Figure 3.30 after weighting by the proportion of hyperbolic signal in the gathers. The regional mid crustal reflector labeled "F" in Figure 3.29 is emphasized.

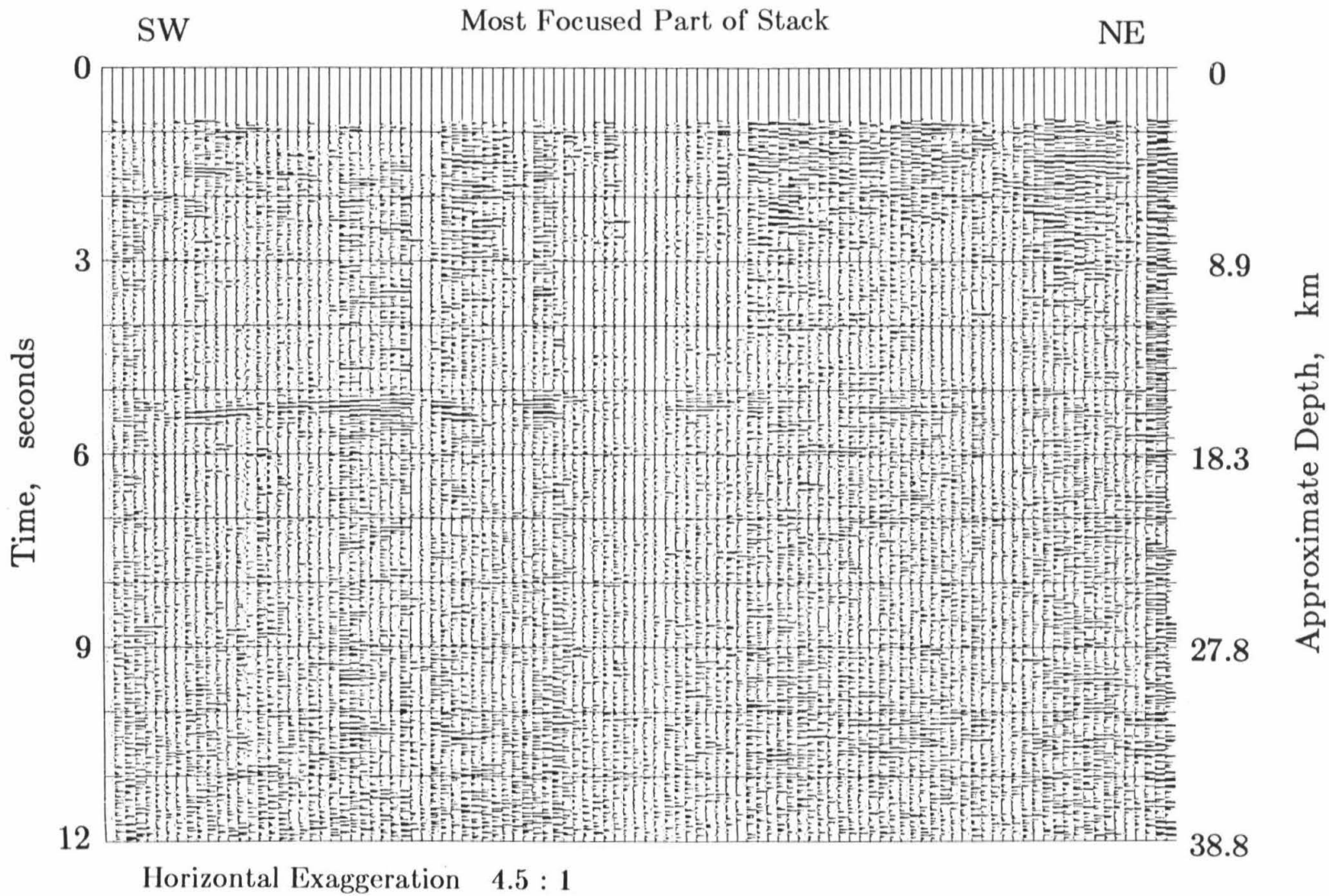


**Fig. 3.32:** Linear amplitude versus offset trend for each point of the COCORP Mojave line 3 stack within the Rand Mountains of Figure 3.31. Dark areas where amplitude increases with offset. Clip level at 0.0001 counts/m. Points for which the multi-offset gathers were examined are circled.

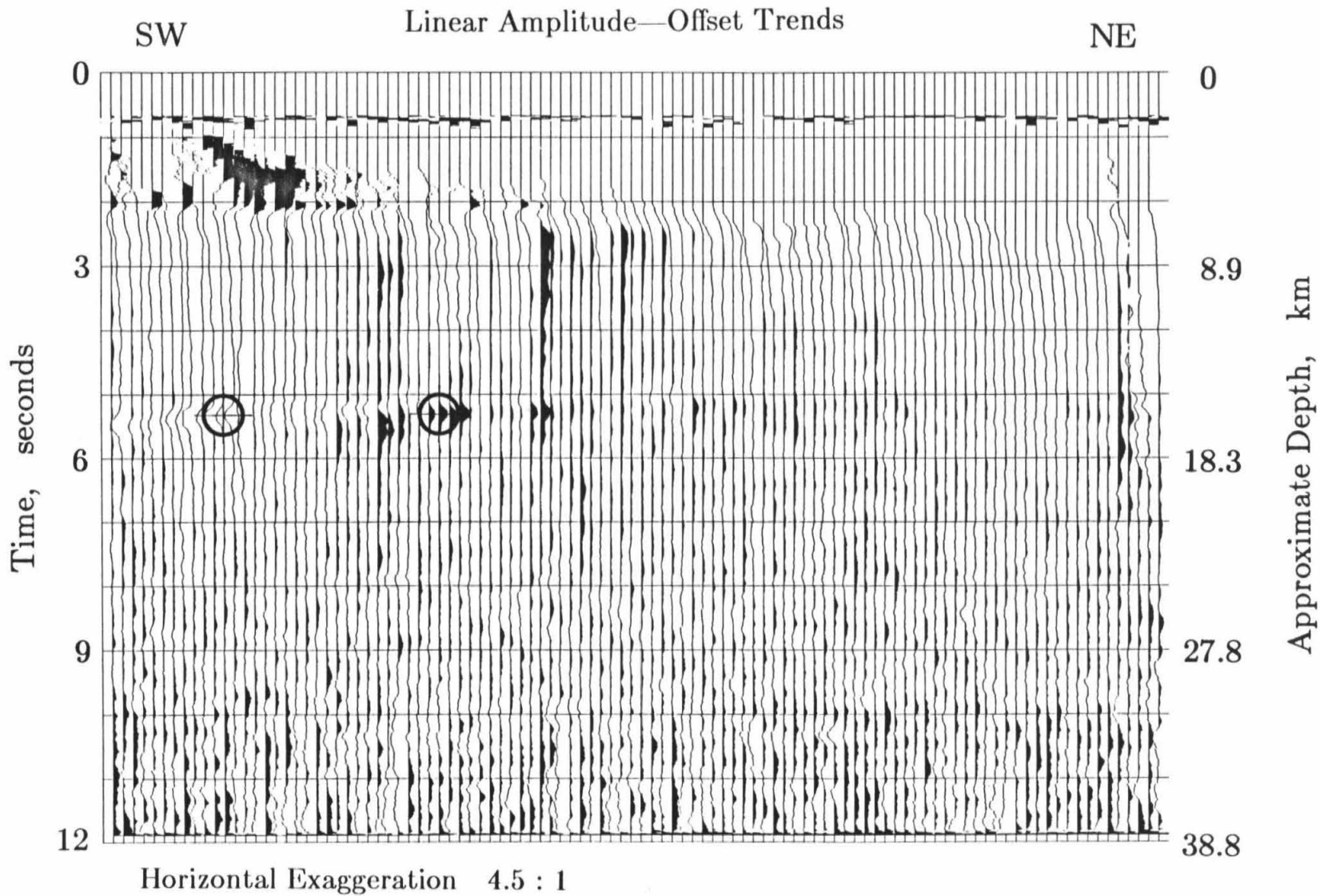
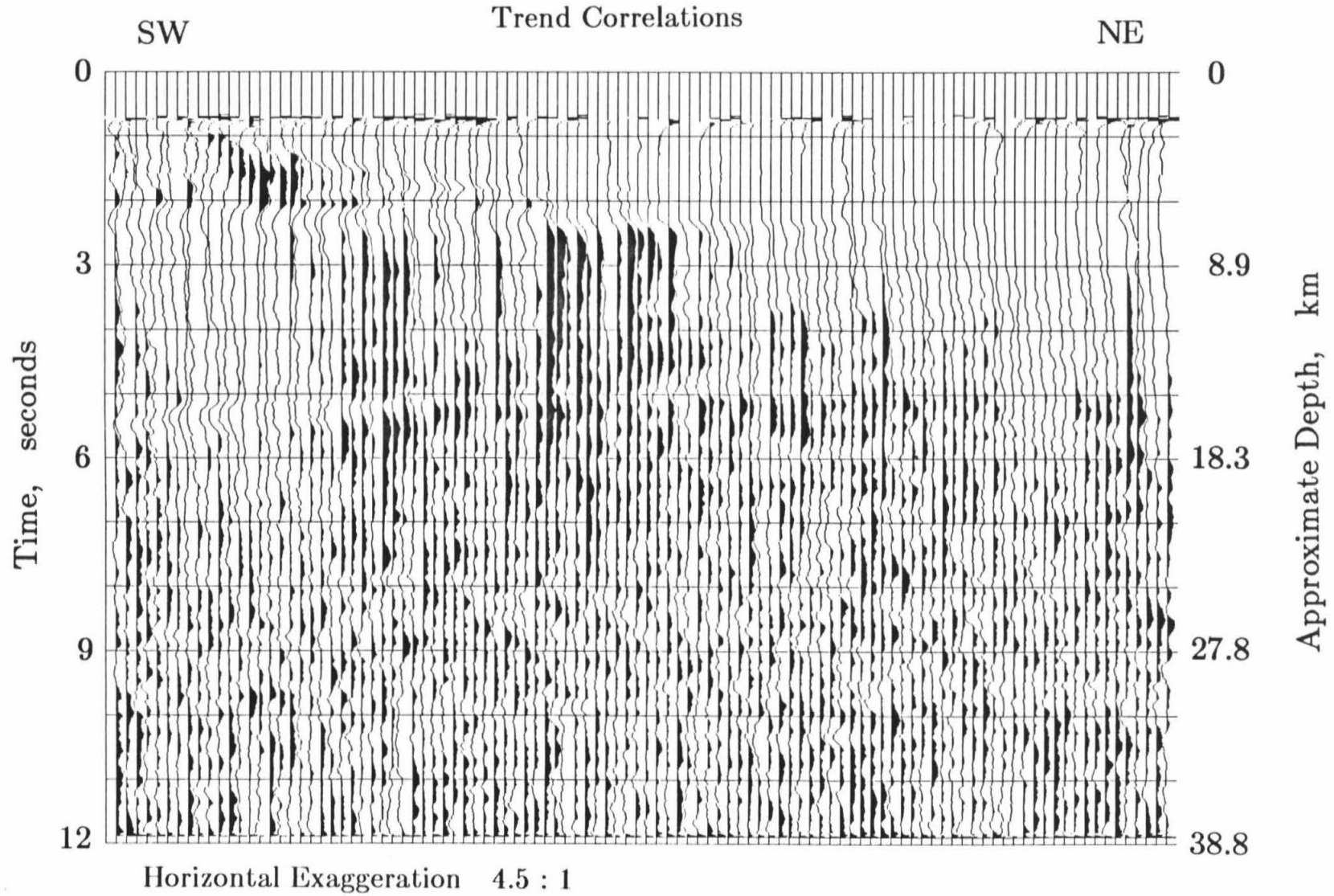


**Fig. 3.33:** Correlations of the linear regressions on amplitude with offset for each point of the COCORP Mojave line 3 Rand Mountains trend stack of Figure 3.32. Dark areas indicate  $r$  positive. Clip at  $r = 0.6$ .



offsets, the range of incidence angles within the deeper parts of the crust is too small to permit analysis of most reflectors there, including this section of the Moho.

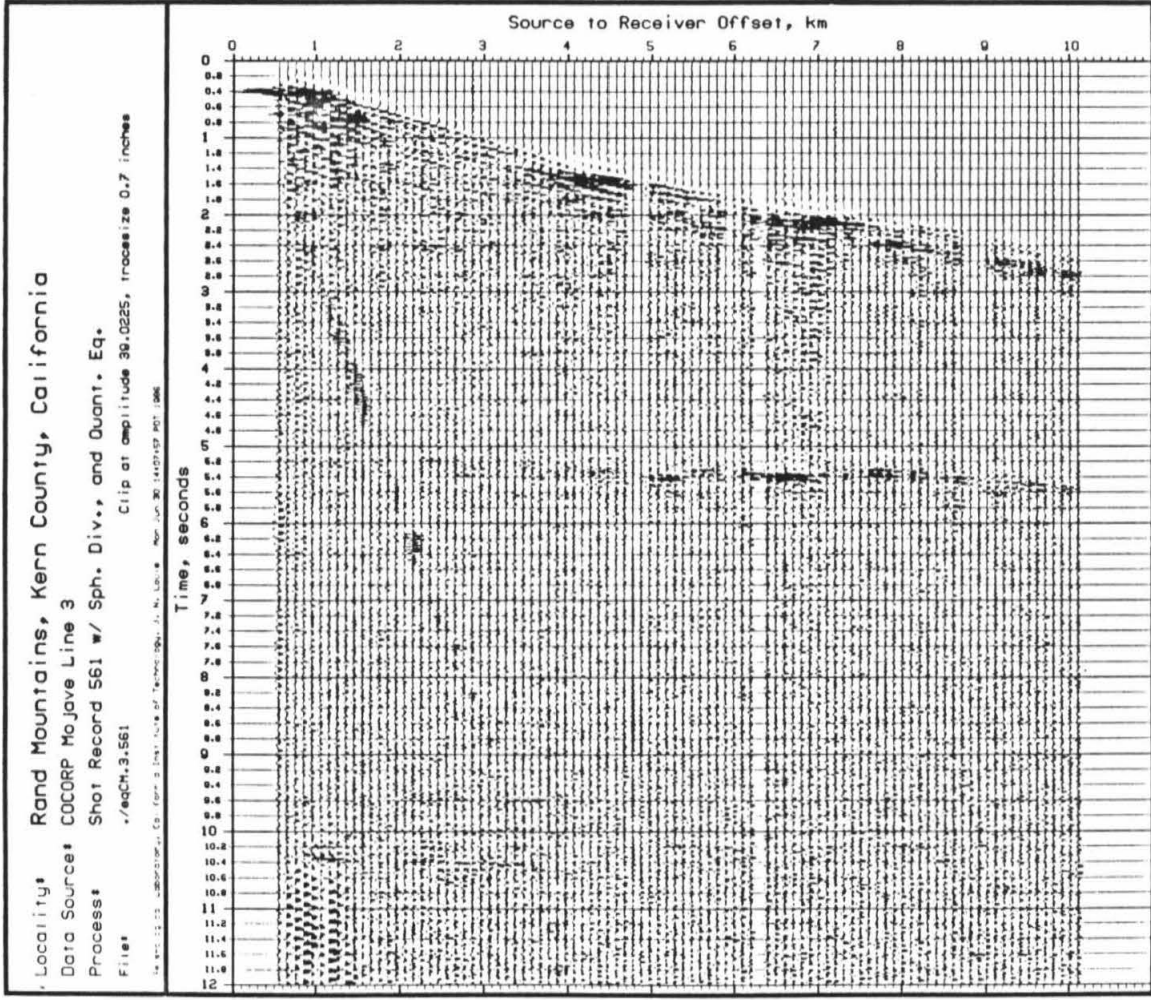
The reflection between 5 and 6 s shows clear amplitude trends with good associated correlations. The trend, however, inverts between the center and the southwest side of the section (Figure 3.32). To find out whether this is due to lateral heterogeneity of the reflector or of the medium overlying the reflector, it is necessary to look at the unstacked data. In the trend stack, the large positive trend on the southwest side between 1 and 2 seconds is a hint that the problem lies along the propagation path. Specifically, it has to do with lateral heterogeneities at the interface between the alluvium and basement, which are the strongest in the entire crust.

Figure 3.34 shows two shot gathers from this part of line 3, 3.34A from near the center of the stack, and 3.34B, from the southwest side. These gathers are plotted with their traces having true relative amplitudes, after the quantile amplitude balancing and spherical divergence correction. In 3.34A the 5 s reflection is easily spotted. It has high amplitudes at a large range of offsets, indicating that energy is penetrating down to it at the full range of incidence angles. This is also indicated by the reasonably high amplitudes of the refracted arrival out to the farthest offsets. On the other hand, the gather in 3.34B shows a much weaker reflection, visible only at the inner offsets. The refracted arrivals have also changed character, with their amplitude decreasing more at the farther offsets.

The reason for these changes lies at the very strong triplication at 1.1 s between 1 and 3 km offset. The transition to the granitic basement has

**Fig. 3.34: A:** COCORP Mojave line 3 field record 561 from vibrator point 527. The offset traces are to the southwest of the vibrator point. The spherical divergence correction has been applied, along with trace equalization of the 75th percentile quantile of the amplitudes between 8 and 10 s. Very strong arrivals are seen at 5.4 s from the reflection "F" of the line drawing in Figure 3.29. **B:** Field record 586 from VP 550, 2.3 km southwest of the record in **A**. Note the strong triplication at 1.2 s, and the diminished amplitude of the 5.4 s and later reflections.

A



B

Locality: Rand Mountains, Kern County, California

Data Source: COCORP Mojave Line 3

Process: Shot Record 586 w/ Sph. Div., and Quant. Eq.

Files: ./eqCH.3.586

Crip at amplitude 77.4793, trace size 1.3 inches

U.S. Geological Survey, Earthquake Hazards Division, Western Region, Menlo Park, California

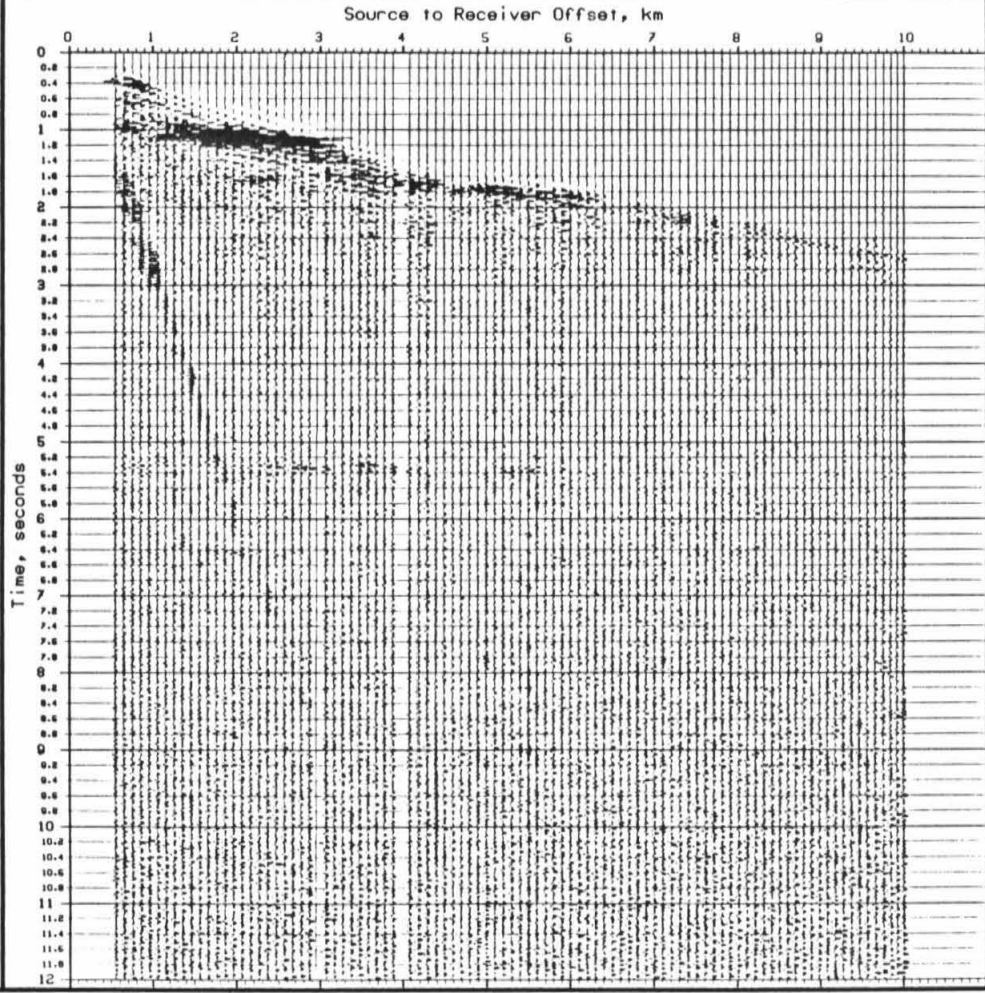
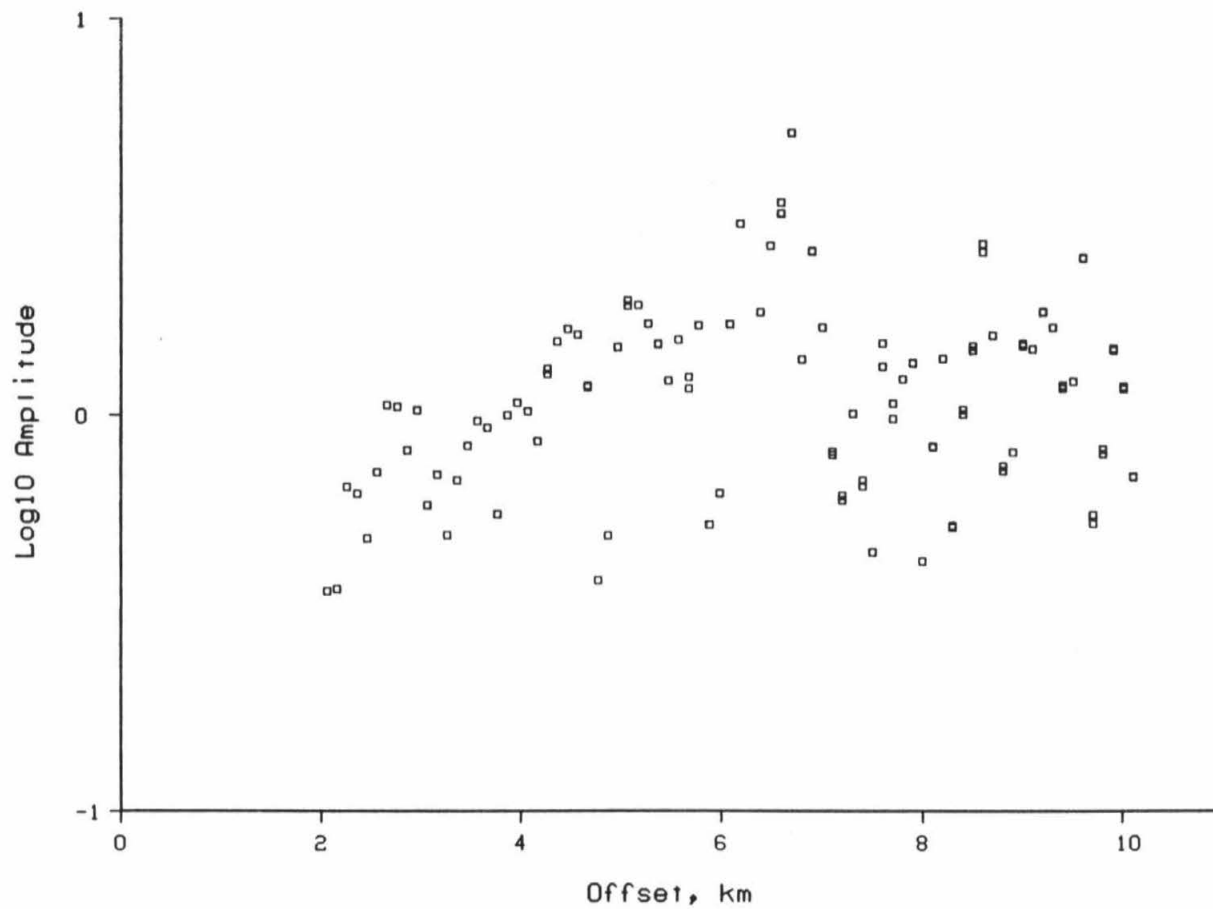


**Fig. 3.35: A:** Plot of the  $\log_{10}$  of the rms amplitude of the 5.4 s reflection of Figure 3.34A, within 0.08 s windows following the hyperbolic path defined by the picked stacking velocity and the paths defined by the velocity varied by  $\pm 0.05$  km/s, versus offset. This mid crustal reflection "F" of Figure 3.29 shows a distinct increase in amplitude with offset that can result only from a strong variation in Poisson's ratio at the reflector. **B:** Similar plot for the gather of Figure 3.34B, showing the attenuation of amplitude at large incidence angles caused by the shallow reflector.

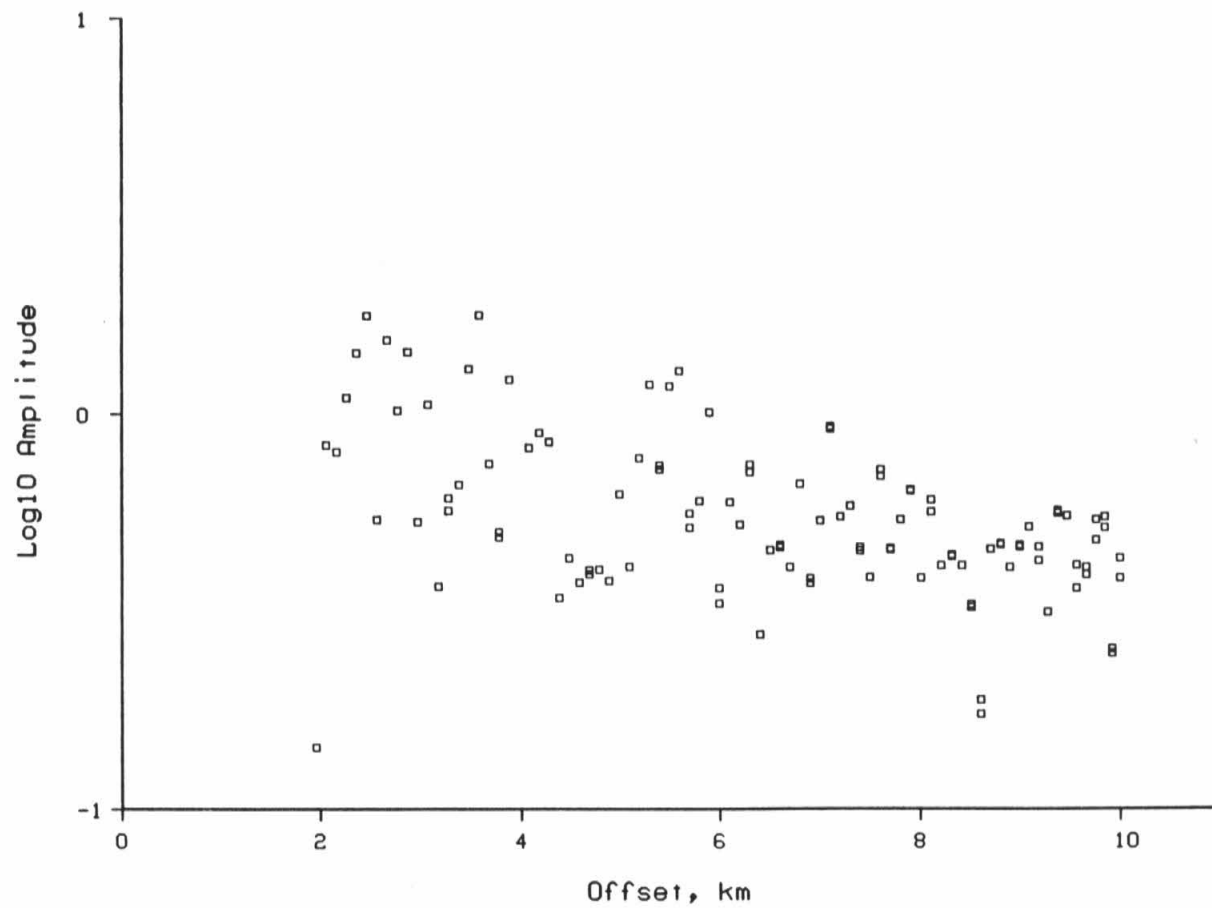
A

Amplitude vs. Offset at Shot Record 561, 5.35 s, ntau=1, nv=3



B

Amplitude vs. Offset at Shot Record 586, 5.35 s,  $\tau=1$ ,  $n_v=3$

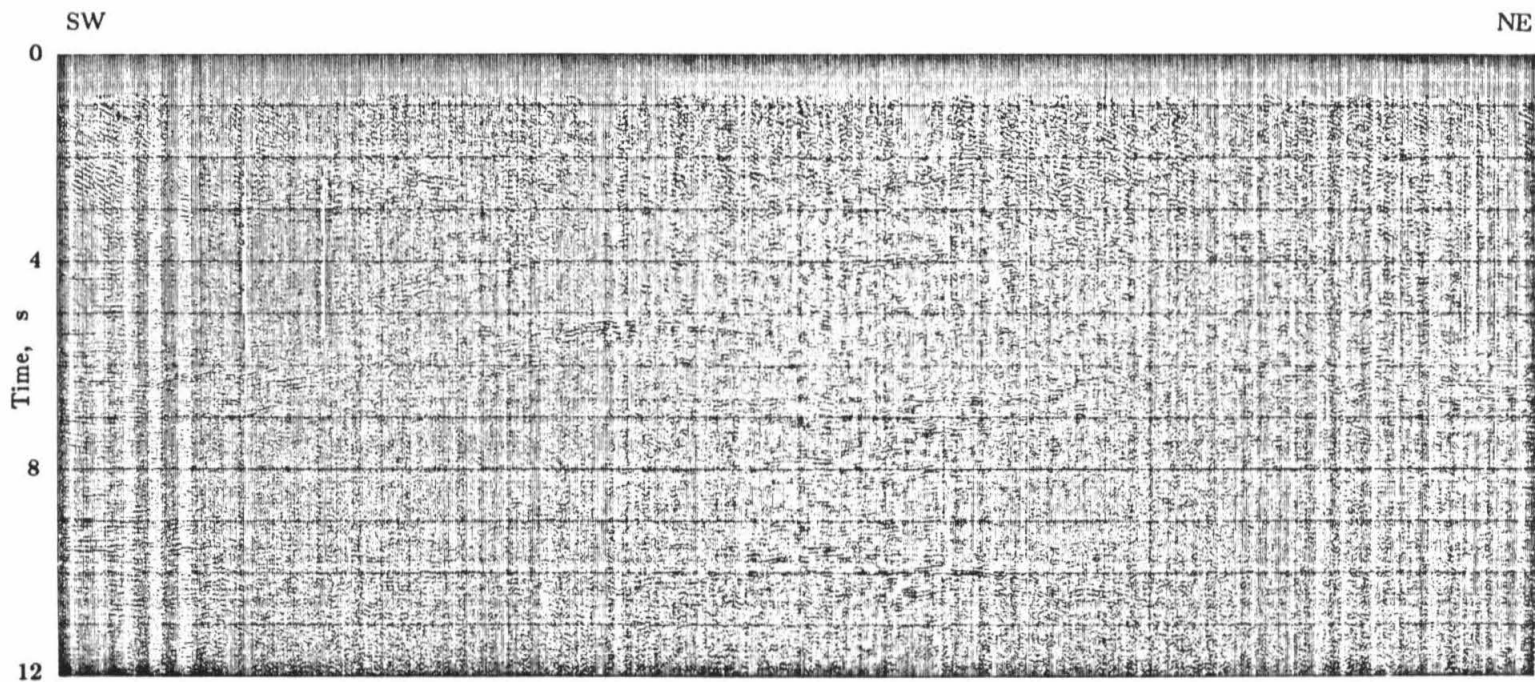


changed its character such that it reflects almost all the energy incident upon it back towards the surface. The deep reflection is depleted at long offset because very little energy penetrates into the basement at larger incidence angles. Figure 3.35 plots the actual amplitudes found for the 5 s reflector over the two gathers. While the near-offset amplitudes are nearly the same in Figures 3.35A and 3.35B, the far offset amplitudes have been depleted in 3.35B. This effect reverses the derived amplitude trend. Fortunately, as can be seen on Figure 3.32, the strong shallow reflector biases the trends of all the reflections beneath it, making its effect easy to identify on the trend stack.

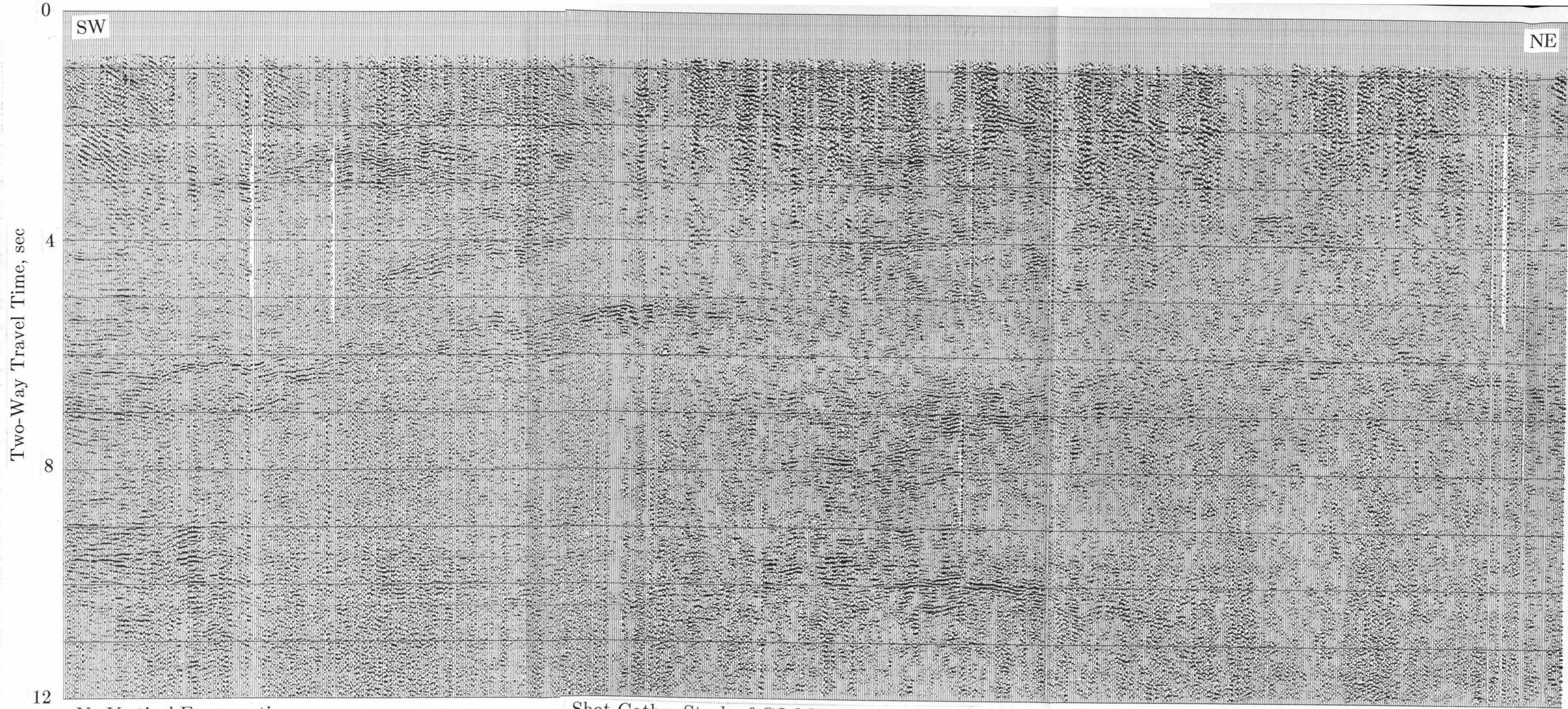
With this analysis in mind, the entire line 3 dataset was stacked in the same manner as the section under the Rand Mountains. The weighted stack is shown by Figure 3.36. All of the reflections identified by Cheadle et al. (1985, 1986) on COCORP's midpoint stacks can be identified on Figure 3.36. The events in the shot stack show, in fact, the same reflection characteristics and locations as those in the midpoint stacks. However, the shot stack, weighted by the signal content, has the advantage that it shows which events best meet the stacking assumptions.

The amplitude trend stack is plotted in Figure 3.38, and the correlation in Figure 3.39. They have been calculated similarly to the stacks of the Rand Mountains area, except that the trend stack has an additional enhancement. The traces of the original trend stack were averaged together over all of line 3, producing the trend profile of Figure 3.37A. Aside from a number of high amplitude glitches caused by summing in a few bad gathers, the profile shows the gradual decline of the influence of effective attenuation with depth. This profile can be modeled, using equation 3.9. The profile in Figure 3.37B gives

**Fig. 3.36:** Shot gather stack of all of COCORP Mojave line 3, weighted by the hyperbolic signal content. The events shown in the line drawing of Figure 3.29 are clearly visible. Clip at 0.0166 counts.



No Vertical Exaggeration



No Vertical Exaggeration

Shot Gather Stack of COCORP Mojave Line 3

**Fig. 3.37: A:** The average of the raw linear amplitude versus offset trends as a function of intercept time from all 804 gathers of COCORP Mojave line 3. The trend is truncated by the direct and refracted arrival mutes at less than 0.9 s. The high-amplitude spikes result from the inclusion of the trends of faulty shot gathers. Both curves are clipped at 3.14 counts/m, with the dark areas indicating increases of amplitude with offset. **B:** Model trend calculated from equation 3.9 for an apparent  $Q$  of 20, with  $A_s = 4.8 \times 10^5$  counts,  $h = 10$  km,  $f = 20$  Hz, and the picked stacking velocities from VP500, to match the above average trend. The fit of these two curves at times of less than 3 s indicates that the average  $Q_{ap}$  over line 3 is  $20 \pm 10$ .

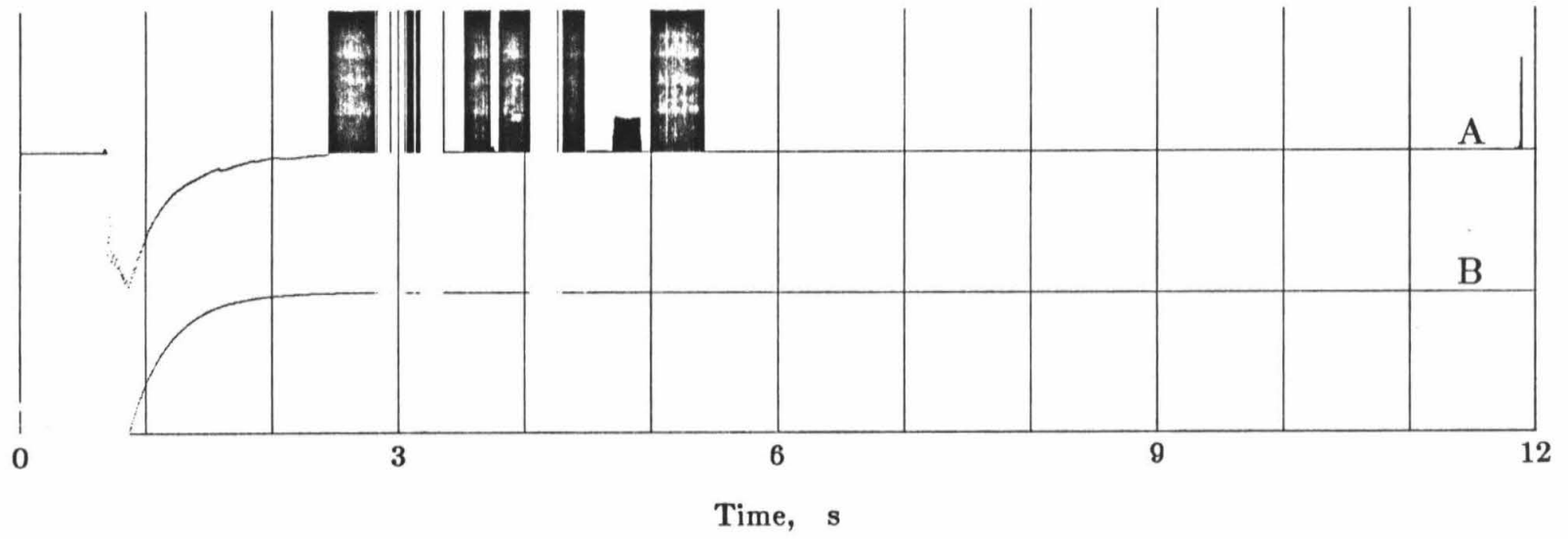
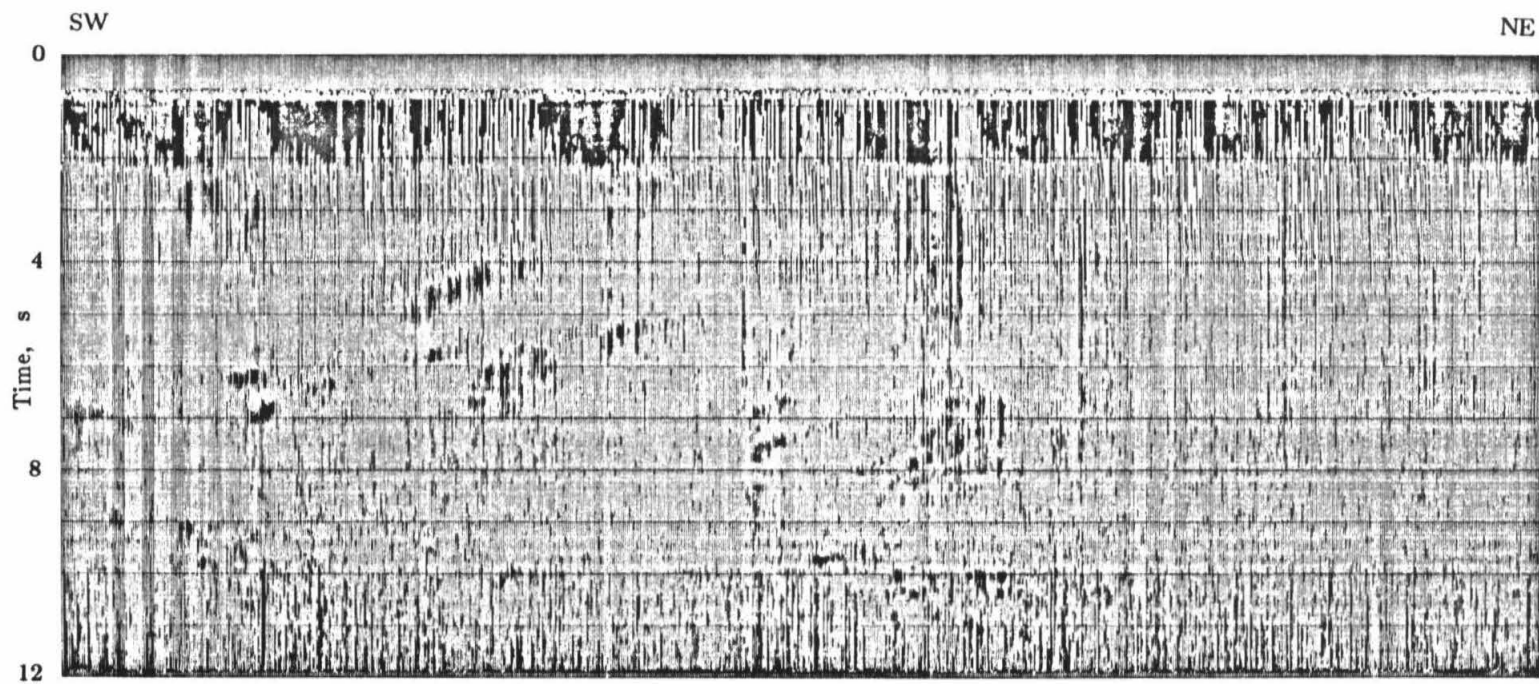
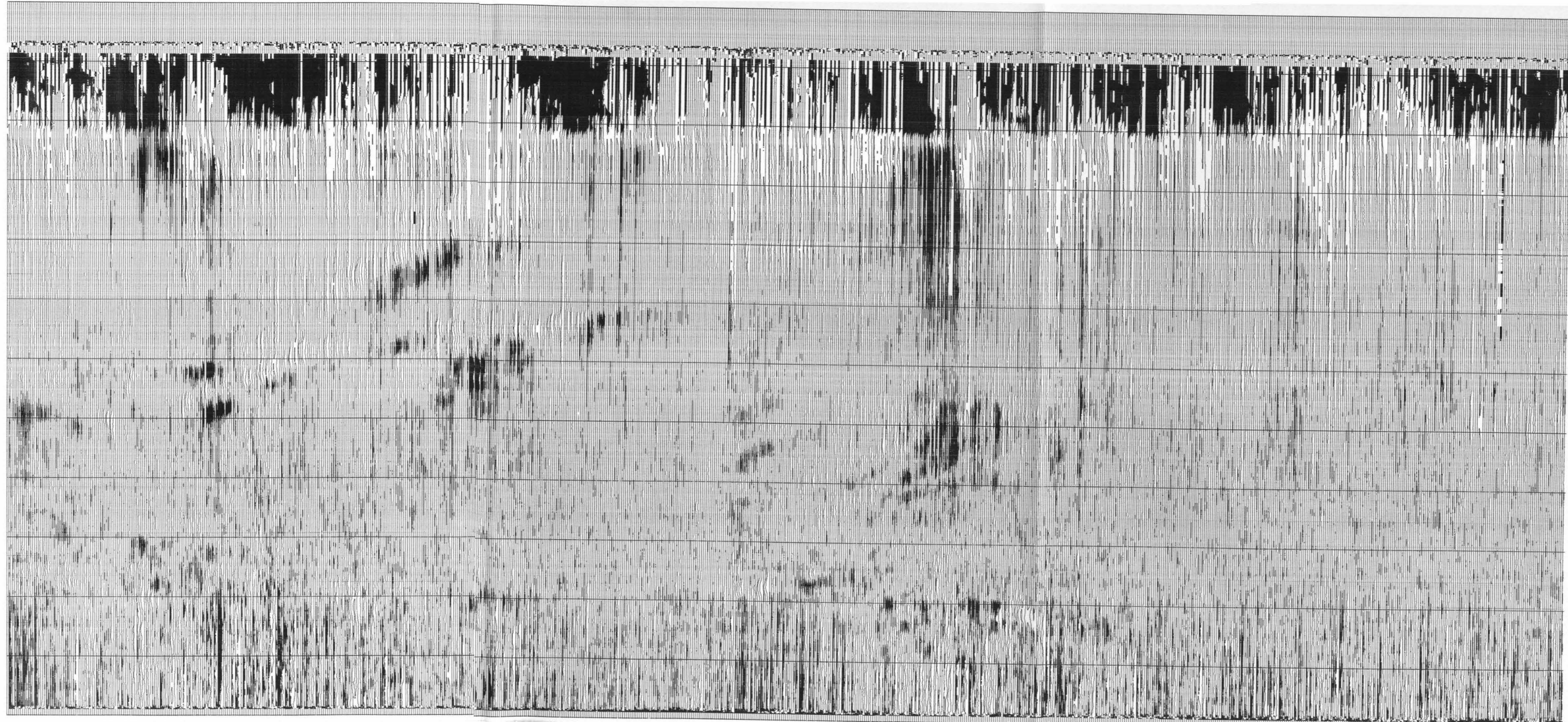


**Fig. 3.38:** Linear amplitude versus offset trend stack of all of COCORP Mojave line 3, for each point of the stack of Figure 3.36. The trend due to an apparent  $Q$  of 20, with the other parameters as shown in Figure 3.37B, has been subtracted out. Clip at 0.0001 counts/m. Dark areas indicate amplitude increases with offset. Plot is on the same scales as Figure 3.36.

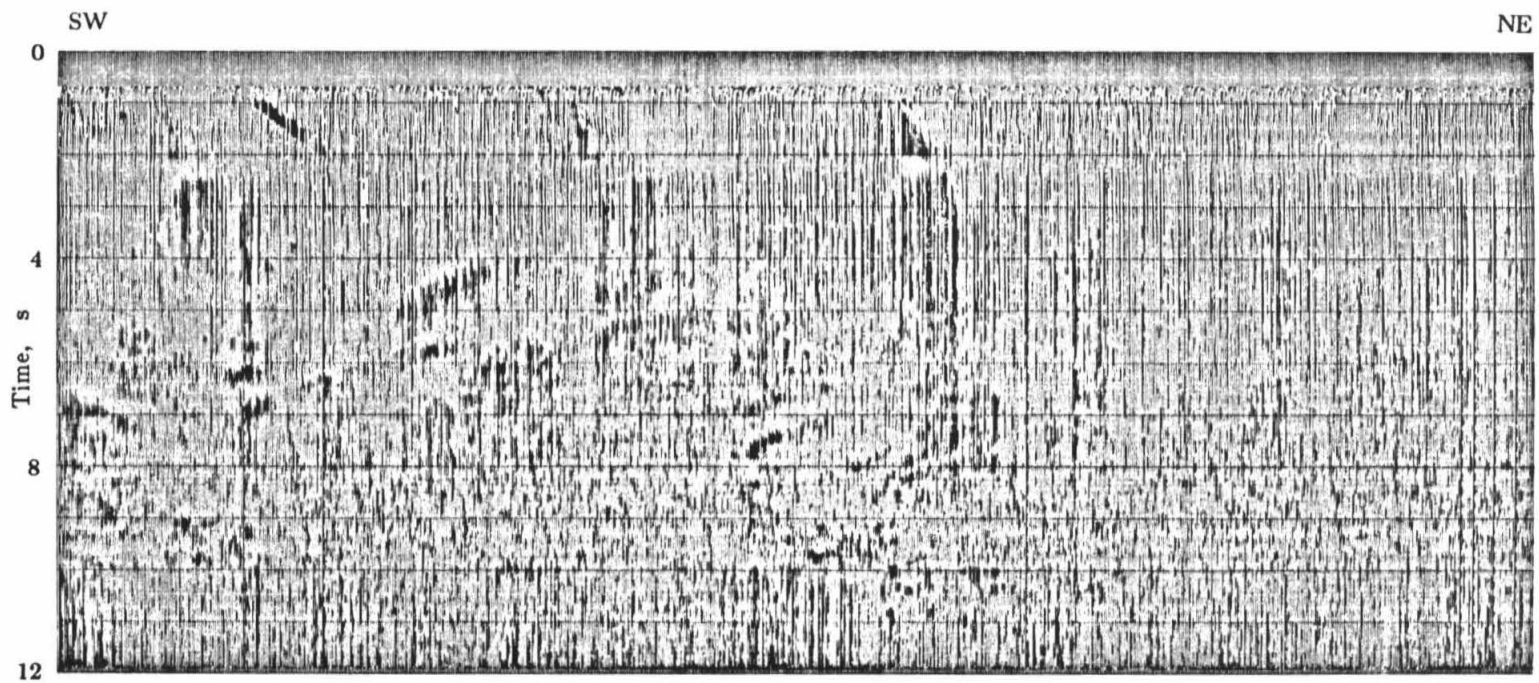


No Vertical Exaggeration

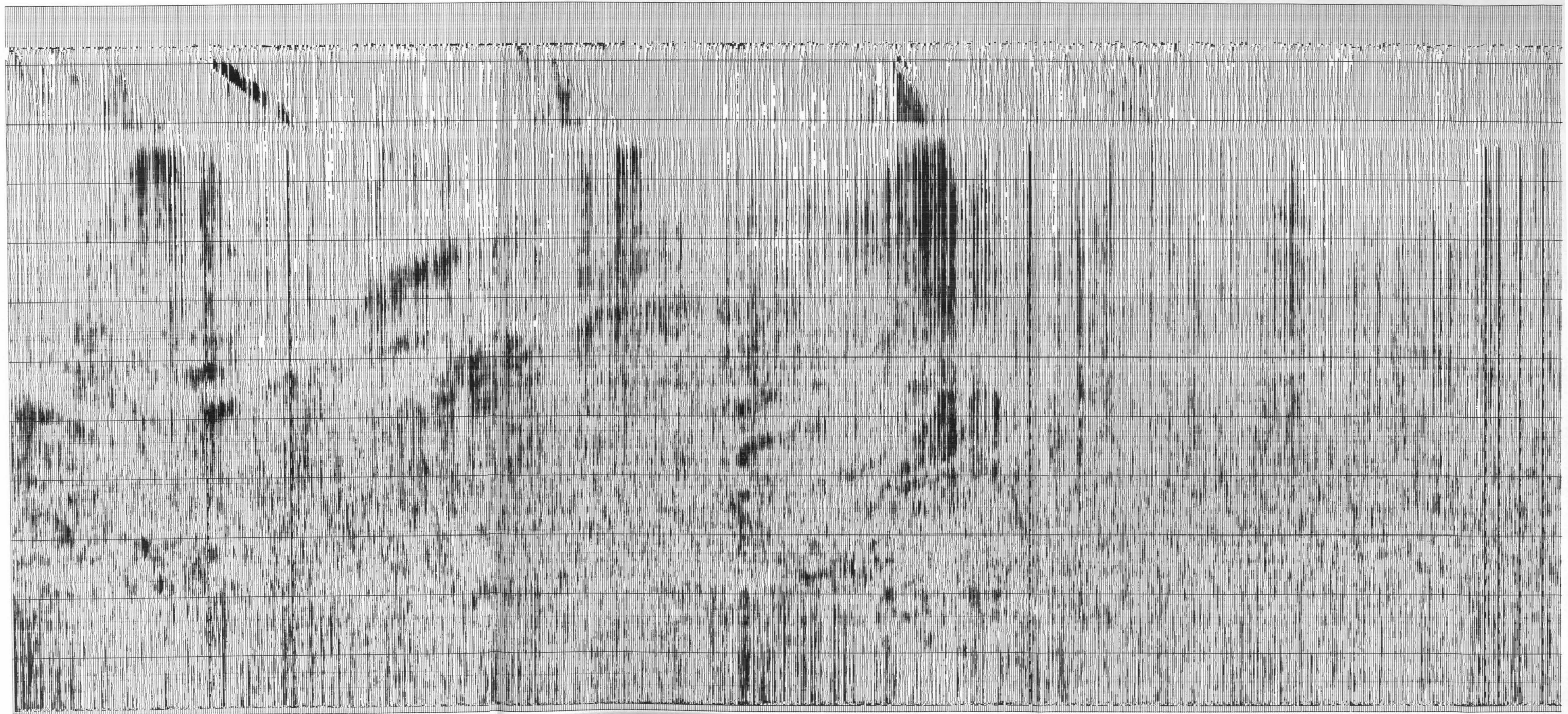


Amplitude-Offset Trend Stack of COCORP Mojave Line 3

**Fig. 3.39:** Correlations of the linear regressions on amplitude versus offset for each point of the stack in Figure 3.36. Clip at  $r=0.6$ . Dark areas indicate positive  $r$ . Plot is on the same scales as Figure 3.36.



No Vertical Exaggeration



Correlation of COCORP Mojave Line 3 Trend Stack

the calculation for a frequency  $f$  of 20 Hz, a characteristic offset  $h$  of 10 km, and an effective attenuation corresponding to a  $Q_{ap}$  of 20. The shape of the curve between 1 and 3 s is so strongly affected by the value of  $Q_{ap}$  that the average  $Q_{ap}$  over line 3 is constrained to be between 10 and 30. Considering the values for effective attenuation reviewed in the section on propagation effects above, such a low value is not at all surprising. The average trend, as modeled, is affected mostly by the shallowest section of the crust, where highly heterogeneous alluvium causes extensive scattering and mode conversion of high-frequency reflections. The fact that the average trend can be modeled so directly indicates that most of the energy in the shot gathers, away from the mutes, is actually due to the presence of direct compressional wave reflections from within the basement. This is apparently the case even though it is very difficult to identify these events individually on the shot gathers or in the stacks.

This model trend, fit to the average amplitude versus offset trend of the entire dataset, was subtracted from each trace of the trend stack to yield the trend stack in Figure 3.38, which is thus the trend corrected for the average effective attenuation. The section shows dark areas, where  $Q_{ap}$  is greater than 20 near the surface, and light areas where it is less than 20. The trend of some reflections is made visible by the correction, such as at 2.2 s just northeast of the center of the line. Overall, except for the influence of a few near-surface reflectors reversing the trends below them, the major southwest dipping mid crustal reflection, "F" on Figure 3.29, shows increasing amplitude with offset. There are also hints near the center of the section that the Moho reflection at 10 s may have a positive trend. It is not strong enough over the

whole section, however, to yield a definite trend from the COCORP experiment. Without corroborating information indicating the contrast in compressional velocity at the regional reflector, the sign of its Poisson's ratio contrast cannot be determined. It is sure, however, that the variation in Poisson's ratio at this structure is large.

The COCORP Mojave line 3 dataset thus provides a regionally extensive analysis of the strongest mid crustal reflections. It unfortunately lacks enough offset coverage to enable a regional analysis of the Moho. Further, the inability to sort it into midpoint gathers forces the assumption of lateral homogeneity over scales of several kilometers. With the major mid crustal reflections, however, comparison of shot and midpoint gather stacks suggests that such an assumption may be made. The derived amplitude trends suffer from interference by a highly heterogeneous near-surface section, but the interference is easy to identify. This surface section also produces effective attenuation to the extent that the average apparent  $Q$  is only 20. The ability to account for all of these considerations should make these multi-offset techniques applicable to many COCORP, and other, datasets.

## 5. CONCLUSIONS

An understanding of the nature of the Earth's crust and its formative processes depends upon knowledge of the physical nature and condition of rocks at deep levels. Seismic reflection surveys in many areas have brought to light the existence of previously unsuspected structures that have led to new models of crustal phenomena. To date, however, they have employed techniques oriented towards defining the geometric structure of these reflectors. While knowledge of reflector geometry allows hypotheses on the geologic nature of the reflectors to be proposed, in many cases it has not provided tests for competing models. In addition, geologists, often regarding seismic reflection results as having some equivalence to geologic sections, have mainly proposed reflector models based on genetic factors associated with the geologic origin of the rocks. Other models, based on factors solely related to the present-day physical condition of the crust, have been ignored. This implied equivalence of geologic boundaries with reflectors is risky, as the deep crust has not yet been sampled or observed directly. Despite their resolution of unprecedented detail, seismic reflection surveys have not yet brought about an improved understanding of such critical processes as volcanism, earthquake generation, and metamorphism, all present-day physical phenomena.

This shortcoming can be addressed through expanding the analysis of seismic data to include the multi-offset information. This can be done in two steps. First, by examining the dependence of reflection frequency on offset, a step discontinuity can be distinguished from thinly layered structures. Thin layers produce an increase in peak frequency with offset, a phenomenon constrained by simple interference relations and elastic wave equation modeling.

If the amount of increase can be measured, the thickness and velocity contrast of the layers can be estimated. This determination reveals whether a reflective structure is the result of broad scale changes in the crust, or due to the more localized effects of phenomena such as fault motion or fluid injection.

The second step is to examine reflection amplitudes as they change with offset. Approximations of elastic scattering phenomena, applicable to crustal reflections, show that whether amplitude increases or decreases with offset in the pre-critical range depends on the sign of the density and rigidity variations relative to the sign of the variation in Lamé's parameter. If the signs are opposed, amplitude increases with offset. If the signs agree, the amplitudes decrease. If the sign of the compressional velocity variation is also known, the sense of variation in Poisson's ratio can be found. These simplified relationships are verified by full plane wave calculations on a set of canonical models. This simple method yields fundamental constraints on the physical properties of deep reflectors.

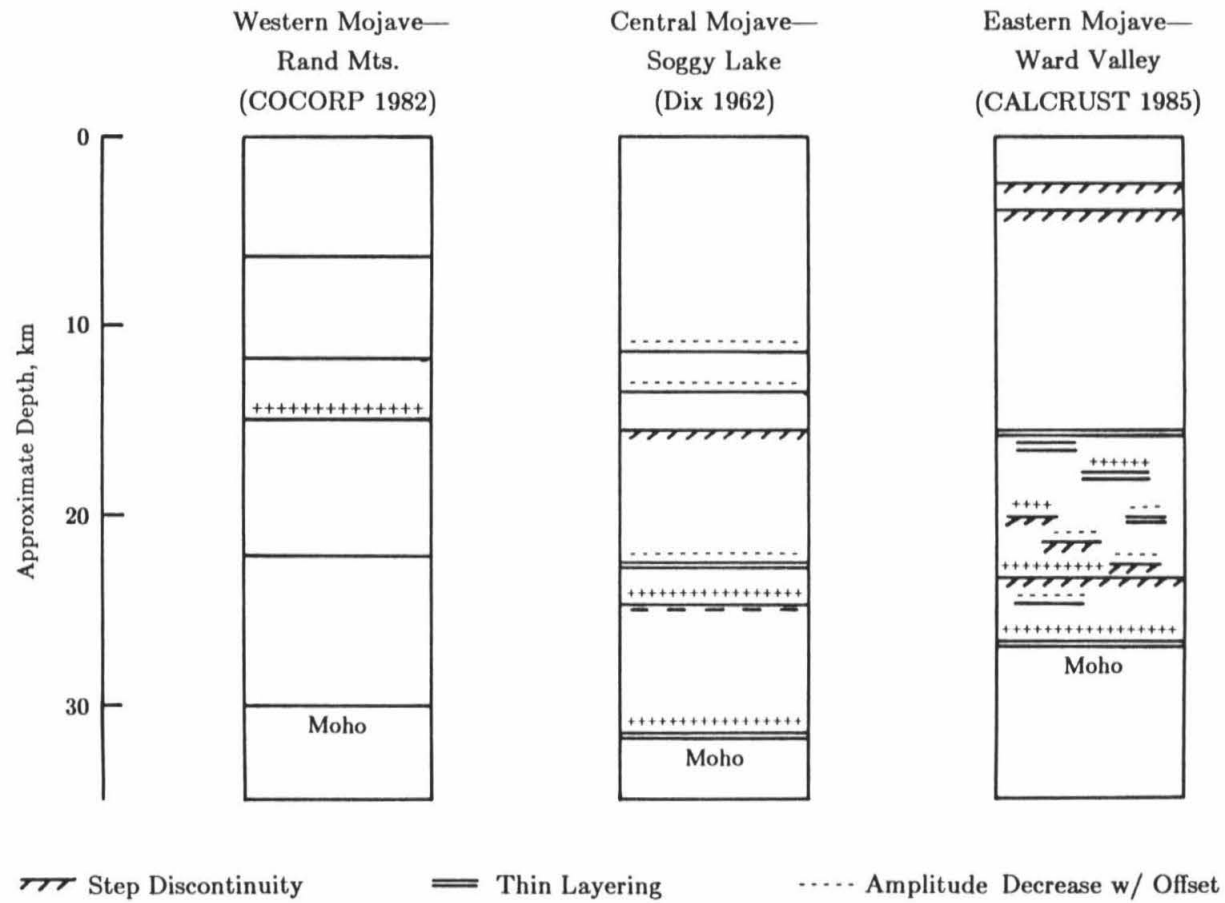
These steps can be applied to a variety of datasets. The results from three surveys in the eastern, central, and western Mojave image structures in the deep crust about which very little is known. The 1985 Calcrust line in the Ward Valley was designed to yield long offset information on the deep crust within a short interval. A single long offset shot gather assembled by C. H. Dix in 1962 contains some of the clearest records of deep events. The COCORP Mojave line 3, although shot in a conventional manner with a limited offset range, provides regional coverage. The coverage and quality of these data are too poor for formal inversions, but they do provide definitive analyses of simple frequency and amplitude trends.

Four classes of factors can affect apparent frequency and amplitude trends. Recording and processing factors include source and receiver calibration and the identification of directly reflected compressional waves. Surface consistent effects result from variations in instrument ground coupling, directivity, and near-surface heterogeneities. The effects of propagation, spherical divergence and effective attenuation, are often exacerbated by heterogeneity and anisotropy. Finally, anisotropy contrasts, layering, and curvature of the reflector itself can complicate the interpretation of multi-offset reflections.

The effects of these factors can be mitigated to the point where useful interpretations can still be made. Only the gross trend of amplitude with offset, whether it increases or decreases, needs to be found. The trend is calculated for each point of a stacked section, which has been weighted by the proportion of hyperbolic events incorporated into each point. Interpretations can then be made from the strongest reflections that best fit the assumptions of the stacking process. The trends of strong reflections stand out as sharp events above the background noise. The trend stack itself can be used to locate the effects of interfering phenomena, while the effects of most types of heterogeneity can be averaged out by conducting an experiment with sufficient multiplicity and reciprocity. The interpretation of the 1985 Calcrust Ward Valley dataset carries all of these advantages. While the datasets from the western and central Mojave have limitations, the trend stacks still show where valid interpretations may be made.

The results of examination of manually selected multi-offset spectra and of weighted stacks and their accompanying trend stacks and trend correlation stacks for the three areas of the Mojave are summarized in Figure 3.40.

**Fig. 3.40:** Generalized crustal columns showing the depths and character of major reflectors in 3 areas of the Mojave Desert (Figure 3.1). The physical nature of selected structures as derived from frequencies and amplitudes of multi-offset reflections are indicated. Increases or decreases of amplitude with offset are indicated by plusses or minuses above each reflector.



This page intentionally left blank.

Although the three areas are separated by at least 100 km, and the quality of the datasets varies, some similarities can be noted. In the middle crust, the most prominent reflectors may show an increase in amplitude with offset. In the eastern Mojave, where spectra indicate that at least one of the predominant reflectors contains thin layering, this increase corresponds with an increase in Poisson's ratio. While this cannot be shown for the other areas, the trends are so prominent that these mid crustal structures must incorporate a strong variation in Poisson's ratio. Such structures can extend over regions of at least 100 km, as seen in the western Mojave. The Poisson's ratio variations imply that, if the thin layering is interpreted to be tectonic, then any motion interpreted must be large enough to offset rock units of entirely different composition. Otherwise the motion must be large enough and recent enough to offset rocks of metamorphic facies equilibrated to quite different levels of the crust, without re-equilibration.

All three sections show some evidence of a basal crustal zone overlain by strong, dipping heterogeneities, which vary on a small scale. The top of the basal zone may have a remarkably constant depth, near 22 km across the Mojave. Where it can be constrained, it is a step discontinuity carrying an increase in Poisson's ratio, producing one of the strongest reflections. The overlying dipping heterogeneities suggest a broad transition zone, possibly composed of the same rocks as the mid crust, but broken or invaded by fluids arising from the basal zone. The basal zone itself shows a high degree of small-scale heterogeneity, but not, at least in the eastern Mojave, great variability of Poisson's ratio.

The Moho discontinuity shows the same characteristics across the Mojave. It includes thin layering and represents a strong increase in Poisson's ratio, observations best constrained in the central and eastern Mojave. This is true despite its difference in depth of at least 5 km between the two areas. The entire amount of thinning of the crust in the eastern Mojave during the Miocene could be accounted for by thinning and boudinage of the basal zone. This implies that the extension process that acted to thin the crust thinned only a pre-existing basal zone, or that the basal zone was created across the entire Mojave after the Miocene extensional event.

The next step in this analysis would be a quantification of the effects of geologic and physical processes on Poisson's ratio. While experimental work on porous rocks at upper crustal conditions suggests that strong changes in Poisson's ratio may be tied to changes in porosity (Toksoz et al., 1976), little is known about the possible range of conditions at deeper levels. Aside from the effects of physical condition, Poisson's ratio contrasts, due to variations in metamorphic grade, have yet to be worked out. On the evidence, presented here, of the great variability of this parameter throughout the crust, geologic models should be constructed to include contrasts having the more incompatible physical properties. Interfaces involving only changes in the present-day physical condition must also be considered.

## RECOMMENDATIONS

In many ways, the interior of Earth is more inaccessible than the far reaches of the solar system. Despite our proximity to it, the dense, opaque nature of rocks has severely limited the amount and quality of the information we can obtain from it. Even for Earth's crust, intensive efforts must be made to discern its properties and the processes that formed it. The seismic reflection technique is one such remote sensing method, which has been useful for providing reconnaissance information on the nature of the crust.

Often, however, reconnaissance seismic reflection methods miss important features of the crust. This was seen in Chapter 1, where standard stacking techniques were unable to indicate the presence of dramatic lateral heterogeneity. A different approach is necessary to prevent a biased view of the crust from emerging. This approach is realizable in two ways. First, the data from previously completed seismic experiments must be examined in their entirety. It is helpful if, in addition, the data can be presented in a format intuitively related to the actual physical experiment that was carried out. One such format is the record sections on which the fault zone reflections at Parkfield could be easily identified. At present the examination of all of the shot records from an average seismic survey is a difficult and time-consuming prospect, because of the enormous volume of data. It is steadily becoming even more difficult, as more surveys employing large numbers of receivers, and three-dimensional acquisition designs, are carried out. This problem can be

mitigated, however, by designing new data processing systems that will allow the retrieval, display, and manipulation of multi-dimensional record sections on a human time scale. As an additional advantage, such systems could make the testing and comprehension of novel transformations of the data more tractable. This will bring about the interpretation of phenomena that are at present too poorly known to handle except by deletion.

The second way of extending the seismic reflection technique beyond its present reconnaissance status is to design reflection experiments with particular scientific objectives. An attempt at this was carried out by the Calcrust consortium and was reported in Chapter 2. Such a consortium, incorporating both geologists and geophysicists, provides a valuable forum for determining what the geologically pressing problems are, and how they might be addressed with geophysical experiments. The design of such an experiment should include not only the routing of the survey, but also specific acquisition methods tailored to observe phenomena that can be expected, from modeling, to arise from the hypothetical structures considered. It should be noted, however, that the expense of seismic experiments makes it necessary to carry out surveys having more than one objective. The 1985 Calcrust survey is an example. Although it was primarily designed to resolve questions on the geometry of structures in the shallow basement, it was perhaps most successful in obtaining constraints on the nature of deep structures, as was seen in Chapter 3. This information was obtained in large part from the long offset arrays specifically designed to image the deep crust.

Any experiment with a deep objective may have to include methods aimed at the shallow section for another reason. As was seen in Chapter 2,

the highly heterogeneous nature of the surface interfered with the receipt of any information from the deeper section. The effects of the surface section had to be evaluated in Chapter 3 before analyses of deep phenomena could proceed. The examination and reduction of multi-offset reflections, while it increases the amount of information available, also does not benefit from the standard methods of mitigating noise through data summing processes. Thus, the nature of the noise, which usually arises close to the surface, must be understood. Because of these considerations, it is suggested that any seismic experiment have several objectives, located in quite different parts of the crustal section.

The 1986 Calcrust experiment in the Apple Valley, in the central Mojave Desert, was designed with these considerations in mind. Its dual nature was driven by having both shallow objectives, some of which crop out along the survey, and deep objectives, such as structure of the Moho. The methods that were applied in Chapter 3 can be applied to this new survey more robustly, since it includes data of higher density and wider offset coverage. It is also one of the first deep crustal surveys to be undertaken in an area of active seismicity, where the activity carries suggestions of boundaries in the present day physical state of the rocks at depth.

The importance of corroborating information cannot be overstressed. Aside from the information available to geologists in outcrops, other physical information on the state of the crust must be brought to bear on interpretations of seismic reflectors. Seismic activity, gravity, electromagnetic, and heat flow information all have the potential of further constraining the nature of structures suggested by reflection work. In fact, extensive laboratory work

may be necessary to understand the connection of observed physical properties, like Poisson's ratio, to geologically understandable processes such as metamorphism. At present, it can only be said that many boundaries that have fundamental importance to the genesis of crustal terranes, such as basement fault offsets, may not have any consistently recognizable contrast in the physical properties observed by the reflection technique. Some of this information may be obtained as more boreholes begin to penetrate reflective basement structures, as is occurring near the Apple Valley.

## REFERENCES

- Aki, K., and Richards, P. G., 1980, Quantitative Seismology, **1**: W. H. Freeman and Co.
- Almoghrabi, H., and Lange, J., 1986, Layers and bright spots: Geophysics, **51**, 699-709.
- Anderson, J. L., and Rowley, M.C., 1980, Synkinematic intrusion of two-mica and associated metaluminous granitoids, Whipple Mountains, California: Canadian Mineralogist, **19**, 83-101.
- Balachandran, K., 1974, Noninterchangeability of sources and receivers in a heterogeneous medium: Geophysics, **39**, 73-80.
- Balch, A. H., Lee, M. W., Miller, J. J., and Ryder, R. T., 1981, Seismic amplitude anomalies associated with thick First Leo sandstone lenses, eastern Powder River basin, Wyoming: Geophysics, **46**, 1519-1527.
- Carpenter, P. J., and Sanford, A. R., 1985, Apparent Q for upper crustal rocks of the central Rio Grande rift: J. Geophys. Res., **90**, 8661-8674.
- Cheadle, M. J., Czuchra, B. L., Ando, C. J., Byrne, T., Brown, L. D., Oliver, J. E., Kaufman, S., 1985, Geometries of deep crustal faults: evidence from the COCORP Mojave survey: *in* Barazangi, M. and Brown, L., Eds., Reflection seismology: the continental crust: Geodynamics series, **14**, Am. Geophys. Union, 305-312.
- Cheadle, M. J., Czuchra, B. L., Byrne, T., Ando, C. J., Oliver, J. E., Brown, L. D., Kaufman, S., Malin, P. E., and Phinney, R. A., 1986, The deep crustal structure of the Mojave Desert, California, from COCORP seismic

reflection data: *Tectonics*, **5**, 293-320.

Chiburis, E. F., 1984, Analysis of amplitude versus offset to detect gas/oil contacts in the Arabian Gulf: Presented at Soc. Expl. Geophys. annual meeting, Atlanta.

Clowes, R. M., and Kanasewich, E. R., 1970, Seismic attenuation and the nature of reflecting horizons within the crust: *J. Geophys. Res.*, **75**, 6693-6705.

Cohen, J. K., and Bleistein, N., 1983, The influence of out-of-plane surface properties on unmigrated time sections: *Geophysics*, **48**, 125-132.

Coney, P. J., 1980, Cordilleran metamorphic core complexes: an overview, *in* Crittenden, M. D., Coney, P. J., and Davis, G. H., Eds., Tectonic significance of metamorphic core complexes of the North American cordillera: *Geol. Soc. Am. Memoir 153*, 7-35.

Dainty, A. M., 1984, High-frequency acoustic backscattering and seismic attenuation: *J. Geophys. Res.*, **89**, 3172-3176.

Daley, P. F., and Hron, F., 1977, Reflection and transmission coefficients for transversely isotropic media: *Bull., Seis. Soc. Am.*, **67**, 661-675.

Davis, G. A., Anderson, J. L., Frost, E. G., and Shackelford, T. J., 1980, Mylonitization and detachment faulting in the Whipple-Buckskin-Rawhide Mountains terrane, southeastern California and western Arizona, *in* Crittenden, M. D., Coney, P. J., and Davis, G. H., Eds., Tectonic significance of metamorphic core complexes of the North American cordillera: *Geol. Soc. Am. Memoir 153*, 79-129.

- Davis, G. A., Anderson, J. L., Martin, D. L., Krummenacher, D., Frost, E. G., and Armstrong, R. L., 1982, Geologic and geochronologic relations in the lower plate of the Whipple detachment fault, Whipple Mountains, southeastern California: a progress report, *in* Frost, E. G., and Martin, D. L., Eds., Mesozoic-Cenozoic tectonic evolution of the Colorado River region, California, Arizona, and Nevada: Cordilleran Publishers, 408-432.
- Davydova, N. I., 1972, Possibilities of the DSS technique in studying properties of deep-seated seismic interfaces, *in* Davydova, N. I., Ed., Seismic properties of the Mohorovicic discontinuity: U. S. Dept. of Commerce, Nat. Technical Inform. Serv., 4-22.
- Davydova, N. I., Ivantsov, Y. F., Tal-Virskii, B. B., Fursov, A. N., and Yaroshevskaya, G. A., 1972, Properties of deep-seated seismic boundaries in western Uzbekistan, *in* Davydova, N. I., Ed., Seismic properties of the Mohorovicic discontinuity: U. S. Dept. of Commerce, Nat. Technical Inform. Serv., 43-57.
- De Bremaecker, J. C. I., Godson, R. H., Watkins, J. S., 1966, Attenuation measurements in the field: *Geophysics*, **31**, 562-569.
- de Voogd, N., and den Rooijen, H., 1983, Thin-layer response and spectral bandwidth: *Geophysics*, **48**, 12-18.
- Dickey, D. D., Carr, W. J., and Bull, W. B., 1980, Geologic map of the Parker NW, Parker, and parts of the Whipple Mountains SW and Whipple Wash quadrangles, California and Arizona: U. S. Geol. Surv. Misc. Invest. Series Map I-1124, 1:24,000.

- Dix, C. H., 1965, Reflection seismic crustal studies: *Geophysics*, **30**, 1068-1084.
- Dokka, R. K., 1983, Displacements on late Cenozoic strike-slip faults of the central Mojave Desert, California: *Geology*, **11**, 305-308.
- Eaton, J. P., O'Neill, M. E., and Murdock, J. N., 1970, Aftershocks of the 1966 Parkfield-Cholame earthquake: a detailed study: *Bull., Seismol. Soc. Am.*, **60**, 1157-1197.
- Fenati, D., and Rocca, F., 1984, Seismic reciprocity field tests from the Italian Peninsula: *Geophysics*, **49**, 1690-1700.
- Feng, R., and McEvilly, T. V., 1983, Interpretation of seismic reflection profiling data for the structure of the San Andreas fault zone: *Bull., Seismol. Soc. Am.*, **73**, 1701-1720.
- Fisher, D. A., and Gardner, G. H. F., 1984, Physical and numerical modeling of reflections from interfaces and thin layers: Presented at Soc. Expl. Geophys. annual meeting, Atlanta.
- Fokhema, J. T., and Ziolkowski, A., 1985, The critical reflection theorem: Presented at Soc. Expl. Geophys. annual meeting, Washington, D. C.
- Frankel, A., and Clayton, R. W., 1986, Finite difference simulations of seismic scattering: implications for the propagation of short-period seismic waves in the crust and models of crustal heterogeneity: *J. Geophys. Res.*, **91**, 6465-6489.
- Frost, E. G., 1981, Structural style of detachment faulting in the Whipple Mountains, California, and Buckskin Mountains, Arizona: *Arizona Geol. Soc. Digest* **13**, 25-30.

- Fuchs, K., 1969, On the properties of deep crustal reflectors: *Z. Geophys.*, **35**, 133-149.
- Fuis, G. S., Mooney, W. D., Healey, J. H., McMechan, G. A., and Lutter, W. J., 1982, Crustal structure of the Imperial Valley region: *U. S. Geol. Surv. Profess. Paper 1254*, 25-49.
- Ganley, D. C., and Kanasewich, E. R., 1980, Measurement of absorption and dispersion from check shot surveys: *J. Geophys. Res.*, **85**, 5219-5226.
- Gassaway, G. S., 1984, Effects of shallow reflectors on amplitude versus offset (seismic lithology) analysis: Presented at Soc. Expl. Geophys. annual meeting, Atlanta.
- Goupillaud, P. L., 1961, An approach to inverse filtering of near-surface layer effects from seismic records: *Geophysics*, **26**, 754-760.
- Gupta, R. N., 1966, Reflection of elastic waves from a linear transition layer: *Bull., Seis. Soc. Am.*, **56**, 511-526.
- Hale, L. D., and Thompson, G. A., 1982, The seismic reflection character of the continental Mohorovicic discontinuity: *J. Geophys. Res.*, **87**, 4625-4635.
- Hamilton, W. B., 1982, Structural evolution of the Big Maria Mountains, northeastern Riverside County, California, *in* Frost, E. G., and Martin, D. L., Eds., *Mesozoic-Cenozoic tectonic evolution of the Colorado River region, California, Arizona, and Nevada*: Cordilleran Publishers, 1-28.
- Hanna, W. F., Burch, S. H., and Dibblee, T. W., 1972, Gravity, magnetics, and geology of the San Andreas fault area near Cholame, California: *U. S. Geol. Surv. Profess. Paper 646-C*.

- Harlan, W. S., Claerbout, J. F., and Rocca, F., 1984, Signal/noise separation and velocity estimation: *Geophysics*, **49**, 1869-1880.
- Hearn, T. M., 1984, Pn travel times in southern California: *J. Geophys. Res.*, **89**, 1843-1855.
- Hearn, T. M., and Clayton, R. W., 1986, Lateral velocity variations in southern California. II. Results for the lower crust from *Pn* waves: *Bull., Seismol. Soc. Am.*, **76**, 511-520.
- Helbig, K., 1984, Anisotropy and dispersion in periodically layered media: *Geophysics*, **49**, 364-373.
- Hilterman, F. J., 1975, Amplitudes of seismic waves— a quick look: *Geophysics*, **40**, 745-762.
- Honeyman, W., 1983, Short note on near-surface faulting effects on seismic reflection times: *Geophysics*, **48**, 1140-1142.
- Howard, K. A., Stone, P., Pernokas, M. A., and Marvin, R. F., 1982, Geologic and geochronologic reconnaissance of the Turtle Mountains area, California: west border of the Whipple Mountains detachment terrane, in Frost, E. G., and Martin, D. L., Eds., *Mesozoic-Cenozoic tectonic evolution of the Colorado River region, California, Arizona, and Nevada*: Cordilleran Publishers, 341-355.
- Hubral, P., 1983, Computing true amplitude reflections in a laterally inhomogeneous Earth: *Geophysics*, **48**, 1051-1062.
- Hubral, P., 1984, Short note on simulating true amplitude reflections by stacking shot records: *Geophysics*, **49**, 303-306.

- Jain, S., and Wren, A. E., 1980, Migration before stack— procedure and significance: *Geophysics*, **45**, 204-212.
- John, B. E., 1982, Geologic framework of the Chemehuevi Mountains, southeastern California, *in* Frost, E. G., and Martin, D. L., Eds., Mesozoic-Cenozoic tectonic evolution of the Colorado River region, California, Arizona, and Nevada: Cordilleran Publishers, 317-325.
- Jones, T. D., 1985, Nature of seismic reflections from the crystalline basement: COCORP Wind River line, Wyoming: *J. Geophys. Res.*, **90**, 6783-6791.
- Jones, T. D., and Nur, A., 1984, The nature of seismic reflections from deep crustal fault zones: *J. Geophys. Res.*, **89**, 3153-3171.
- Kahler, S., and Meissner, R., 1983, Radiation and receiver pattern of shear and compressional waves as a function of Poisson's ratio: *Geophys. Prosp.*, **31**, 421-435.
- Kanamori, H., and Hadley, D., 1975, Crustal structure and temporal velocity change in southern California: *Pure Appl. Geophys.*, **113**, 257-280.
- Knopoff, L., and Gangi, A. F., 1959, Seismic reciprocity: *Geophysics*, **24**, 681-691.
- Koefoed, O., 1955, On the effect of Poisson's ratios of rock strata on the reflection coefficients of plane waves: *Geophys. Prosp.*, **3**, 381-387.
- Kosminskaya, I. P., 1964, On layering of the Earth's crust: *J. Geophys. Res.*, **69**, 802-805.
- Krail, P. M., and Brysk, H., 1983, Reflection of spherical seismic waves in elastic layered media: *Geophysics*, **48**, 655-664.

- Krohn, C. E., 1984, Geophone ground coupling: *Geophysics*, **49**, 722-731.
- Long, A., and Richgels, J., 1985, A practical application of amplitude versus offset effects: Presented at Soc. Expl. Geophys. annual meeting, Washington, D. C.
- Le Bras, R., 1985, Methods of multiparameter inversion of seismic data using the acoustic and elastic Born approximations: Ph.D. thesis, Calif. Institute of Technology.
- Liu, H.-L., 1983, Interpretation of near-source ground motion and implications: Ph.D. thesis, Calif. Institute of Technology.
- Long, G. H., 1981, A COCORP deep seismic reflection profile along the San Andreas fault, Parkfield, California: M.Sc. thesis, Cornell Univ.
- Louie, J. N., Le Bras, R. J., and Clayton, R. W., 1984, 3-d imaging of steeply dipping structure near the San Andreas fault, Monterey Co., California: Presented at Soc. Expl. Geophys. annual meeting, Atlanta.
- Lyle, J. H., 1982, Interrelationship of late Mesozoic thrust faulting and mid-Tertiary detachment faulting in the Riverside Mountains, southeastern California, in Frost, E. G., and Martin, D. L., Eds., Mesozoic-Cenozoic tectonic evolution of the Colorado River region, California, Arizona, and Nevada: Cordilleran Publishers, 470-492.
- Mair, J. A., and Lyons, J. A., 1976, Seismic reflection technique for crustal structure studies: *Geophysics*, **41**, 1272-1290.
- Mayne, W. H., 1962, Common reflection point horizontal depth stacking techniques: *Geophysics*, **27**, 927-938.

- Mazzotti, A., 1984, Prestack analysis of seismic amplitude anomalies: Presented at Soc. Expl. Geophys. annual meeting, Atlanta.
- McBride, J. H., and Brown, L. D., 1986, Reanalysis of the COCORP deep seismic reflection profile across the San Andreas fault, Parkfield, California: Bull., Seismol. Soc. Am., **76**, 1668-1686.
- McMechan, G. A., Clayton, R. W., and Mooney, W. D., 1982, Application of wave field continuation to the inversion of refraction data: J. Geophys. Res., **87**, 927-935.
- McMechan, G. A., and Fuis, G. S., 1987, Ray equation migration of wide-angle reflections from southern Alaska: J. Geophys. Res., **92**, 407-420.
- Meissner, R., 1967, Exploring deep interfaces by seismic wide angle measurements: Geophys. Prosp., **15**, 598-617.
- Meissner, R., 1973, The "Moho" as a transition zone: Geophys. Surveys, **1**, 195-216.
- Meissner, R., and Meixner, E., 1969, Deformation of seismic wavelets by thin layers and layered boundaries: Geophys. Prosp., **17**, 1-27.
- Mikhota, G. G., 1972, Frequency spectrum of waves generated at the M discontinuity, in Davydova, N. I., Ed., Seismic properties of the Mohorovicic discontinuity: U. S. Dept. of Commerce, Nat. Technical Inform. Serv., 23-42.
- Miller, G. F., and Pursey, H., 1954, The field and radiation pattern of mechanical radiators on the free surface of a semi-infinite isotropic solid: Proc. Royal Soc. (London), series A, **223**, 521-541.

- Newman, P., 1973, Divergence effects in a layered Earth: *Geophysics*, **38**, 481-488.
- Newman, P. J., and Worthington, M. H., 1982, In-situ investigation of seismic body wave attenuation in heterogeneous media: *Geophys. Prosp.*, **30**, 377-400.
- O'Doherty, R. F., and Anstey, N. A., 1971, Reflections on amplitudes: *Geophys. Prosp.*, **19**, 430-458.
- Okaya, D. A., 1985, Seismic profiling of the lower crust: Dixie Valley, Nevada, *in* Barazangi, M., and Brown, L., Eds., *Reflection seismology: the continental crust: Geodynamics Series 14*, Am. Geophys. Union, 269-279.
- Onstott, G. E., Backus, M. M., Wilson, C. R., and Phillips, J. D., 1984, Color display of offset dependent reflectivity in seismic data: Presented at Soc. Expl. Geophys. annual meeting, Atlanta.
- Ostrander, W. J., 1984, Plane-wave reflection coefficients for gas sands at non-normal angles of incidence: *Geophysics*, **49**, 1637-1648.
- Patton, H. J., and Taylor, S. R., 1984, Q structure of the Basin and Range from surface waves: *J. Geophys. Res.*, **89**, 6929-6940.
- Pullan, S. E., and Hunter, J. A., 1985, Seismic model studies of the overburden-bedrock reflection: *Geophysics*, **50**, 1684-1688.
- Richards, T. C., 1961, Motion of the ground on arrival of reflected longitudinal and transverse waves at wide-angle reflection distances: *Geophysics*, **26**, 277-297.
- Robinson, W. B., 1945, Refraction waves reflected from a fault zone: *Geophysics*, **10**, 535-545.

- Safar, M. H., 1984, On the determination of the downgoing P-waves radiated by the vertical seismic vibrator: *Geophys. Prosp.*, **32**, 392-405.
- Savit, C. H., 1950, Reflected energy variations resulting from small changes in shot hole and spread locations: *Geophysics*, **15**, 219-226.
- Schoenbeger, M., and Levin, F. K., 1978, Apparent attenuation due to intrabed multiples, II: *Geophysics*, **42**, 730-737.
- Shuey, R. T., 1985, A simplification of the Zoeppritz equations: *Geophysics*, **50**, 609-614.
- Shuey, R. T., Banik, N. C., and Lerche, I., 1984, Amplitude from curved reflectors: Presented at Soc. Expl. Geophys. annual meeting, Atlanta.
- Shugart, T. R., 1944, Frequency discrimination in the low velocity zone: *Geophysics*, **9**, 19-28.
- Sibson, R. H., 1984, Roughness at the base of the seismogenic zone: contributing factors: *J. Geophys. Res.*, **89**, 5791-5799.
- Stainsby, S. D., and Worthington, M. H., 1985,  $Q$  estimation from vertical seismic profile data and anomalous variations in the central North Sea: *Geophysics*, **50**, 615-626.
- Tan, T. H., 1985, The elastodynamic field of  $N$  interacting vibrators (two-dimensional theory): *Geophysics*, **50**, 1229-1252.
- Taner, M. T., and Koehler, F., 1981, Surface consistent corrections: *Geophysics*, **46**, 17-22.
- Thorson, J. R., and Claerbout, J. F., 1985, Velocity-stack and slant-stack stochastic inversion: *Geophysics*, **50**, 2727-2741.

- Toksoz, N. M., Cheng, C. H., and Timur, A., 1976, Velocity of seismic waves in porous rocks: *Geophysics*, **41**, 621-645.
- Tulina, Y. V., Zverev, S. M., Mikhota, G. G., and Zaitseva, E. N., 1972, Characteristic features of waves from the Mohorovicic discontinuity in the ocean and the transition zone, *in* Davydova, N. I., Ed., *Seismic properties of the Mohorovicic discontinuity*: U. S. Dept. of Commerce, Nat. Technical Inform. Serv., 58-65.
- Ursin, B., 1986, Zero-offset reflections from a curved interface: *Geophysics*, **51**, 50-53.
- Vidale, J. E., and Helmberger, D. M., 1987 in press, Path effects in strong motion seismology, *in* Bolt B. A., Ed., *Seismic strong motion synthetics: Methods of computational physics series*, Academic Press.
- Welder, J., and Nur, A., 1984, Porosity reduction and crustal pore fluid pressure development: *J. Geophys. Res.*, **89**, 11 539-11 548.
- Wen, J., and McMechan, G. A., 1985, Application of two-dimensional synthetic seismogram modeling to interpretation of wide-angle seismic data from the Wind River, Wyoming: *J. Geophys. Res.*, **90**, 3617-3625.
- Widess, M. B., 1973, How thin is a thin bed?: *Geophysics*, **38**, 1176-1180.
- Wiggins, R., Kenny, G. S., and McClure, C. D., 1985, Common-depth point method for determining and displaying the shear-velocity reflectivities of a geologic formation: U. S. Patent 4 534 019.
- Wilson, J., McCarthy, J., and Fuis, G., 1986, Preliminary 2-d velocity modeling of the Whipple Mountains metamorphic core complex (abstract): *EOS Trans. Am. Geophys. Union*, **67**, 1096.

- Wright, J., 1984, The effect of anisotropy on reflectivity-offset: Presented at Soc. Expl. Geophys. annual meeting, Atlanta.
- Wright, J. E., Anderson, L., and Davis, G. A., 1986, Timing of and decompression in a metamorphic core complex, Whipple Mountains, CA: Geol. Soc. Am. Abstracts with programs, **18**, 201.
- Wu, R., and Aki, K., 1985a, Scattering characteristics of elastic waves by an elastic heterogeneity: Geophysics, **50**, 582-595.
- Wu, R. S., and Aki, K., 1985b, Elastic wave scattering by a random medium and the small-scale inhomogeneities in the lithosphere: J. Geophys. Res., **90**, 10 261-10 273.
- Yu, G., 1985, Offset-amplitude variation and controlled-amplitude processing: Geophysics, **50**, 2697-2708.

## Appendix

### Acquisition Parameters of the 1985 Calcrust Survey

Details of the acquisition parameters used during the 1985 Calcrust Mojave-Sonoran project are given here for reference. Chapter 2 discusses how these parameters were chosen. Table A-1 gives the geographic coordinates of the ends of the survey lines to an accuracy of 30 m. Table A-2 summarizes the final acquisition parameters used on both the primary roll-along lines and the long offset stationary spreads. Parameters not listed did not change between lines and are as follows: Four vibrators made linear upsweeps from 8 to 36 Hz, with a 3 s cosine taper at the low end. The Sercel SN-348 recorder listened for 12 s in addition to the sweep time, applying a 72 dB/octave high cut filter at 62.5 Hz and a notch filter at 60 Hz, with a preamp gain of  $2^7$ , before digitizing at 0.004 s intervals. The Sercel SN-338 recorder listened for 9 s in addition to the sweep time, applying a 72 dB/octave high cut filter at 62.5 Hz, a 12 dB/octave low cut filter at 8 Hz, and a notch filter at 60 Hz, with a preamp gain of  $2^7$ , before digitizing at 0.004 s intervals.

Table A-2 is divided into two parts, giving source and receiver parameters. The "record line" is the name of the line associated with the records in the observers' reports, while the "source line" is the name of the line on which the vibrators were operating. The range of vibrator points (VPs) over which they operated is also noted. The "source interval" is the nominal, or in-line,

distance between consecutive shots by the vibrators. The moveup "interval" gives the creep distance between sweeps of the vibrators within the moveup pattern, which forms a source array "size" long and weighted centrally about a point displaced by "disp." away from the nominal VP in the direction indicated. This is not the true bearing, but indicates direction either parallel or perpendicular to the local course of the line. The "group interval" is the nominal, in-line distance between consecutively recorded receiver channels. The "spread type" indicates the geometry of the receiver spreads, with all of the split spreads being symmetrical about the vibrators and all of the off-end spreads being pushed by the vibrators. These spreads progressed with the sources; the "static" spreads did not. The array "type" gives the shape of the receiver group array at each channel, with the "geoph. inter." being the distance between individual seismometers of the group, and aspect being the greatest overall dimension of the array. The center of the group array is displaced from the nominal receiver VP by "disp." in the direction indicated, parallel or perpendicular to the local course of the line.

<b>Table A-1</b>			
Calcrust 1985 Mojave-Sonoran Project			
Line End Geographic Coordinates			
Line	VP	Latitude N	Longitude W
WM-1	101	34 ° 26' 58"	115 ° 02' 13"
	1193	34 ° 12' 29"	115 ° 05' 34"
WM-2	201	34 ° 16' 34"	115 ° 08' 43"
	1305	34 ° 04' 47"	114 ° 49' 52"
WM-3	101	34 ° 05' 15"	114 ° 51' 44"
	1297	34 ° 11' 29"	114 ° 35' 13"
WM-4	101	34 ° 11' 53"	114 ° 35' 15"
	445	34 ° 16' 01"	114 ° 33' 50"
WM-5	101	34 ° 04' 54"	114 ° 51' 03"
	602	33 ° 56' 30"	114 ° 51' 18"
Rice (WM-6)	25	34 ° 02' 10"	114 ° 47' 39"
	120	34 ° 04' 15"	114 ° 43' 47"

**Table A-2 A**  
Calcrust 1985 Mojave-Sonoran Project Source Acquisition Parameters

Record Line	Source				Max. Fold	Sweeps per Point	Moveup Array			Sweep Length, s
	Line	VP Range	Progression	Interval, m			Interval, m	Size, m	Disp. from VP, m	
WM-1	WM-1	101-300	N→S	75.4	32	12	2.1	50.3	0	16
		285-1113	N→S	75.4	32	8	3.1	50.3	0	31
WM-2	WM-2	201-1305	NW→SE	100.6	32	8	4.8	67.1	0	31
WM-3	WM-3	102-1297	SW→NE	75.4	32	8	3.1	50.3	0	31
WM-4	WM-4	101-388	S→N	75.4	32	8	3.1	50.3	0	31
WM-5	WM-5	101-143	N→S	100.6	32	8	4.8	67.1	0	31
		147-423	N→S	134.1	24	8	4.8	67.1	0	31
WM-5 (Refr.)	Rice	100-49	N→S	402.3	—	16	3.4	75.4	12.6N	31
Danby N	WM-1	438-876	N→S	75.4	—	8	3.1	50.3	0	31
Danby S	WM-1	438-876	N→S	75.4	—	8	3.1	50.3	0	31
Ward	WM-1	882-1113	N→S	75.4	—	8	3.1	50.3	0	31
Freda	WM-2	201-621	NW→SE	100.6	—	8	4.8	67.1	0	31
Milligan	WM-2	627-1305	NW→SE	100.6	—	8	4.8	67.1	0	31
Rice (WM-6)	WM-3	120-700	W→E	75.4	—	8	3.1	50.3	0	31
		1093-1297	SW→NE	75.4	—	8	3.1	50.3	0	31
	WM-4	101-388	S→N	75.4	—	8	3.1	50.3	0	31
	WM-5	101-143	N→S	100.6	—	8	4.8	67.1	0	31
		147-423	N→S	134.1	—	8	4.8	67.1	0	31
Savahia	WM-3	718-1084	S→N	75.4	—	8	3.1	50.3	0	31
	Rice	100-49	N→S	402.3	—	16	3.4	75.4	12.6N	31

**Table A-2 B**  
Calcrust 1985 Mojave-Sonoran Project Receiver Acquisition Parameters

Record Line	Source		Group Inter., m	Spread			Group Array				Rec. Sys.
	Line	VP Range		Type	No. Chan.	Offset Range, m	Type	Geoph. Inter., m	Aspect, m	Disp. from VP, m	
WM-1	WM-1	101-300	25.15	split	192	138-2527	online	2.3	25.1	12.6S	348
		285-1113	25.15	split	192	138-2527	online	2.3	25.1	12.6S	348
WM-2	WM-2	201-1305	33.53	split	192	184-3370	online	3.0	33.5	16.8SE	348
WM-3	WM-3	102-1297	25.15	split	192	138-2527	online	2.3	25.1	12.6NE	348
WM-4	WM-4	101-388	25.15	split	192	138-2527	online	2.3	25.1	12.6N	348
WM-5	WM-5	101-143	33.53	offend	192	138-6588	online	3.0	33.5	16.8S	348
		147-423	33.53	offend	192	138-6588	online	3.0	33.5	16.8S	348
WM-5 (Refr.)	Rice	100-49	33.53	static	48	—	online	3.0	33.5	16.8S	348
Danby N	WM-1	438-876	75.44	static	48	—	circ.	6.7	30	15W	338
Danby S	WM-1	438-876	75.44	static	48	—	L	6.7	47	12W, 37S	338
Ward	WM-1	882-1113	75.44	static	96	—	circ.	6.7	30	15W	338
Freda	WM-2	201-621	100.58	static	96	—	oval	6.7	45	5NE	338
Milligan	WM-2	627-1305	100.58	static	96	—	circ.	6.7	30	15NE	338
Rice (WM-6)	WM-3	120-700	100.58	static	96	—	circ.	6.7	30	15N,W	338
		1093-1297	100.58	static	96	—	circ.	6.7	30	15N,W	338
	WM-4	101-388	100.58	static	96	—	circ.	6.7	30	15N,W	338
	WM-5	101-143	100.58	static	96	—	circ.	6.7	30	15N,W	338
		147-423	100.58	static	96	—	circ.	6.7	30	15N,W	338
Savahia	WM-3	718-1084	75.44	static	96	—	circ.	6.7	30	15E	338
	Rice	100-49	75.44	static	96	—	circ.	6.7	30	15E	338